

21906

İSTANBUL TEKNİK ÜNİVERSİTESİ ★ FEN BİLİMLERİ ENSTİTÜSÜ

DAR BİR KANAL İÇİNDE ISI ÜRETEK DİKDÖRTGEN BLOKLAR  
ETRAFINDA LAMİNER AKIŞIN SAYISAL BENZEŞİMİ

DOKTORA TEZİ

Yük. Müh. İbrahim ÖZKOL

Ana Bilim Dalı : UÇAK MÜHENDİSLİĞİ

Programı : UÇAK MÜHENDİSLİĞİ

MART 1992

ISTANBUL TECHNICAL UNIVERSITY ★ INSTITUTE OF SCIENCE AND TECHNOLOGY

NUMERICAL SIMULATION OF 2-D LAMINAR FLOW, HEAT GENERATION AND  
FORCED CONVECTION FROM RECTANGULAR BLOCKS IN A NARROW CHANNEL

Ph.d. THESIS  
İbrahim ÖZKOL, M.Sc.

Date of Submission : 26 November 1991

Date of Approval : 24 March 1992

Examination Committee :

Supervisor	: Assoc. Prof. Dr. C. Ruhi KAYKAYOĞLU
Member	: Prof. Dr. Oğuz BORAT
Member	: Assoc. Prof. Dr. Osman ISIKAN

**İ.T. YÜKSEKÖĞRETİM KURULU**  
**DOKÜMANTASYON MERKEZİ**

MARCH 1992

## ACKNOWLEDGEMENTS

Before doing ordinary statements about the valuable persons who have helped me in the way of completing this thesis as well as in the way of life, I would really like to say my deepest thankfulness to my supervisor, Assoc. Prof. Dr. C.Ruhi Kaykayoglu for his encouragement and unfinished support at each step of this study.

To get such a reward and have a triumph, someone must have the help of a person who has the magic word in his finger tips, it is Dr.Kaykayoglu. Whatever he touches he reveals its holiest secret; liberates it from enhancement and restores it to its pristine loveliness.

I would also like to thank to my dear friend Metin.O.Kaya for his moral support and valuable criticism. And I would not pass to the next word without mentioning about Kerim Can Bayar, for his unforgettable help in preparing the color graphics programs and his fair behavior in ordering.

I would like to thank to my colleagues, Salih Bozkurt, Hakan Erdun and Orhan Gökçöl for their help in printing my thesis.

And, last my thanks goes to the Computing Center of Istanbul Technical University which enabled the computational facilities for my research.

## CONTENTS

ACKNOWLEDGEMENTS .....	ii
LIST OF SYMBOLS .....	vi
SUMMARY .....	ix
OZET .....	x

## CHAPTER 1

INTRODUCTION .....	1
1.1 Experimental Models of The Flow in a Narrow Channel With Obstacles .....	3
1.2 Computational Models of The Flow in a Narrow Channel With Obstacles ...	5

## CHAPTER 2

2.FUNDAMENTAL EQUATIONS .....	9
2.1 Flow Field .....	9
2.1.1 Clasical Primitive Function Variables Equation Form of The Navier-Stokes Equations .....	14
2.1.1 Vorticity-Stream Function Variables Equation Form of The Navier-Stokes Equation .....	16
2.2 Thermal Field .....	18
2.2.1 Energy Equation For Fluid Domain .....	19
2.2.2 Energy equation For Solid Domain .....	20
2.2.3 Solid-Fluid Interaction and Conjugate Solution .....	20

## CHAPTER 3

3. A REVIEW OF FINITE DIFFERENCE TECHNIQUES .....	22
3.1 General Ideas and Short History Review .....	22
3.2 A Finite Difference Formulation .....	23
3.2.1 Taylor Series Approach .....	25
3.2.2 Polyonomial Approach .....	27
3.2.3 Integral Method Approach .....	27
3.2.4 Control Volume Approach .....	28

## CHAPTER 4

4. PYHSICAL PROBLEM .....	34
4.1 Models .....	34



4.1.1 Phisycal Model .....	34
4.1.2 Flow Model .....	37
4.1.3 Thermal Model .....	37
4.1.4 The Implicit Numerical Solution Method .....	37
4.1.4.1 Governing Equations For Flow Field .....	41
4.1.4.2 Governing Equations For Thermal Field .....	42
4.2 Boundary Conditions .....	43
4.2.1 Boundary Conditions For Fluid and Heat Transfer Equations .....	45
4.3 Directional Implicit Finite Difference Formulation and Solution .....	48
4.3.1 Flow Equations .....	52
4.3.2 Energy Equation .....	60
4.3.3 Solution Procedure .....	63

## CHAPTER 5

5. NUMERICAL APPROXIMATION OF BOUNDARY CONDITIONS .....	66
5.1 Boundary Conditions of Flow Field .....	66
5.2 Boundary Conditions of Thermal Field .....	72
5.2.1 Prescribed Temperature Boundary Condition .....	72
5.2.2 Prescribed Heat Flux Boundary Condition .....	74
5.2.3 Convection Boundary Condition .....	79
5.3 Numerical Treatment of The Critical Points .....	82

## CHAPTER 6

6. FLOW FIELD .....	88
---------------------	----

## CHAPTER 7

7. THERMAL FIELD .....	119
7.1 One-Step Thermal Field .....	121
7.2 Two-Step Thermal Field .....	121
7.3 Three-Step Thermal Field .....	122
7.4 Iso Temperature Counters .....	122

## CHAPTER 8

HEAT TRANSFER CHARACTERISTICS .....	164
-------------------------------------	-----

CHAPTER 9	
COLOR GRAPHIC PRESENTATIONS .....	173
 CHAPTER 10	
RECOMMENDATIONS AND FUTURE ASPECTS .....	189
 REFERENCES .....	191
 APPENDIX A .....	192
 CURRICULUM VITAE .....	199

## LIST OF SYMBOLS

$a$	: Coefficient
$A$	: Area
$B_h$	: Block height
$B_L$	: Block length in flow direction
$B_T$	: Block length in transverse direction
$C$	: Specific heat
$C_p$	: Specific heat at constant pressure
$C_v$	: Specific heat at constant volume
$dQ$	: Externally added heat
$dQ_c$	: Heat addition by conduction
$dQ_f$	: Heat addition by friction
$\frac{D}{Dt}$	: Material derivative
$Ec$	: Eckert number
$E_L$	: Channel entrance length
$f$	: Body forces
$f$	: Function
$g$	: Gravitational acceleration constant
$H$	: Channel height
$i$	: Grid point in x direction
$j$	: Grid point in y direction
$k$	: Thermal conductivity
$k_b$	: Thermal conductivity of block
$k_f$	: Thermal conductivity of fluid
$k_s$	: Thermal conductivity of substrate
$L$	: Length
$m$	: Subscript

$n$  : Superscript  
 $\vec{n}$  : Surface normal  
 $Nu$  : Nusselt number  
 $p$  : Presssure  
 $Pr$  : Prandtl number  
 $q$  : Generated heat  
 $q$  : Heat flux  
 $Q$  : Heat source  
 $Q''$  : Nondimensionalized heat source  
 $Re$  : Reynolds number  
 $S_{ij}$  : Stress tensor  
 $S_L$  : Distance between two blocks in flow direction  
 $S_T$  : Length between two blocks in transverse direction  
 $t^*$  : Nondimensionalized time  
 $T$  : Temperature  
 $T_{in}$  : Inlet temperature  
 $T_w$  : Wall temperature  
 $T_{w,b}$  : Channel outer wall temperature  
 $T_{w,l}$  : Channel lower wall temperature  
 $T_{w,u}$  : Channel upper wall temperature  
 $T_\infty$  : Temperature of the ambient fluid  
 $u^*, v^*, w^*$  : Nondimensionalized velocity components  
 $U_\infty$  : Free stream velocity  
 $\vec{w}$  : Vector of Vorticity  
 $\vec{V}$  : Velocity vector  
 $u, v, w$  : Velocity components  
 $x_0, y_0$  : Considered point coordinates  
 $x, y, z$  : Spatial coordinate components in rectangular coordinate system

$\Delta x$  : Finite difference length in x direction between two grids

$\Delta y$  : Finite difference length in y direction between two grids

$\Delta G$  : Elementary weight

$\Delta V$  : Elementary volume

$\varepsilon$  : Small enough quantity

$\Theta$  : Nondimensionalized temperature

$\Theta_\infty$  : Nondimensionalized temperature of the ambient air

$\mu$  : Viscosity

$\nu$  : Kinematic viscosity

$\rho$  : Density

$\rho^*$  : Nondimensionalized density

$\Phi$  : Dissipation

$\psi$  : Stream function

$\vec{\nabla}$  : Operator

## SUMMARY

In this study, a directional-implicit Computational Fluid Dynamics (CFD) finite difference code is developed so as to simulate the direct and indirect heat removal through conduction and convection processes from the rectangular blocks attached to the lower surface of a narrow channel geometry.

Two dimensional, unsteady, incompressible, laminar form of the Navier - Stokes (N-S) equations are considered. Using the stream function-vorticity approach, they are discretized via finite difference technique, under the assumption of the Taylor series expansions. The discretized equations than reduced to a three-banded form of a matrix equality ready to be used conjugate solution formulation. In the same manner, two dimensional unsteady energy equation discretized with the source term included into three-banded matrix form.

Two field equations are solved numerically for various channel-rectangular block geometries so as to study the steady-state heat transfer characteristics inside channel with possible heat generation inside the blocks. It is shown that the numerical model is capable of simulating the main features of the flow field. Detailed benchmarks of the present numerical model is attempted so as to validate the developed algorithm. The streamwise extension of the recirculation zone behind the rectangular block which is a function of the Reynolds number is very well simulated. Furthermore, it was shown that the heat transfer characteristics of the zone agrees well with the experimental and theoretical observations in the literature. Prepared algoritmh is a highly stable algorithm but showing slow convergence to a steady state value. Conjugate solution property of the present approach enables one to study complex thermal characteristics of fluid-solid and solid-solid interactions.

Beside the classical boundary conditions of the thermal field, the problem domain is further complicated by the presence of discrete heat sources in the rectangular blocks in form of the infinite small heat generating sheet. Heat generated at various transfer positions are convected by the fluid downstream. The near wall flow temperature and the Nusselt number distributions over the surface depict the most features of the complex fluid-solid interaction. The steady-state temperature inside the blocks and in the substrate are found to be functions of the flow Reynolds number, Prandtl number, heat source position and substrate bottom surface temperature. Due to the heat generation the flow is heated well above its inlet value. This causes continous heat flow from fluid to the lower plate in the recirculating regions of the rectangular blocks and in the cavities where there are more than one obstacle. The present model can simulate the chip cooling problems for integrated circuit components, i.e, chips, on a horizontal printed curcuit board which is contain-ing heat generating rectangular blocks attached to a single layer substrate. Results consistency with other studies, which are reported in literature, is discussed.

## ÖZET

### DAR BİR KANAL İÇİNDE DİKDÖRTGEN BLOKLAR ETRAFINDA LAMİNER AKIŞ, ISI ÜRETİMİ VE ZORLANMIŞ TAŞIMANIN 2 BOYUTLU BENZEŞİMİ

Bu çalışmada dar bir kanal içine yerleştirilmiş dikdörtgen bloklar üzerinde viskoz, laminar, 2-Boyutlu akış çeşitli Reynolds sayılarında modellenmiştir. Ayrıca bloklar içinde üretilen yapay ısının taşımın yoluyla akışkana ve iletim yolu ile alt takaba geçişi birleşik çözüm yöntemi ile modellenmiştir. Problem blok ve alt tabaka malzemesi olarak değişik iletim ve ısı kaynakları gerektirmektedir. Ayrıca akışkan ile etkileşim nedeniyle katı ve akışkan bölgelerinin ortak çözümünün yapılması gerekmektedir. Bu nedenle çalışmada bütün bölge bir anda çözüme alınarak ortak çözüm elde edilmiştir. Bu çözüm yöntemi birleşik çözüm olarak bilinmektedir. Aşağıda problem çözümünde kullanılan denklemler özetlendikten sonra çalışmada izlenen yöntem tanıtılmıştır.

Akışkanlar mekaniğinin temel denklemleri, korunum yasaları kullanılarak çıkarılmıştır. Kütlenin korunumu kullanılarak süreklilik denklemi, momentum korunumu kullanılarak vektör formundaki momentum denklemi ve enerjinin korunumundan ise enerji denklemi elde edilir. Momentum denklemi viskoz akış alanı için Navier-Stokes denklemleri ile ifade edilmektedir. En genelde bu denklemler iki boyutlu sıkıştırılamaz viskoz ve daimi olmayan akış alanı için aşağıdaki gibidir.

Süreklilik Denklemi

$$\nabla \cdot \vec{V} = 0 \quad (1)$$

Momentum Denklemi

$$\frac{D\vec{V}}{Dt} = -\frac{1}{\rho} \vec{\nabla} p + \nu \nabla^2 \vec{V} + \vec{f} \quad (2)$$

Enerji Denklemi

$$\rho c_p \frac{DT}{Dt} = k \left( \frac{\partial^2 T}{\partial x^2} + \frac{\partial^2 T}{\partial y^2} \right) + \mu \Phi \quad (3)$$

Akış alanının çözümü için bu çalışmada 2-Boyutlu girdaplılık akım fonksiyonu tercih edilmiştir. Çalışmada kullanılan girdaplılık akım fonksiyonları yöntemi önce girdaplılık denkleminin tanımıyla başlatılmıştır. Sonra hız alanının bileşenleri akım fonksiyonu cinsinden ifade edilmiştir. Bu bileşenlerin girdaplılık denklemine taşınmasıyla, kısmi diferensiyel denklem formundaki eliptik Poisson denklemi elde edilmiştir. Aynı şekilde girdaplılık tanımının, momentum denklemine taşınması ve gerekli düzenlemelerin yapılması ile iki boyutlu parabolik girdaplılık taşınım denklemi elde edilmektedir.

Bu denklemler sırasıyla,

İki boyutlu Girdaplılık alanının tanımı;

$$\omega = \frac{\partial V}{\partial x} - \frac{\partial U}{\partial y} \quad (4)$$

Hız alanının akım fonksiyonu cinsinden tanımı;

$$U = \frac{\partial \psi}{\partial y} \quad V = -\frac{\partial \psi}{\partial x} \quad (5)$$

Poisson denklemi;

$$\nabla^2 \psi = -\omega \quad (6)$$

Girdaplılık taşınım denklemi boyutsuz değerler cinsinden;

$$\nabla^2 \omega = Re \left( \frac{\partial \psi}{\partial y} \frac{\partial \omega}{\partial x} - \frac{\partial \psi}{\partial x} \frac{\partial \omega}{\partial y} + \frac{\partial \omega}{\partial t} \right) \quad (7)$$

şeklinde ifade edilir.

Akış alanını denklemlerinden sonra sıcaklık alanına ait enerji denklemi ifade edilmiştir.

En genel haldeki enerji denklemi,

$$\rho C_p \frac{DT}{Dt} = k \left( \frac{\partial^2 T}{\partial x^2} + \frac{\partial^2 T}{\partial y^2} \right) + \mu \Phi \quad (8)$$



şeklinde tanımlanır.

Bu denklemde,

$$\Phi = 2 \left[ \left( \frac{\partial U}{\partial x} \right)^2 + \left( \frac{\partial V}{\partial y} \right)^2 + \left( \frac{\partial V}{\partial x} + \frac{\partial U}{\partial y} \right)^2 \right]$$

Bu denklem boyutsuz değişkenler cinsinden çözüme uygun şekilde aşağıda tanımlanmıştır.

Akış alanı için enerji denklemi

$$\frac{\partial \theta}{\partial t} + \frac{\partial \psi}{\partial y} \frac{\partial \theta}{\partial x} - \frac{\partial \psi}{\partial x} \frac{\partial \theta}{\partial y} = \frac{Ec}{Re} \Phi + \frac{1}{RePr} \left[ \frac{\partial^2 \theta}{\partial x^2} + \frac{\partial^2 \theta}{\partial y^2} \right] \quad (10)$$

Katı cisim için enerji denklemi ise

$$\frac{\partial \theta}{\partial t} = \frac{1}{PrRe} \nabla^2 \theta + q \quad (11)$$

şeklinde ifade edilir. 11 denkleminde  $q$  katı cisim içinde birim hacimde üretilen ısı kaynağını göstermektedir. Ayrık ısı kaynağı dikdörtgen bloklar içinde çeşitli konumlarda bulunmaktadır.

Kısmi diferensiyel denklemleri çözme yöntemlerinden biri de Sonlu Farklar Yöntemidir (SFY). Sonlu Farklar Yöntemini; süreklilik gösteren ve fiziksel olayı modelleyen denklemleri, süreklilik bölgesi içinde, verilen belirli bir noktadan başlayarak çok küçük artımlarla ayrık noktalarda bu süreklilik bölgesi içinde verilen belirli başlangıç koşulları ve sınır şartları ile çözmek olarak tanımlayabiliriz. Sonlu farklar yöntemi; Taylor serisi yaklaşımı, Polinom yaklaşımı, Integral yöntem yaklaşımı ve Kontrol hacmi yaklaşımından birini ya da aynı anda bir kaçını, aynı problemde, modellemesini gerektirmektedir. Bunlardan integral yöntem ve Taylor serisi yöntemindeki kabul, verilen kısmi diferensiyel denklemin verilmiş formunun doğru olduğu ve bu formunda fiziksel olayın gerçekleştiği konservativ form olduğu kabul edilip denklem cebrik denklemler formuna sadece matematiksel teknikler kullanılarak indirgenmektedir. Özellikle sınırlarda, kontrol hacmi yaklaşımı daha hasas çözümler vermektedir, ancak uygulamada sınırlarda alan büyüklüklerinin her biri sınırı geçtiği yerde bu büyüklük cinsinden yazılmış denge denkleminde elde edilmektedir. Eğer Taylor serisi ve Kontrol Hacmi yaklaşımı arasında bir karşılaştırma yapmak istersek; Taylor serisi yaklaşımı kullandığımızda verilen kısmi diferensiyel denklemi tamamen modellemek mümkün olduğu gibi değişik Taylor serisi modellemeleri kullanarak bunların kombinasyonundan yeni modellemeler çıkarmak mümkündür. Fakat Kontrol

Hacmi yaklaşımında konservatif form gerektiğinden bunu sadece alan değişkeninin türevi olması halinde yapmak mümkün olmayabilir. Bundan dolayı, sınırlar boyunca alınmış türevler için gereken sonlu farklar modelinin nasıl olacağına karar vermemiz zorlaşacaktır. Yani kontrol hacmi yaklaşımında kullanacağımız sonlu farklar modelinin konservatif özellik taşıması zorunlu hale gelmiştir.

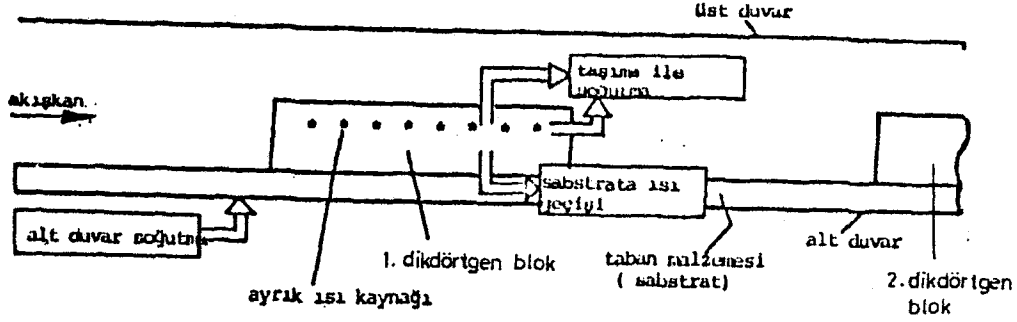
Çok sayıda örnek olmadan hangi sonlu farklar indirgeme metodun ya da yaklaşımın daha uygun sonucu vereceğini söylemek zordur. Fakat birçok basit durumda farklı dört yöntemin aynı sonucu vermesi mümkün olabilir. Geliştirilen sonlu farklar modelinin sayısal olarak kararlı olmaması halinde ise hangi yöntem ya da yaklaşım kullanılmış olursa olsun sonuç anlamsızdır.

Bu çalışmada ağırlıklı olarak Taylor serisi yaklaşımı kullanılmıştır. Birinci derece türevler için ileri farklar, geri farklar ve merkezi farklar formülleri de ikinci dereceden türevler için merkezi farklar modelleri problem fiziğine uygun olarak verilmiştir.

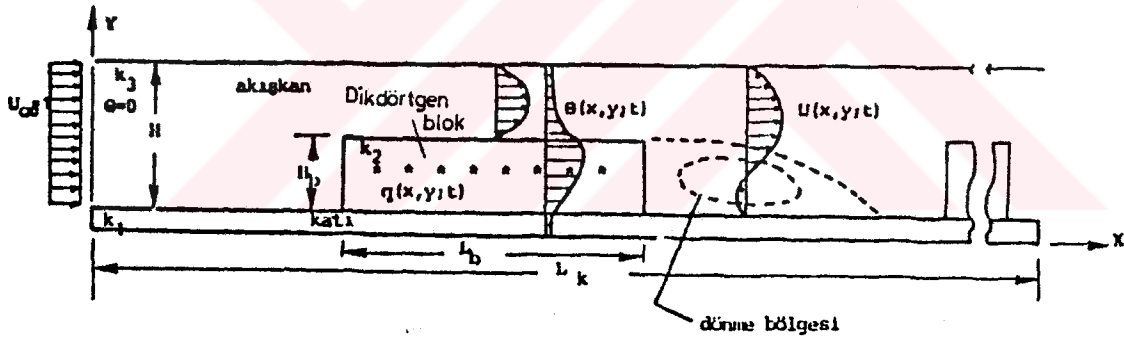
Şekil 1 bu çalışmada kullanılan geometrinin önemli özelliklerini göstermektedir. Problemin uygulama alanı daha çok elektronik baskılı devre kartlar üzerindeki yongaların soğutulması olarak literatürden gözlenebilir. Ancak bu çalışmada yaklaşım daha genel ve fiziksel parametrelerin araştırılması olarak seçilmiştir.

Modelin fiziksel özellikleri gerçekte varolan fiziksel modelinkine yakın alınmıştır. Burada modellenen bilgisayar yongasıdır (chip) ve yongalar dikdörtgen bloklar olarak modellenmişlerdir. Denklemlerin akış alanı ve sıcaklık alanı için yazılmasından ve gerekli sonlu farklar modellerinin geliştirilmesinden sonra yaptığımız sayısal modellemeye uygun bir fiziksel model olarak HaCohen [1] tarafından yapılan deneysel çalışmada kullanılan geometri benzeri geometriler sayısal olarak modellenmiştir.

Bu modellemede uzunluklar kanalın yüksekliği ile boyutsuzlaştırılmış olup, anında değiştirilebilir durumda tutulmuştur. Akım modeli olarak, dar bir kanala impulsiv olarak gönderilen akışkanın durumu göz önüne alınmıştır. Sıcaklık alanının modellenmesi ise; akışkan sıfır boyutsuz sıcaklığı ile gönderilirken katı yüzeylerinde katı-sıvı iletişim dengesi yazılmıştır. Bloklar içinde belirli güçte ısı üreten kaynaklar alınmış ve kanalın alt üst duvarları sabit sıcaklıkta tutulmuştur.



Şekil 1a) Fiziksel modelin geometrisi.



Şekil 1b) Fiziksel modelin geometrisi için kullanılan numerik model

Bu durumu modelleyen diferensiyel denklemler olarak süreklilik ve girdaplılık denklemleri seçilen parametrelerle boyutsuz hale getirilip 2 boyutlu hal için uygun şekilde yazılarak akım alanı modellenmiştir. Aynı şekilde enerji denkleminin 2 boyutlu hal için boyutsuz durumu disipasyon terimi ve kaynak teriminin eklenmesiyle verilmiştir.

Bilindiği üzere bir fiziksel olayın modellenmesinde kullanılan denklemler önemli olduğu gibi bu denklemlerin çözümünde kullanılan sınır koşullarının da önemi büyüktür. Bunların fiziksel olaya uygun bir şekilde gerçekçi olarak verilmesi gerekir.

Göz önüne alınan kanalın içinde dikdörtgen bloklar birbiri arkasına seri halde belirli mesafelerde konumlandırılmıştır. Girişte sadece akıma paralel yön olarak seçilen  $x$  ekseninde hız vardır; dik yönde ise hız sıfırdır ( $U = U_\infty, V = 0$  dır). Yine girişte girdaplılık için alınan değer  $\omega = 0$ , fakat akım fonksiyonunu ise hız alanına uygun birinci dereceden bir fonksiyon ile tanımlanmıştır.

Akış alanı içinde duvarlarda kaymama koşuluna uygun olarak katı yüzeylerde hız vektörü sıfırdır yani  $V = U = 0$ . Akım fonksiyonunun değeri sabit olup 0 olarak alınmıştır. Girdaplılık için kullanılan sınır şartları olarak duvarlarda girdaplılık denkleminin seri açılımından elde edilen değerler kullanılmaktadır girişte ise sabit 0 olarak alınmaktadır.

Sıcaklık alanı için kullanılan sınır şartlarında, akışkan  $\theta = 0$  boyutsuz sıcaklığı ile dar bir kanala girmektedir. Akış alanı içinde taşınım denklemi; katı içinde ise iletim denklemi çözülmektedir. Katı ile sıvının birleştiği yerlerde bir ortamdan diğer ortama geçen ısıların eşitliği yazılmaktadır. Fakat seçilen sınır şartına bağlı olarak duvarların izole edilmiş olması söz konusu olabileceği gibi sabit sıcaklıkta tutulması da söz konusu olabilir.

Bütün alan büyüklükleri, akış alanının ve sıcaklık alanın, göz önüne alınan geometrinin sonunda, akış alanına paralel eksen boyunca değişmeyen türevlere sahip büyüklükler olarak kabul edilmişlerdir. Denklemlerin seçilen fiziksel geometri için uygun durumu verildikten sonra, geometriye uygun sınır koşulları verilmiştir. “Akış alanına paralel eksen boyunca değişmeyen türevlerdir” demekle anlatılmak istenen şudur:

$$\frac{\partial U}{\partial x} = \frac{\partial V}{\partial x} = \frac{\partial \psi}{\partial x} = \frac{\partial \omega}{\partial x} = \frac{\partial \theta}{\partial x} = 0$$

Şimdi bu denklemlerin ayrışlaştırılması yapılmalıdır. Birinci merteye türevlerde akıma paralel yönde geri farklar kullanılırken dik yönde merkezi farklar kullanılmış; zamanda ise geri farklar alınmıştır. İkinci merteye türevler merkezi farklara göre açılmıştır. Ayrışlaştırma denklemlerinin düzenlenmesinden sonra akıma paralel yöndeki alan büyüklükleri merkezi terimi hariç diğer terimler bir zaman adımı geriden alınmıştır ve zaman adımı küçük tutulmuştur. Seçilen zaman adımı CFL şartını sağlamaktadır. Bu değerlerin bir zaman adımı geriden alınmasının faydası

şu şekilde açıklanabilir. Ayrıklaştırılmış denklemlerin oluşturduğu cebrik denklemlerin matris formunda yazılması karşımıza 5 bandlı bir matris çıkarmaktadır. Bunun bellek gereksinimi, eğer bu 3 bandlı matris olarak saklanırsa daha az olacaktır ve kullanacağı bilgisayar zamanında azalacaktır. Bundan dolayı bir zaman adımı geriden alınan değerler bize bu durumu sağlamaktadır. Böylece daha fazla noktada daha kısa zamanda çözüm yapılabilir. Bunun yanında ödenen diyet ise seçilen çok küçük zaman adımı ile daimi koşula yakınsamadaki iterasyon sayısı çok yüksek sayılara ulaşmaktadır. Bilgisayar programının yapım nedeni ile bu pek sorun yaratmamaktadır.

Ana denklemlerin istenilen şekilde ayrıklaştırılmasından sonra sınır şartlarının uygun bir durumda ayrıklaştırılması gerekmektedir. Akış alanına ait büyüklüklerin ayrıklaştırılmasında uygun görülen yerlerde polinom yaklaşımı kullanılmıştır. Aynı şekilde sıcaklık alanın çözümünde kullanılan sınır şartları detaylı bir şekilde tezde anlatılmıştır. Akış alanı ve sıcaklık alanı içinde yer alan kritik noktalardaki çözümlerde özel yaklaşımlar kullanılarak bu noktalardaki büyüklüklerin değerlerinin hassas hesaplanması yapılmıştır. Bu hesapların nasıl yapıldığı şekillerle iyice açıklanmış ve ayrıklaştırma noktaları üzerinde gösterilmiştir.

Buraya kadar yapılan açıklamaların ışığı altında yazılan bilgisayar programında yukarıda anlatılan yöntemler ve yaklaşımlar kullanılarak çözümler yapılmıştır.

Elde edilen sonuçlar, akım alanı ve sıcaklık alanı için, grafiklerle verilmiş bu grafiklerin yorumları yapılmıştır sıcaklık alanının anlatılmasında, üç farklı geometri için üç farklı kaynak yerleştirme durumunda sıcaklık dağılımları çıkartılmış ve bunların birbirlerine göre karşılaştırılmalı yorumları yapılmıştır.

Bu sonuçlardan hareketle en iyi soğutmanın, benzer geometriler için ve yapılan kabuller dahilinde nasıl olabileceği hakkında yorum getirilmiş ve öneriler yapılmıştır.

## CHAPTER 1

### INTRODUCTION

Increasing demand in high speed computer technology makes us to realize an immediate engineering approach to the problems which are dealing with combined fluid-heat transfer engineering. The need for an immediate solution is playing an increasingly important role in the advancement of electronic technology. Removing of heat from the large scale computer chips is becoming among the major technical problems which need to be solved to achieve higher data processing speeds.

From small scales to large ones, there are many vehicles having electronic devices which will confront a multitude of heat transfer problems that will affect their reliability. Furthermore, attention must be taken on that the heat transfer problems in electronic equipment are strongly coupled with considerations of electronic performance [1].

From the deep search one understands that in most devices the geometry of heat conduction paths and coolant paths are dictated by the arrangement of the electronic circuits. Finally, for one there arises an increasing need to the under-

standing of heat transfer processes within the equipment. In addition to that, the majority of heat transfer problems have not as yet been solved to a satisfactory degree due to the interrelationship of the many geometrical operative parameters.

An increase in speed of data processing needs a new model system on the basis of the types of cooling systems. These include the kind of coolant, the candidate schemes of enhancement measures for heat transfer at the package and board levels, and the schemes of coolant circulation at the board and system levels [2]. From above explanation one sees that the geometric and operative parameters, such as the size of the cooling device and the flow rate of the coolant, should fall in certain ranges of permissible values considering the design criteria and the constraints imposed by the bounds on the electrical connection distances, and also performing approximate heat transfer analyses, the ranges of parameter values can be delineated for each candidate scheme.

Since development of the first electronic digital computers, heat removal has played an important role in maintaining reliable operation. An important trend that initially alleviated, and subsequently exacerbated, the heat removal problem involved the integration of monolithic circuits on a silicon chip and the development of very large scales of circuit integration [3]. From the large-scale integration (LSI) technologies of the 1970s, which involved up to 1000 gates per chip, to the very large-scale integration (VLSI) of the 1980s, which involved up to 100.000 gates per chip, there has been a steady increase in heat dissipation at the chip, module and system levels. Such increases have made the role of heat transfer and thermal design more important than ever, and the development of future large-scale, high speed

circuits may well be limited by the inability to maintain effective cooling [3].

Similar to the chip cooling problem, transfer of heat from walls to the fluid flow occurs in various engineering application. The heat generated from obstacles inside channels are convected downstream to the rest of the fluid and also to the recirculation zone behind the block. If there happens to be more than one block there is a possibility of having cavity type flow and heat transfer becomes very important.

An understanding of the basic features of the heat and momentum transfer inside the narrow channels having obstacles attached to the lower surface is still an intergoing challenge to the predictor in the numerical simulation area. In this research work, author attempts to generate a practical but highly accurate numerical prediction algorithm so as to study complex heat transfer characteristics inside the narrow channel.

### 1.1 Experimental Models of The Flow in A Narrow Channel With Obstacles

Due to the geometric dimension of the narrow channels which are in operation in the practical it is desirable to do detailed, accurate and effective measurements by using highly sophisticated experimental techniques. Therefore extensive experimental studies are usually made on prototype models of prespective designs to verify that the required board and component temperatures are maintained.



Flow and thermal field distributions in channels formed by stacked PCBs containing heated components are usually quite difficult to obtain without the use of sophisticated test equipment, i.e hot wire and hot film anemometry or laser doppler anemometry, and experienced personel. Furthermore, preparation of the test rig for the experiments require sensitive mechanical operations. Small dimensions of the components make difficulty for one who wants to take data on the velocity and thermal fields without disturbing the local fields themselves [4]. Flow field visualization can be accomplished by use of smoke or trace materials injected into the fluid streams [4-7]. Prediction of component surface convective coefficients and finally the component temperatures can be done indirectly, i.e by evaporation of naphthalene-constructed components [8].

Prediction of the the amount of heat generation in a component through electrical measurments, embedding thermocouples and measuring freee-stream or inlet temperature is needed to compute the average convective heat transfer coefficient on the surface of a component in the channel. In general, as the components become smaller, the experimental predictions begin to fail due to practical reasons.

It is worth noting that although it is customary to speak about the experimental results reliability, unfortunately in this field, there does not exist extensive data to make comparisons with numerical prediction due to the above practical reasons.

## 1.2 Computational Models of The Flow In a Narrow Channel With Obstacles

The variation in the geometric parameters and measurement difficulties brought about by the small physical size of the component array under consideration lead one to investigate various means of experimental studies by using other prediction techniques. Then attentions turn on the searching the possibility of using numerical experimentation. In all areas of engineering, Computational Fluid Dynamics (CFD) is becoming an increasingly powerful tools. The use of the CFD in the aeronautics industry is well known and documented by Bradly [9]. On the other hand the use of CFD in more practical engineering areas are just starting.

A comparison between experimental and numerical studies yields the following important advantageous points for the numerical approach.

- a) The ability to see implications of design changes within short time intervals to increase design flexibility.
- b) Getting out the detailed information on all field variables through out the domain.
- c) Elimination of external disturbance effect on the field variables which may have occurred during measurements.
- d) Simulation ability of severe operating conditions
- e) Least expensive time values and material costs [4].

The capability of finite difference or finite element CFD codes to provide design and packing engineers with an easily usable tool to visualize complex flow fields and evaluate the thermal performance using various cooling situations illustrated by many investigators [10–15]. In the present computational model finite difference technique will be used to discretize field equations. All the boundary conditions, will be given later in all details, suitably fitted into finite difference form considering physical significancies as well as their geometric positions on the physical model.

Before describing the approach in this study, it will be usefull to review similar studies in this field.

Mahaney, Incropera and Ramadhyani [16] investigated mixed convection heat transfer from a four-row, in line array 12, square heat sources which are flush mounted to the lower wall of a horizontal rectangular channel was investigated. The variation of the row-average Nusselt number with Reynolds number exhibits a minimum, suggesting, that due to the buoyancy-induced flow, heat transfer may be enhanced.

J. T. Lin, B. F. Armaly and T. S. Chen [17] show that the influence of the buoyancy force on the velocity distribution. To study the effects that the buoyancy has on the heat transfer in laminar flow inside a vertical duct with a backward-facing step. The buoyancy force changes significantly the shape of the main recirculation region behind step it causes the reattachment length to decrease as its magnitude increases. This study show that bouncy effects should be consider in simulation

model if one studies the vertical duct problem with a backward facing step.

Fluid flow and heat transfer in a two dimensional finned passages were analyzed for constant property laminar flow conduction by Kelkar and Patankar [18]. In this study, the temperature of the plate was kept constant and the cross-sectional area of the channel was varied periodically. This causes the flow and the temperature fields to be periodic after a certain streamwise length. Computations were performed for different values of the Reynolds number, the Prandtl number, geometric ratios and the material thermal conductance. The placement of the fins in the channel changes the heat transfer significantly since it changes the velocity significantly as well.

Hsieh and Huang [19] solved two-dimensional Navier-Stokes equations by applying different numerical schemes for the convective term discretization. Particularly, they applied various numerical schemes to analyze numerical errors for the predictor of the laminar recirculation zone. As the conclusions of their study, the Quadratic Upstream Weighted Schemes (QUDS) or the Hybrid Central/Skew Upwind Schemes (CSUDS) are shown to be more accurate than the standard upwind scheme or the schemes.

Ghia, Osswald and Ghia [20] formulated the unsteady incompressible Navier-Stokes equation in terms of vorticity and streamfunction. The numerical method developed solves the conservative form of the vorticity transport equation using the Alternating Direction Implicit method, whereas the streamfunction equation is solved by Direct Block Gaussian elimination. The results are in good agreement,

in the entire laminar range for the back step channel problem, with the available experimental data.

Pereira and Durst [21] studied steady-state laminar flow characteristics over surface-mounted ribs by using the finite-difference numerical scheme with uniform/nonuniform grid systems to examine grid dependence. In addition the variation of Reynolds number effects on the drag were examined

Two-dimensional time dependent Navier-Stokes equations are formulated into stream function vorticity equations by Cheng and Huang [22]. The conservative form of the vorticity transport equation is solved by using the Alternating Direction Implicit Method, whereas stream function equation is solved by Direct Block Gaussian Elimination. This method is applied to a model problem of flow over a back step in a doubly infinite channel with suitable grid distribution in the separation and reattachment regions, as well as in the inflow and outflow regions. In order to avoid artificial viscosity in the discretization of the problem, central differences for the spatial derivatives are used. They observed the shedding of vortices at the corner of the step, the formation of additional separation bubbles at the lower wall and the occurrence of the upper wall separation bubbles.

## CHAPTER 2

### FUNDAMENTAL EQUATIONS

#### 2.1 Flow Field

In this chapter, governing equations for the fluid motion and the temperature field will be presented. There will be no detailed derivation of the fundamental equations, since it is readily available in most of the texts written on the subject [23]. The classical form of the flow equations, which will be used primarily for computational purposes are reviewed in the following lines.

The fundamental equations of fluid flow are based on the following universal laws of conservation;

- a) Conservation of mass.
- b) Conservation of momentum.
- c) Conservation of energy.

Very short presentation of above the conservation equations will be presented below for the sake of the countinuty in the presentation.

a) Conservation of mass

When the conservation of mass law applied to a fluid passing through an infinitesimal volume, the following continuity equation is obtained, [24];

$$\frac{D\rho}{Dt} + \rho(\vec{\nabla} \cdot \vec{V}) = 0 \quad (2.1)$$

with the assumption of incompressible flow hence,

$$\frac{D\rho}{Dt} = 0 \quad (2.2)$$

Equation (2.1) reduces to  $\nabla \cdot \vec{V} = 0$ . For 3-D flows, in differential form, this takes the following form;

$$\frac{\partial U}{\partial x} + \frac{\partial V}{\partial y} + \frac{\partial W}{\partial z} = 0 \quad (2.3)$$

where,

$$\vec{V} = U\vec{i} + V\vec{j} + W\vec{k} \quad (2.4)$$

b) Conservation of momentum

When Newton's second law is applied to a fluid passing through an infinitesimal, fixed control volume, momentum conservation is obtained in the following form;

$$\frac{\partial}{\partial t}(\rho\vec{V}) + \vec{\nabla} \cdot \rho\vec{\nabla}\vec{V} = \rho\vec{f} + \vec{\nabla} \cdot S_{ij} \quad (2.5)$$

Making use of the continuity equation, the momentum equation reduces to

$$\rho \frac{D\vec{V}}{Dt} = \rho\vec{f} + \vec{\nabla} \cdot S_{ij} \quad (2.6)$$

The first term on the right hand-side of equation (2.6),  $\vec{f}$ , is the body force vector per unit volume. The second term on the right-hand side of equation (2.6),  $S_{ij}$ , represents the surface forces per unit volume. These forces are created by the external stresses on the fluid element boundary. The stresses consist of normal and shearing stresses and are represented by the components of the stress tensor  $S_{ij}$ . After inserting each component of the stress tensor  $S_{ij}$  which were obtained through series of assumptions known as Stokes assumptions, Navier-Stokes equations are obtained. In addition, with the assumptions of incompressibility and constant viscosity coefficient final form of equation 2.5. will be

$$\frac{D\vec{V}}{Dt} = \vec{f} - \frac{1}{\rho}\vec{\nabla}p + \nu\nabla^2\vec{V} \quad (2.7)$$



## b) Conservation of energy

Generally, for an incompressible fluid the energy balance is determined by the internal energy, the conduction of heat, the convection of heat with the stream and generation of heat through friction. In a compressible fluid there is an additional term due the work of volume changing. In all cases radiation may also be present, but its contribution is small at moderate temperatures, and it is neglected completely. In the present thesis based on the first law of thermodynamics, considering on elementray volume  $\Delta V$  of weight,

$$\Delta G = \Delta V \cdot \rho \cdot g \quad (2.8)$$

Writing a balance between externally added heat  $dQ$ , internal energy and expansion work;

$$dQ = \Delta G \cdot C_v \cdot dT + p \cdot d(\Delta V) \quad (2.9)$$

The quantity of heat  $dQ$  consists of two terms:

- 1) Heat  $dQ_c$  added through conduction
- 2) Heat  $dQ_f$  added through friction

With Fourier's law help one can calculate the quantity of heat added through conduction

$$\frac{dQ_c}{A \cdot dt} = q = -k \frac{\partial T}{\partial n} \quad (2.10)$$

$q$ =Heat flux: Crossing an area  $A$  of heat per unit area and time

Using this law to calculate conduction part, and using shear stresses and normal stresses on the element to calculate friction, calculate the work by means of expansion or compression. Put these terms into a balance, with the addition of dissipation, one finally derives the energy equation;

$$\rho g C_p \frac{DT}{Dt} = \frac{Dp}{Dt} + \frac{\partial}{\partial x} \left( k \frac{\partial T}{\partial x} \right) + \frac{\partial}{\partial y} \left( k \frac{\partial T}{\partial y} \right) + \frac{\partial}{\partial z} \left( k \frac{\partial T}{\partial z} \right) + \mu \Phi \quad (2.11)$$

Assuming the independency of  $C_p$  and  $k$  from temperature ,energy equation becomes;

$$\rho g C_p \frac{DT}{Dt} = \frac{Dp}{Dt} + k \left( \frac{\partial^2 T}{\partial x^2} + \frac{\partial^2 T}{\partial y^2} + \frac{\partial^2 T}{\partial z^2} \right) + \mu \Phi \quad (2.12)$$

For incompressible fluid the work of compression,  $DP/DT$ , vanishes and  $C_p = C_v = C$  Final form of the energy equation,

$$\rho g C \frac{DT}{Dt} = k \left( \frac{\partial^2 T}{\partial x^2} + \frac{\partial^2 T}{\partial y^2} + \frac{\partial^2 T}{\partial z^2} \right) + \mu \Phi \quad (2.13)$$

Where

$$\Phi = 2 \left[ \left( \frac{\partial U}{\partial x} \right)^2 + \left( \frac{\partial V}{\partial y} \right)^2 + \left( \frac{\partial W}{\partial z} \right)^2 \right] + \left( \frac{\partial V}{\partial x} + \frac{\partial U}{\partial y} \right)^2 + \left( \frac{\partial W}{\partial y} + \frac{\partial V}{\partial x} \right)^2 - \frac{2}{3} \left( \frac{\partial U}{\partial x} + \frac{\partial V}{\partial y} + \frac{\partial W}{\partial z} \right)^2 \quad (2.14)$$

### 2.1.1 Classical Primitive Function Variables Equation Form of The Navier-Stokes Equations

The vorticity-stream function approach, which will be mentioned in the next section loses its attractiveness when applied to a three-dimensional flow field because a single scalar stream function does not exist in this case. Consequently, the incompressible N-S equations are normally solved in their primitive variable form  $(U, V, W, P)$  for a three dimensional problem. The incompressible Navier-Stokes equations in nondimensional, primitive variable form for a cartesian coordinate system are given as follows [23];

Continuity:

$$\frac{\partial U^*}{\partial x^*} + \frac{\partial V^*}{\partial y^*} + \frac{\partial W^*}{\partial z^*} = 0 \quad (2.15)$$

X-Momentum:

$$\frac{\partial U^*}{\partial t^*} + U^* \frac{\partial U^*}{\partial x^*} + V^* \frac{\partial U^*}{\partial y^*} + W^* \frac{\partial U^*}{\partial z^*} = -\frac{\partial P^*}{\partial x^*} + \frac{1}{Re_L} \left( \frac{\partial^2 U^*}{\partial x^{*2}} + \frac{\partial^2 U^*}{\partial y^{*2}} + \frac{\partial^2 U^*}{\partial z^{*2}} \right) \quad (2.16)$$

Y-momentum

$$\frac{\partial V^*}{\partial t^*} + U^* \frac{\partial V^*}{\partial x^*} + V^* \frac{\partial V^*}{\partial y^*} + W^* \frac{\partial V^*}{\partial z^*} = -\frac{\partial P^*}{\partial y^*} + \frac{1}{Re_L} \left( \frac{\partial^2 V^*}{\partial x^{*2}} + \frac{\partial^2 V^*}{\partial y^{*2}} + \frac{\partial^2 V^*}{\partial z^{*2}} \right) \quad (2.17)$$

Z-momentum

$$\frac{\partial W^*}{\partial t^*} + U^* \frac{\partial W^*}{\partial x^*} + V^* \frac{\partial W^*}{\partial y^*} + W^* \frac{\partial W^*}{\partial z^*} = -\frac{\partial P^*}{\partial z^*} + \frac{1}{Re_L} \left( \frac{\partial^2 W^*}{\partial x^{*2}} + \frac{\partial^2 W^*}{\partial y^{*2}} + \frac{\partial^2 W^*}{\partial z^{*2}} \right) \quad (2.18)$$

where above equations are nondimensionalized using the following definitions;

$$u^* = \frac{U}{U_\infty}, \quad x^* = \frac{x}{L}, \quad \rho^* = \frac{\rho}{\rho_\infty}, \quad v^* = \frac{V}{U_\infty}, \quad y^* = \frac{Y}{L},$$

$$t^* = \frac{t U_\infty}{L}, \quad W^* = \frac{W}{U_\infty}, \quad z^* = \frac{Z}{L}, \quad Re_L = \frac{U_\infty L}{\nu} \quad (2.19)$$

These equations are written in an Eulerian frame of reference, i.e. in a space-fixed reference frame through which the fluid flows. The boundary conditions for primitive variables  $U$ ,  $V$  and  $W$  along a no-slip wall are just  $U = 0$ ,  $V = 0$  and  $W = 0$  for all the time. This is evidently a great advantage for the use of the implicit methods, since no iteration is required for the boundary conditions. However, there

is an impediment to the succesful application of implicit methods to the primitive equations, due to a nonlinear instability of the pressure term during the solution procedure [25]. One of the early techniques for solving the incompressible N-S in primitive-variable form is the artifical compressibility method. In this method, the continuity equation is modified to include an artifical compressibility term which vanishes when the steady-state solution is reached. With the addition of this term to the continuity equation and the resulting N-S equations are mixed to form set of hyperbolic-parabolic equations which can be solved using a standart time dependent approach. The artifical compressibility method, is one of the techniques for solving the incompressible N-S equations in primative variable form. This method uses a Poisson equation formulation for the pressure in place of continuity equation. This is done to separate the majority of the pressure effects into a single equation so that the elliptic nature of the flow can be suitably modelled.

### 2.1.2 Vorticity-Stream Function Variables Equation Form of The Navier–Stokes Equation

The vorticity–stream function approach is one of the most popular methods for solving 2–D incompressible N–S equations [23,26]. This approach, introduces the vorticity component ( $\omega$ ) and the stream function ( $\psi$ ). The vorticity vector ( $\vec{\omega}$ ) is defined as;

$$\vec{\omega} = \nabla \times \vec{V} \quad (2.20)$$

where the magnitude of the vorticity vector will be

$$|\vec{\omega}| = \omega = |\nabla \times \vec{V}| \quad (2.21)$$

For a 2-D flow field Eq. 2.21 can be written explicitly as;

$$\omega = \frac{\partial V}{\partial x} - \frac{\partial U}{\partial y} \quad (2.22)$$

In 2-D cartesian coordinate system, the stream function  $\psi$  is defined in the usual way as follows

$$U = \frac{\partial \psi}{\partial y} \quad V = -\frac{\partial \psi}{\partial x} \quad (2.23)$$

Using these new dependent variables and also eliminating the pressure term in both equations vorticity transport equation is obtained. The two-dimensional, unsteady flow of an incompressible Newtonian fluid formulated in terms of the stream function( $\psi$ ) and the vorticity( $\omega$ ) values take the following forms, in terms of nondimensional values [23].

Definition of vorticity;

$$\nabla^2 \psi = -\omega \quad (2.24)$$

Vorticity transport equation;

$$\nabla^2 \omega = Re \left( \frac{\partial \psi}{\partial y} \frac{\partial \omega}{\partial x} - \frac{\partial \psi}{\partial x} \frac{\partial \omega}{\partial y} + \frac{\partial \omega}{\partial t} \right) \quad (2.25)$$

or,

$$\frac{\partial \omega}{\partial t} + U \frac{\partial \omega}{\partial x} + V \frac{\partial \omega}{\partial y} = \frac{1}{Re} \nabla^2 \omega \quad (2.26)$$

or,

$$\frac{D\omega}{Dt} = \frac{1}{Re} \nabla^2 \omega \quad (2.27)$$

This is a parabolic Partial Differential Equation having of marching type.

On the other hand, stream function equation, so called Poisson equation, has an elliptic character having a jury type solution.

## 2.2 Thermal Field

Generally, for an incompressible fluid the energy balance is determined by the rate of change of internal energy in the field with the conduction of heat with in the flow field and the generation of heat through viscous friction. For compressible fluids, there is an additional term due the work of volume change. In all cases radiation heat transfer may also present in the physics of the problem. Its contribution is small at moderate temperatures, and we shall neglect it completely in the present work.

The first of law of thermodynamics constitutes the balance of the various work terms in the flow field with the input of heat transfer. Hence the energy equation is [27],

$$\rho C_p \frac{DT}{Dt} = \frac{Dp}{Dt} + \frac{\partial}{\partial x} \left( k \frac{\partial T}{\partial x} \right) + \frac{\partial}{\partial y} \left( k \frac{\partial T}{\partial y} \right) + \frac{\partial}{\partial z} \left( k \frac{\partial T}{\partial z} \right) + \mu \Phi + Q \quad (2.28)$$

Assuming the constant  $C$  and  $k$  energy equation becomes;

$$\rho C \frac{DT}{Dt} = \frac{Dp}{Dt} + k \left( \frac{\partial^2 T}{\partial x^2} + \frac{\partial^2 T}{\partial y^2} + \frac{\partial^2 T}{\partial z^2} \right) + \mu \Phi + Q \quad (2.30)$$

For incompressible fluid flow the work of compression,  $Dp/Dt$ , vanishes. The final form of the energy equation which will be used through out the computations will

be

$$\rho C \frac{DT}{Dt} = k \left( \frac{\partial^2 T}{\partial x^2} + \frac{\partial^2 T}{\partial y^2} + \frac{\partial^2 T}{\partial z^2} \right) + \mu \Phi + Q \quad (2.30)$$

where, the dissipation term is represented as follows

$$\begin{aligned} \Phi = 2 \left[ \left( \frac{\partial U}{\partial x} \right)^2 + \left( \frac{\partial V}{\partial y} \right)^2 + \left( \frac{\partial W}{\partial z} \right)^2 \right] + \\ \left( \frac{\partial V}{\partial x} + \frac{\partial U}{\partial y} \right)^2 + \left( \frac{\partial W}{\partial y} + \frac{\partial W}{\partial x} \right)^2 \end{aligned} \quad (2.31)$$

### 2.2.1 The Energy Equation for Fluid Domain

Before presenting the governing equations, for the fluid domain, it is necessary to introduce some dimensionless quantities which will be used for the nondimensionalization of energy equation. These are as follows;

$$U = \frac{U}{U_\infty}, \quad V = \frac{V}{U_\infty}, \quad x = \frac{X}{L}, \quad y = \frac{Y}{L}, \quad t = \frac{t U_\infty}{L}, \quad \theta = \frac{T - T_{in}}{T_w - T_{in}} \quad (2.32)$$

Above nondimensional terms are introduced into equation 2.29 to obtain the following form,

$$\frac{D\theta}{Dt} = \frac{1}{RePr} \nabla^2 \theta + \frac{Ec}{Re} \Phi + Q'' \quad (2.33)$$

where,

$$Re = \frac{U_\infty L}{\nu}, \quad Pr = \frac{\mu}{k/\rho c}, \quad Ec = \frac{U_\infty^2}{c(T_w - T_{in})} \quad (2.34)$$

Eq. 2.33 written in cartesian coordinate system will be as follows

$$\frac{\partial \theta}{\partial t} + U \frac{\partial \theta}{\partial x} + V \frac{\partial \theta}{\partial y} + = \frac{Ec}{Re} \Phi + \frac{1}{RePr} \left[ \frac{\partial^2 \theta}{\partial x^2} + \frac{\partial^2 \theta}{\partial y^2} + \right] + Q'' \quad (2.35)$$



### 2.2.2 Energy Equation for Solid Domain

Consider the time dependent conduction energy equation for the solid domain [27],

$$\rho C_p \frac{\partial T}{\partial t} = k \nabla^2 T + Q'' \quad (2.36)$$

Introducing the nondimensional quantities of Eq.2.31, the following form yields

$$\frac{\partial \theta}{\partial t} = \frac{k}{L^2} \frac{1}{\rho C_p} \frac{L}{U_\infty} \nabla^2 \theta + Q'' \quad (2.37)$$

now multiply the numerator and denominator of the right hand side by  $\nu$

$$\frac{\partial \theta}{\partial t} = \frac{k}{\rho C_p} \frac{1}{LU_\infty} \frac{\nu}{\nu} \nabla^2 \theta + Q'' \quad (2.38)$$

now regrouping the right side terms and use the definition of Pr and Re then

$$\frac{\partial \theta}{\partial t} = \frac{k}{\rho C_p} \frac{1}{\nu} \frac{\nu}{LU_\infty} \nabla^2 \theta = \frac{1}{Pr} \frac{1}{Re} \nabla^2 \theta + Q'' \quad (2.39)$$

Hence, the energy equation for the solid domain becomes

$$\frac{\partial \theta}{\partial t} = \frac{1}{Pr Re} \nabla^2 \theta + Q'' \quad (2.40)$$

### 2.2.3 Solid-Fluid Interaction and Conjugate Solution

Solution of the combined thermal field in the fluid and solid domain requires conjugate solution techniques since the boundary condition at the interface changes during the solution. In the problem domain, heat convects in the fluid and conducts

in the solid domain part. On the boundaries conduction and convection processes should be in balance.

Take energy equation into consideration again in nondimensional form,

$$\frac{\partial \theta}{\partial t} + U \frac{\partial \theta}{\partial x} + V \frac{\partial \theta}{\partial y} = \frac{1}{Pr Re} \nabla^2 \theta + \frac{Ec}{Re} \Phi + Q'' \quad (2.41)$$

This equation was written for a media which contained fluid-solid together must be valid everywhere in such kind of media. Let's make an assumption that we were moving with a fluid particle, if we had velocity in three-dimension different from zero, the temperature around us would be given by this complete energy equation. If we had zero velocity in three- dimension this would mean  $U = V = W = 0$  then energy equation would become;

$$\frac{\partial \theta}{\partial t} = \frac{1}{Pr Re} \nabla^2 \theta + Q \quad (2.42)$$

That is the equation which is valid for only the solid media. The equation which is written in general sense modified itself conveniently where the physical phenomenon takes place. Therefore no additional efforts required to check its correctness.

## CHAPTER 3

### A REVIEW ON FINITE DIFFERENCE TECHNIQUES

#### 3.1 General Ideas and Short Historical Review

The development of the high-speed digital computers has had a great impact on the way in which principles for the sciences of fluid mechanics and heat transfer which are applied to problems of design in modern engineering practice. Problems can now be solved at a very little cost in few seconds of computer time which would have taken years to work out with the analytical methods and the first generation computers available twenty years ago. The ready availability of previously unimaginable computing power has stimulated many changes [23].

Traditionally, both experimental and theoretical methods have been used to develop new designs for equipment and vehicles involving fluid flow and heat transfer problem. With the advents of the digital computer, a third method, the numerical approach, has become available [23]. Below short review of the finite difference techniques will be presented.

The rise of a new methodology of attacking the complex problems in fluid mechanics and heat transfer which is known as Computational Fluid Dynamics (CFD) involves the solution of continuity, momentum and energy equations. The equations which correspond to physical phenomena of interest are solved numerically. The evaluation of numerical methods, particularly finite difference methods for solving ordinary and partial differential equations have begun at about the turn of the century.

### 3.2 A Finite Difference Formulation

In many text books and research papers it is possible to find general remarks for Finite Difference Method (FDM). For this reason, a brief explanation for the purpose of general understanding will be considered in this section. One of the first step to be taken in establishing a finite-difference procedure for solving a PDE is to replace the continuous problem domain by a finite-difference procedure by solving a Partial Difference Equations (PDE) for which  $f(x, y)$  is the dependent variable. In the square domain  $0 \leq x \leq 1$ ,  $0 \leq y \leq 1$  discrete point representation replaces the continuous field variable  $f(x, y)$  by  $f(i\Delta x, j\Delta y)$ . Points can be located according to the values of  $i$  and  $j$  difference equations which are written in terms of general points  $(i, j)$  and its neighbouring points. This labeling is illustrated in Figure 3.1.

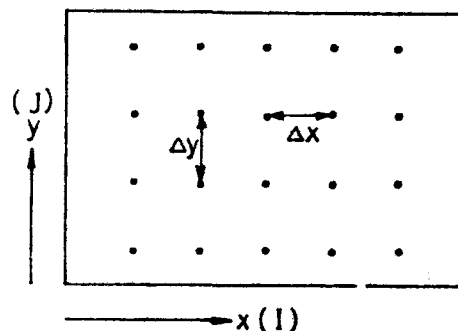


Figure 3.1) Finite difference grid.

If  $f(x_0, y_0)$  replaces  $f(i, j)$ , then the following definitions can be deduced;

$$\begin{aligned} f(i+1, j) &= f(x_0 + \Delta x, y_0) & f(i, j+1) &= f(x_0, y_0 + \Delta y) \\ f(i-1, j) &= f(x_0 - \Delta x, y_0) & f(i, j-1) &= f(x_0, y_0 - \Delta y) \end{aligned}$$

Often in the solution of the time dependent marching problems, the variation of the marching coordinate is indicated by a superscript, such as  $f^{n+1}(i, j)$ . Many different finite-difference representations are possible for any given PDE and it is usually impossible to establish a best form on absolute basis. The accuracy of a finite difference scheme may depend on the exact form of the equation and the problem being solved. And secondly, on the selection of a best “scheme” which will be influenced by the aspect of the procedure which are being optimized, i.e. accuracy, economy, programing simplicity.

The idea of a finite-difference representation for a derivative can be introduced by recalling the definition of derivative for the function  $f(x, y)$  at  $x = x_0$ ,  $y = y_0$ , i.e.,

$$\frac{\partial f(x, y)}{\partial x} = \lim_{\Delta x \rightarrow 0} \frac{f(x_0 + \Delta x, y_0) - f(x_0, y_0)}{\Delta x} \quad (3.1)$$

Here, if  $f$  is continuous, it is expected that  $[f(x_0 + \Delta x, y_0) - f(x_0, y_0)]/\Delta x$  will be a ‘reasonable’ approximate to  $\partial f/\partial x$  for a “sufficiently” small but finite  $\Delta x$ . But the main value theorem assures that the difference representation is exact for some points within a  $\Delta x$  interval. There are various ways of generating finite difference approximations [23]. These approaches are;

- a) Taylor series approach
- b) Polynomial approach
- c) Integral method approach
- d) Control volume approach

Using these four different approaches it is possible to obtain exactly the same finite-difference representation. These techniques are briefly reviewed in the following sections.

### 3.2.1 Taylor Series Approach

A Taylor series expansion approach to develop a difference approximation for  $df/dx(i, j)$  having a truncation error of  $O(dx)^2$  will be described in this section by using at most values  $f(i-2, j)$ ,  $f(i-1, j)$  and  $f(i, j)$ . It would be logical to write Taylor series expressions for the point  $f(i-2, j)$  and  $f(i-1, j)$  expanding about the point  $(i, j)$  and attempt to solve for  $df/dx(i, j)$  from the resulting equations in such a way as to obtain a truncation error of  $O(dx)^2$ . Hence,

$$f(i-1, j) = f(i, j) + \left. \frac{\partial f}{\partial x} \right|_{(i, j)} (-\Delta x) + \left. \frac{\partial^2 f}{\partial x^2} \right|_{(i, j)} \frac{(\Delta x)^2}{2!} + \left. \frac{\partial^3 f}{\partial x^3} \right|_{(i, j)} \frac{(-\Delta x)^3}{3!} + \dots \quad (3.2)$$

$$f(i-2, j) = f(i, j) + \frac{\partial f}{\partial x} \Big|_{(i,j)} (-2\Delta x) + \frac{\partial^2 f}{\partial x^2} \Big|_{(i,j)} \frac{(2\Delta x)^2}{2!} + \frac{\partial^3 f}{\partial x^3} \Big|_{(i,j)} \frac{(-2\Delta x)^3}{3!} + \dots \quad (3.3)$$

Using the above expansions, it is possible to get the value of  $\frac{\partial f}{\partial x} \Big|_{(i,j)}$ .

Hence,

$$\frac{\partial f}{\partial x} \Big|_{(i,j)} = \frac{\partial^2 f}{\partial x^2} \Delta x - \frac{f(i-2, j)}{2\Delta x} + \frac{f(i, j)}{2\Delta x} + O(\Delta x)^2 \quad (3.4)$$

writing more explicitly and using the definition for  $\frac{\partial^2 f}{\partial x^2}$  which will be given later hence,

$$\frac{\partial f}{\partial x} \Big|_{(i,j)} = \frac{f(i-2, j) - 4f(i-1, j) + 3f(i, j)}{(2\Delta x)} + O(\Delta x^2) \quad (3.5)$$

A careful check on the details of the above derivation reveals that it was really necessary to include terms involving  $\frac{\partial^3 f}{\partial x^3} \Big|_{(i,j)}$  in the Taylor-series expansions in order to determine whether or not these terms would cancel in the algebraic operations and reduce the truncation error even further to  $O(dx^3)$ .

### 3.2.2 Polynomial Approach

Using polynomial approach, it is also possible to develop a finite difference formulation in fluid mechanics and heat transfer problem. It is easy to notice that arbitrary decisions are need to be made in the process of polynomial fitting which will influence the form truncation error of the result. Particularly, these decisions influence the choice of points in the finite difference expressions. It is also possible to see that there is nothing unique about the procedure of polynomial approach which guaranties that the difference approximation for the PDE is the best in any sense or that numerical scheme is stable [23].

### 3.2.3 Integral Method Approach

Integral method approach is one of the other ways of producing a difference approximation to PDE's. The use of this approach will be illustrated with an example below.

Consider the equation,

$$\frac{\partial f}{\partial t} = a \frac{\partial^2 f}{\partial x^2} \quad (3.6)$$

The strategy is to develop an algebraic relationship among the  $f$ 's at neighboring grid points by integrating above equation with respect to the independent variables  $t$  and  $x$  over the local neighborhood of point  $(m, n)$ . The point  $(m, n)$  will also be identified as a point  $(t_o, x_o)$ . Grid points are spaced at intervals of  $\Delta x$  and  $\Delta t$ . An arbitrary integration on both side of the equation (3.6) over the interval  $t_o$  to  $t_o + \Delta t$  and  $x_o - \Delta x/2$  to  $t_o + \Delta t/2$  would lead to an inherently unstable difference



equation.

Hence, it is not obvious which of the above choices for the integration interval would be the right for the efficient stability of the solution method. Using the advantage of exact differentials the following formulation is obtained.

$$\int_{x_o - \Delta x/2}^{x_o + \Delta x/2} \left( \int_{t_o}^{t_o + \Delta t} \frac{\partial f}{\partial t} dt \right) dx = a \int_{t_o}^{t_o + \Delta t} \left( \int_{x_o - \Delta x/2}^{x_o + \Delta x/2} \frac{\partial^2 f}{\partial x^2} dx \right) dt \quad (3.7)$$

Further using the Mean-Value Theorem [23] simplify the equation within the intervals of integration;

$$[f(t_o + \Delta t, x_o) - f(t_o, x_o)] \Delta x = a \left[ \frac{\partial f}{\partial x}(t_o + \Delta t, x_o + \Delta x/2) - \frac{\partial f}{\partial x}(t_o + \Delta t, x_o - \Delta x/2) \right] \Delta t \quad (3.8)$$

Hence;

$$\frac{\partial f}{\partial x}(t_o + \Delta t, x_o + \Delta x/2) \cong \frac{f(t_o + \Delta t, x_o + \Delta x) - f(t_o + \Delta t, x_o)}{\Delta x} \quad (3.9)$$

after doing necessary rearrangings and using n for time, m for space variables one obtains the following form;

$$\frac{f_m^{n+1} - f_m^n}{\Delta t} = \frac{a}{(\Delta x)^2} (f_{m-1}^{n+1} - 2f_m^{n+1} + f_{m+1}^{n+1}) \quad (3.10)$$

### 3.2.4 Control Volume Approach

For Integral Methods and Taylor-Series expansions the assumptions made that the PDE as the correct and appropriate form of the conservation principle governing the physical problem and only turned the mathematical tools to develop algebraic approximations to derivatives. One never considered again the physical

law represented by the proceed in a rather formal, mechanical way operation on the PDE.

The discrete nature of a finite difference model must be recognized at the outset. Now, one proceeds to work out a mathematical statement of the physical conservation principle. The following steps somewhat reminiscent of procedure used some to derive PDE's from physical laws except that one should not take the limit of shrinking to control volume to a point. After putting PDE's into a divergence form one can use this process by employing the Gauss divergence theorem.

Practically, control volume approach brings out more accurate solution, especially on the boundaries. However, in the control volume approach one is forced to observe that there is some material associated with the boundary. The field variable balance on the control volume would account for possible transfer accross all boundaries.

Therefore, one would not know how to respond to a request to develop a difference representation of the derivatives along the boundaries. The discrete nature of the problem is always taken into account in the control volume approach which implies that the physical law satisfied over a finite region rather than only at a point as the mesh dimensions approach zero.

As it is seen clearly that the difference equations developed by the control volume approach would almost certainly have the conservative property.

Now, if one tries to put out a comparison between Taylor-series and control volume approach, one should note that the Taylor-series method readily provided difference approximations to derivatives and the representation for the complete PDE was made up from the addition of several such representations. However, the control volume approach employs the conservation statement or physical law represented by the entire PDE and appear insufficient of providing a finite difference representation just to a derivative alone.

Without having a large number of examples in hand, it is difficult to say which method or approach is the best to get out subtle differences. Probably for many simple cases the resulting difference equation derived from four different approaches can be identical. Shortly, no guarantee that difference equations developed by any of the methods will be numerically stable.

After these critical but brief review on finite difference formulae, Taylor series expansion method will be utilized on this work. The difference approximation can be put on a formal basis through the use of either a Taylor-Series expansion or Taylor's formula with remainder.

Developing a Taylor series expansion for  $f(x_0 + \Delta x, y_0)$  about  $(x_0, y_0)$  gives:

$$\begin{aligned}
 f(x_0 + \Delta x, y_0) = & f(x_0, y_0) + \frac{\partial f}{\partial x} \Big|_{(x_0, y_0)} \Delta x + \frac{\partial^2 f}{\partial x^2} \Big|_{(x_0, y_0)} \frac{(\Delta x)^2}{2!} + \frac{\partial^3 f}{\partial x^3} \Big|_{(x_0, y_0)} \frac{(\Delta x)^3}{3!} + \dots \\
 & + \frac{\partial^{n-1} f}{\partial x^{n-1}} \Big|_{(x_0, y_0)} \frac{(\Delta x)^{n-1}}{(n-1)!} + \frac{\partial^n f}{\partial x^n} \Big|_{(x_0, y_0)} \frac{(\Delta x)^n}{n!}
 \end{aligned} \tag{3.11}$$

$$x_0 \leq \varepsilon < (x_0 + \Delta x) \tag{3.12}$$

In the expansion the last term can be identified as the remainder. Thus "forward" difference form can be formed by rearranging general expansion.

$$\frac{\partial f}{\partial x} \Big|_{(x_0, y_0)} = \frac{f(x_0 + \Delta x, y_0) - f(x_0, y_0)}{\Delta x} - \frac{\partial^2 f}{\partial x^2} \Big|_{(x_0, y_0)} \frac{\Delta x}{2!} \dots \tag{3.13}$$

Changing the notation  $(x_0, y_0)$  into  $(i, j)$  for the sake of generality, the following form is obtained;

$$\frac{\partial f}{\partial x} \Big|_{(i, j)} = \frac{f(i+1, j) - f(i, j)}{\Delta x} + \text{Truncation error} \tag{3.14}$$

The truncation error is the difference between the partial derivative and its finite difference representation. One can characterize the limiting behaviour of the truncation error (T.E) by using the order of ( $O$ ) notation. Hence;

$$\left. \frac{\partial f}{\partial x} \right|_{(i,j)} = \frac{f(i+1,j) - f(i,j)}{\Delta x} + O(\Delta x) \quad (3.15)$$

$$f(x_0 - \Delta x, y_0) = f(x_0, y_0) - \left. \frac{\partial f}{\partial x} \right|_{(x_0, y_0)} \Delta x + \frac{\partial^2 f}{\partial x^2} \bigg|_{(x_0, y_0)} \frac{(\Delta x)^2}{2!} - \frac{\partial^3 f}{\partial x^3} \bigg|_{(x_0, y_0)} \frac{(\Delta x)^3}{3!} + \dots \quad (3.16)$$

and obtain the "backward" difference representation

$$\left. \frac{\partial f}{\partial x} \right|_{(i,j)} = \frac{f(i,j) - f(i-1,j)}{\Delta x} + O(\Delta x) \quad (3.17)$$

Take difference between the forward and the backward, one gets central difference formulae

$$\left. \frac{\partial f}{\partial x} \right|_{(i,j)} = \frac{f(i+1,j) - f(i-1,j)}{2\Delta x} + O(\Delta x)^2 \quad (3.18)$$

In the same manner adding the forward difference expansion to the backward difference expansion, second order derivative is presented,

$$\left. \frac{\partial^2 f}{\partial x^2} \right|_{(i,j)} = \frac{f(i+1,j) - 2f(i,j) + f(i-1,j)}{\Delta x^2} + O(\Delta x)^2 \quad (3.19)$$

## CHAPTER 4

### PHYSICAL PROBLEM

#### 4.1 Models

##### 4.1.1 Physical Model

So far we have developed flow field and thermal field to solve them individually or together for a conjugate problem in which fluid and solid were considered simultaneously. If we turn our attention to literature whether or not we find out a real physical system in which our approached and developed formulas can easily be applied. So, we have chosen the physical model and the physical system which were used for the experimental study by HaCohen [1].

In this experimental study the physical model was 4x4 array of heated aluminium blocks mounted or embedded in a wood base. The dimensions of the blocks were 34x34 square with varying, but equal array heights. The spacing between the array components was 14 both in the longitudinal and transversal directions. The channel height was allowed to vary. It is understood that if it is used a compu-

tational model, in a nondimensionalized form it would be able to keep immediately all changibility in a real given physical model.

The geometry and the materials, which are used in this physical system, can be depicted in Figure 4.1a and 4.1b

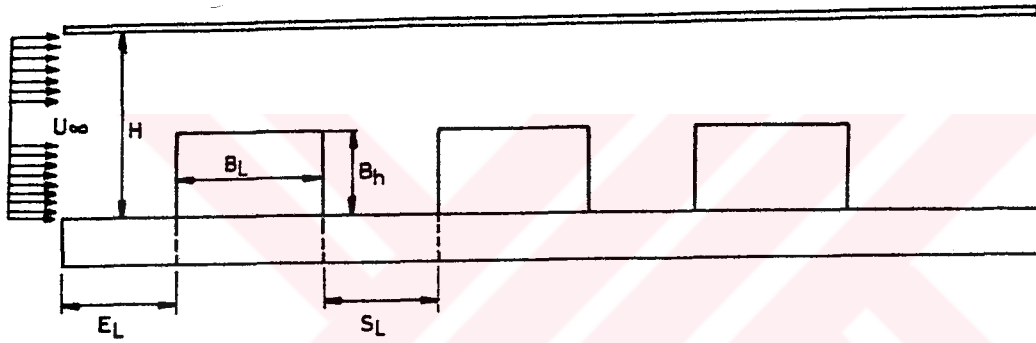


Figure 4.1a) Side view of used geometry

We solved the flow field making all dimensions as a ratio of channel height. Some ratios are important in the physical behavior of the flow field. The ratio of channel height to component height,  $H/B_h$ , characterizes the friction of the total flow around a component which affects the heat transfer.  $S_L/B_L$  characterizes the flow disturbance due to the interaction of: outer flow with cavity flow between two neighbouring components.  $S_L/B_L$  is dealing with the separation reattachment and redevelopment of boundary layer flows on individual components. The ratio  $S_T/B_T$  explains the amount of channelization which occurs between columns of components and therefore the three-dimensionality of the flow. Above given parameters in the range



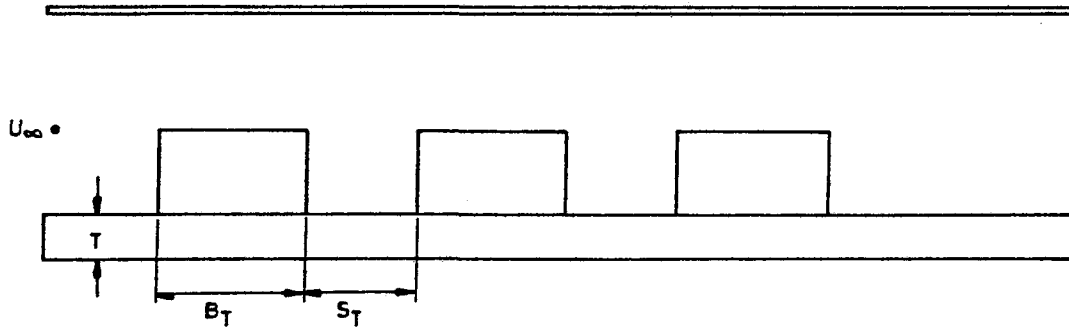


Figure 4.1b) Front view of the used geometry

$$\begin{aligned}
 0.2 &< B_h/H < 1 \\
 0.25 &< S_L/B_h < 12 \\
 0.083 &< S_L/B_L < 0
 \end{aligned}$$

These ranges are the common ones which cover most of the actual board component packing densities currently in use. In most of the studies and experiments substrates can be made of ceramic copper or plywood. Chips mostly can be made of aluminum or silicon and some alloys of both. As a criteria in the design stage the upper ceiling of the populated chips for the junction temperature is set from failure rate data taken in the field and from high temperature acceleration testing. For the new chip design or a package, the experience in field operation produces a learning factor which enhances the predictability of physical effects of using materials for having the successful construction are becoming more important.

#### 4.1.2 Flow Model

The considered channel is populated with obstacles and posing a cooling fluid on them. And it is narrow enough when its height is compared to its length and obstacles' geometries are regular in squares or rectangles and top of the channel is closed which means we are dealing with internal flow. At the entrance flow sent into the channel impulsively.

#### 4.1.3 Thermal Model

The computer code developed for internal flows mentioned above is also capable to solve entire thermal field for such geometries with various boundary conditions. At the entrance flow sent into obstacle-populated channel with the nondimensional temperature which is equal to zero. The heat sources which are placed into obstacles at various height from the substrate. The top and bottom of the channel walls are held at constant temperatures.

#### 4.1.4 The Implicit Numerical Solution Method

Some form of an iteration procedure has to be used in order to solve the set of linear finite difference algebraic equations that results from the discretization of Navier-Stokes equations and the energy equation [28]. These are :

- a) the point iteration / explicit methods.
- b) the line iteration / implicit methods.

The goal of the present study is to set up an iterative solution procedure which be classified under the category of general implicit methods for solving the algebraic equations arising from the stream function  $\psi$ -vorticity  $\omega$  formulation of Navier Stokes equations and the energy equation.

Generally implicit methods appear to be much more stable and faster than the explicit methods. Implicit methods are line methods. The field variables in the implicit methods are solved implicitly along lines. Alternating Direction Implicit (ADI) techniques involve rows and columns operation while the Modified Strongly Implicit (MSI) methods involve diagonal lines. These lines are named as "implicit lines" [29]. The field variables are solved in a coupled manner along the implicit line. Hence, the effect of boundary conditions are felt immediately in the field. Implicit line runs between two boundary points and all the equations along this line are coupled. Implicit methods are formulated by defining spatial ordering among the grid points in physical domain. This ordering creates the structure of the implicit lines and finally the system of equations to be solved. The final system of equations can be solved by efficient block tri-diagonal or penta-diagonal solvers such as the generalized Thomas algorithm [23].

Lin [29] discusses the nature of general implicit lines. Furthermore he comments on the optimization of general implicit lines by choosing cut-off points as the grid points where the convection is much smaller than the diffusion. In most of the cases, the grid points near a solid boundary are the cut-off points of the general implicit lines.

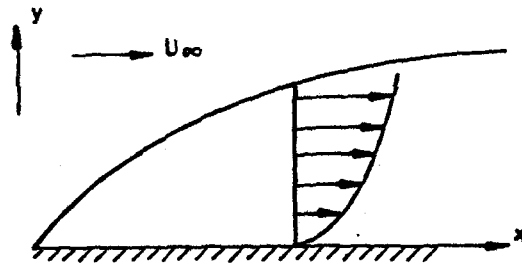
The application of implicit methods for the solution of boundary layer like

flows involves general implicit lines which are normal to the flow direction. Hence, general implicit procedure resembles marching technique for a boundary layer. Figure 4.2a shows a boundary layer like flow. Usually such kind of flows are solved by marching techniques along  $x$  in which  $u$  and  $v$  velocities are solved implicitly along the transverse direction  $y$ . Figure 4.2b shows the computational domain with the essentials of grid points. Implicit lines are drawn by joining the point  $(i, j)$  with one of the next points  $(i, j + 1)$ ,  $(i, j - 1)$ ,  $(i, j + 1)$  or  $(i, j - 1)$ . Finally, Figure 4.2c shows the structure of the implicit lines which represent the basics of the standart marching procedure.

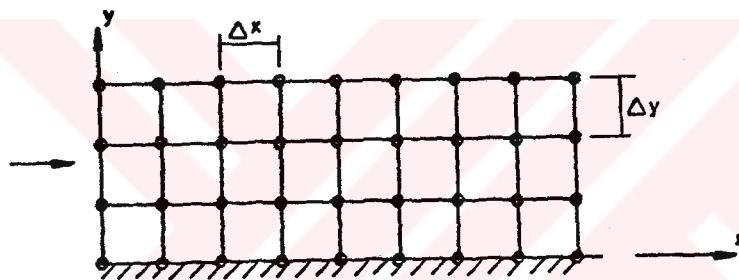
Depending on the nature of the flow physics it is possible to arrange various other optimum general implicit lines [29]. Lin has made a survey on various implicit line structure for many fluid problems including the flow over a backward facing step [29].

In the present study, general implicit line method which involves implicit line construction similar to Figure 4.2c was employed. The resulting finite difference algebraic equations are solved by a fast Thomas algorithm.

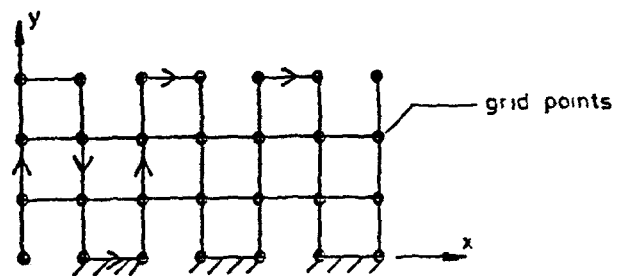
In this section, the discretization of the governing equations will be presented. First, the final form of the governing momentum equations of flow and thermal field will be reviewed. The boundary and initial condition will be described in details next. Finally, the solution method will be presented ready to be implemented as a solution algorithm.



4.2a A boundary-layer-like flow



4.2b Computational domain for the boundary-layer flow



4.2c Generation of implicit line algorithm.

#### 4.1.4.1 Governing Equations for Flow Field

An impulsively generated flow of an incompressible, laminar, 2-D flow develops between parallel plates of a channel with and without rectangular blocks over the lower plate. Steady state flow field is the primary interest of the modelling.

The differential equations which govern unsteady, incompressible, viscous two-dimensional flow field are stated in their non-dimensional form as;

$$\nabla^2 \psi = -\omega \quad (4.1)$$

$$\frac{\partial \omega}{\partial t} + U \frac{\partial \omega}{\partial x} + V \frac{\partial \omega}{\partial y} = \frac{1}{Re} \left( \frac{\partial^2 \omega}{\partial x^2} + \frac{\partial^2 \omega}{\partial y^2} \right) \quad (4.2)$$

where non-dimensional quantities are represented by

$$Re = \frac{U_\infty 2H}{\nu}, \quad U = \frac{U}{U_\infty}, \quad V = \frac{V}{U_\infty}, \quad x = \frac{X}{2H}, \quad y = \frac{Y}{2H}, \quad t = \frac{\tilde{t} U_\infty}{2H} \quad (4.3)$$

Equations 4.1 and 4.2 will be solved simultaneously under the boundary conditions which will be described in the next section.

#### 4.1.4.2 Governing Equations for Thermal Filed

Physical domain which was described at the opening section of this chapter involves generation of heat in rectangular blocks. This heat is conducted in the solid portion and then convected through the walls to the flow. Energy equation for the flow domain in a non-dimensional form will be

$$\frac{\partial \theta}{\partial t} + U \frac{\partial \theta}{\partial x} + V \frac{\partial \theta}{\partial y} = \frac{1}{RePr} \left( \frac{\partial^2 \theta}{\partial x^2} + \frac{\partial^2 \theta}{\partial y^2} \right) + \frac{Ec}{Re} \Phi + Q \quad (4.4)$$

Where,

$\Phi$  = Nondimensionanlized Viscous heat dissipation term.

$Q$  =Nondimensionlized Uniform heat source term.

$$\theta = \frac{(T - T_{in})}{(T_{w,u} - T_{in})} \quad (4.5a)$$

$$Pr = \alpha / \nu \quad (4.5b)$$

$$Ec = \frac{U_{\infty}^2}{c(T_w - T_{in})} \quad (4.5c)$$

## 4.2 Boundary Conditions

In this section detailed boundary conditions which complete the definition of the flow and thermal field variables in the physical domain will be presented. Physical domain is presented in Figure 4.3. Geometry of the problem consists of two separate regions; fluid and solid. Moreover solid domain has two different solid regions with different thermal properties. Bottom part, substrate, has a low thermal conductivity in comparison with the block material where heat sources are embedded at various optional elevations from the substrate top surface in the form of an infinitesimal sheets with no thickness.

In many analytical and numerical studies of the past, usually the heat transfer problem was solved by considerations of only the fluid region and by specifying the boundary conditions directly at the solid-fluid interface. Although finite, thin and high thermal conductivity allows to the such kind of a procedure, this is not correct for low thermal conductivity walls. This implies that, the temperature distribution in the wall and the fluid must be solved simultaneously. This analysis is called conjugate formulation and the problem is called a conjugate problem. Luikov et.al [30] and Mari et.al [31] applied this technique to solve heat transfer to flow in circular tubes. More recently Bayazıtıoğlu [32] and F. P. Incropera et.al [33] applied this approach to study the heat transfer between parallel plates similar approach is utilized in the present study.



Due to the nature of the problem two different kinds of boundary conditions will be considered; Dirichlet type boundary conditions and the Neuman type boundary conditions. Flow field boundary condition will be a classical condition over the solid surfaces, thus involving no slip properties. Exit and inlet flow conditions will be the conditions of the fully developed and uniform flow conditions respectively. Thermal field involves either prescribed or flux conditions. Although there involves other options only the results for a limited amount of conditions will be presented in this study. However, it is worth noting that the solution algorithm is capable of modeling various thermal boundary options which can be chosen interactively by the user.

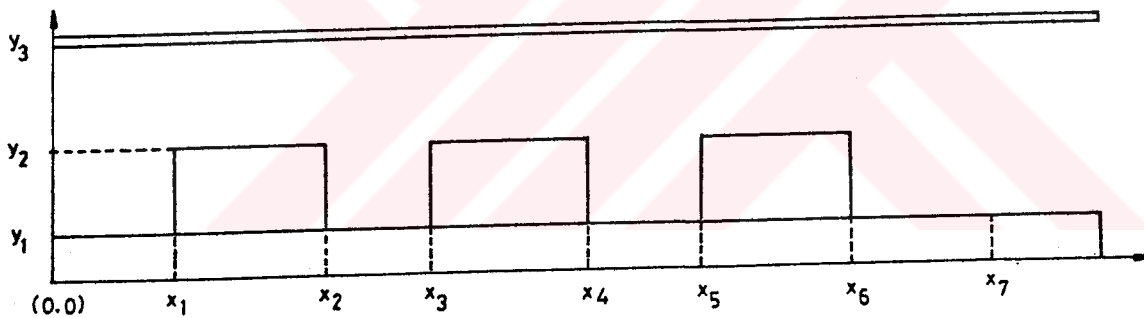


Figure 4.3) Geometry of the flow between parallel plates with rectangular obstacles attached to the lower wall.

#### 4.2.1 Boundary Conditions for Fluid and Heat Transfer

##### Equations

In this section, boundary conditions for both the flow field and thermal field will be presented. Problem variables are  $\psi$ ,  $\omega$  and  $\theta$

Inlet conditions;

$$\begin{aligned}
 x = 0 \quad 0 \leq y \leq y_1, \quad U = V = \omega = \theta = 0 \quad \psi = 0 \\
 y_1 < y \leq y_3, \quad U = 1, V = \omega = \theta = 0 \quad \psi = \Delta y \quad \text{constant.} \\
 \text{wall conditions;} \\
 x = x_1 \quad y_1 \leq y \leq y_2, \quad U = V = 0, \omega = f_1(\psi) \quad \psi = \text{constant} \\
 -k_f \frac{\partial \theta}{\partial x} = -k_b \frac{\partial \theta}{\partial x} \quad (4.6a)
 \end{aligned}$$

$f_1$  function will be described in chapter 5.

$$\begin{aligned}
 x = x_2 \quad y_1 \leq y \leq y_2, \quad U = V = 0, \omega = f_2(\psi) \quad \psi = \text{constant,} \\
 -k_f \frac{\partial \theta}{\partial x} = -k_b \frac{\partial \theta}{\partial x} \quad (4.6b)
 \end{aligned}$$

$f_2$  function will be described in chapter 5.

Similar type of boundary condition will be applied for the  $x$ -stations at  $x_3, x_4, x_5, x_6$  respectively.

Boundary conditions at constant transverse locations will be described below;

$$\begin{aligned}
 y = 0 \\
 0 \leq x < x_7 \quad U = V = \omega = \psi = 0, \theta = \text{constant} \\
 y = y_1 \\
 0 \leq x \leq x_1 \quad U = 0 = V, \omega = f_2(\psi), \psi = \text{constant} \\
 -k_s \frac{\partial \theta}{\partial y} = -k_f \frac{\partial \theta}{\partial y} \quad (4.7a)
 \end{aligned}$$

$$\begin{aligned}
 x_2 \leq x \leq x_3 \quad U = V = 0, \omega = f_2(\psi), \psi = \text{constant}, \\
 -k_s \frac{\partial \theta}{\partial y} = -k_f \frac{\partial \theta}{\partial y} \quad (4.7b)
 \end{aligned}$$

$$\begin{aligned}
 x_1 < x < x_2 \quad U = V = \omega = \psi = 0, \\
 -k_s \frac{\partial \theta}{\partial y} = -k_b \frac{\partial \theta}{\partial y} \quad (4.7c)
 \end{aligned}$$

$$\begin{aligned}
 y = y_2 \quad x_1 < x < x_2 \quad U = V = 0, \psi = \text{constant}, \omega = f_2(\psi) \\
 -k_b \frac{\partial \theta}{\partial y} = -k_f \frac{\partial \theta}{\partial y} \quad (4.7d)
 \end{aligned}$$

$$y = y_3 \quad 0 \leq x \leq x_7 \quad U = V = 0, \psi = \text{constant}, \omega = f_3(\psi), \theta = \theta_\omega$$

Similar types of boundary conditions will be applied for the other  $x$ -station in the channel.

Exit conditions;

$$x = x_7 \quad 0 < y \leq y_1, U = V = w = \psi = 0, \frac{\partial \theta}{\partial x} = 0 \quad (4.8a)$$

$$x = x_7 \quad y_1 < y < y_3, \frac{\partial U}{\partial x} = \frac{\partial V}{\partial x} = \frac{\partial \omega}{\partial x} = \frac{\partial \theta}{\partial x} = 0 \quad (4.8b)$$

Solution algorithm involves various other boundary conditions for the temperature field. Since only the results for the pure convective heat transfer cases

will be presented in this work, other possible thermal conditions will be discussed very briefly are of these possible conditions which involves the definition of insulated lower channel walls at  $y = y_1$  for  $0 < x < x_1$  and  $x_2 < x < x_3$ . Secondly, during the initial phases of the solution code validation, prescribed wall temperature condition was also considered.

#### Initial conditions;

a) For flow field:

at the entry plane

$$U = u_{\infty} = 1$$

$$V = 0$$

$$\psi = \Delta y \star constant$$

$$\omega = 0$$

at the exit plane  $\frac{\partial U}{\partial x} = \frac{\partial V}{\partial x} = \frac{\partial \omega}{\partial x} = 0$

b) For thermal field;

at the entry plane  $\theta = \frac{(T - T_{in})}{(T_{w,u} - T_{in})} = 0$

at the exit plane  $\frac{\partial \theta}{\partial x} = 0$

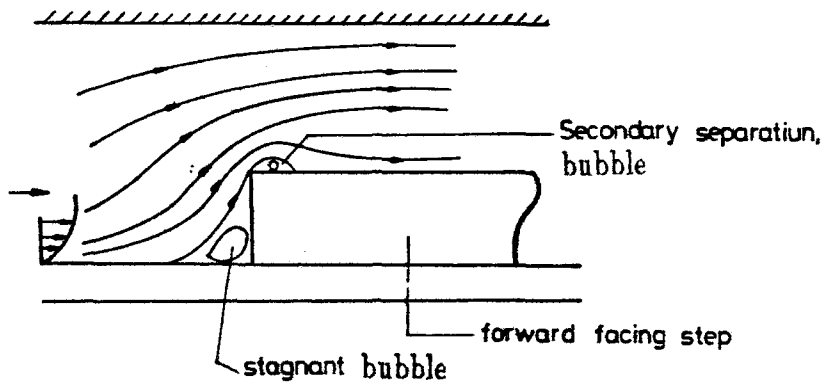
#### 4.3 Directional Implicit Finite Difference Formulation and The Solution

Steady state flow field of the problem under investigation involves four basic flow regimes;

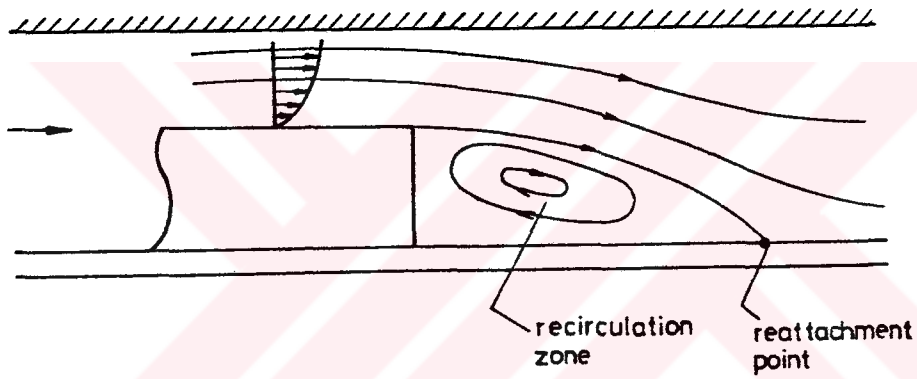
- a) flow over forward facing steps
- b) flow over backward facing blocks
- c) cavity type flow between the blocks
- d) boundary layer like flow both near the top channel wall and over the block surfaces.

Figure 4.4 shows four possible types of flow structure involved in a flow field in a channel with rectangular block and their governing equations

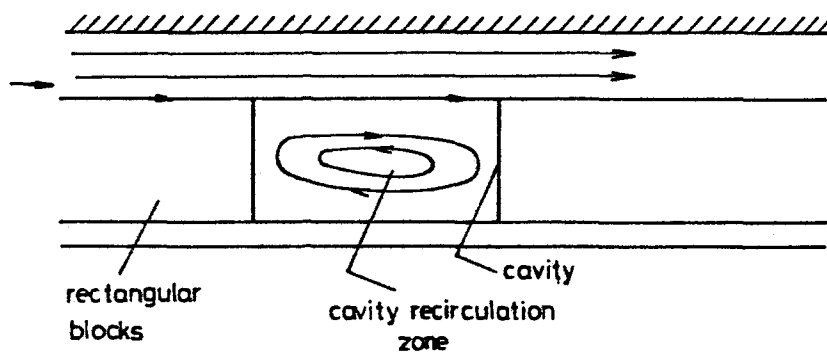
The basic essentials of these four types of flow to be predicted by the present finite difference algorithm. There is a vast amount of literature in all of these types of flows [34-39]. It is well known that flows over forward and backward facing steps are very sensitive to the proposed finite difference algorithms [21]. The goal of the present work is to generate a common algorithm so as to simulate all of these basic



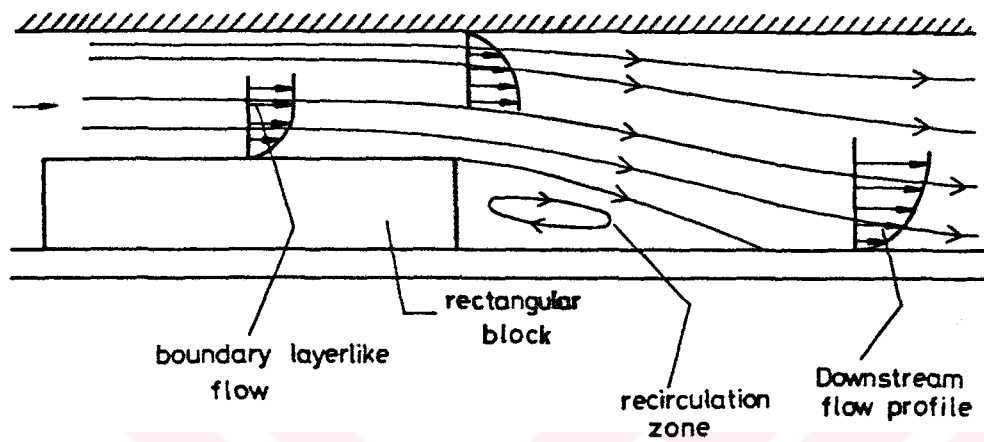
4.4a) Forward facing step



4.4b) Backward facing step



4.4c) Cavity type flow



4.4 d) Boundary layer like flow

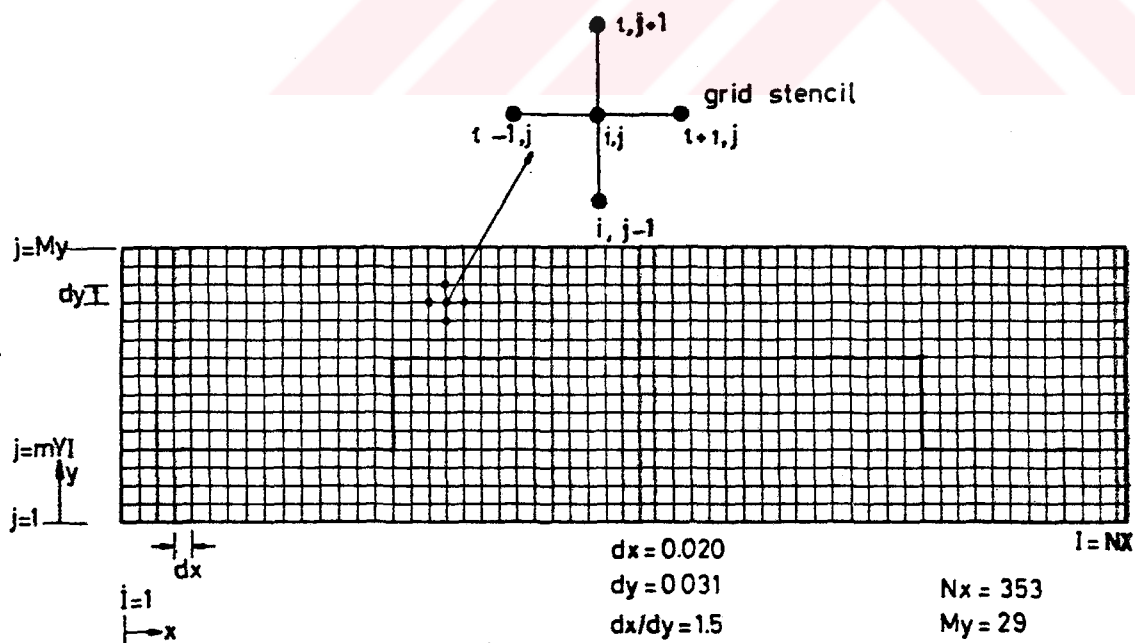


Figure 4.5 Grid Network

regimes. So a reader should judge the efficiency of the proposed method of solution with some reservations. Results will be compared with the available data.

Equations that will be solved simultaneously are presented below;

$$\nabla^2 \psi = -\omega \quad (4.9)$$

$$\frac{D\omega}{Dt} = \frac{1}{Re} \nabla^2 \omega \quad (4.10)$$

or more explicitly,

$$\frac{\partial^2 \psi}{\partial x^2} + \frac{\partial^2 \psi}{\partial y^2} = -\omega \quad (4.11)$$

$$\frac{\partial \omega}{\partial t} + U \frac{\partial \omega}{\partial x} + V \frac{\partial \omega}{\partial y} = \frac{1}{Re} \left( \frac{\partial^2 \omega}{\partial x^2} + \frac{\partial^2 \omega}{\partial y^2} \right) \quad (4.12)$$

Equation (4.12) involves convective and diffusion terms. These terms will be discretized in time and spatial coordinates. Equations will be directly approximated in the physical plane so there is no need to the successive plane transformation. Due to the nature of the boundaries it is relatively easy to generate a grid network.



$dy = (1/48)$  hence  $dx/dy = 1.5$  combination yields the best stable steady results ready to be compared with the available literature data. Total domain consist of  $NX \times NY = 353 \times 29 = 10273$  grid points. Discretized field equations involve the variables at time  $t$  and  $t + \Delta t$  where the expressions  $()^n$  and  $()^{n+1}$  denote the value of variables at  $t$  and  $t + \Delta t$  respectively. Unsteady term was be approximated by an upwind formulation.

#### 4.3.1 Flow Equations

Second order accurate central differencing applied to the terms of Eq. 4.8 yields the following approximate equation;

$$\nabla^2 \psi = \frac{\psi^{n+1}(i+1, j) - 2\psi^{n+1}(i, j) + \psi^{n+1}(i-1, j)}{(\Delta x)^2} +$$

$$\frac{\psi^{n+1}(i, j+1) - 2\psi^{n+1}(i, j) + \psi^{n+1}(i, j-1)}{(\Delta y)^2} = -\omega^n(i, j) \quad (4.13a)$$

Although the stream function values are implicit in time, the right hand side of the equation (4.10a) involves explicit variables for the vorticity value at the grids. The discretization of the vorticity transport equation term will be as follows;

unsteady term;

$$\frac{\partial \omega}{\partial t} = \frac{\omega^{n+1}(i, j) - \omega^n(i, j)}{\Delta t} \quad (4.13b)$$

Convective terms are linearized in time. Streamwise convective term will be approximated by a backward differencing. On the other hand transverse convective term will be approximated by central differencing which is a second order accurate discretization. Lin [29] discussed various approaches for the approximations of these linearized terms.

Final form for the convective terms will be as follows;

$$U \frac{\partial \omega}{\partial x} = u^n \left[ \frac{\omega^{n+1}(i, j) - \omega^{n+1}(i-1, j)}{\Delta x} \right] \quad (4.14)$$

$$V \frac{\partial \omega}{\partial y} = v^n \left[ \frac{\omega^{n+1}(i, j+1) - \omega^{n+1}(i, j-1)}{2\Delta y} \right] \quad (4.15)$$

Terms representing the diffusion of the vorticity are approximated by a second-order central differencing formula as follows;

Final form for the viscous terms will be as follows:

$$\frac{1}{Re} \frac{\partial^2 \omega}{\partial x^2} = \frac{1}{Re} \left[ \frac{\omega^{n+1}(i+1, j) - 2\omega^{n+1}(i, j) + \omega^{n+1}(i-1, j)}{(\Delta x)^2} \right] \quad (4.16)$$

$$\frac{1}{Re} \frac{\partial^2 \omega}{\partial y^2} = \frac{1}{Re} \left[ \frac{\omega^{n+1}(i, j+1) - 2\omega^{n+1}(i, j) + \omega^{n+1}(i, j-1)}{(\Delta y)^2} \right] \quad (4.17)$$

Now, by combining equations 4.10 through 4.14 one approximates the equation 4.9. The relation between the values of  $\omega$  of  $t$  and  $t + \Delta t$  will be;

$$\omega^n(i, j) = \omega^{n+1}(i+1, j) \left[ -\frac{\Delta t}{Re(\Delta x)^2} \right] +$$

$$\omega^{n+1}(i-1, j) \left[ -\frac{\Delta t}{Re(\Delta x)^2} - \frac{u^n \Delta t}{\Delta x} \right] + \omega^{n+1}(i, j-1) \left[ -\frac{\Delta t}{Re(\Delta y)^2} - \frac{v^n \Delta t}{2\Delta y} \right] +$$

$$\omega^{n+1}(i, j+1) \left[ -\frac{\Delta t}{Re(\Delta y)^2} + \frac{v^n \Delta t}{2\Delta y} \right] + \omega^{n+1}(i, j) \left[ 1 + \frac{2\Delta t}{Re(\Delta x)^2} + \frac{2\Delta t}{Re(\Delta y)^2} + \frac{u^n \Delta t}{2\Delta x} \right] \quad (4.18)$$

thus

$$\omega^n(i, j) = A\omega^{n+1}(i+1, j) + B\omega^{n+1}(i-1, j) + C\omega^{n+1}(i, j-1)$$

$$+D\omega^{n+1}(i, j+1) + E\omega^{n+1}(i, j) \quad (4.19)$$

where

$$\begin{aligned} A &= \left[ -\frac{\Delta t}{Re(\Delta x)^2} \right] & B &= \left[ -\frac{\Delta t}{Re(\Delta x)^2} - \frac{u^n \Delta t}{\Delta x} \right] \\ C &= \left[ -\frac{\Delta t}{Re(\Delta y)^2} - \frac{v^n \Delta t}{2\Delta y} \right] & D &= \left[ -\frac{\Delta t}{Re(\Delta y)^2} + \frac{v^n \Delta t}{2\Delta y} \right] \\ E &= \left[ 1 + \frac{2\Delta t}{Re(\Delta x)^2} + \frac{2\Delta t}{Re(\Delta y)^2} + \frac{u^n \Delta t}{2\Delta x} \right] \end{aligned}$$

An implicit finite difference procedure where the channel is discretized into  $N \times N$  rectangular grids is used here to solve the equation.  $U^n, V^n, \psi^n, \omega^n, \theta^n$  and  $U^{n+1}, V^{n+1}, \psi^{n+1}, \omega^{n+1}, \theta^{n+1}$  are assumed to be the values of the variables at the  $t^n$  and  $t^{n+1}$  respectively. There exist several numerical solution techniques for solving two-dimensional elliptic vorticity-stream function equations. Generally, the values of  $\omega^{n+1}(i, j)$  are calculated by using the  $n$ th time step values. An implicit form of the nonlinear vorticity equation uses Central Differencing Scheme for the convective terms. Thoman and Szezewyk [40] used this method to investigate the unsteady fluid motion around a circular cylinder. This method is known as the Directional Difference Explicit Method (DDE). Gauss-Seidel iteration (GSI) is required to compute the stream functions iteratively. On the other hand, Strongly Implicit Procedure (SIP) proposed by Stone [41] uses a technique of matrix factorization elimination. The Alternating Directional Implicit (ADI) methods use half time implicit finite difference formulation in the direction of independent spatial coordinates [42]. Similarly to the DDE method, the values of  $\psi(i, j)$  at the  $n$ th time step are used to calculate the values of  $\omega(i, j)$  at  $n+1$ th time step with Successive Over-Relaxation (SOR) method. In all of the above techniques, the procedures

were repeated for the successive time-steps until steady state solutions were reached. Normally, with the above formulation a five point stencil forms and equations are solved by fully implicit methods. Hence, coefficients of equation 4.13a forms a five banded matrix as final algebraic equations. The solution of equation 4.13a coupled with the described version of equation 4.9 is known as a Strongly Implicit Solution Method SISM. SISM involves pentadiagonal matrix solvers which need large memory and CPU time [29,30]. The coefficients form five diagonal banded matrix. It is more practical to convert this matrix into a three banded tridiagonal matrix where there are very fast solution procedures.

Five banded matrix can be turned out into three-banded or tridiagonal matrix by choosing a small time step for integration and also by replacing  $n$ th values of any field variable on the coordinates  $i + 1$  and  $i - 1$  into the  $n + 1$ th values of the same field variable. This substitution reduces the order of the matrix and it can be solved much more faster than the strongly implicit form. Hence, the final form of the flow field equations will become;

$$\frac{\psi^n(i+1, j) - 2\psi^{n+1}(i, j) + \psi^n(i-1, j)}{(\Delta x)^2} + \frac{\psi^{n+1}(i, j+1) - 2\psi^{n+1}(i, j) + \psi^{n+1}(i, j-1)}{(\Delta y)^2} = -\omega^n(i, j) \quad (4.20)$$

Since the values of  $\psi^n(i+1, j)$  and  $\psi^n(i-1, j)$  become constant at a given time step, no longer one can consider them as variables. These terms are considered as knowns for the implicit solution. Hence, it becomes,

$$\begin{aligned} \psi^{n+1}(i, j) \left[ -\frac{2}{(\Delta x)^2} - \frac{2}{(\Delta y)^2} \right] + \psi^{n+1}(i, j+1) \left[ \frac{1}{(\Delta y)^2} \right] + \psi^{n+1}(i, j-1) \left[ \frac{1}{(\Delta y)^2} \right] = \\ -\omega^n(i, j) - \psi^n(i+1, j) \left[ \frac{1}{(\Delta x)^2} \right] - \psi^n(i-1, j) \left[ \frac{1}{(\Delta x)^2} \right] \end{aligned} \quad (4.21a)$$

Hence,

$$\begin{aligned} A\psi^{n+1}(i, j) + B\psi^{n+1}(i, j+1) + C\psi^{n+1}(i, j-1) = \\ -\omega^n(i, j) - D\psi^n(i+1, j) - E\psi^n(i-1, j) \end{aligned} \quad (4.21b)$$

where,

$$A = \left[ -\frac{2}{(\Delta x)^2} - \frac{2}{(\Delta y)^2} \right] \quad B = \left[ \frac{1}{(\Delta y)^2} \right]$$

$$C = \left[ \frac{1}{(\Delta y)^2} \right] \quad D = \left[ \frac{1}{(\Delta x)^2} \right]$$

$$E = \left[ \frac{1}{(\Delta x)^2} \right]$$

Vorticity transport equation takes the following finite difference form after employing the new discretization approach explained above;

$$\frac{\omega^{n+1}(i, j) - \omega^n(i, j)}{\Delta t} + u^n(i, j) \left[ \frac{\omega^{n+1}(i, j) - \omega^n(i, j)}{\Delta x} \right] +$$

$$v^n(i, j) \left[ \frac{\omega^{n+1}(i, j+1) - \omega^n(i, j-1)}{2\Delta y} \right] = \frac{1}{Re} \left[ \frac{\omega^n(i+1, j) - 2\omega^{n+1}(i, j) + \omega^n(i-1, j)}{(\Delta x)^2} + \right. \\ \left. \frac{\omega^{n+1}(i, j+1) - 2\omega^{n+1}(i, j) + \omega^{n+1}(i, j-1)}{(\Delta y)^2} \right] \quad (4.22)$$

or it can be expressed in the following form

$$\omega^{n+1}(i, j) \left[ \frac{1}{\Delta t} - \frac{u^n(i, j)}{\Delta x} - \frac{2}{Re} \left( \frac{1}{(\Delta x)^2} + \frac{1}{(\Delta y)^2} \right) \right] + \omega^{n+1}(i, j+1) \left[ \frac{v^n(i, j)}{2\Delta y} + \frac{1}{Re(\Delta y)^2} \right] +$$

$$\omega^{n+1}(i, j-1) \left[ -\frac{v^n(i, j)}{2\Delta y} + \frac{1}{Re(\Delta y)^2} \right] = \omega^n(i, j) \left[ \frac{1}{\Delta t} \right] +$$

$$\omega^n(i+1, j) \left[ \frac{1}{Re(\Delta x)^2} \right] + \omega^n(i-1, j) \left[ \frac{1}{Re(\Delta x)^2} \frac{u^n(i, j)}{\Delta x} \right] \quad (4.23a)$$

Hence,

$$A\omega^{n+1}(i, j) + B\omega^{n+1}(i, j+1) + C\omega^{n+1}(i, j-1) =$$

$$D\omega^n(i, j) + E\omega^n(i+1, j) + F\omega^n(i-1, j) \quad (4.23b)$$

where,

$$A = \left[ \frac{1}{\Delta t} - \frac{u^n(i, j)}{\Delta x} - \frac{2}{Re} \left( \frac{1}{(\Delta x)^2} + \frac{1}{(\Delta y)^2} \right) \right]$$

$$B = \left[ \frac{v^n(i, j)}{2\Delta y} + \frac{1}{Re(\Delta y)^2} \right] \quad C = \left[ -\frac{v^n(i, j)}{2\Delta y} + \frac{1}{Re(\Delta y)^2} \right]$$

$$D = \left[ \frac{1}{\Delta t} \right] \quad E = \left[ \frac{1}{Re(\Delta x)^2} \right]$$

$$F = \left[ \frac{1}{Re(\Delta x)^2} \frac{u^n(i, j)}{\Delta x} \right]$$

Right hand side of the equation is taken as constant at each time step.

Central differencing is applied for all the terms except for the convective term in the streamwise direction. The first order backward differencing which allows marching type solutions in the streamwise direction requires very fine mesh distribution in the x-direction. Boundary layer like flow structure of the present problem in various domains of the geometry will certainly involve marching like solutions with the information coming from backward differencing.



### 4.3.2 Energy Equation

By using the approach of section 4.3.1 the energy equation will be discretized in this section. The governing equation for the thermal field was;

$$\frac{\partial T}{\partial t} + u \frac{\partial T}{\partial x} + v \frac{\partial T}{\partial y} = \frac{1}{PrRe} \left( \frac{\partial^2 T}{\partial x^2} + \frac{\partial^2 T}{\partial y^2} \right) + \frac{E_c}{Re} \Phi + Q \quad (4.24)$$

where,

$$\Phi = 2 \left[ \left( \frac{\partial U}{\partial x} \right)^2 + \left( \frac{\partial V}{\partial y} \right)^2 \right] + \left( \frac{\partial V}{\partial x} + \frac{\partial U}{\partial y} \right)^2 \quad (4.25)$$

Similar types of discretization scheme yields;

$$\frac{T^{n+1}(i,j) - T^n(i,j)}{\Delta t} + u^n(i,j) \left[ \frac{T^{n+1}(i,j) - T^n(i-1,j)}{\Delta x} \right] +$$

$$v^n(i,j) \left[ \frac{T^{n+1}(i,j+1) - T^{n+1}(i,j-1)}{2\Delta y} \right] =$$

$$\frac{1}{PrRe} \left[ \frac{T^n(i+1,j) - 2T^{n+1}(i,j) + T^n(i-1,j)}{(\Delta x)^2} \right] +$$

$$\frac{1}{PrRe} \left[ \frac{T^{n+1}(i,j+1) - 2T^{n+1}(i,j) + T^{n+1}(i,j-1)}{(\Delta y)^2} \right] + \frac{E_c}{Re} \Phi^n(i,j) + Q \quad (4.26)$$

or by collecting the similar terms the following forms can be obtained;

$$\begin{aligned}
& T^{n+1}(i, j) \left[ \frac{1}{\Delta t} + \frac{u^n(i, j)}{\Delta x} + \frac{1}{PrRe} \left( \frac{2}{(\Delta x)^2} + \frac{2}{(\Delta y)^2} \right) \right] + \\
& T^{n+1}(i, j+1) \left[ \frac{v^n(i, j)}{2\Delta y} - \frac{1}{PrRe(\Delta y)^2} \right] + T^{n+1}(i, j-1) \left[ -\frac{v^n(i, j)}{2\Delta y} - \frac{1}{PrRe(\Delta y)^2} \right] = \\
& T^n(i, j) \left[ \frac{1}{\Delta t} \right] + T^n(i-1, j) \left[ \frac{u^n(i, j)}{\Delta x} + \frac{1}{PrRe(\Delta x)^2} \right] + T^n(i+1, j) \left[ \frac{1}{PrRe(\Delta x)^2} \right] + \\
& \frac{E_c}{Re} \Phi^n(i, j) + Q \tag{4.27}
\end{aligned}$$

Hence;

$$\begin{aligned}
& A T^{n+1}(i, j) + B T^{n+1}(i, j-1) + C T^{n+1}(i, j+1) = \\
& D T^n(i, j) + E T^n(i-1, j) + F T^n(i+1, j) + G \Phi^n(i, j) + H Q^n(i, j) \tag{4.28a}
\end{aligned}$$

$$C \mathbf{C}_n = D T^n(i, j) + E T^n(i-1, j) + F T^n(i+1, j) + G \Phi^n(i, j) + H Q^n(i, j) \tag{4.28b}$$

This equation can be cast into matrix form hence,

$$\begin{bmatrix} B & C & 0 & 0 & \cdots & 0 & 0 & 0 \\ A & B & C & 0 & \cdots & 0 & 0 & 0 \\ 0 & A & B & C & \cdots & 0 & 0 & 0 \\ \vdots & \vdots & \vdots & \vdots & \vdots & \vdots & \vdots & \vdots \\ \vdots & \vdots & \vdots & \vdots & \vdots & \vdots & \vdots & \vdots \\ 0 & 0 & 0 & 0 & \cdots & A & B & C \\ 0 & 0 & 0 & 0 & \cdots & 0 & B & C \end{bmatrix} \begin{bmatrix} T_1 \\ T_2 \\ T_3 \\ \vdots \\ \vdots \\ \vdots \\ T_N \end{bmatrix} = \begin{bmatrix} CC_1 \\ CC_2 \\ CC_3 \\ \vdots \\ \vdots \\ \vdots \\ CC_n \end{bmatrix} \quad (4.28c)$$

Again the right hand side of the energy equation is treated as a completely constant term. The viscous dissipation term is approximated as;

$$\begin{aligned} \Phi^n(i, j) = 2 \left\{ \left[ \left( \frac{u^n(i, j) - u^n(i-1, j)}{\Delta x} \right)^2 + \left( \frac{v^n(i, j+1) - v^n(i, j-1)}{2\Delta y} \right)^2 \right] \right. \\ \left. + \left[ \left( \frac{v^n(i, j) - v^n(i-1, j)}{\Delta x} \right) + \left( \frac{u^n(i, j+1) - u^n(i, j-1)}{2\Delta y} \right) \right]^2 \right\} \quad (4.29) \end{aligned}$$

$Q$  is a nondimensionalized source term representing the heat generation inside the rectangular block. During solution, source term  $Q$  was introduced into discretized thermal equations as a constant value at the special node points where the source is embedded. Similar to vorticity transport equation energy equation is represented by a tridiagonal matrix and solved by Thomas algorithm [23].

Boundary conditions are also discretized and combined to the main field equation for a conjugate solution. Numerical details of the boundary condition discretization will be discussed in details in Chapter 5.

#### 4.3.3 Solution Procedure

After accomplishing finite difference approach to governing flow and thermal equations by means of Taylor series expansion of first and second order derivatives, solution procedure will be presented in this section. The technique is well known and explained by Roache [25] in details for flow field approximation. This technique adopted and modelled with the energy equation

The steps of the solution procedure are given below.

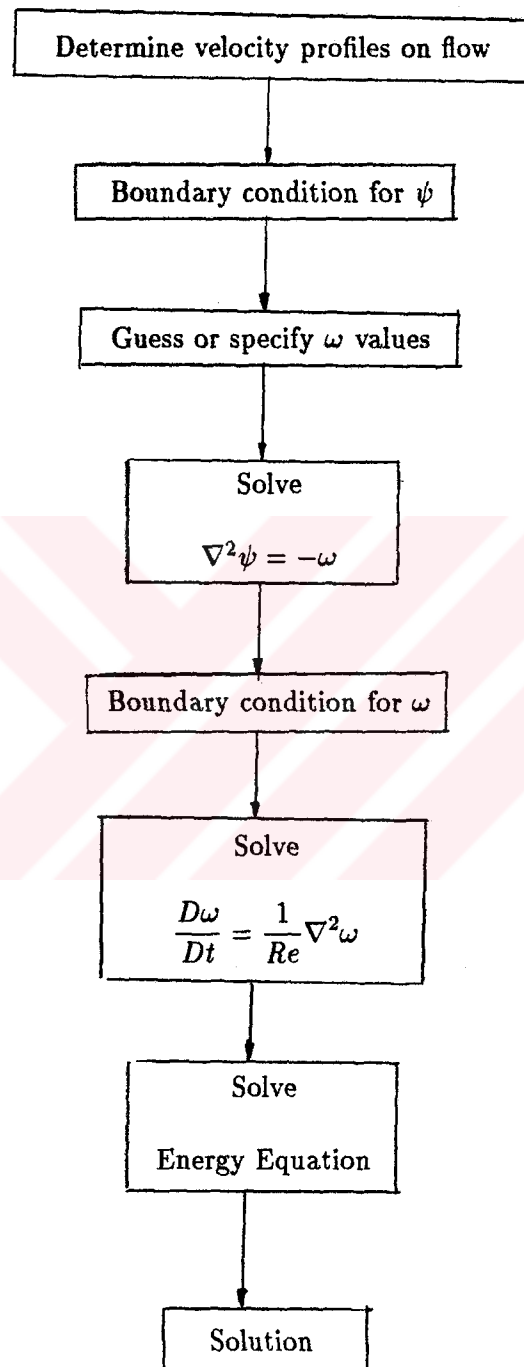
1. Specify initial values for  $\omega$  and  $\psi$  at time  $t=0$ .
2. Solve the vorticity transport equation for  $\omega$  at each interior grid point at each time interval (Eq 4.18).
3. Iterate for new  $\psi$  values at all points by solving the Poisson equation using new  $\omega$ 's at the interior points (Eq 4.21).
4. Compute the velocity field components from  $U = \frac{\partial \psi}{\partial y}$  and  $V = -\frac{\partial \psi}{\partial x}$
5. Determine values of  $\omega$  on the boundaries using  $\psi$  and  $\omega$  values at interior points.
6. Solve the energy equation and obtain the values of  $\theta$  (Eq 4.27)

7. Return to step 2 if the solution is not converged. If the flow field is converged return to step 6 and perform iterations until energy field converges.

After completing the above steps with the prerequired accuracy, the solution is assumed to be converged and final data is presented. Solution procedure is given with a small chart below.



## Solution procedure steps



## CHAPTER 5

### NUMERICAL APPROXIMATION OF BOUNDARY CONDITIONS

In this chapter, the details of the boundary conditions will be presented. Particularly, the attention will focus on the numerical approximation of the boundary conditions. Due to the nature of the problem considered, special care is needed at various grid locations in the process of discretization.

#### 5.1 Boundary Conditions of Flow Field

The equations which govern the flow field, without making any assumptions, have elliptic character. In order for the elliptic problems to be well posed one must specify either the prescribed values (Dirichlet condition) or the normal derivatives (Neumann Condition) of the stream function. Implicit procedure include boundary conditions during the solution process [21]. On the other hand, vorticity is always difficult to be set along boundaries. Implicit vorticity conditions are very difficult to be treated by numerical algorithms since it is very costly. For this reason, explicit method of considering this condition is preferred [21]. In this study this way of formulation consists the current value of a vorticity on the boundary is approximated

by using the previous set of values by making a time dependency in the development of the vorticity.

In order to solve equations 4.1 and 4.2, boundary conditions of stream function  $\psi$  and vorticity,  $\omega$  should be described. The relevant boundaries are shown in Figure 5.1 Below, details of these conditions are presented along each section of the boundary. Hence

$$\text{Along AB: } \omega^n(i, j) = \psi^n(i, j) = 0 \quad j=1, my1 \quad 5.1$$

$$\text{Along BC: } U = 1 \quad V = 0$$

$$U = \frac{\partial \psi}{\partial y} = 1; \quad -\frac{\partial \psi}{\partial x} = V = 0 \quad (5.2)$$

then;

$$\psi = \int U dy + C_0 \quad (5.3)$$

$$\psi = y + C_0 \quad (5.4)$$

Hence;

$$\psi(i, j) = dy \times j + C_0 \quad j = my1, my \quad (5.5)$$



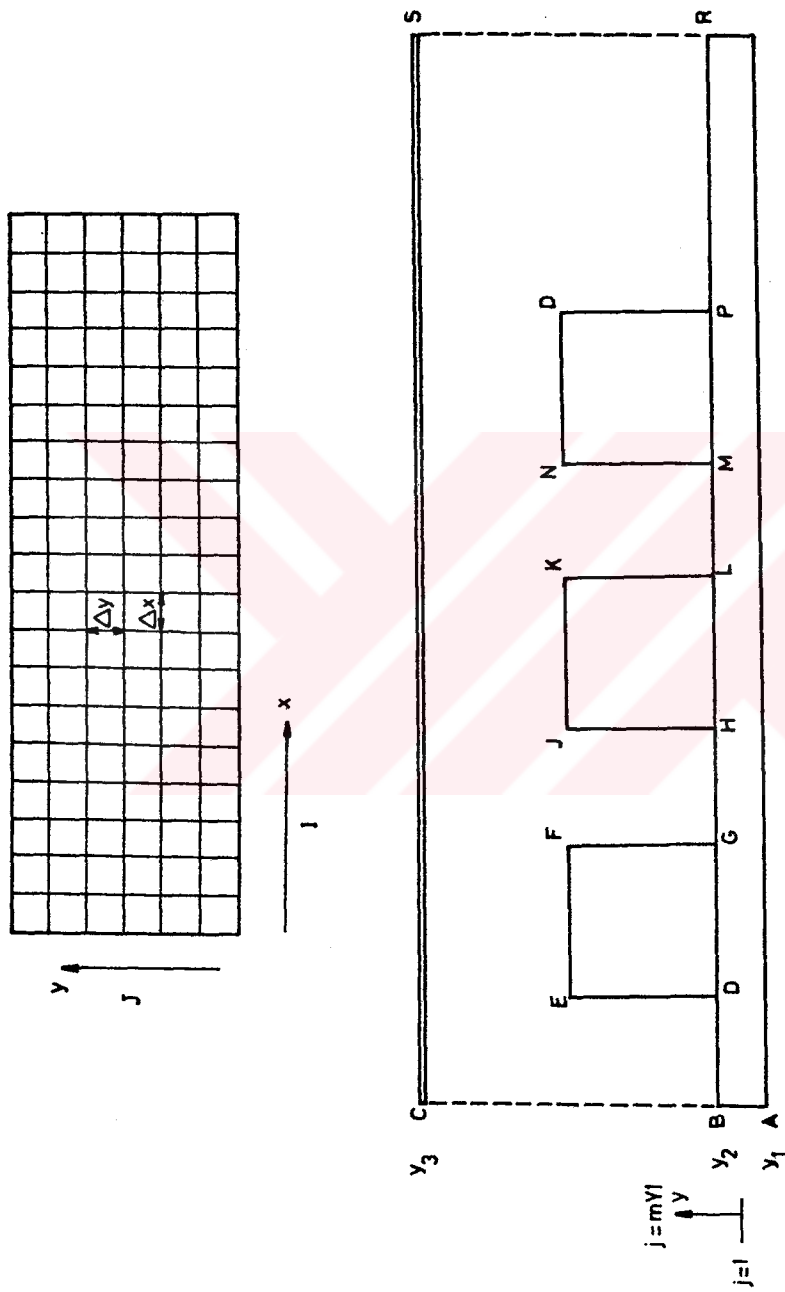


Figure 5.1) The geometry of flow field and thermal field.

For the vorticity boundary condition

Along AB:

$$\omega = \frac{\partial v}{\partial x} - \frac{\partial u}{\partial y} = 0 \quad (5.6)$$

Hence;

$$\omega(i, j) = 0 \quad j = my1, my \quad (5.7)$$

Along BD:  $U = V = 0$ , then

$$\psi(i, my1) = 0 \quad (5.8)$$

Along wall BD, the definition of vorticity requires detailed modelling. Vorticity  $\omega$ , distribution will be determined by using the expansion of the stream function  $\psi$  near the wall point  $(i, j)$  between B and D. Figure 5.2 shows the direction of expansion.

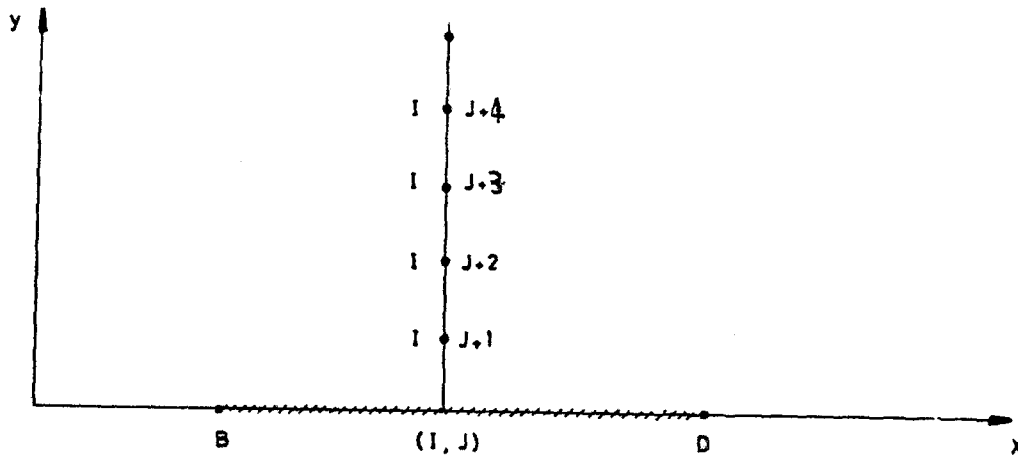


Figure 5.2) Expansion of stream function near wall.

Figure 5.2 expansion of stream function near wall for to be prediction of vorticity condition.

Then;

$$\psi(i, j+1) = \psi(i, j) + \frac{\partial \psi(i, j)}{\partial y} \Delta y + \frac{1}{2!} \frac{\partial^2 \psi(i, j)}{\partial y^2} \Delta y^2 + \dots \quad (5.9)$$

it is known that

$$\left. \frac{\partial \psi}{\partial y} \right|_{(i, j)} = U(i, j) = 0 \quad (5.10)$$

from no-slip boundary condition. However, the second derivative of  $\psi$  is not zero.

Hence;

$$\left. \frac{\partial^2 \psi}{\partial y^2} \right|_{(i, j)} = \left. \frac{\partial U}{\partial y} \right|_{(i, j)} \quad (5.11)$$

near wall  $|v| \ll |u|$  (basic boundary layer assumption). If one neglects the variation of  $v$  along flow direction then by using the definition of vorticity one gets the following definition

$$\omega(i, j) = \left( \frac{\partial v}{\partial x} - \frac{\partial u}{\partial y} \right) = - \left. \frac{\partial^2 \psi}{\partial y^2} \right|_{(i, j)} \quad (5.17)$$

By expanding the second derivatives by an upwind approximation, first order vorticity definition is obtained. Hence;

$$\omega(i, j) = 2 \left( \frac{\psi(i, j) - \psi(i, j+1)}{\Delta y^2} \right) + O(dy) \quad (5.13)$$

Similarly along the boundary ED.

$$\omega(i, j) = 2 \left( \frac{\psi(i, j) - \psi(i + 1, j)}{\Delta x^2} \right) + O(dx) \quad (5.14)$$

Along the boundary CS;

$$\omega(i, j) = 2 \left( \frac{\psi(i, j) - \psi(i, j + 1)}{\Delta y^2} \right) + O(dy) \quad (5.15)$$

The exit plane is selected well downstream so that flow becomes parallel to the channel walls and can be considered fully developed. Hence;

$$\frac{\partial U}{\partial x} = 0, \quad \frac{\partial V}{\partial x} = 0, \quad \frac{\partial \omega}{\partial x} = 0 \quad (5.16)$$

hence

$$U(i, j) = U(i - 1, j) \quad V(i, j) = V(i - 1, j) \quad \omega(i, j) = \omega(i - 1, j) \quad (5.17)$$

or being more precise, one can approximate Eq. 5.12 as 3 point approximations as

$$3U(i, j) - 4U(i - 1, j) + U(i - 2, j) = 0 \quad (5.18)$$

$$3V(i, j) - 4V(i - 1, j) + V(i - 2, j) = 0 \quad (5.19)$$

$$3\omega(i, j) - 4\omega(i - 1, j) + \omega(i - 2, j) = 0 \quad (5.20)$$

Equations 5.16 through 5.18 are considered implicit with the fundemantal equations during the solution procedure.

## 5.2 Boundary Conditions for Thermal Field

### 5.2.1 Prescribed Temperature Boundary Condition

$$\theta = \frac{(T - T_{in})}{(T_{wu} - T_{in})} \quad (5.21)$$

$\theta$ :Dimensionless Temperature

$T_{in}$ :Inlet Temperature

$T_{w,u}$ :Upper wall Temperature

Along AB and AC temperature,  $\theta$ , is chosen to be constant and this constant was set to zero.

In this study three kinds of boundary conditions were considered. Generalized characters of more common ones will be described first. When the temperature varies with the space variables, the energy equation involves a second derivative in space. If only the conduction equation would be necessarily solved, two boundary conditions were needed in addition to the initial condition. The boundary conditions specify the thermal conditions imposed on the boundary surfaces of the solid. For example, at a given surface one may specify either the temperature or the heat flux or convection into the media in which the temperature specified.

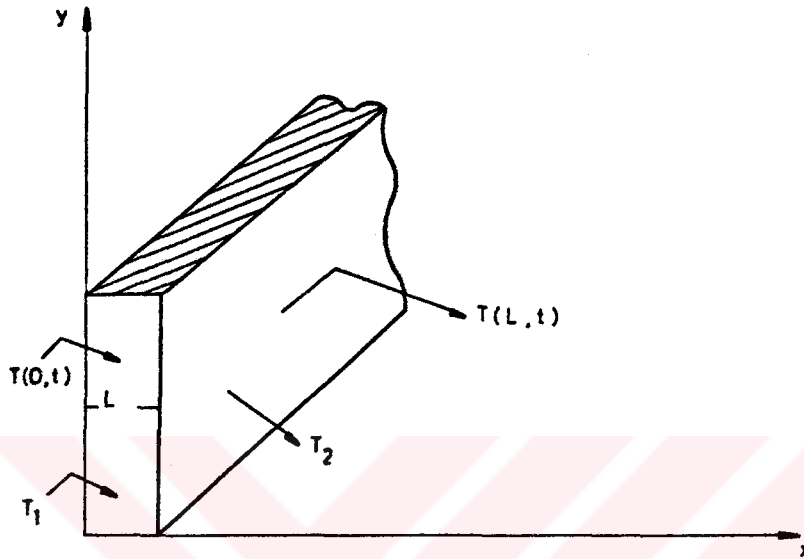


Figure 5.3) Prescribed temperature boundary condition.

Above figure shows the application of the prescribed temperature boundary condition for a solid domain. The front and back surfaces are kept at constant temperature. Depending on the relative magnitudes of these conduction a thermal energy flows from one surface to another.

There are numerous applications in which the temperature of the boundary surface is considered to be known. When the value of the temperature at the boundary surface is specified, for it said to be prescribed. In the present model temperature prescribed in domain which means that is known everywhere.

### 5.2.2 Prescribed Heat Flux Boundary Condition

There are situations in which the rate at which heat is supplied to or removed from a boundary surface is known. For example, at an electrically heated surface, the rate of heat flow entering the solid known; at a thermally insulated surface, the heat flux is zero; at a surface subjected to a solar radiation, the rate of energy absorbed can be estimated, and hence the heat flux is as regarded as known. Also, there are situations in which the surface heat flux may vary with time. When the magnitude of the heat flux at a boundary surface is specified, the boundary condition is said to be prescribed heat flux boundary condition.

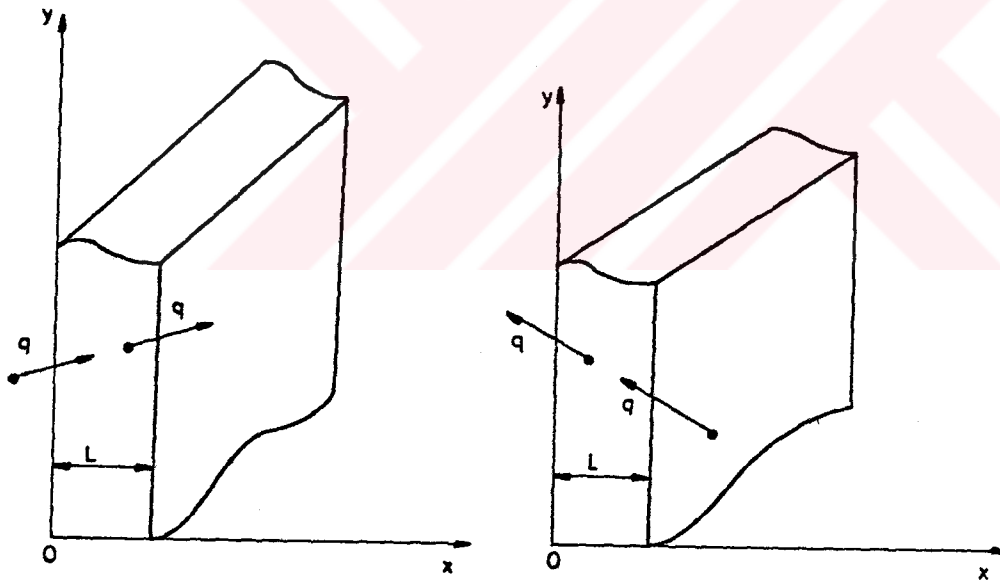


Figure 5.4) Prescribed heat flux boundary condition.

$$q = -k \frac{\partial T(x, t)}{\partial x} \Big|_{x=0} \qquad q = +k \frac{\partial T(x, t)}{\partial x} \Big|_{x=0} \qquad (5.22)$$

A numerical approximation of heat flux condition needs the finite difference form of these equation considering energy balance on boundaries. Suppose the heat flux entering the plane wall through the boundary surface at  $x = 0$ , is prescribed

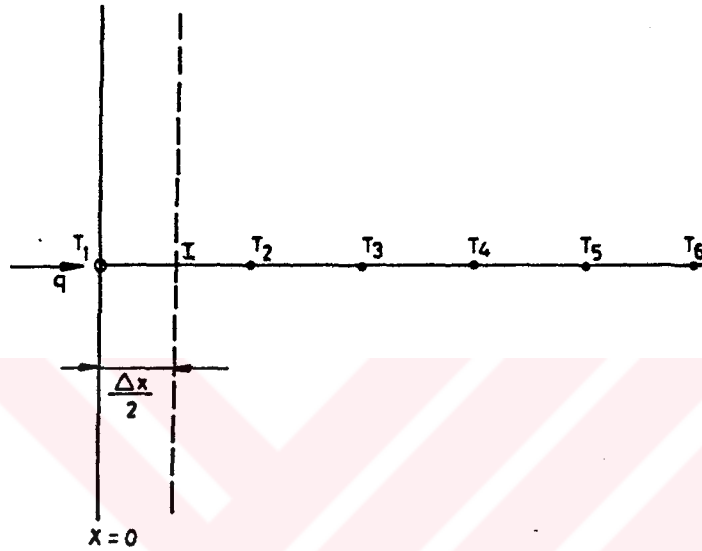


Figure 5.5) Prescribed heat flux on the boundary.

To develop an additional finite difference equation for the node at  $x = 0$ , we write energy balance equation for a volume element of thickness  $dx/2$  at the node  $i$ , as illustrated above.

$$\left\{ \begin{array}{l} \text{Rate of heat} \\ \text{entering through} \\ \text{boundary surface} \end{array} \right\} + \left\{ \begin{array}{l} \text{rate of heat} \\ \text{entering by} \\ \text{conduction} \end{array} \right\} + \left\{ \begin{array}{l} \text{Rate of} \\ \text{energy} \\ \text{generation} \end{array} \right\} = 0 \quad (5.23)$$



If on area  $A$  is considered, the mathematical expression for each of these three terms in the brackets can be written as follows.

$$qA + kA \frac{(T_2 - T_1)}{\Delta x} + \frac{\Delta x}{2Ag} = 0 \quad (5.24)$$

$g$ : Generated heat in area

if  $g$  is zero, thus

$$k \frac{(T_2 - T_1)}{\Delta x} + q = 0 \quad (5.25)$$

In the present problems, applications commonly there are two different materials, and also interface between solid and fluid. This case is depicted in figure 5.5.

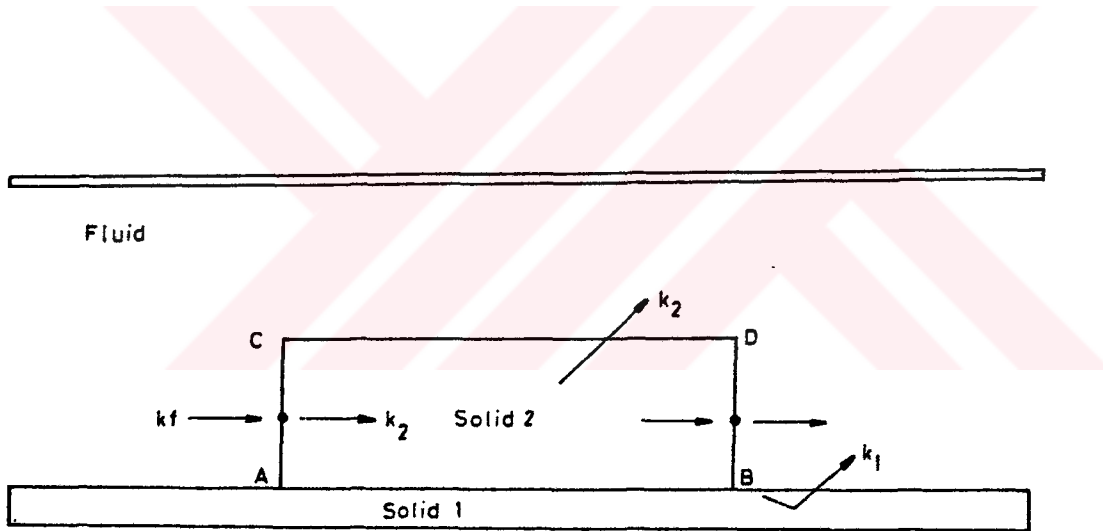


Figure 5.6) The balance of heat flux in Y direction for two different materials boundary.

The income heat flux must be equal to outcome heat flux namely at the considered point  $(i,j)$

$$-k_2 \frac{\partial T}{\partial y} \Big|_{(i,j)} = -k_1 \frac{\partial T}{\partial y} \Big|_{(i,j)} \quad (5.26)$$

and expanding them into Taylor series,

$$\left. \frac{\partial T}{\partial y} \right|_{(i,j)} = \frac{-3T(i,j) + 4T(i,j+1) - T(i,j+2)}{2\Delta y} \quad (5.27)$$

hence;

$$k_2[-3T(i,j) + 4T(i,j+1) - T(i,j+2)] = k_1[-3T(i,j) + 4T(i,j-1) - T(i,j-2)] \quad (5.28)$$

$$T(i,j)[3(k_1 - k_2)] + T(i,j+1)[4k_2] + T(i,j-1)[-4k_1] = T(i,j+2)[k_2] + T(i,j-2)[-k_1] \quad (5.29)$$

right hand side's terms are taken as knowns at each time step. The same balance will be written in the connectory boundary between fluid and solid. Again consider the same geometry shown in figure 5.7.

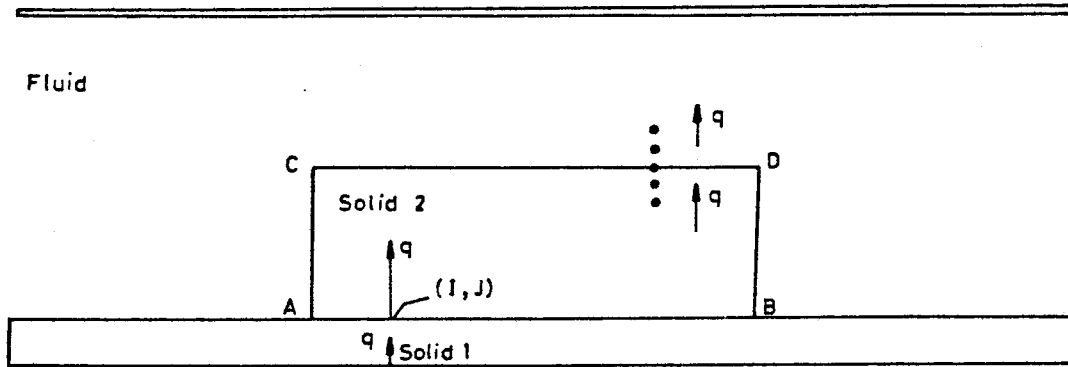


Figure 5.7) The balance of heat flux in X direction for two different materials boundary.

To treat the same boundary condition in  $x$  direction heat transfer balance should be written. Hence;

$$-k_2 \frac{\partial T}{\partial x} \Big|_{(i,j)} = -k_f \frac{\partial T}{\partial x} \Big|_{(i,j)} \quad (5.30)$$

$$k_2[-3T(i,j)+4T(i+1,j)-T(i+2,j)] = k_f[-3T(i,j)+4T(i-1,j)-T(i-2,j)] \quad (5.31)$$

rearrange the equality,

$$T(i,j)[3(k_f-k_2)] + T(i,j+1)[4k_2] + T(i,j-1)[-4k_f] = T(i,j+2)[k_2] + T(i,j+2)[-k_f] \quad (5.32)$$

on the point  $(i,j)$  an equation for  $T(i,j)$  becomes;

$$T(i,j) = \frac{\{T(i+1,j)[-4k_2] + T(i-1,j)[4k_f] + T(i+2,j)[k_2] + T(i-2,j)[-k_f]\}}{3(k_f - k_2)} \quad (5.33)$$

The case of zero flux condition considers isolated solid body in given direction. it is shown in figure 5.8

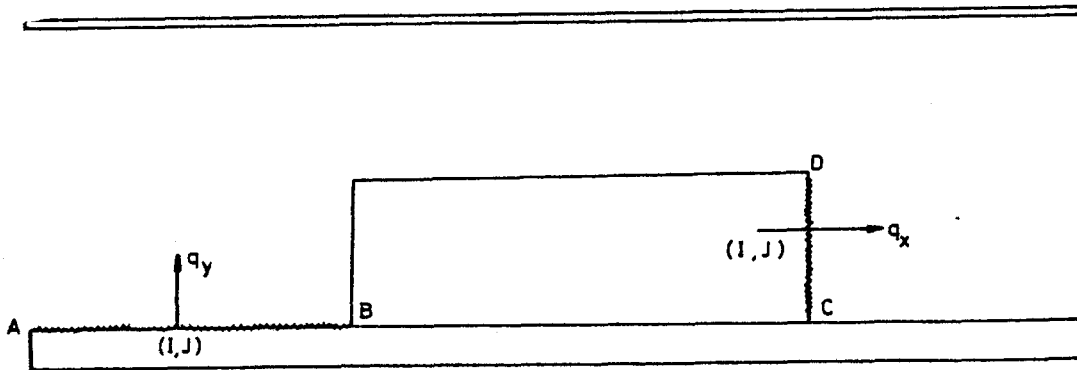


Figure 5.8) Isolated boundary in considered direction.

If  $q_y = 0$  then  $q_y = -k_y \partial T / \partial y = 0$

Now, already driven equation (5.32) becomes,

$$\left. \frac{\partial T}{\partial y} \right|_{(i,j)} = \frac{-3T(i,j) + 4T(i,j+1) - T(i,j+2)}{2\Delta y} = 0 \quad (5.34)$$

then

$$T(i,j) = \frac{[4T(i,j+1) - T(i,j+2)]}{3} \quad (5.35)$$

In the  $x$  direction same equation becomes,

$$\left. \frac{\partial T}{\partial x} \right|_{(i,j)} = \frac{-3T(i,j) + 4T(i+1,j) - T(i+2,j)}{2\Delta x} = 0 \quad (5.36)$$

Hence;

$$T(i,j) = \frac{4T(i+1,j) - T(i+2,j)}{3} \quad (5.37)$$

### 5.2.3 Convection Boundary Condition

In this section, details of the application of convective heat transfer boundary conditions will be presented.

Suppose the solid boundary surface at  $x = 0$  is subjected to a convective heatloss with a heat transfer convective coefficient  $h_{\infty}$  into an ambient at temperature  $T_{\infty}$ . Furthermore assumed that a heat source of  $q$  is generated per unit area in the solid domain.

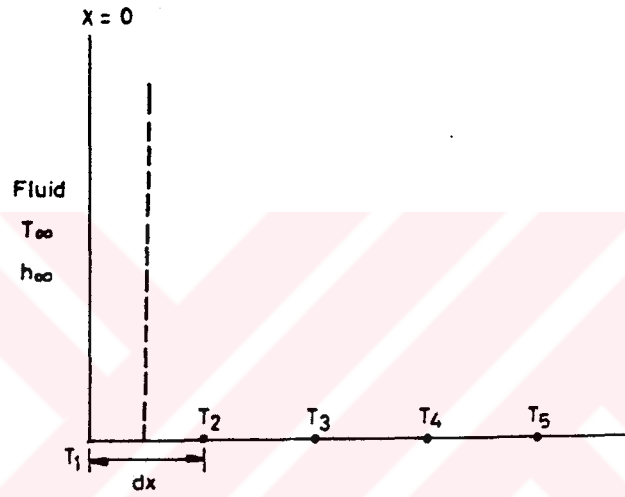


Figure 5.9) Convective heat transfer for a solid region.

By considering an energy balance for a volume element of thickness  $\Delta x/2$  at the node  $i = 1$  near the solid surface, the following balance can be observed,

$$\left\{ \begin{array}{l} \text{Rate of heat} \\ \text{entering through} \\ \text{the surface} \\ \text{by convection} \end{array} \right\} + \left\{ \begin{array}{l} \text{rate of heat} \\ \text{entering by} \\ \text{conduction} \end{array} \right\} + \left\{ \begin{array}{l} \text{Rate of} \\ \text{energy} \\ \text{generation} \end{array} \right\} = 0 \quad (5.38)$$

Considering arbitrary chosen area  $A$ , the mathematical expression can be written as

$$h_{\infty}A(T_{\infty} - T_1) + kA\frac{(T_2 - T_1)}{\Delta x} + \frac{\Delta x}{2}Aq \quad (5.39)$$

$q$ : Generated heat per unit area

$h_{\infty}$ : Natural or convective heat transfer coefficient  $k$ : Thermal conductivity of the solid

With the assumption of no heat generation above equation becomes

$$2T_2 - (2 + 2\Delta x \frac{h_{\infty}}{k})T_1 + 2\Delta x h_{\infty} \frac{T_{\infty}}{k} = 0 \quad (5.40)$$

Finally, very brief outline of the exit boundary condition is given below. At the exit plane, a fully developed flow condition approximates the temperature profile.

Hence;

$$\frac{\partial T}{\partial x} = -\frac{3T(i, j) + 4T(i + 1, j) - T(i + 2, j)}{2\Delta x} = 0 \quad (5.41)$$

or after simplification, condition at the exit boundary SR becomes;

$$T(i, j) = \frac{[4T(i - 1, j) - T(i - 2, j)]}{3} \quad (5.42)$$

### 5.3 Numerical Treatment of The Critical Points

During the calculations of the field variables such as  $\psi, \omega$ , for flow field, and  $\theta$ , for temperature field, one faces up same difficulties on the corners where field variables become discontinues. On these such points one gets value of little infinite or highly irregular values from the neighbouring points.

These kinds of points must be treated separately and continuously controlled by their time dependent values whether they become stable or unstable. They must behave timely convergent as well as become consistent with its neighbours. The approximations of the boundary conditions will be presented in this section. Thermal field involves many critical surfaces and points. Figure 5.9 shows these loctions. These treatments introduced below were succesfully used for flow field and thermal field under considerations.

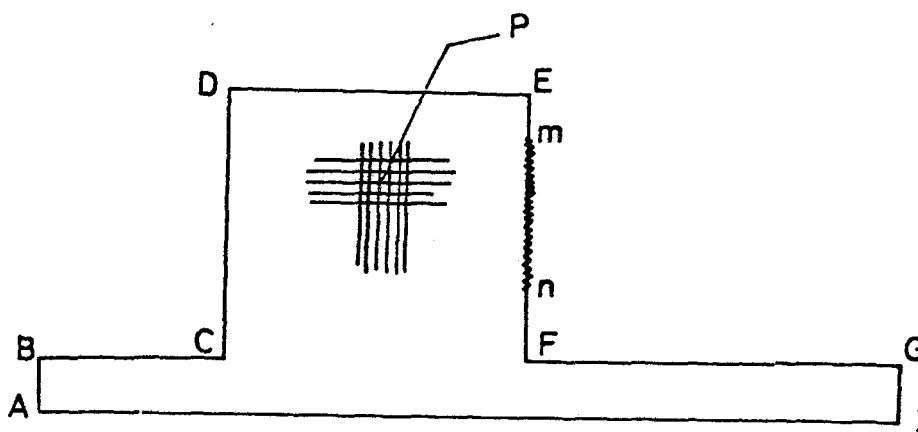


Figure 5.10) Critical points for thermal field consideration.

Case A)

Generation of heat at an interior grid point and energy balance. Rectangular blocks carries infinitely thin heat source layer embedded at various elevations. Steady state energy balance at a point, for example at P yields the following balance inside a typical block.

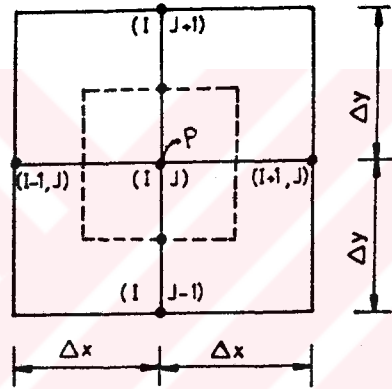


Figure 5.11) The energy balance for an interior point P.

Case A1)

without heat source;

$$\theta(i, j) + \theta(i, j + 1) + \theta(i - 1, j) + \theta(i, j - 1) - 4\theta(i, j) = 0 \quad (5.43)$$

by the assumption that  $\Delta x = \Delta y$



Case A2)

with heat source; If there is a source on the point (i,j) then equation becomes

$$\theta(i+1, j) + \theta(i, j+1) + \theta(i, j-1) - 4\theta(i, j) = q(i, j) \quad (5.44)$$

$q(i, j)$  is the amount of heat generate per unit area

Case B)

Heat transfer from a solid surface having heat sources embeded at an interior point. Heat generated in rectangular blocks will be transferred to the ambaient fluid through convection.

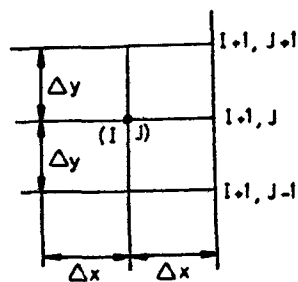


Figure 5.12) Convective heat transfer from a solid surface with heat generation near the surface.

Hence the energy balance will yield;

$$\frac{h_{\infty} \Delta x}{k} \theta_{\infty} + \frac{1}{2}(\theta(i-1, j) + \theta(i, j+1) + \theta(i, j-1)) - \left( \frac{h_{\infty} \Delta x}{k} + 1 \right) \theta(i, j) = q(i, j) \quad (5.45)$$

Case C) Exterior corner such as D or E with convection boundary

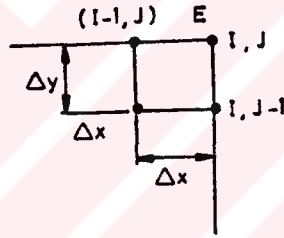


Figure 5.13) Convection boundary condition for an exterior corner.

The energy balance at a point (i,j) yields the following formulae, Figure 5.13

$$q(i, j) = \frac{2h_{\infty} \Delta x}{k} \theta_{\infty} + (\theta(i-1, j) + \theta(i, j-1)) - \left( \frac{2h_{\infty} \Delta x}{k} + 2 \right) \theta(i, j) \quad (5.46)$$

Case D) Interior corner such as C or F with convection boundary

The energy balance at a point (i,j) yields the following formulae; Figure 5.14

$$q(i,j) = 2h_{\infty} \frac{\Delta x}{k} \theta_{\infty} + 2\theta(i-1,j) + 2\theta(i,j+1) + \theta(i+1,j) + \theta(i,j-1) - 2(3 + h_{\infty} \frac{\Delta x}{k})\theta(i,j) \quad (5.47)$$

Case E) Insulated boundary

The energy balance at (i,j) yields the following formulae;

$$q(i,j) = \theta(i,j+1) + \theta(i,j-1) + 2\theta(i-1,j) - 4\theta(i,j) \quad (5.48)$$

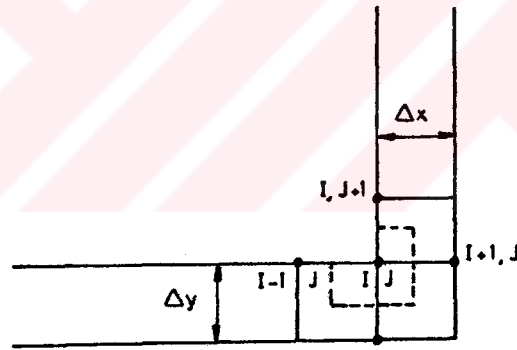


Figure 5.14) Convection boundary condition for an interior corner.

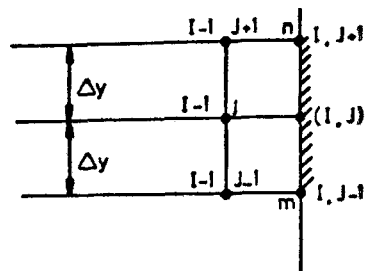


Figure 5.15) Boundary condition for an insulated surface.

## CHAPTER 6

### FLOW FIELD

This section presents the approximate flow field solutions of the Directional Implicit Finite Difference Algorithm to the problem under consideration. In order to test the computer code that was prepared two cases of a starting flow between two parallel plates will be considered first. Due to the vast experimental and analytical literature available for such a flow condition, the efficiency of the computer code was tested for this particular geometry. The length of the channel plates are chosen to be long enough to allow a fully developed flow conditions at the exit plane. The geometry of the test problem with essential feature is presented in Figure 6.1. Figure 6.2a and 6.2b presents the numerical solution precision and correctness. The axial velocity profile at the exit plane (Figure 6.2a) compared with the analytical solution given by [27].

Second test case involves flow between parallel plates but with an obstacle attached to the lower plate. As it is depicted agreement seem to be excellent. Reattachment length variation behind the step is presented in Figure 6.2b for ranges of Reynolds numbers. This length is almost a linear function of the Reynolds number. Similar observation are also made by [20]. The variation of the reattachment

length is compared with with the experimental works in Figure 6.2c. The agreement is satisfactory.

Figure 6.3 shows centerline velocity development along the flow direction for various Reynolds numbers. These development trends are tested with the results given by Arpaci [43]. It is expected that as the Reynolds number increases, centerline velocity reaches its steady state value in relatively small streamwise distances.

Figure 6.4 shows the model geometries for which computations will be carried out. The geometric dimensions were taken from a physical real system which can be considered as the printed circuit board system with chips attached to the lower plate. Similar geometries and dimensions have been given in references [4]. The computer code developed here suitably simulates the geometric dimensions and the nondimensionalized numbers of practical interest.

Figure 6.5 and 6.6 and 6.7 are the schematic representations of the geometries for the flow field and temperature field equations which will be solved in this thesis. At each figure several windows are selected to visualize the flow and temperature fields. These windows cover the whole flow domain and labeled in these figures.

Figure 6.8 shows the velocity field distribution for a one-step channel case. For this velocity field the stream function distribution is depicted in figure 6.9a and 6.9b. The vorticity distribution for the same velocity field is shown in Figure 6.10.

Boundary layer development and also bubble formation behind the block are well captured. For the velocity field and its stream function, vorticity distributions for two and three step channel case are shown through Figure 6.11 and 6.16.

In order to show the computer code's efficiency for the flow as well as the heat field, channel case run profiles are shown in progressive regions. At the entrance, rectangular uniform velocity enters impulsively into a channel. After the region three profiles slightly change. Before region nine no change in profiles is observed. Then, quite smooth profiles are observed. These developing profiles are shown in Figure 6.17a and 6.17b.

Figure 6.18a and 6.18b show the profiles at various sections for three-step channel case. On the steps profiles reached the maximum at about 3.

Over the steps, channel width reduces to half of its entrance height and for the channel case developed profile maximum velocity is about 1.5. Therefore, consequently, on the steps maximum velocity reaches at about 3. In region 4 and 7 flow has the cavity type, there its profiles have the negative velocities. Similar negative values can be seen for the region 10, which is the recirculation region behind the step.



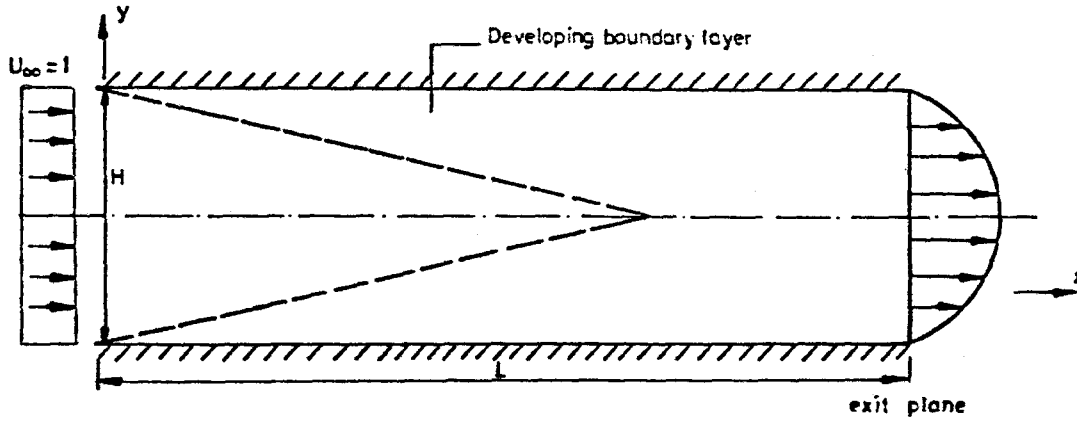


Figure 6.1 Test geometry for the validation of the computer algorithm.

$L/H=20$   $N_x=(\text{Number of grid points in X direction})=320$   $M_y=(\text{Number of grid points in Y direction})=24$



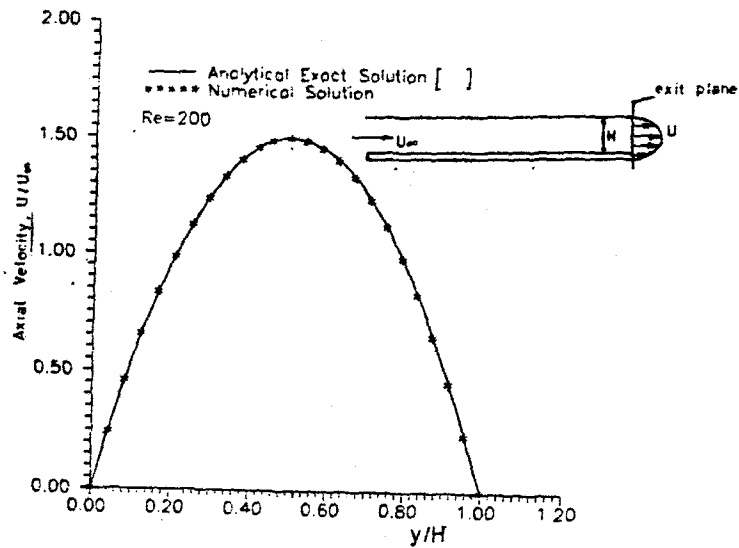


Figure 6.2a) Comparison of present numerical solution to the analytical exact solution for the channel case.

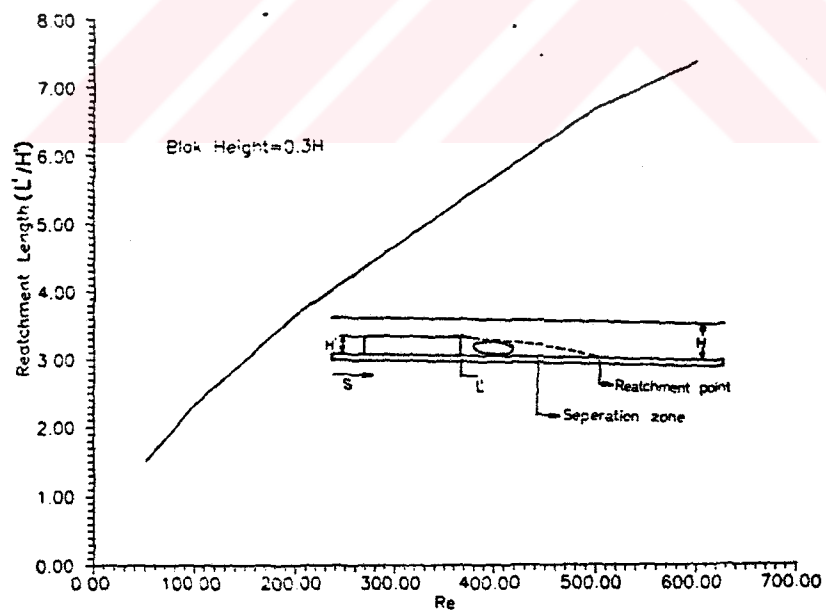


Figure 6.2b) Variation of reattachment length at various Reynolds numbers.

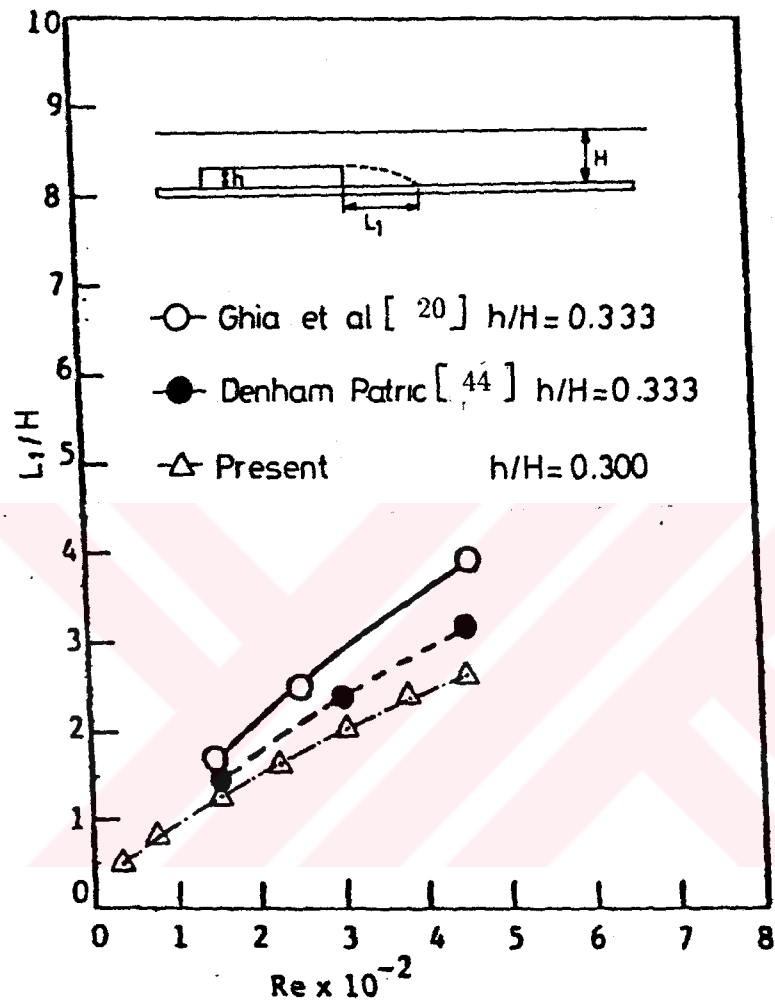


Figure 8.2c) Reattachment length for various studies.

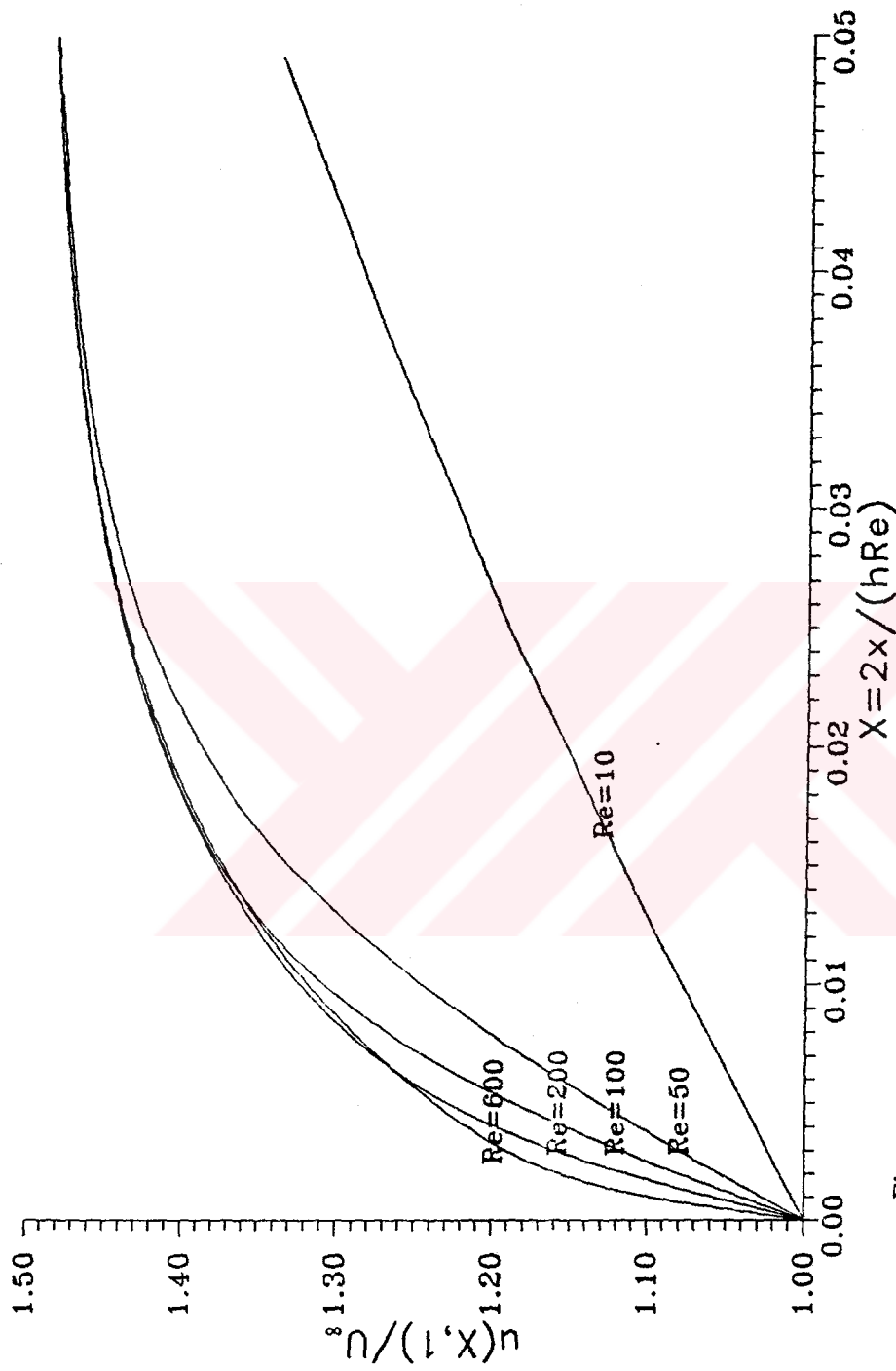


Figure 6.3 Centerline velocity development along the flow direction for various Reynolds numbers.

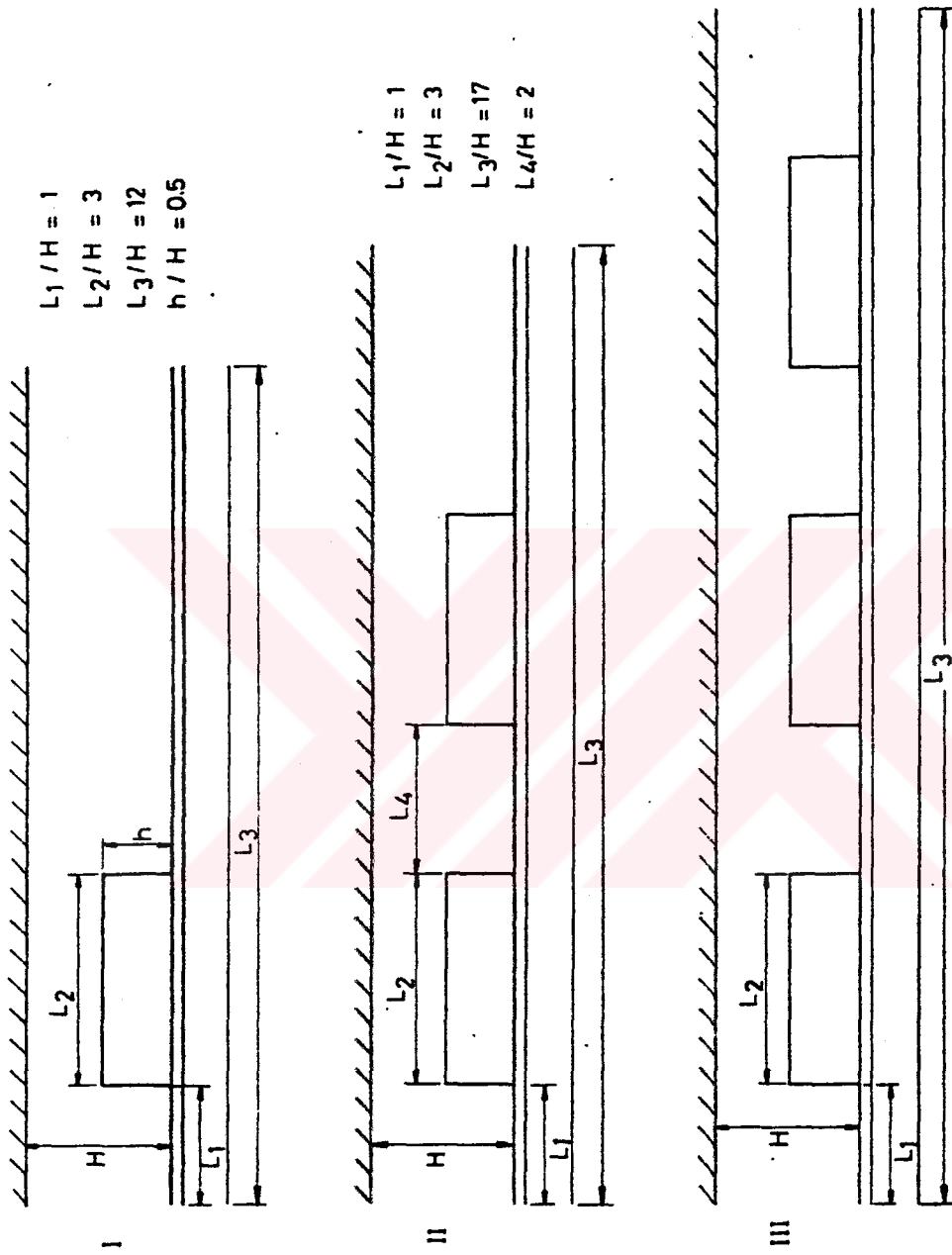


Figure 6.4 The model geometries as the physical system.



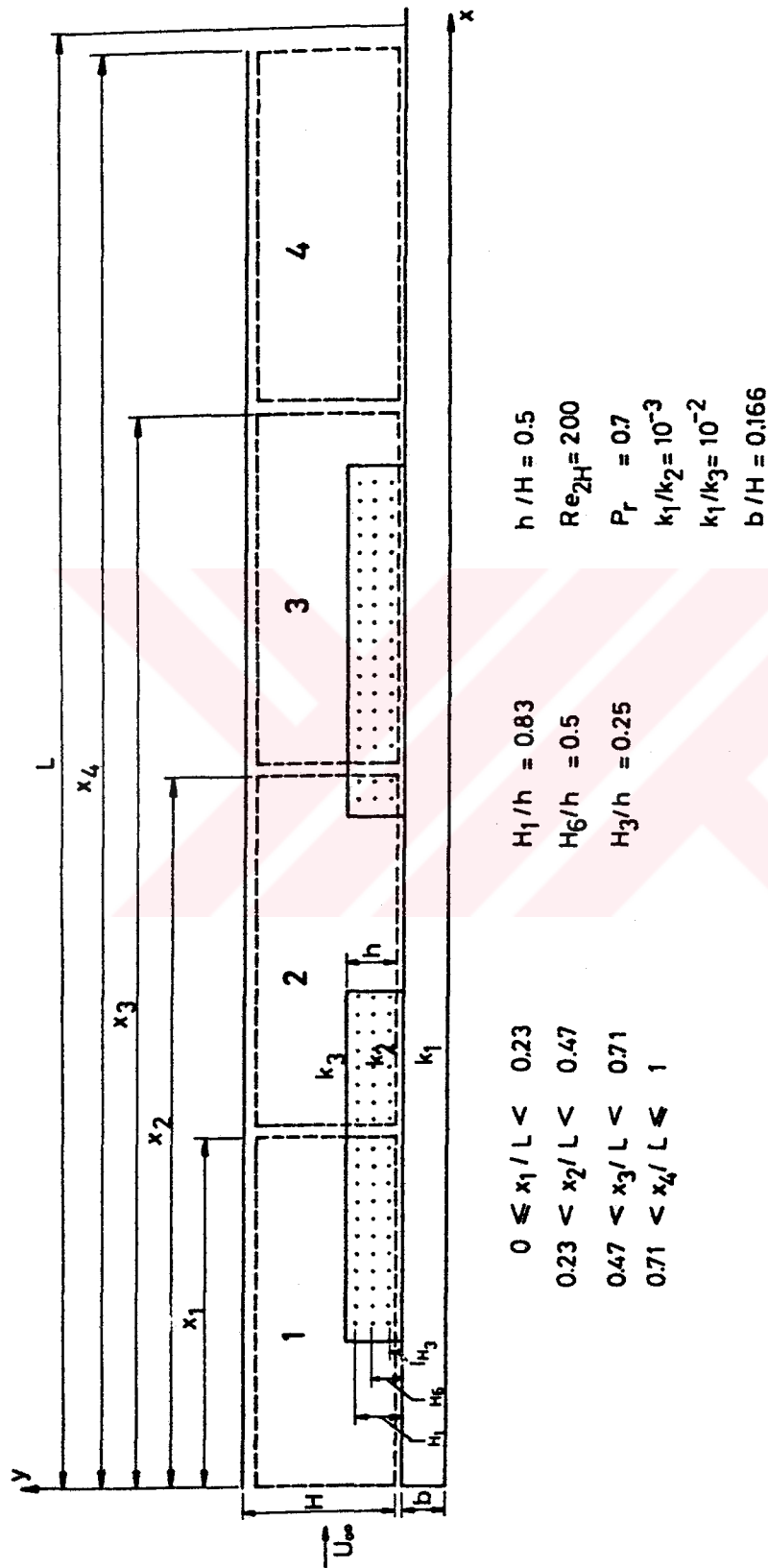


Figure 6.6 The model geometry for two-step channel case with nondimensionalized parameters.

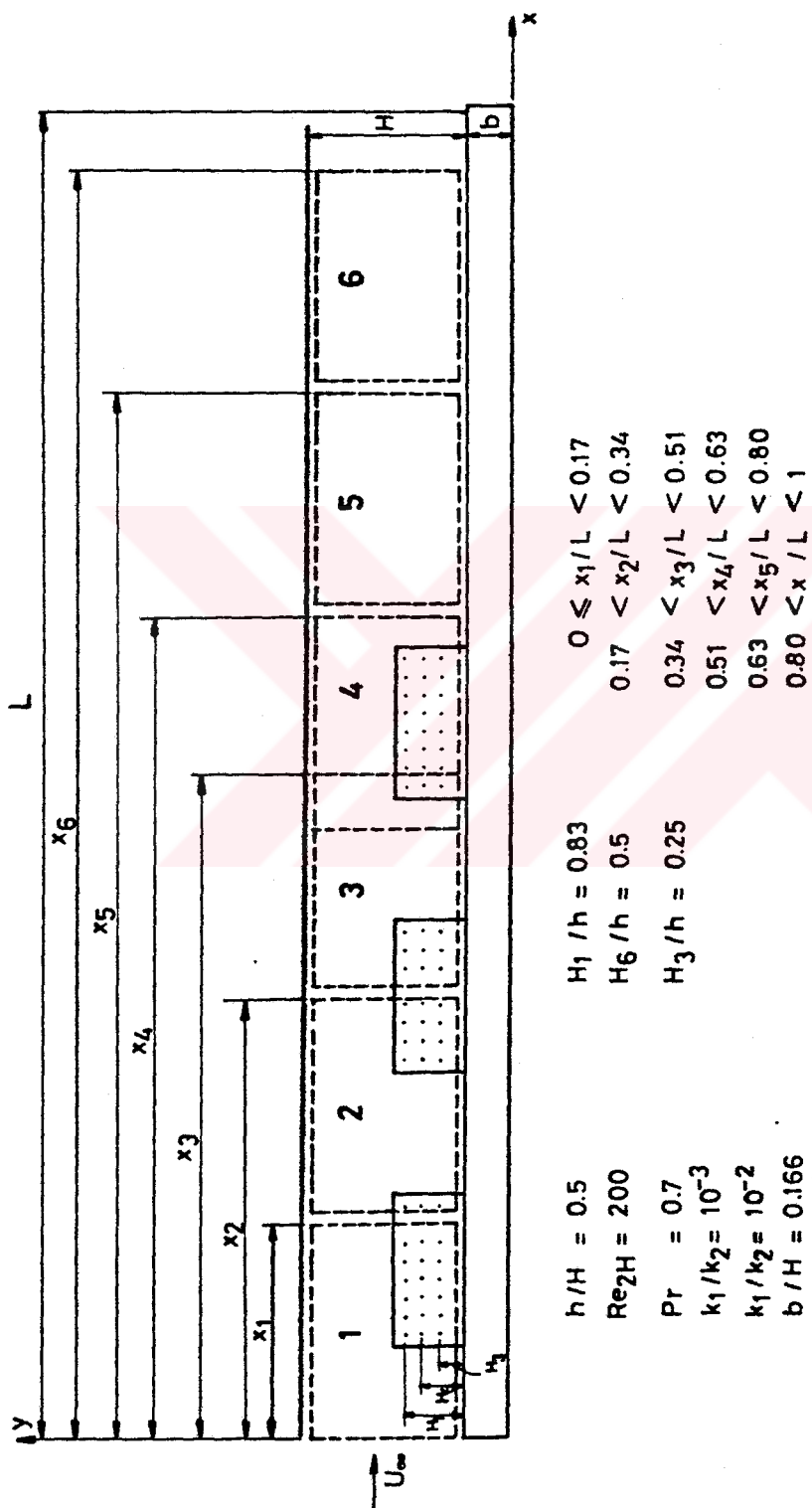


Figure 6.7 The model geometry for three-step channel with nondimensionalized parameters.

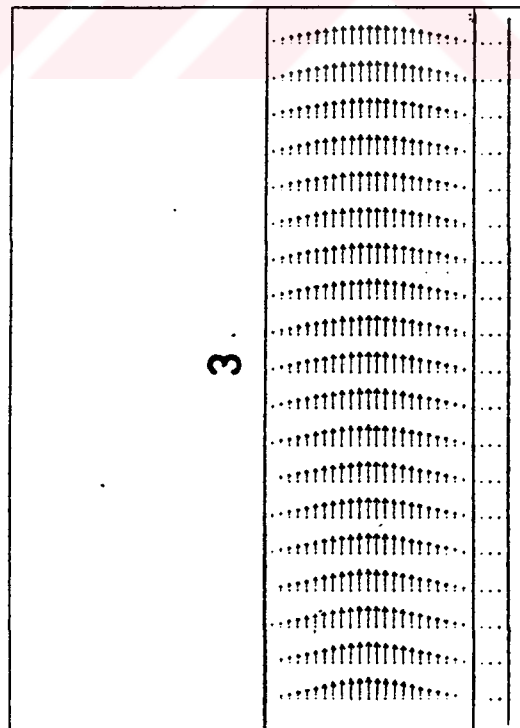
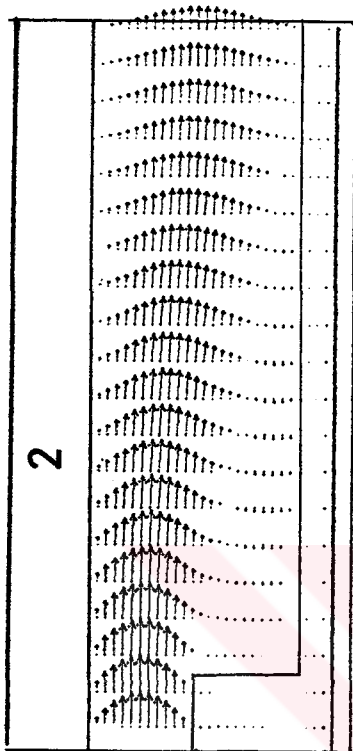
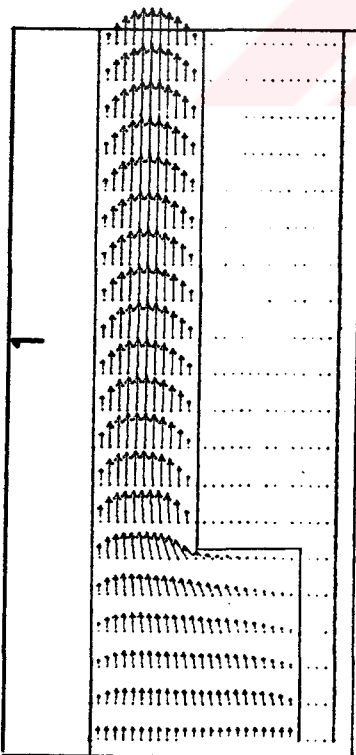


Figure 6.8 The velocity field for one-step channel case.



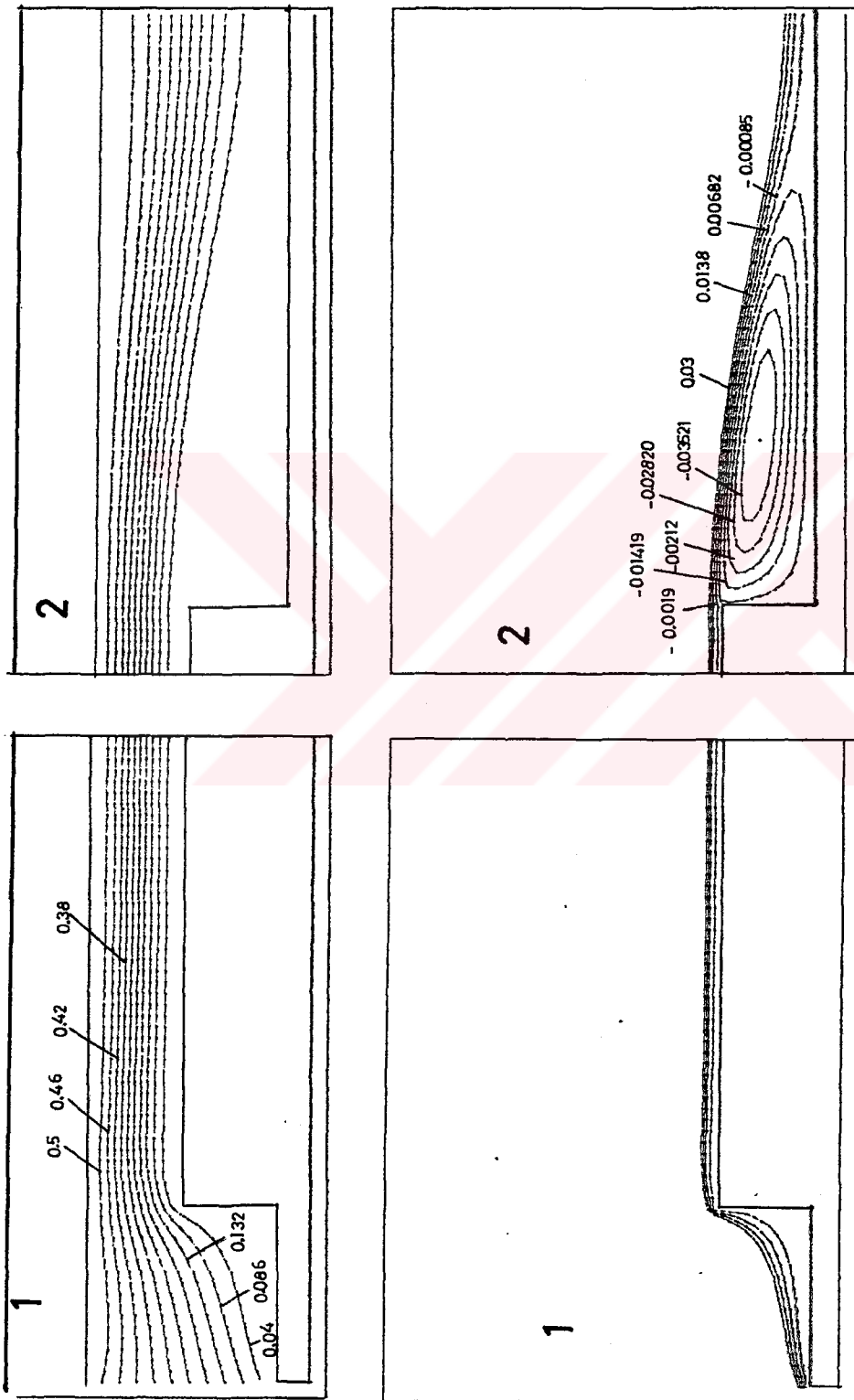


Figure 6.9a) The stream function distribution for one step channel case.

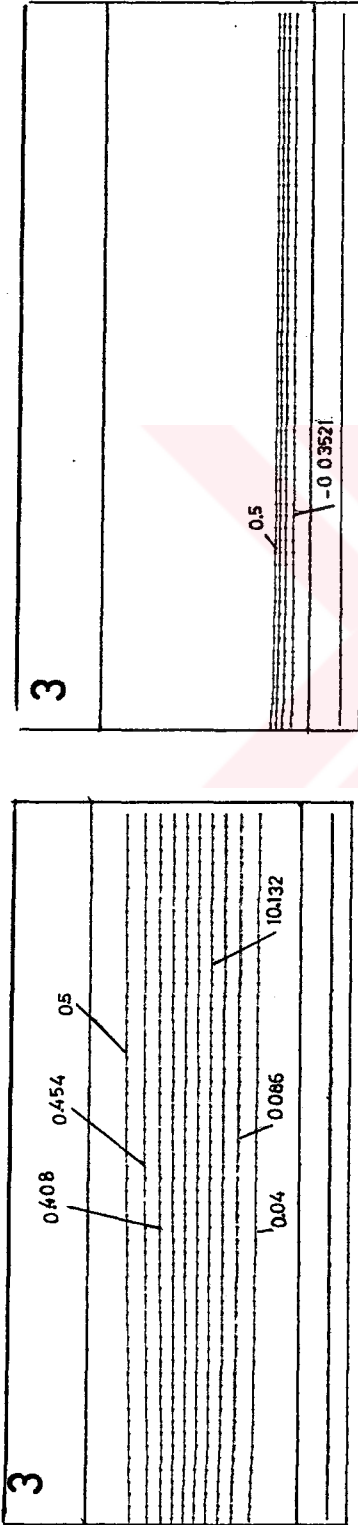


Figure 6.9b) The stream function distribution for one-step channel case.

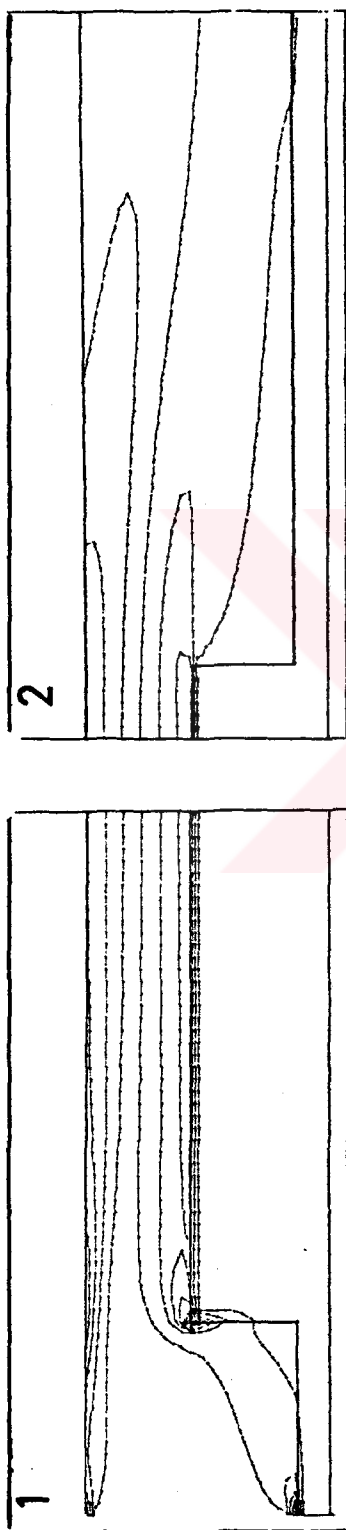


Figure 6.10 Vorticity distribution for one-step channel case.

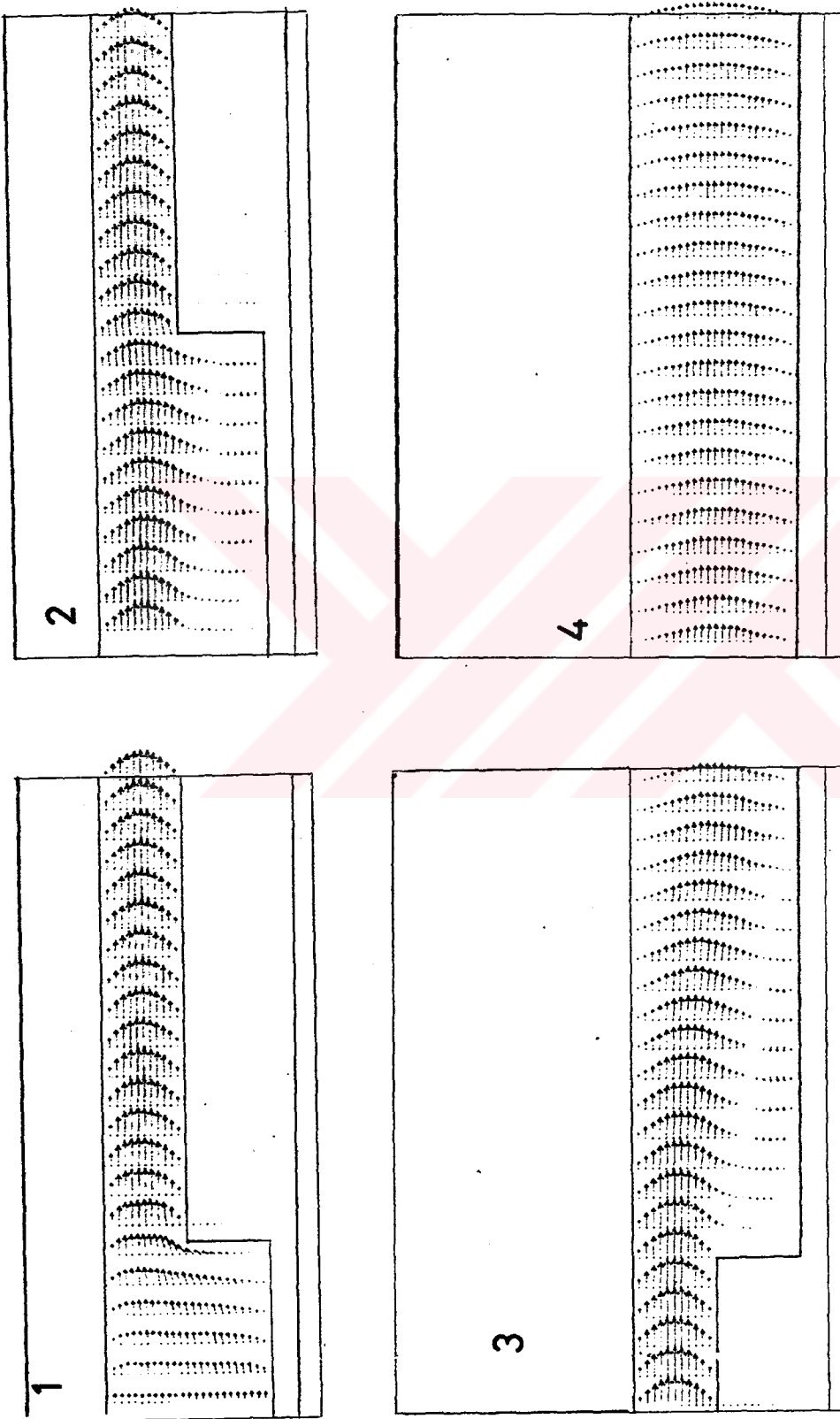


Figure 6.11 Velocity field for two step channel case.

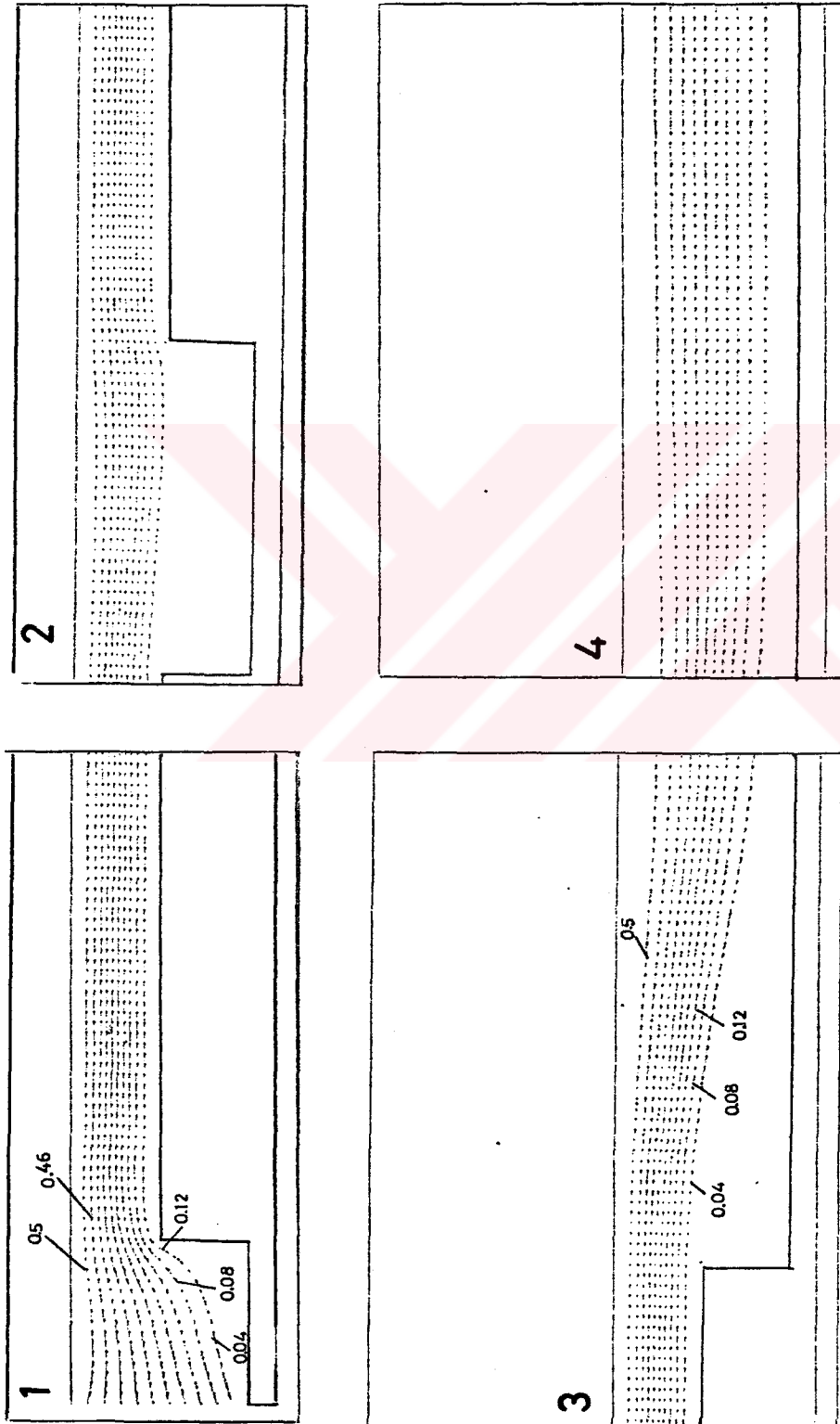


Figure 6.12a) Stream function distribution for two-step channel case.

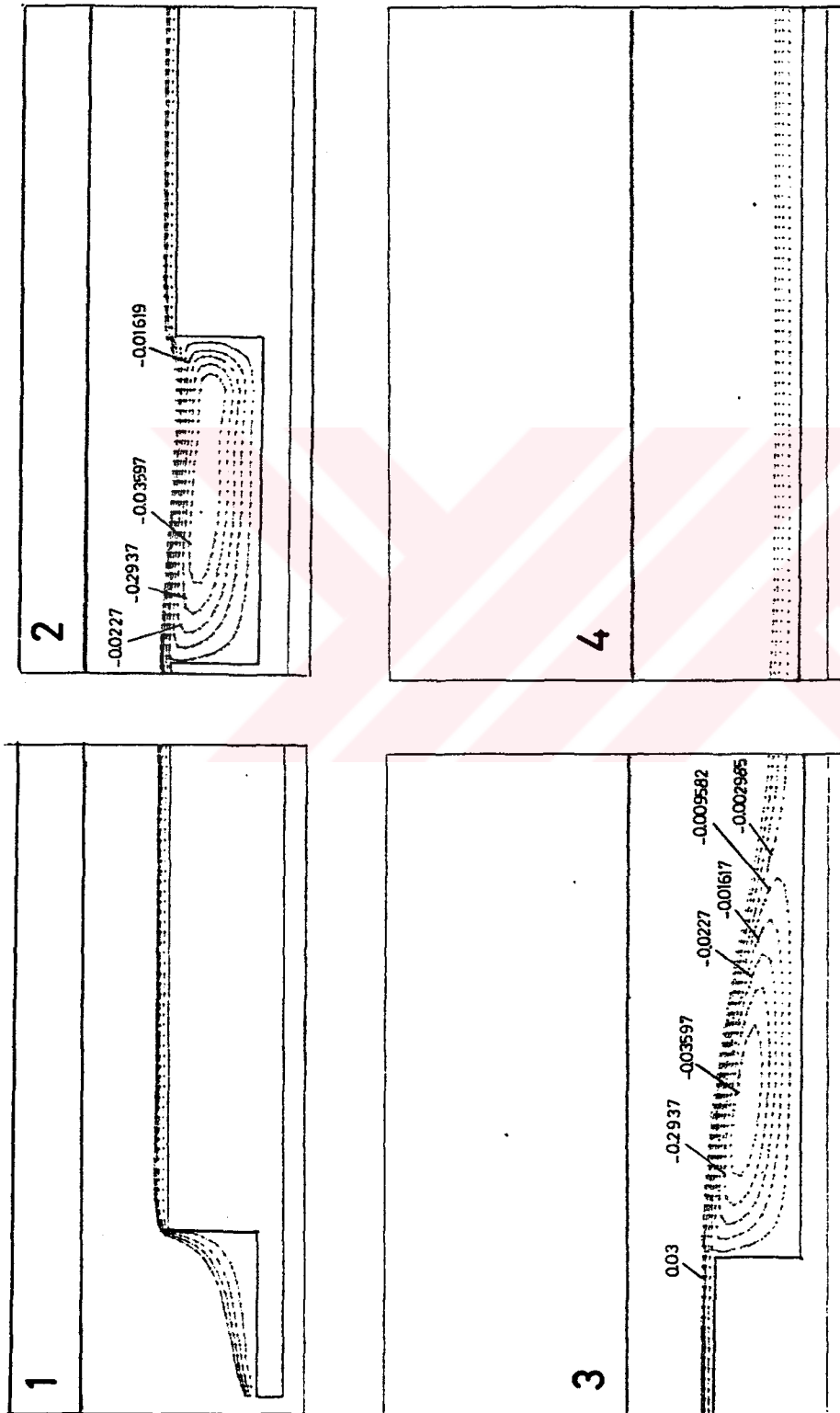


Figure 6.12b) Stream function distribution for two-step channel case.

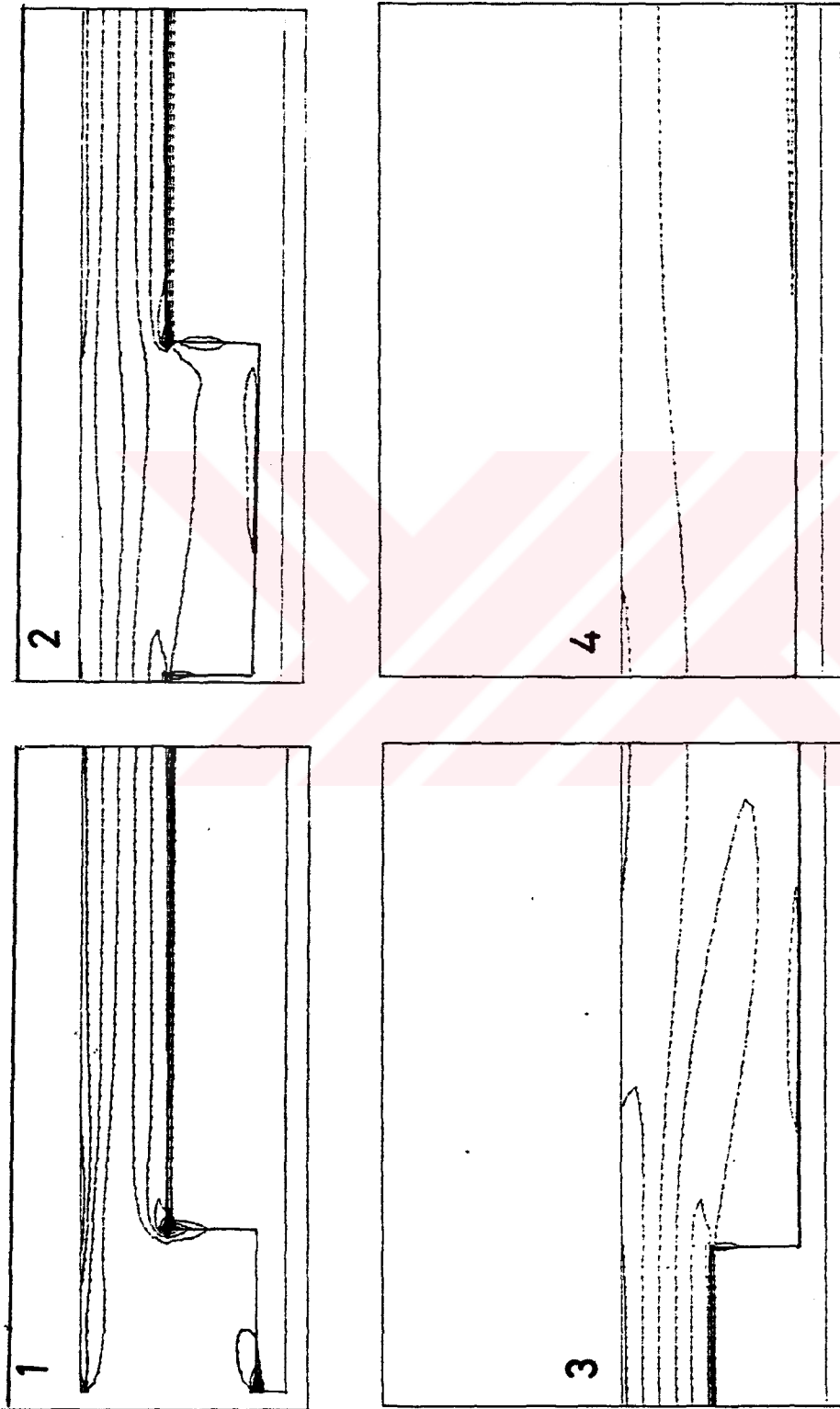


Figure 6.13 Vorticity distribution for two-step channel case.

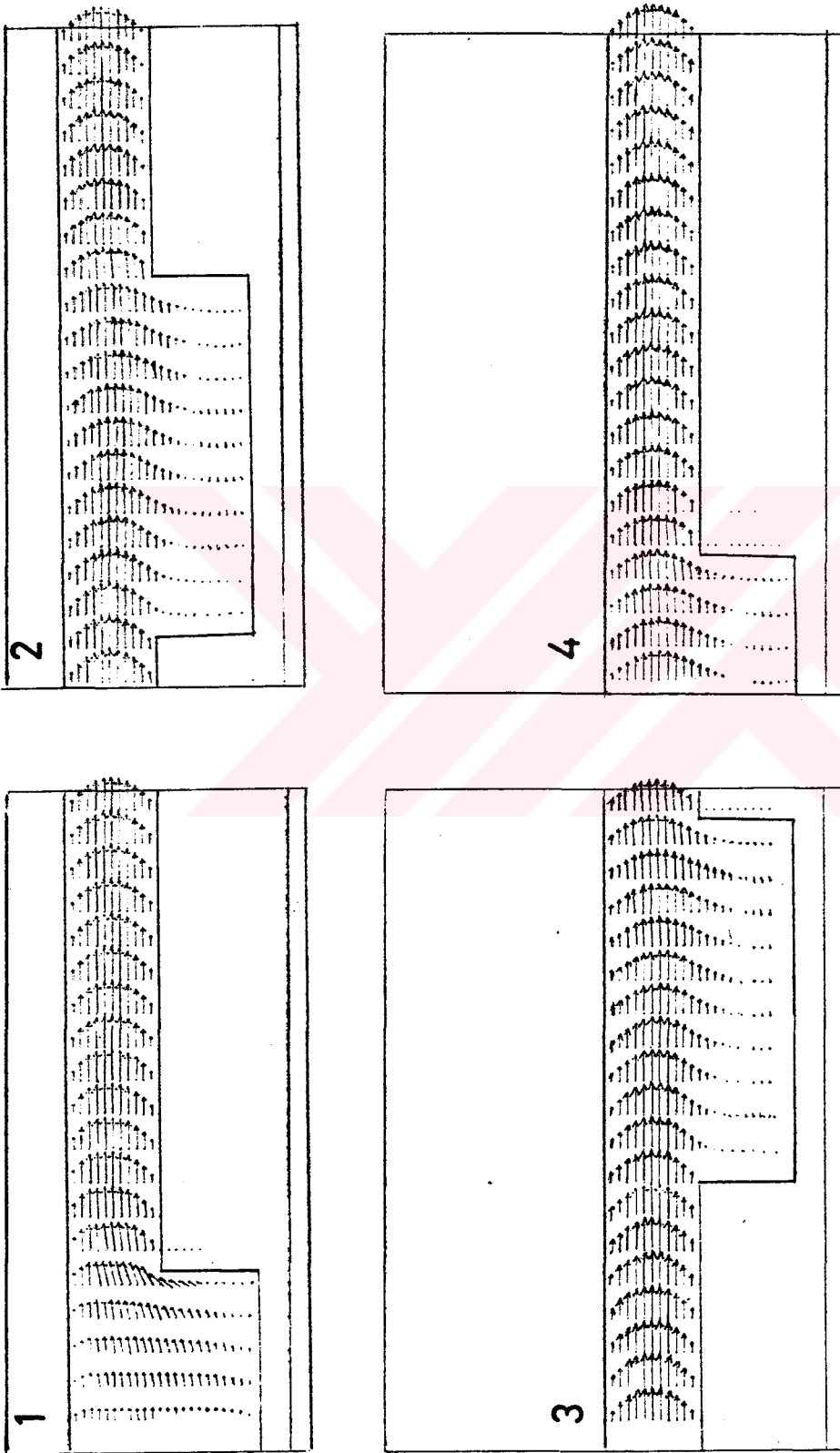


Figure 6.14a) Velocity field for three step-channel case



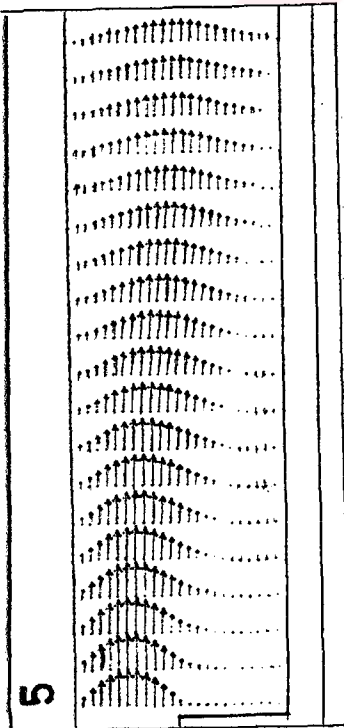
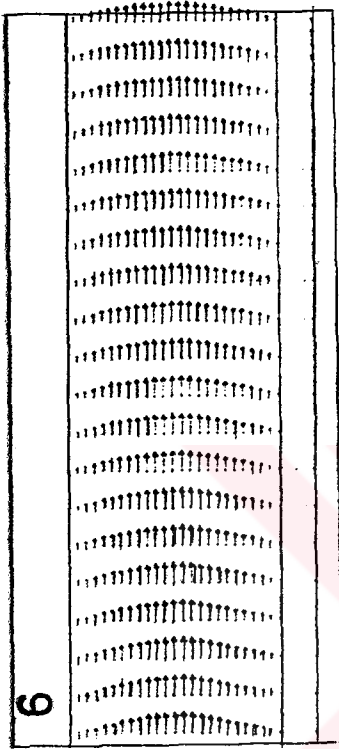


Figure 6.14b) Velocity field for three step-channel case

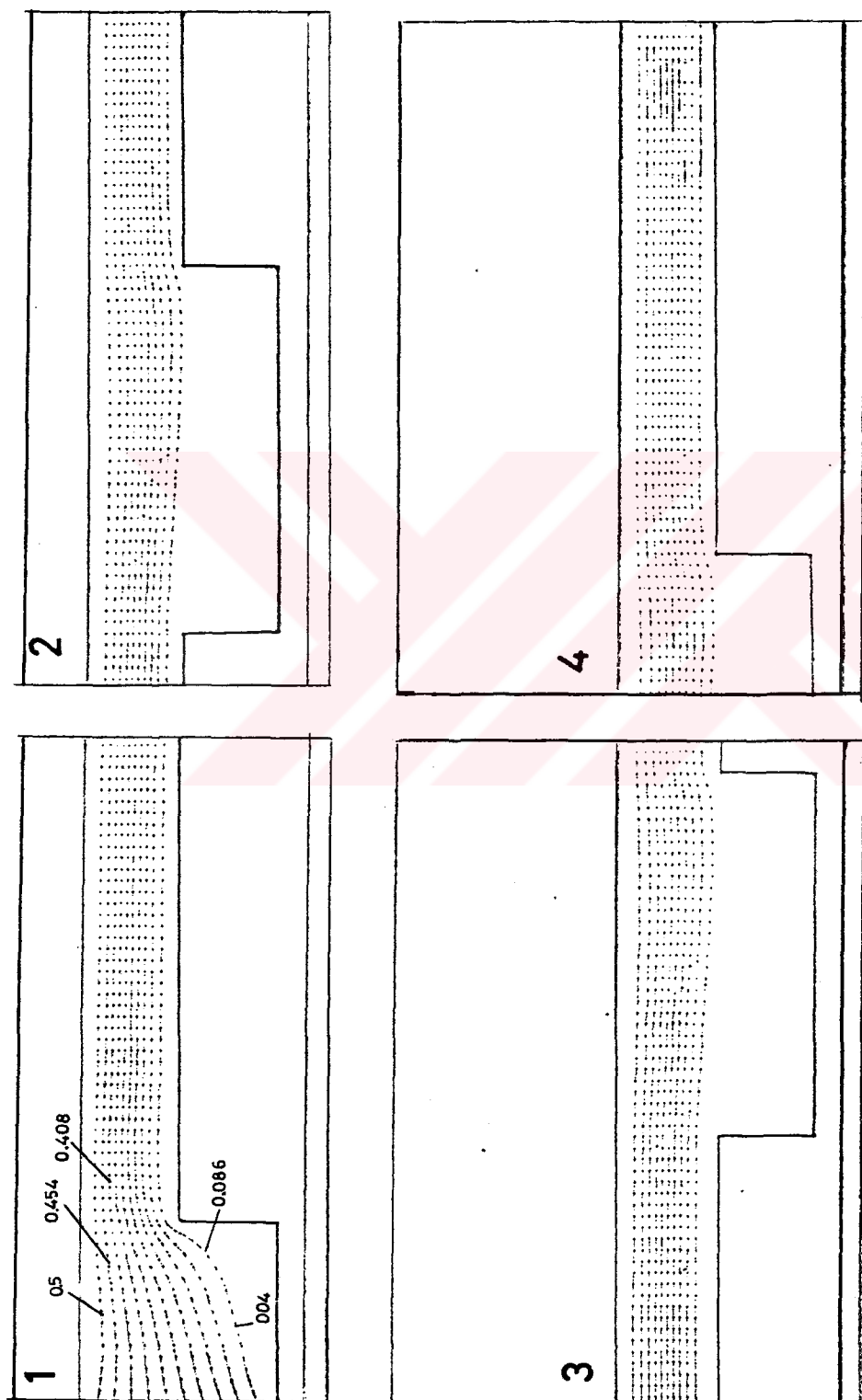


Figure 6.15a) Stream function distribution for three-step channel case.

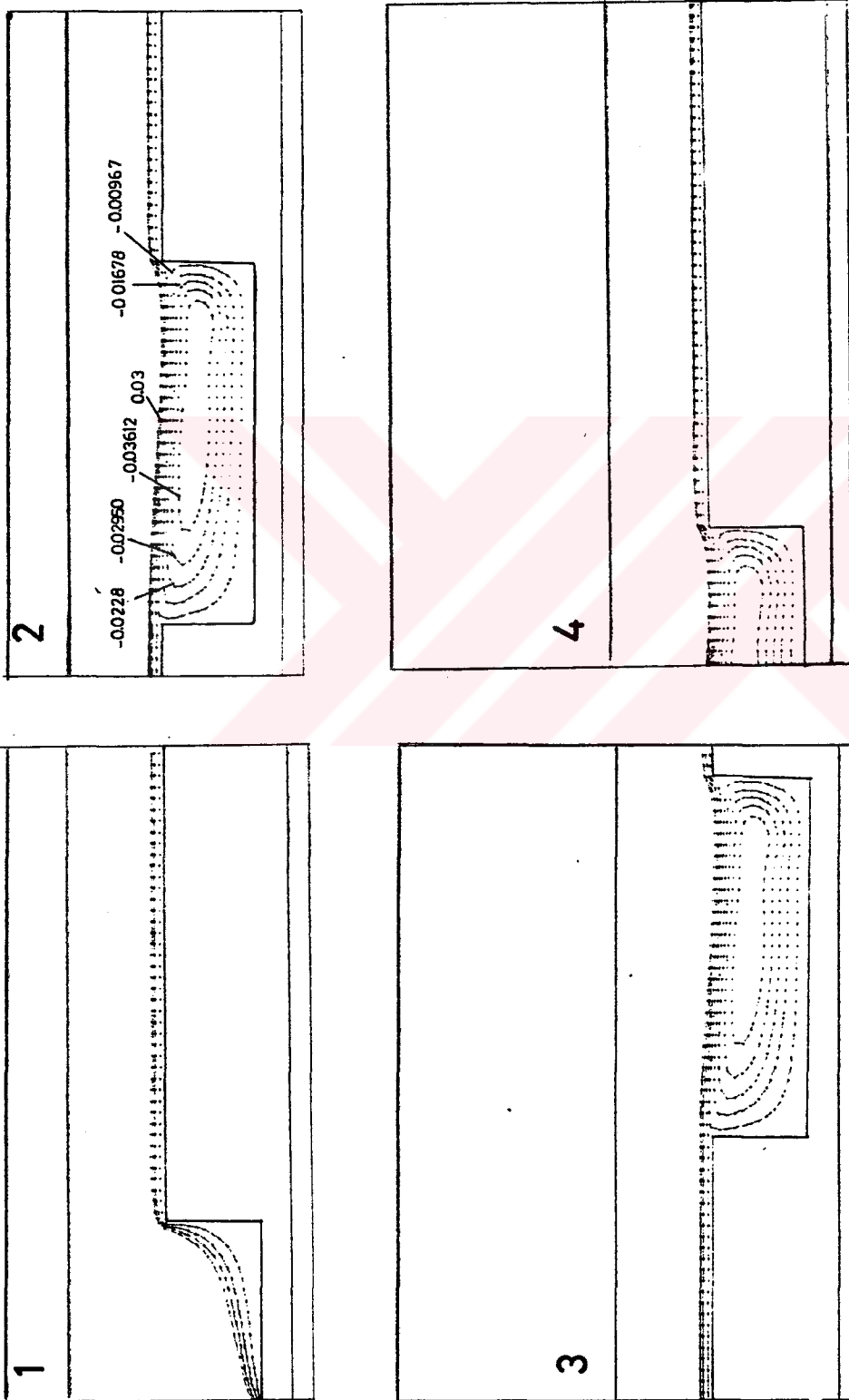


Figure 6.15b) Stream function distribution for three-step channel case.

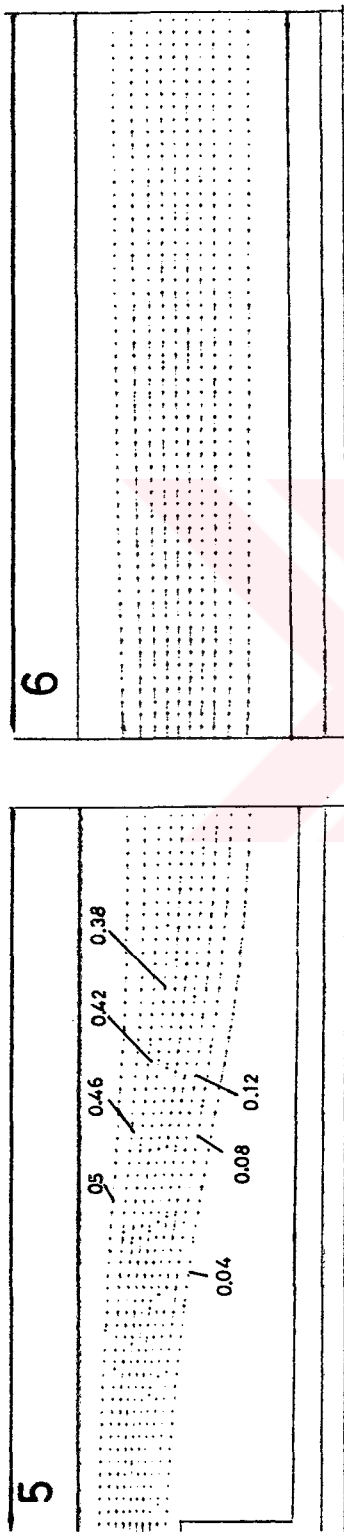


Figure 6.15c) Stream function distribution for three-step channel case.

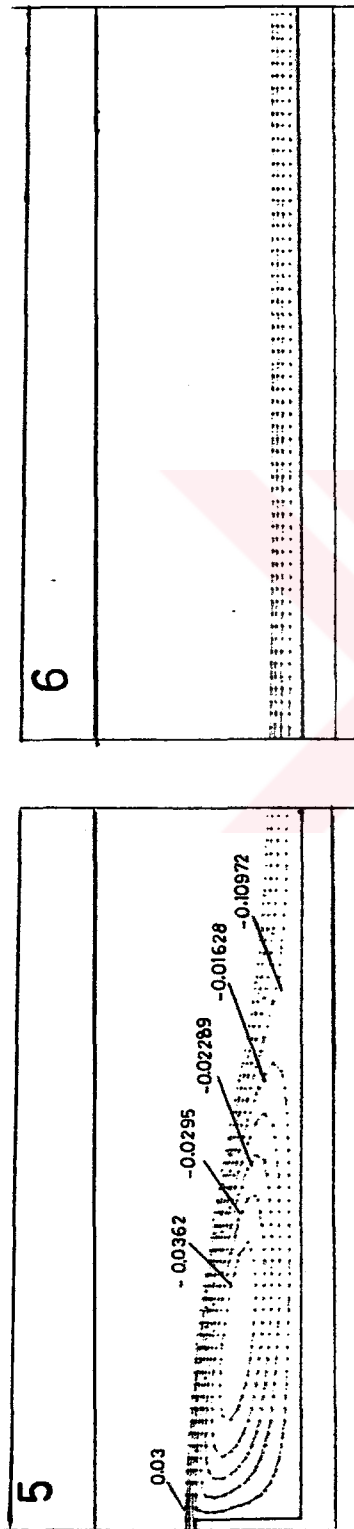


Figure 6.15d) Stream function distribution for three-step channel case.

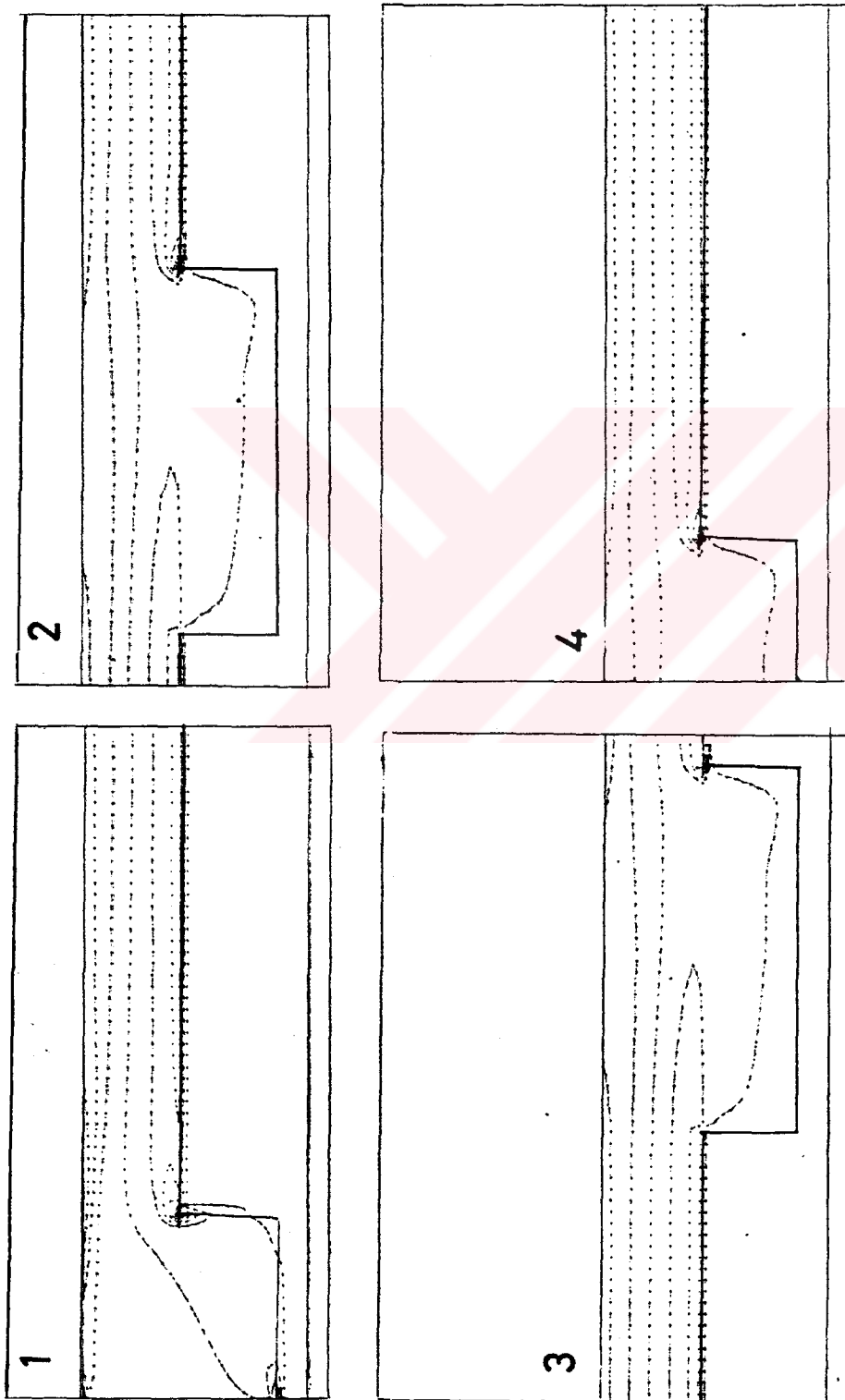


Figure 6.16a) Vorticity distribution for three-step channel case.

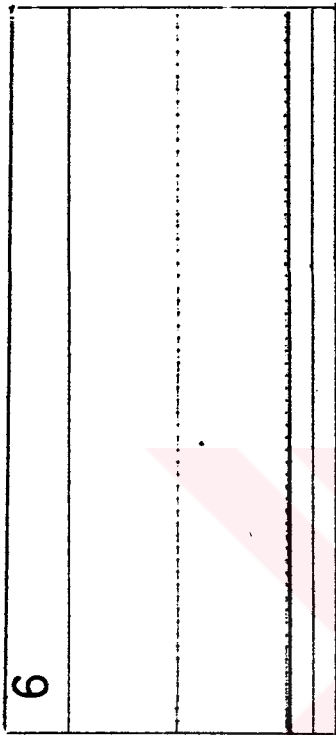
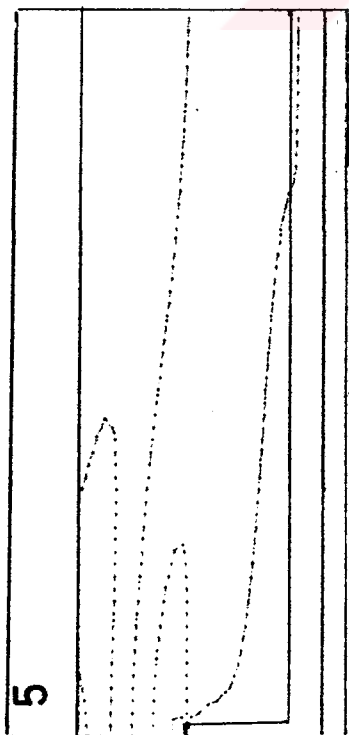


Figure 6.16b) Vorticity distribution for three-step channel case.

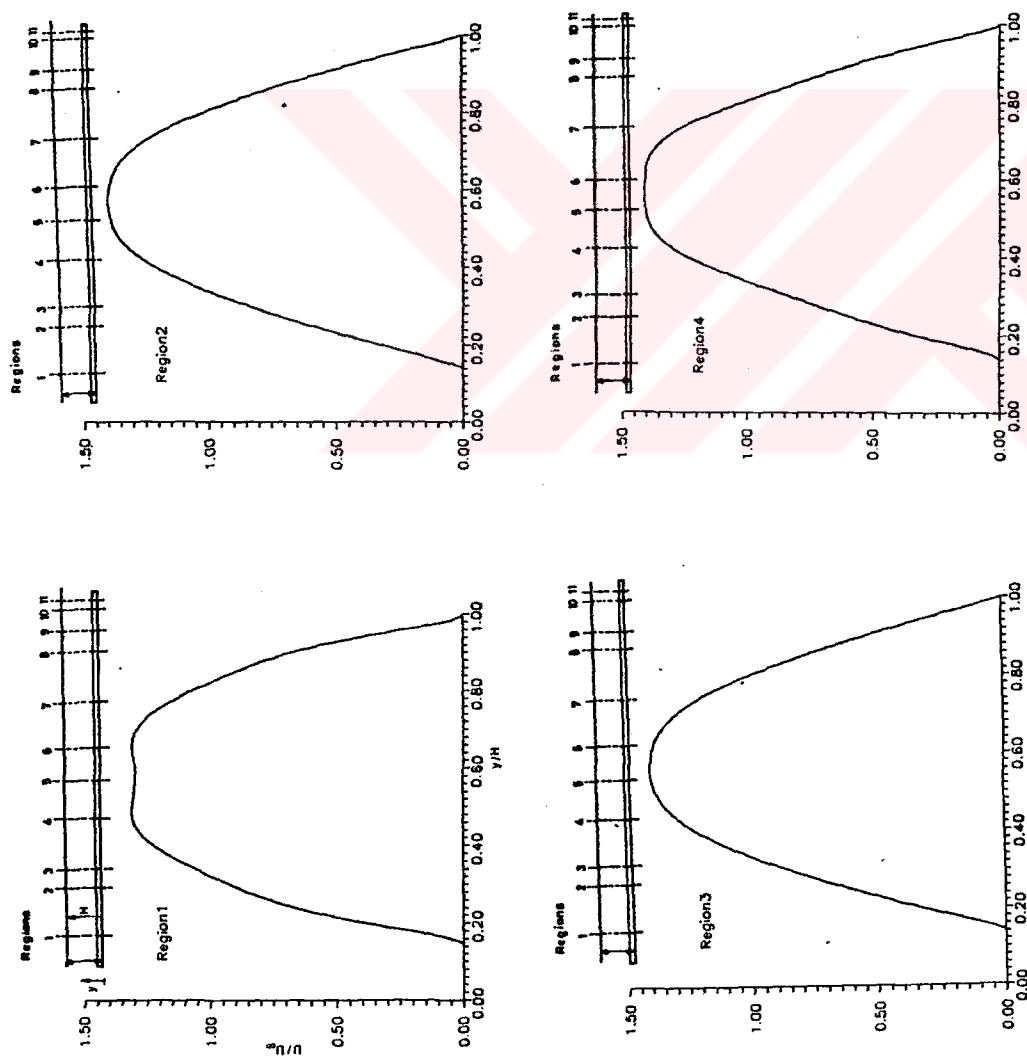


Figure 6.17a) The velocity profiles at various sections for the channel case.



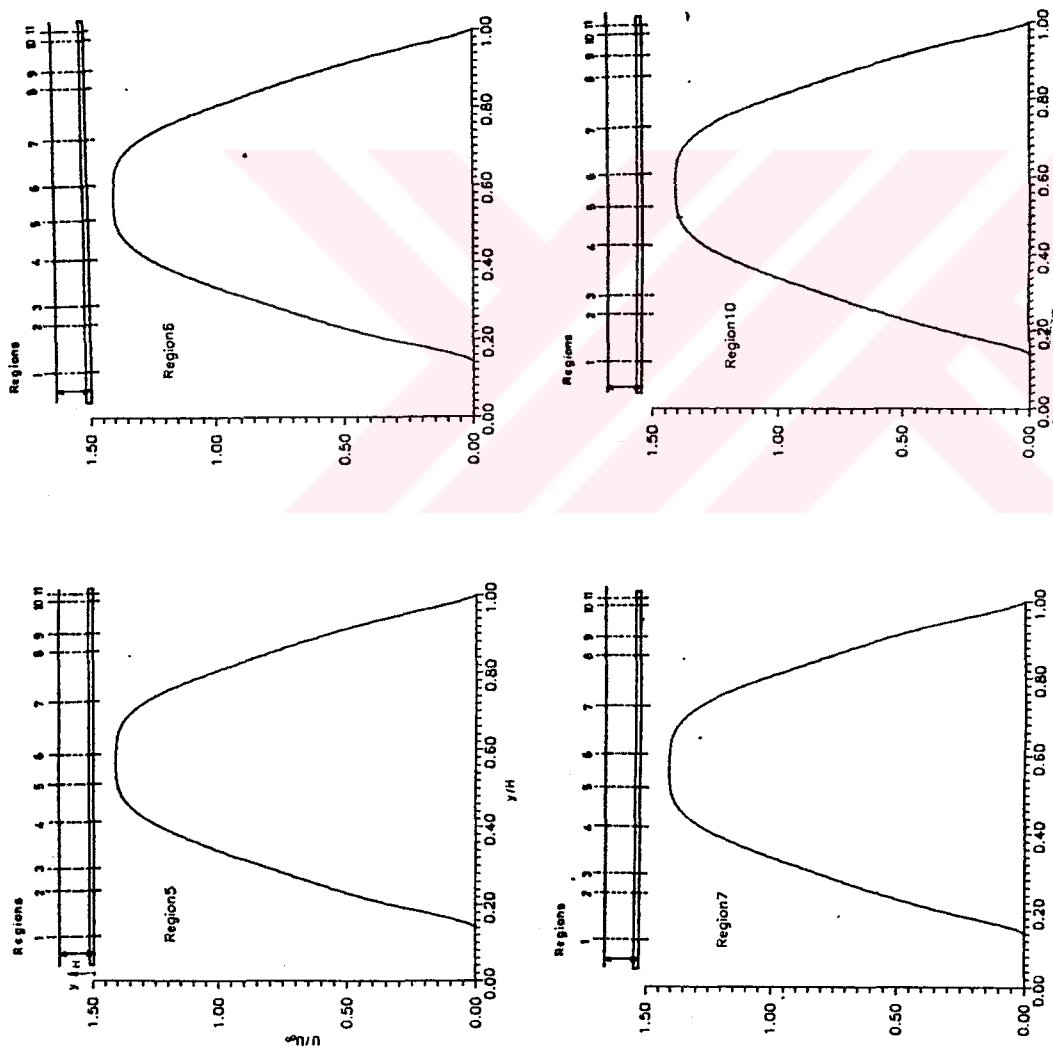


Figure 6.17b) The velocity profiles at various sections for the channel case.

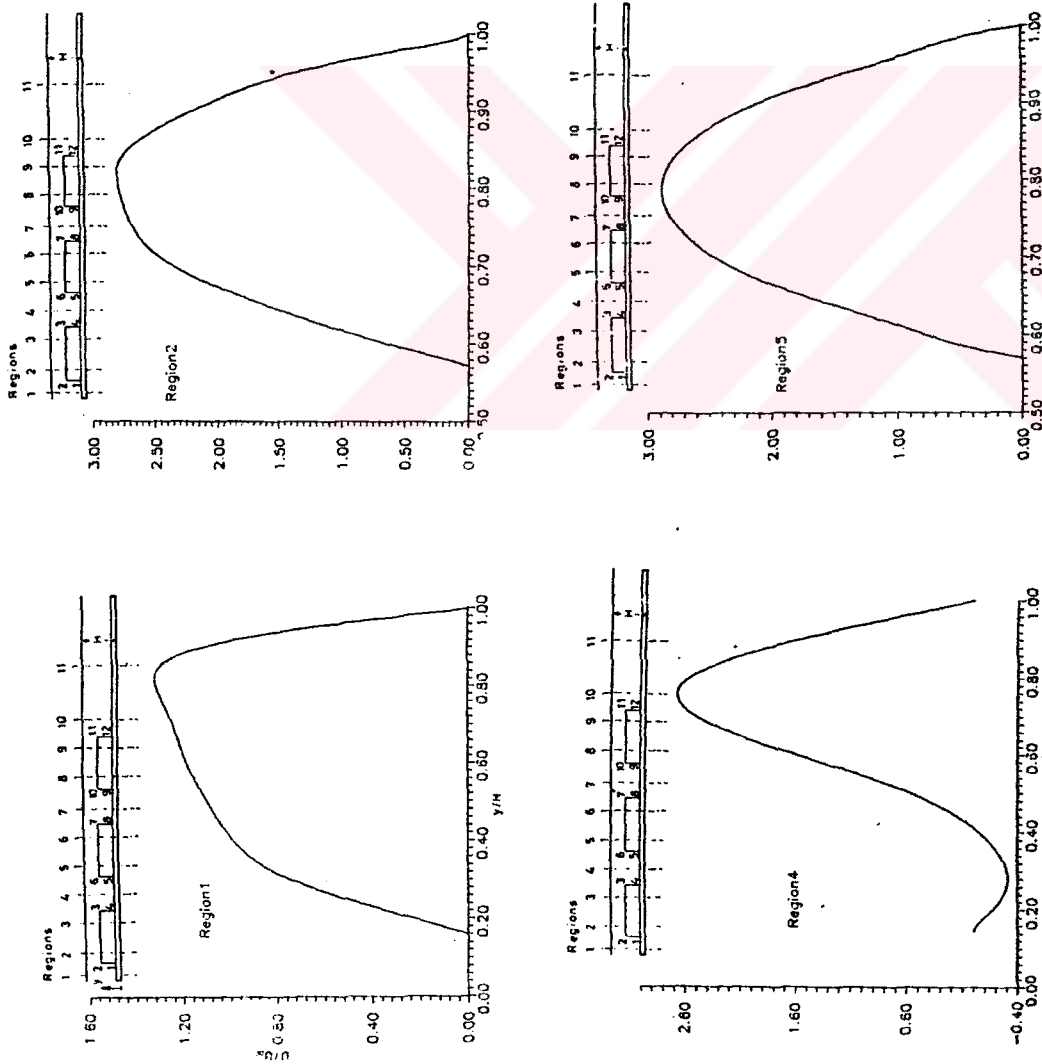


Figure 6.18a.) The velocity profiles at various sections for the three-step channel case.

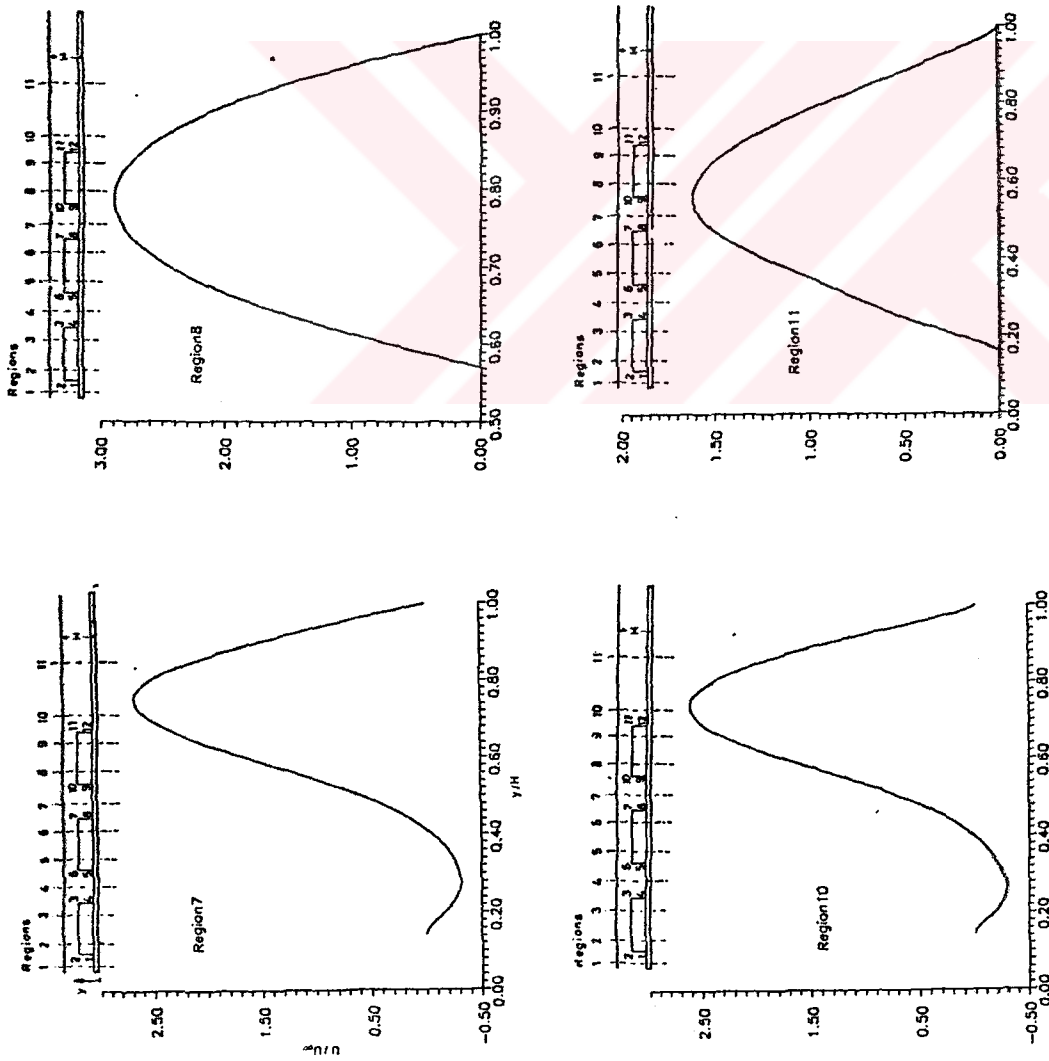


Figure 6.18b) The velocity profiles at various sections for the three-step channel case.

## CHAPTER 7

### THERMAL FIELD

The computer code is validated with some known analytical results which are the exact solutions of the Navier–Stokes and energy equation. First check was conducted inside a narrow channel with constant wall temperature. Flow starts impulsively and develops inside the channel. Corresponding Reynolds number is  $Re = 200$  and Prandtl number is  $Pr = 0.7$ . The upper wall is at temperature,  $T_{u,w} = 1$ , and the lower wall is at  $T_{l,w} = 3$ . Figure 7.1a shows the resultant steady Nusselt number,  $Nu$ , distribution. Steady state solution for a constant upper and lower wall temperature case supplied from Arpaci [43] shows that mean averaged Nusselt number is  $Nu = 3.77$ . For the same geometry and boundary conditions, the bulk temperature distribution is depicted in Figure 7.1b. Its distribution shows rather smooth development with channel length. In Figure 7.1c at the exit plane, the computer solution is checked against the analytical solution. Computed results show an excellent agreement near the walls although some numerical errors occur near the centerline.

Figure 7.2 shows the variation of temperature along the channel axial station where solid–fluid interaction is simulated by using a conjugate solution technique. Relevant parameters and temperature boundary conditions are shown on the first sketch of Figure 7.2. At the entrance, temperature profile in the fluid domain shows a curvilinear change whereas in the solid domain profiles are linear with linear increments from the bottom wall temperature,  $T_{w,b} = 6$ , to the lower wall temperature  $T_{w,l} = 3$ . Near the exit the fluid temperature distribution nearly keeps its property with the sign of the fully developed conditions. Changes in the middle domains are naturally expected since the fluid starts impulsively with the nondimensionalized temperature of zero. This is clearly seen in region one. In the progressing regions fluid temperatures increase since the heat conducted from the solid portion is being convected into the fluid. The rate of heat transfer becomes steady after region five. This is also due to the conduction in fully developed flow conditions.

In Figure 7.3, steady–state temperature profiles are shown at various regions of a one-step channel with heat sources which are located at the upper level of the step ( $H'/H = 5/6$ ). Heat source presence is shown, clearly in all regions of the channel. Therefore profiles change their slopes in the region where heat sources are located. Maximum temperature reaches a nondimensional value of 4.

Figure 7.4 shows additional various temperature profiles for a one-step channel case. Sources located upper part of the step as it was in Figure 7.3. In order to understand the effect of the source magnitude, for a comparison, two other cases with higher source magnitude are considered. Practically, one says that increasing

source magnitude results in increasing maximum temperature at the fluid and solid domain while the fluid properties are kept the same.

### 7.1 One-Step Thermal Field

Figure 7.4, 7.6, and 7.7 show one-step channel profiles for three different source location positions. In the region one, for three different source location positions profiles are almost the same. In the region two, profiles become quite different, particularly around the center of the channel. Higher the location source in the step higher the maximum temperature in the domain but thinner the temperature layer which is around the maximum. One sees same thing in the region four and the region five where profiles show same trend but different maximum temperature values. When the source location is at the lowest position, maximum temperature distribution captures comparatively thick part in the solid domain, but the maximum temperature is comparatively low. When the location of the source position is highest, the maximum temperature distribution captures thinner part in the solid and it becomes the highest one of three cases considered.

### 7.2 Two-Steps Thermal Field

In Figure 7.8, two step channel temperature profiles are shown. Sources are located at the higher position in the step. Profiles on the steps are similar and these profiles are the maximum temperature profiles. It is important to note that in the fluid portions the maximum temperature profile is seen in region seven. However in the region eight, the temperature profile shows higher values than the temperature

profile in the region four.

### 7.3 Three-Steps Thermal Field

Figure 7.9 shows various profiles of temperatures in three-step channel. Sources are located at higher position in the steps. The maximum temperature profiles are seen on the steps as in two-step channel case. Profiles on the steps show comparatively slight changing to the cavity profiles, region 4 and 5, naturally having increased values in the flow direction. One sees that in the recirculation zone (Region 10) profile values are higher than ones in the cavity zones. In the cavity region velocities are not high and fluid moves slowly. This causes effective losses of heat by the conduction into the cooled substrate.

### 7.4 Iso Temperature Contours

In Figure 7.10a and 7.10b wall temperature distributions are shown. Corresponding  $Re$  is 200 and  $Pr$  is 0.7. On the steps, for each different step cases, wall temperatures are maximum. This is quite natural since sources are located in the steps. It can be seen that critical temperature values can be reached on the steps. For each case the general trend is the same except maximum values of the considered case.

Figure 7.10c and 7.10d show one-step channel temperature contours with the source at the higher position. One sees here that higher temperature contours show themselves in a thin solid part, but are enough to reach critical temperature of the structure. Figure 7.10e shows some detailed contours of these critical ones indicating that critical values take place in a thin solid part.

Figure 7.10f and 7.10g show temperature contours for the case of one-step channel with the source position at the middle. Careful inspection tells one that, comparatively low temperature contours are shown, but these temperature contours take place thicker part in the solid than the case in which sources are located at the higher position. Above explanations become more clear in Figure 7.10c where temperature contours are depicted in one step-channel with the source location at the lower position. Maximum temperature contours take place in more thicker solid part than two other cases, but with lower values. In this case maximum temperature is three times lower than the case with the higher source location position.

Figure 7.11a and 7.11b show temperature contours in two-step channel with the source location at the higher position. Naturally, higher temperature contours take place at the upper part of the step therefore high temperature contours extend far enough away from the solid parts. In the cavity region, top and bottom walls contours do not make a contact.

Figure 7.11c, 7.11d and 7.11e show the temperature contours for the middle position of two-step channel case. Again higher temperature contours take more thicker solid part than one, where sources placed in higher position. At this case in



the cavity, upper and lower walls temperature contours make a contact. In Figure 7.11f and 7.11g heat sources are located the lower position in the solid part. Temperature contours at the higher value, take more thicker place than the other two cases. But the maximum temperature comparatively quite low. This can be easily seen from Figure 7.11g which is the detailed from of the Figure 7.11f.

Figures 7.12a, b, c, d, e show temperature contours in three step channel with source location at the higher position, Figures 7.12f, g, h, k, l, show temperature contours in three step channel with source location at the middle position and Figures 7.12m, n, o, show temperature contours for the same geometry with the source location at the lower position. For step one, two and three geometries, the general trend in temperature contours and the contours at the higher value are the same. When the step number increase in the channel, the temperature values in the cavity regions become higher along the flow direction and more heat carried away by the fluid.

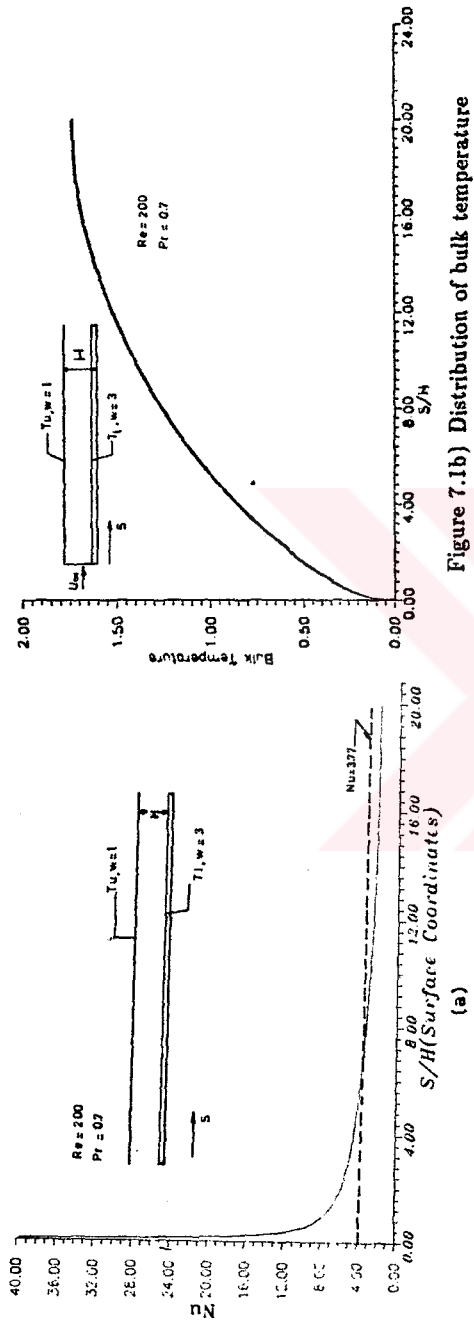


Figure 7.1b) Distribution of bulk temperature

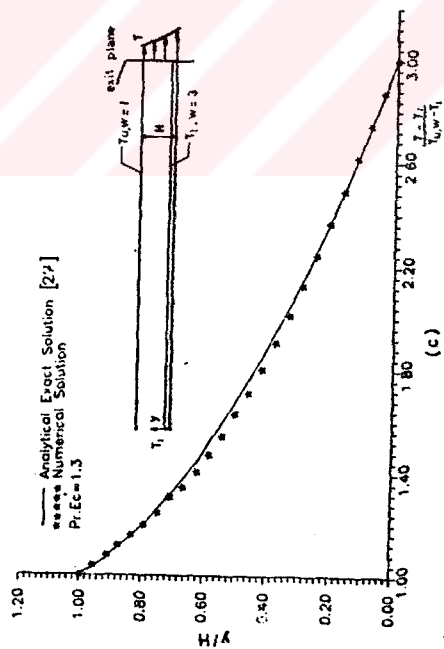
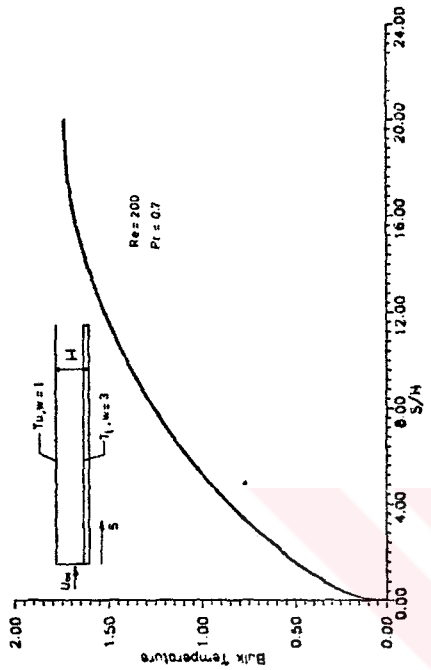


Figure 7.1a) Nusselt number distribution along the lower plate for constant wall temperature.

Figure 7.1c) Distribution of temperature for constant wall case at the exit.

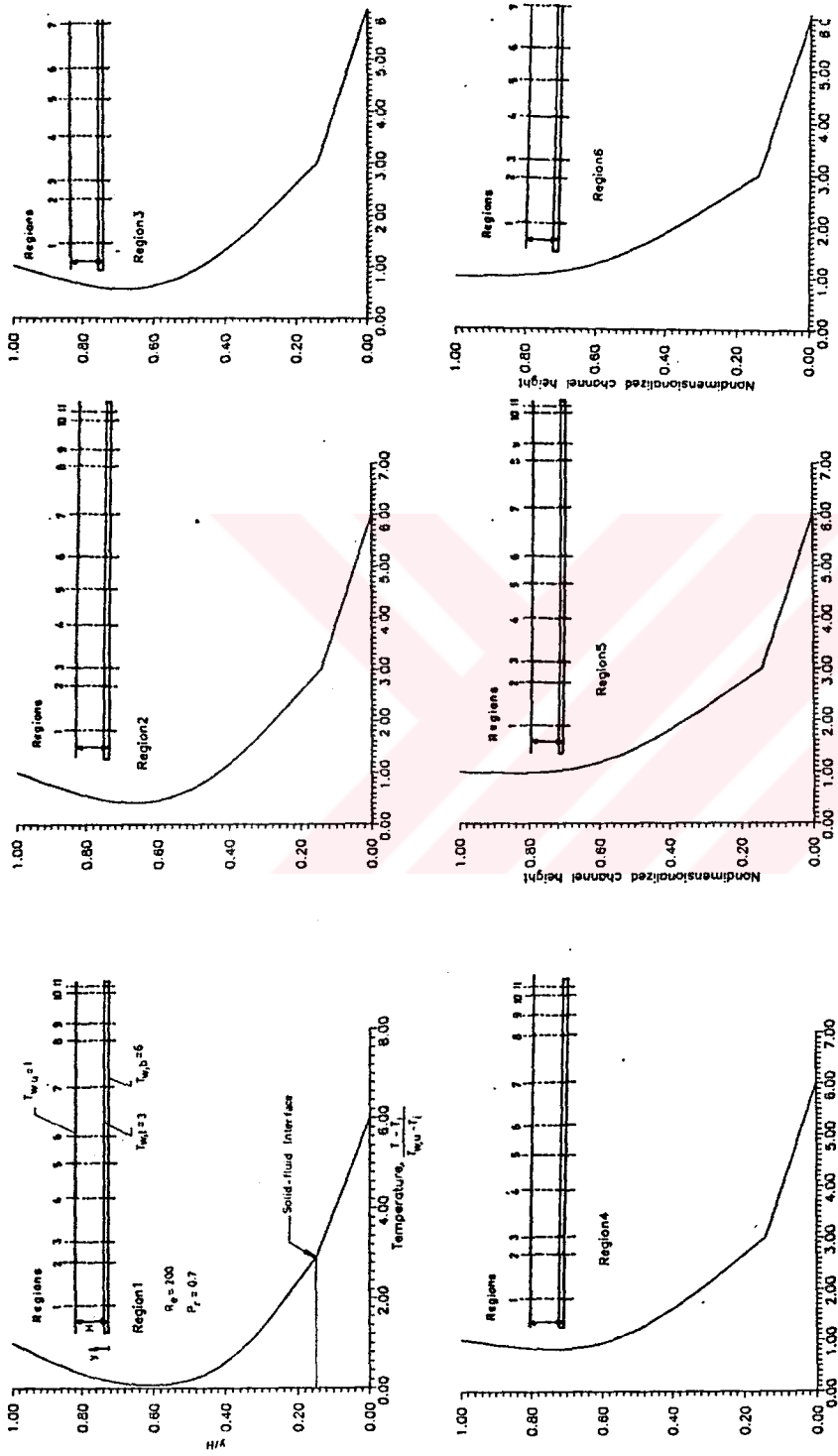


Figure 7.2 Solid wall-fluid interaction and temperature profiles at various axial station.  
( $Re=200$ ,  $Pr=0.7$ )

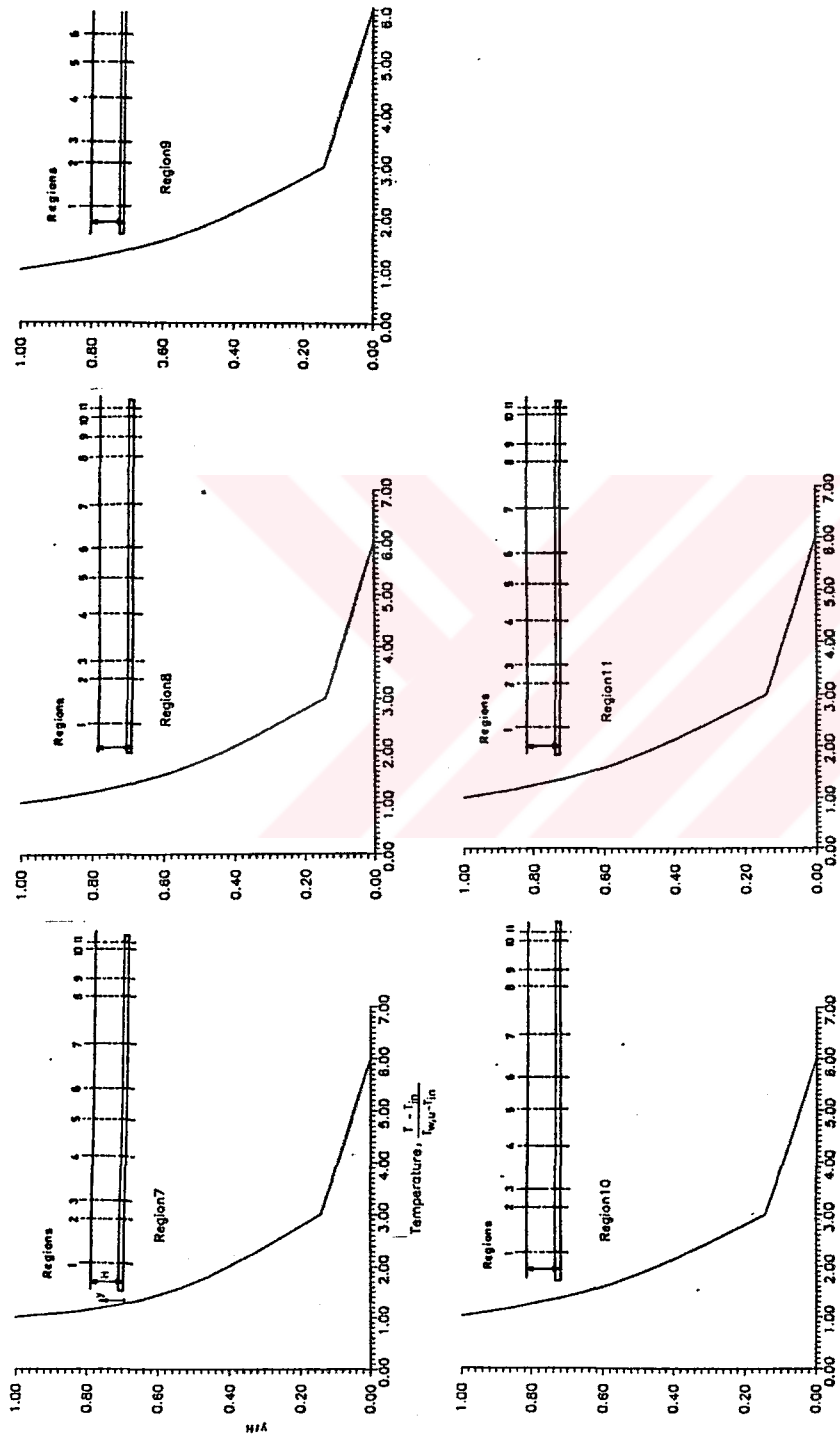


Figure 7.2 Solid wall-fluid interaction and temperature profiles at various axial station.  
( $Re=200$ ,  $Pr=0.7$ )

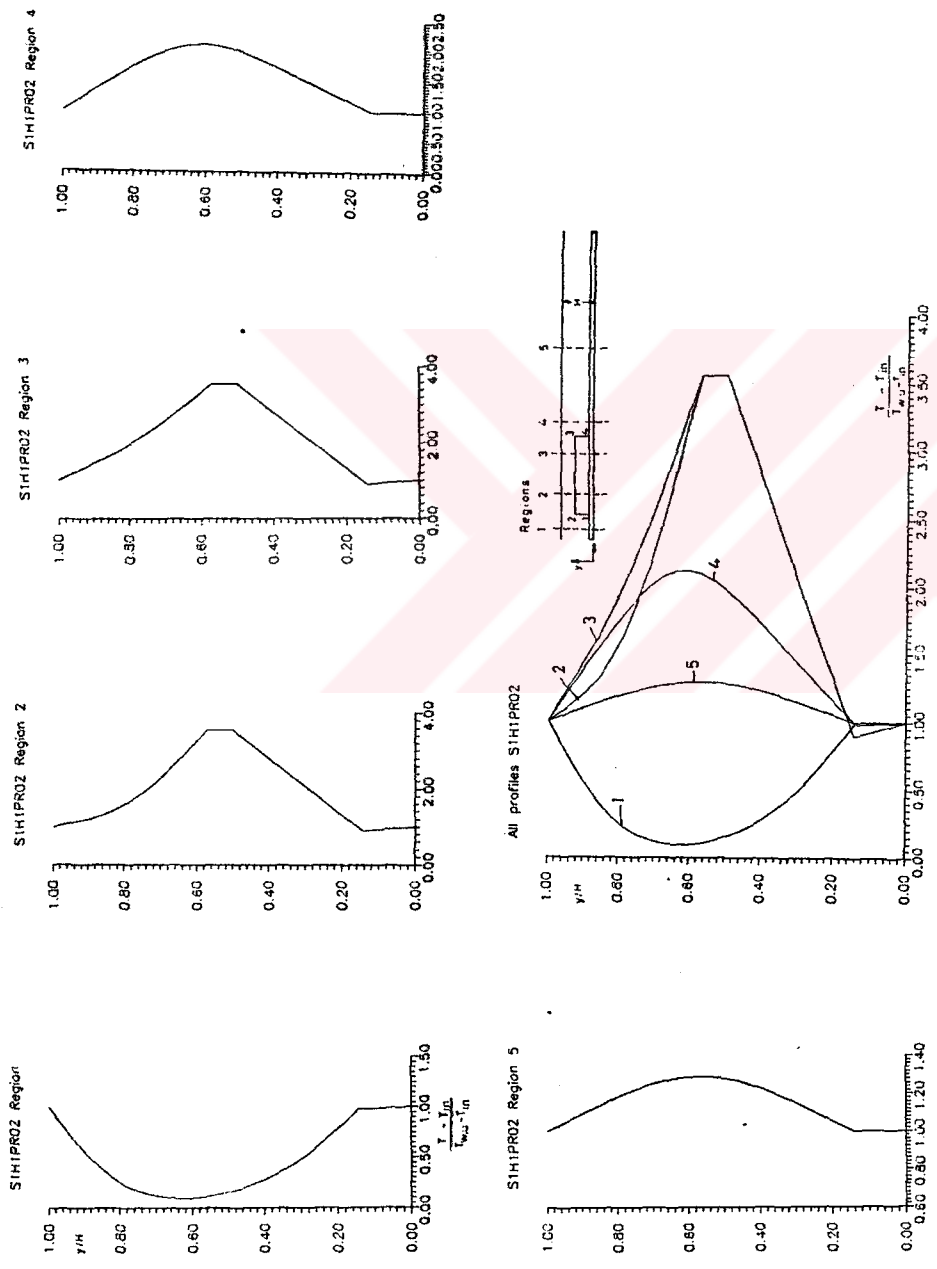


Figure 7.3 Temperature distribution at various sections in one-step channel case with source location at a position,  $H'/H=5/6$ , ( $Re=200$ ,  $Pr=0.2$ )

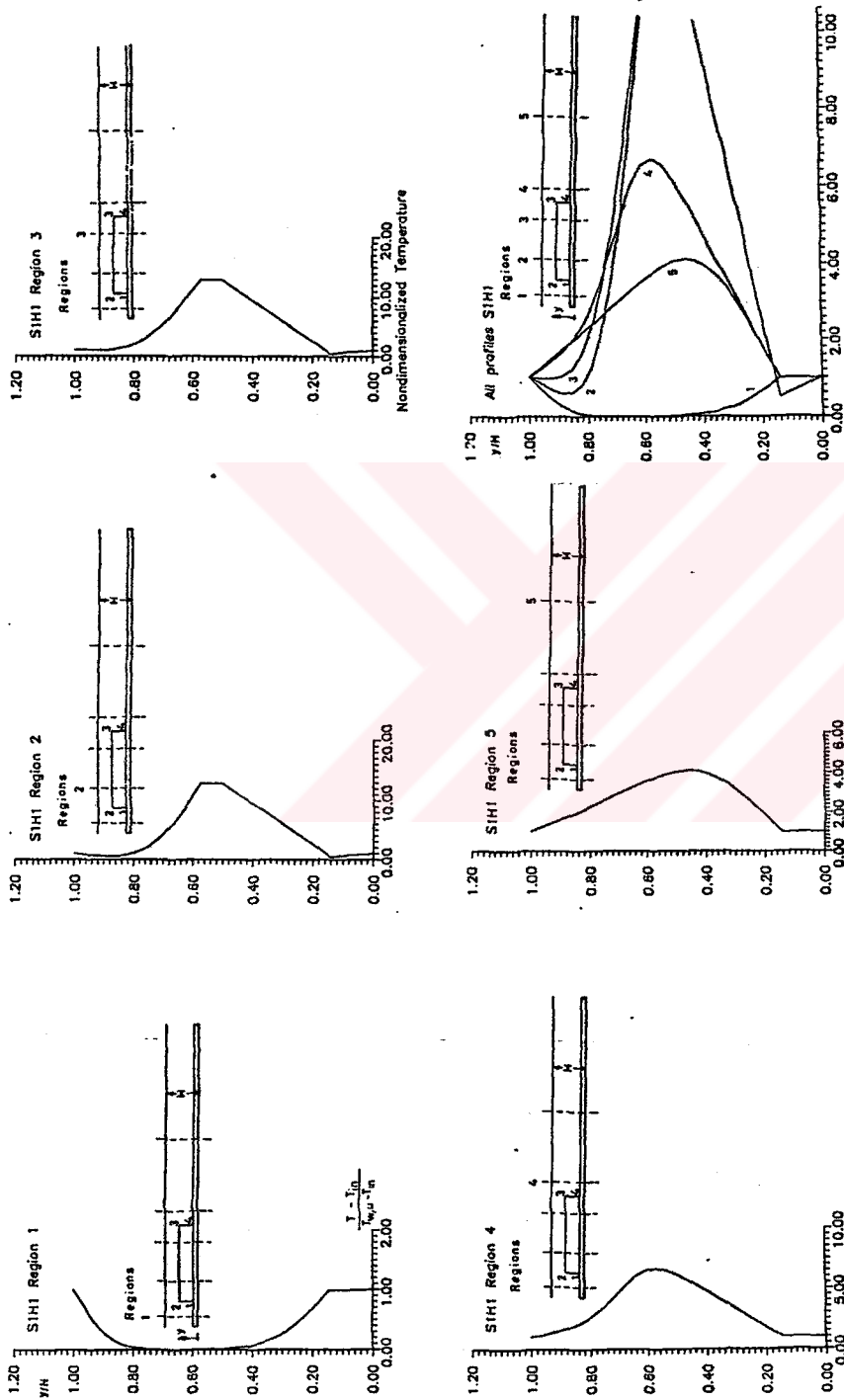


Figure 7.4 Temperature distribution at various section in one-step channel case with source location at a position,  $H'/H=5/6$ , ( $Re=200$ ,  $Pr=0.7$ )

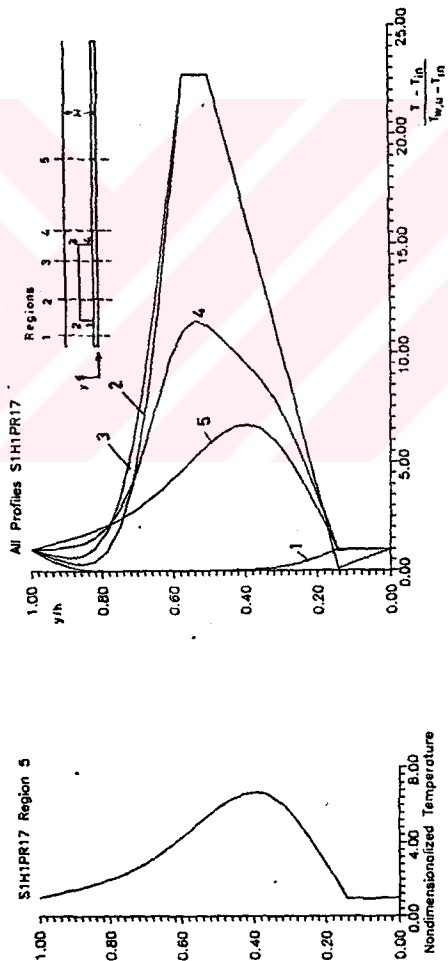
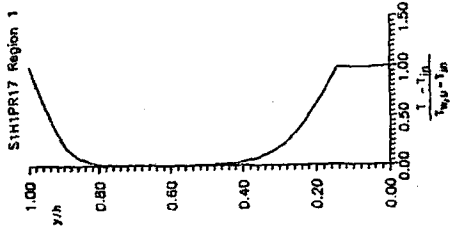
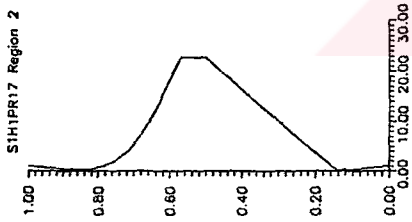
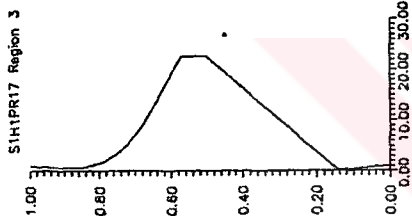
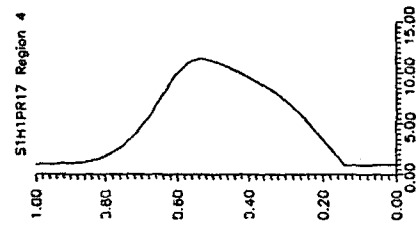


Figure 7.5 Temperature distribution at various section in one-step channel case with source location at a position,  $H'/H=5/6$ , ( $Re=200$ ,  $Pr=1.7$ )

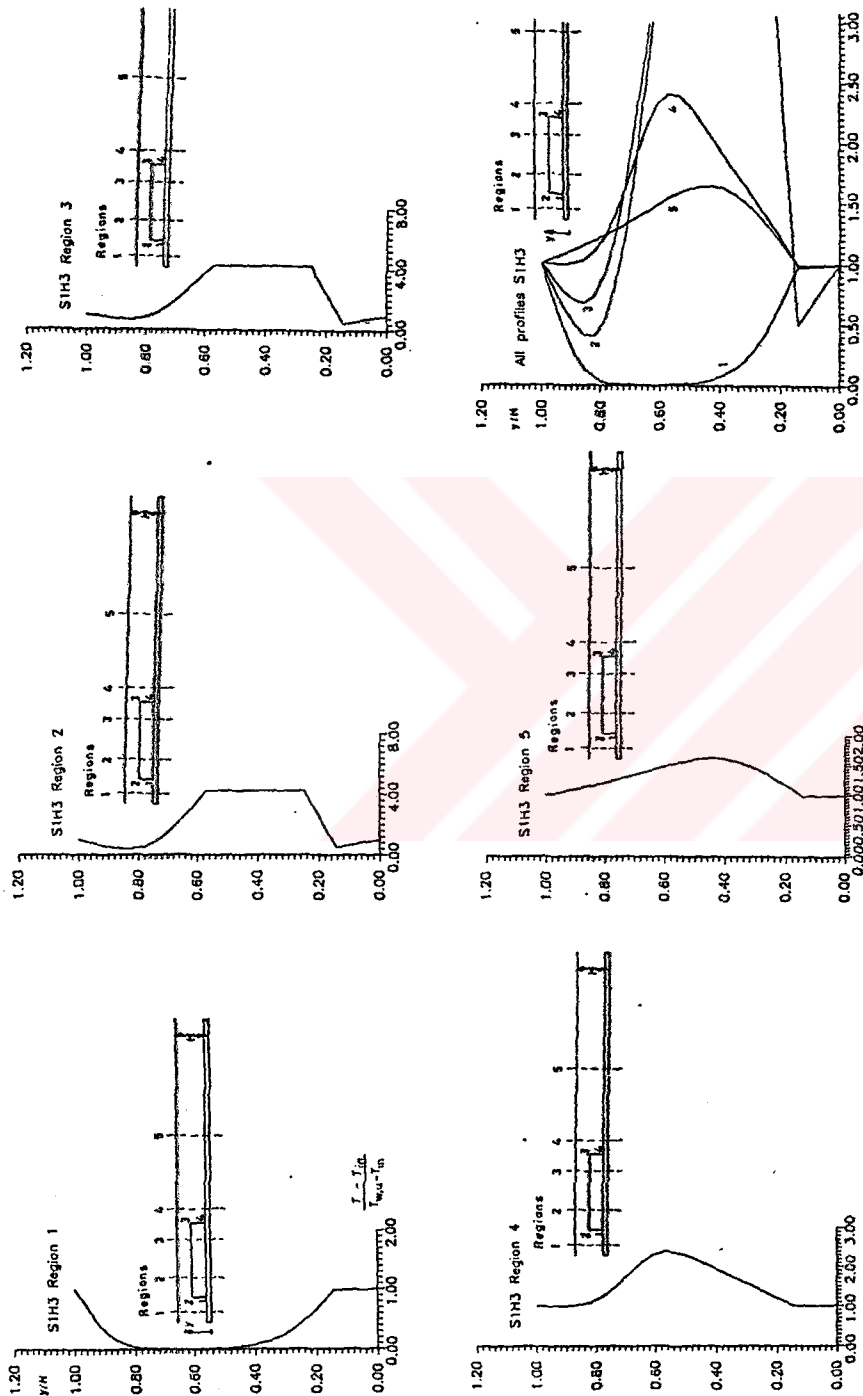


Figure 7.6 Temperature distribution at various section in one-step channel case with source location at a position,  $H'/H=1/4$ , ( $Re=200$ ,  $Pr=0.7$ )



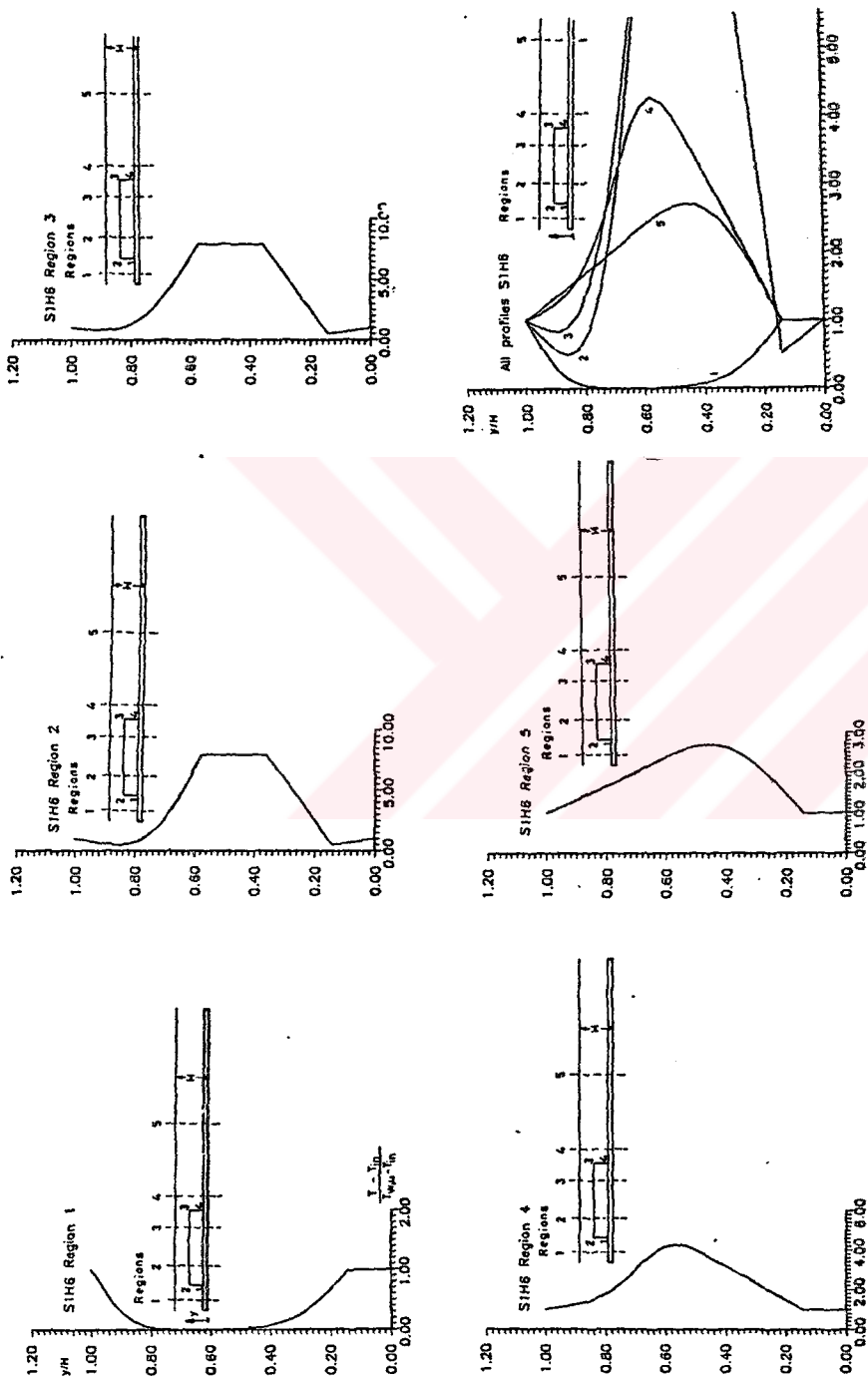


Figure 7.7 Temperature distribution at various section in one-step channel case with source location at a position,  $H/H=1/2$ , ( $Re=200$ ,  $Pr=0.7$ )

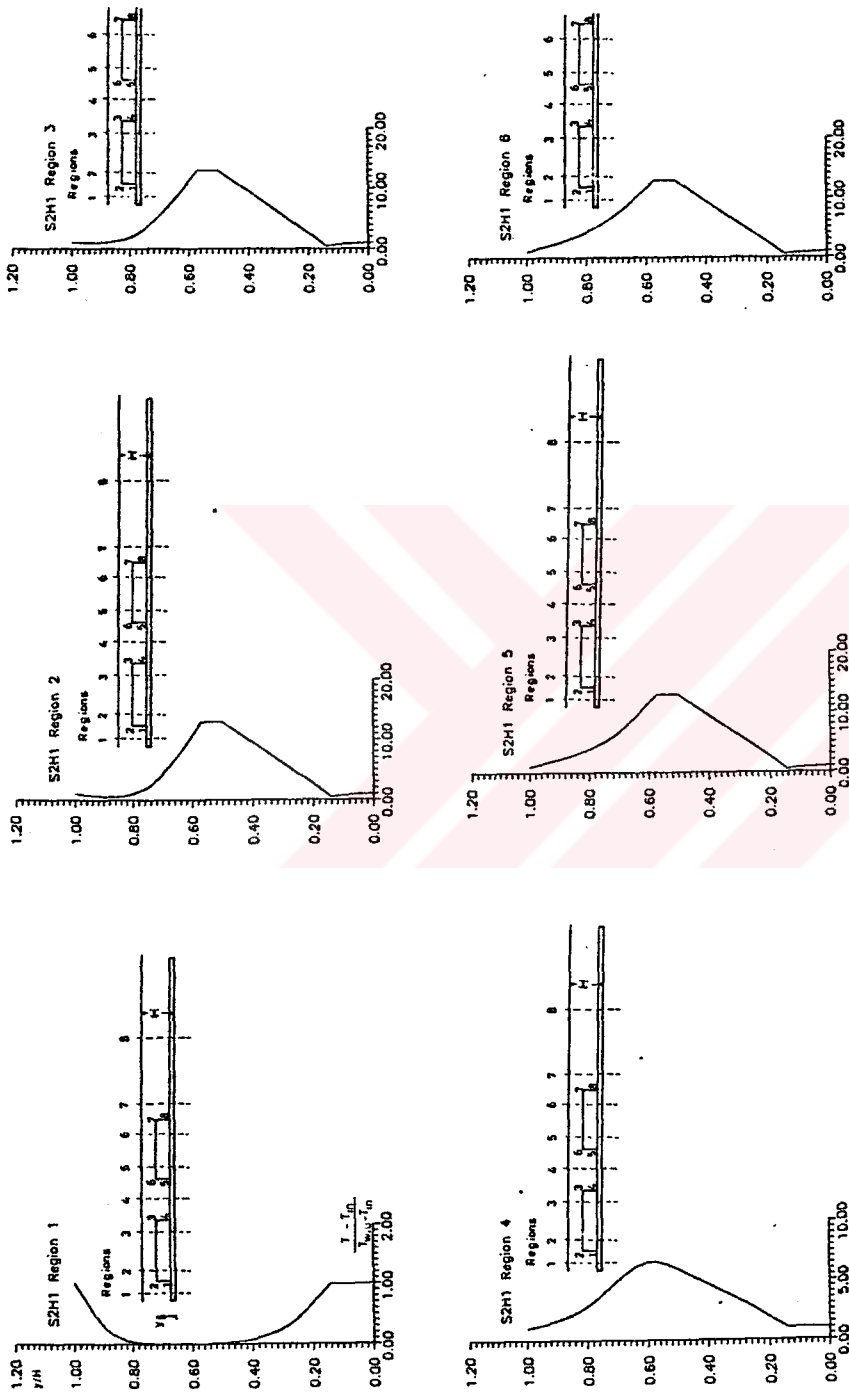


Figure 7.8 Temperature distribution at various section in two-step channel case with source location at a position,  $H'/H=5/6$ , ( $Re=200$ ,  $Pr=0.7$ )

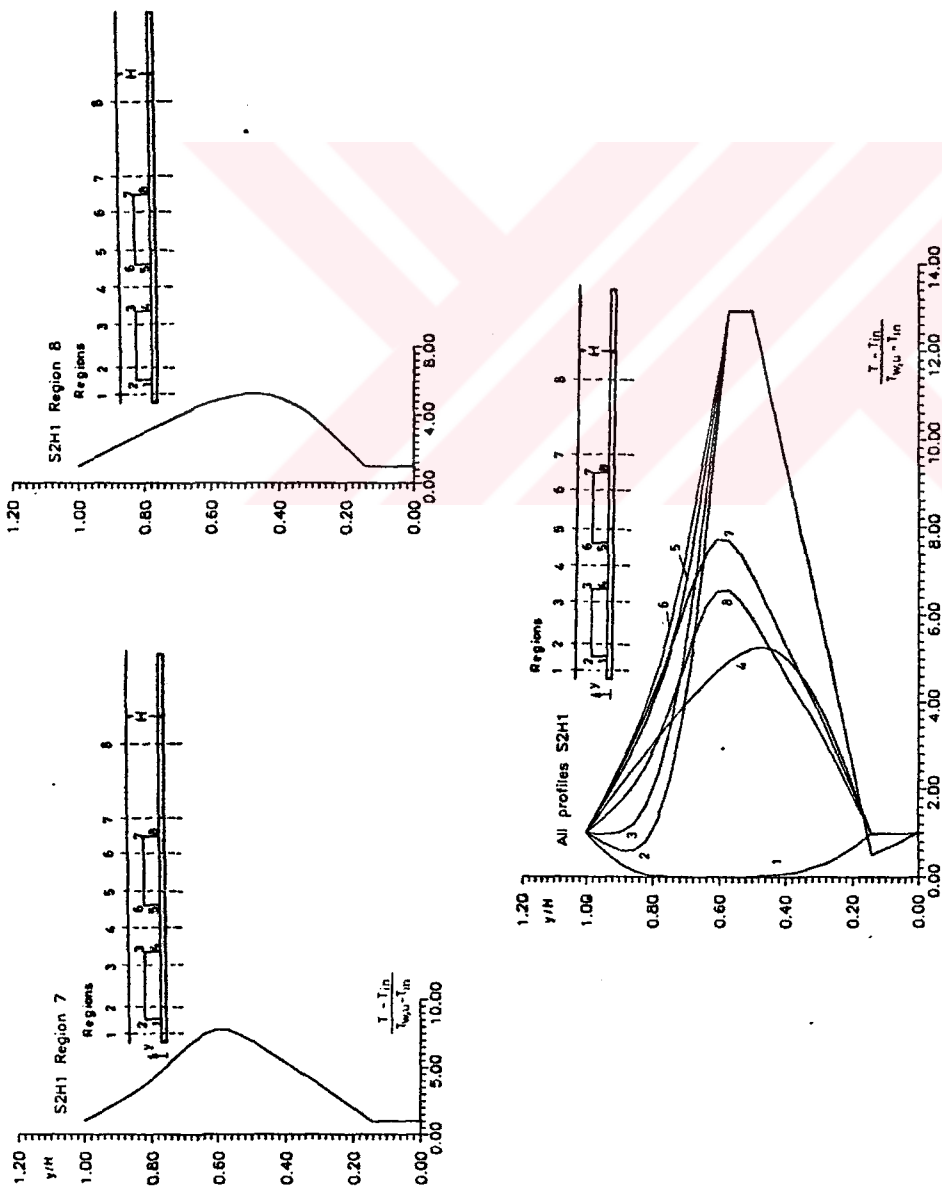


Figure 7.8 Temperature distribution at various section in two-step channel case with source location at a position,  $H'/H=5/6$ , ( $Re=200$ ,  $Pr=0.7$ )

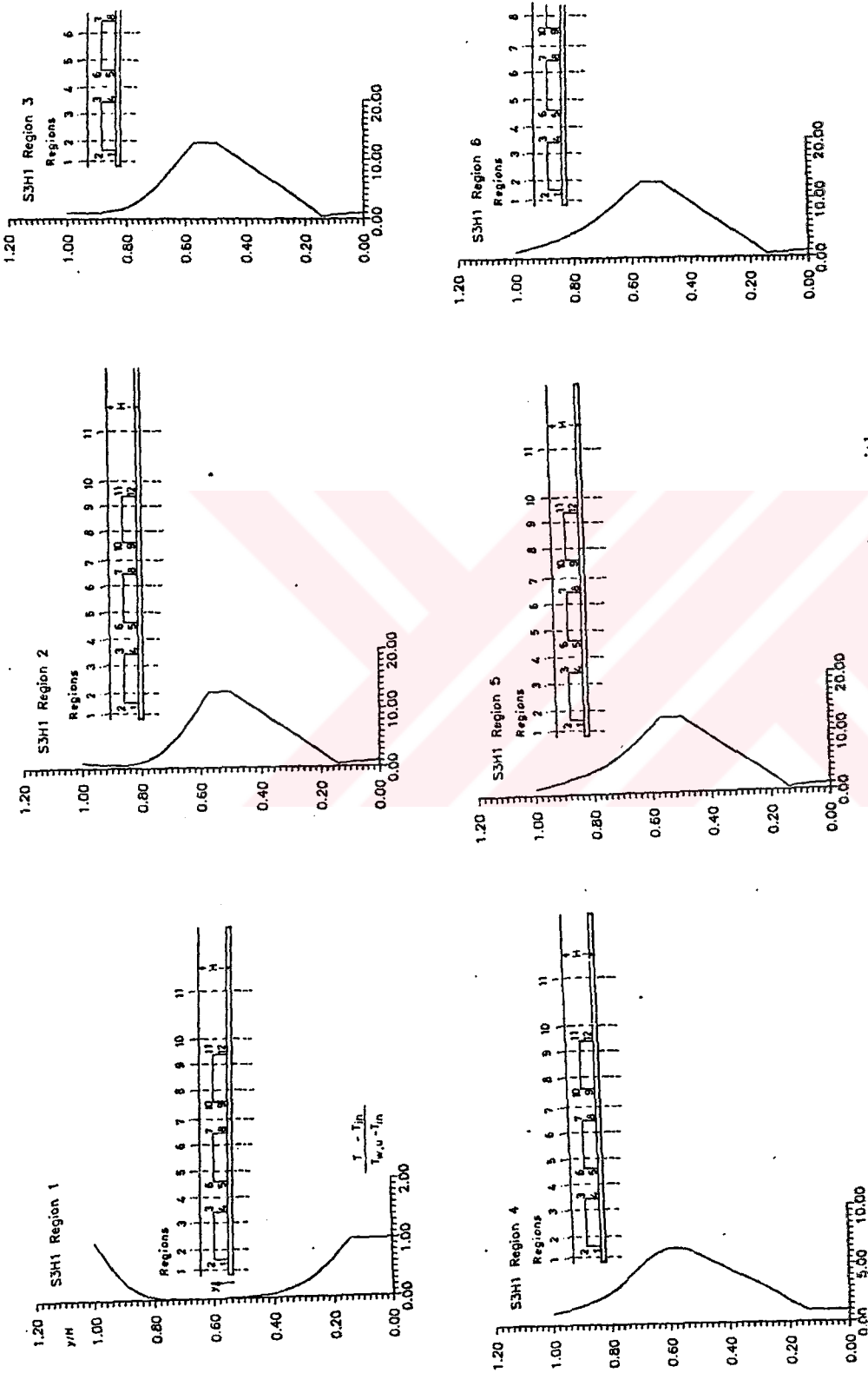


Figure 7.9 Temperature distribution at various section in three-step channel case with source location at a position,  $H'/H=5/6$ , ( $Re=200$ ,  $Pr=0.7$ )

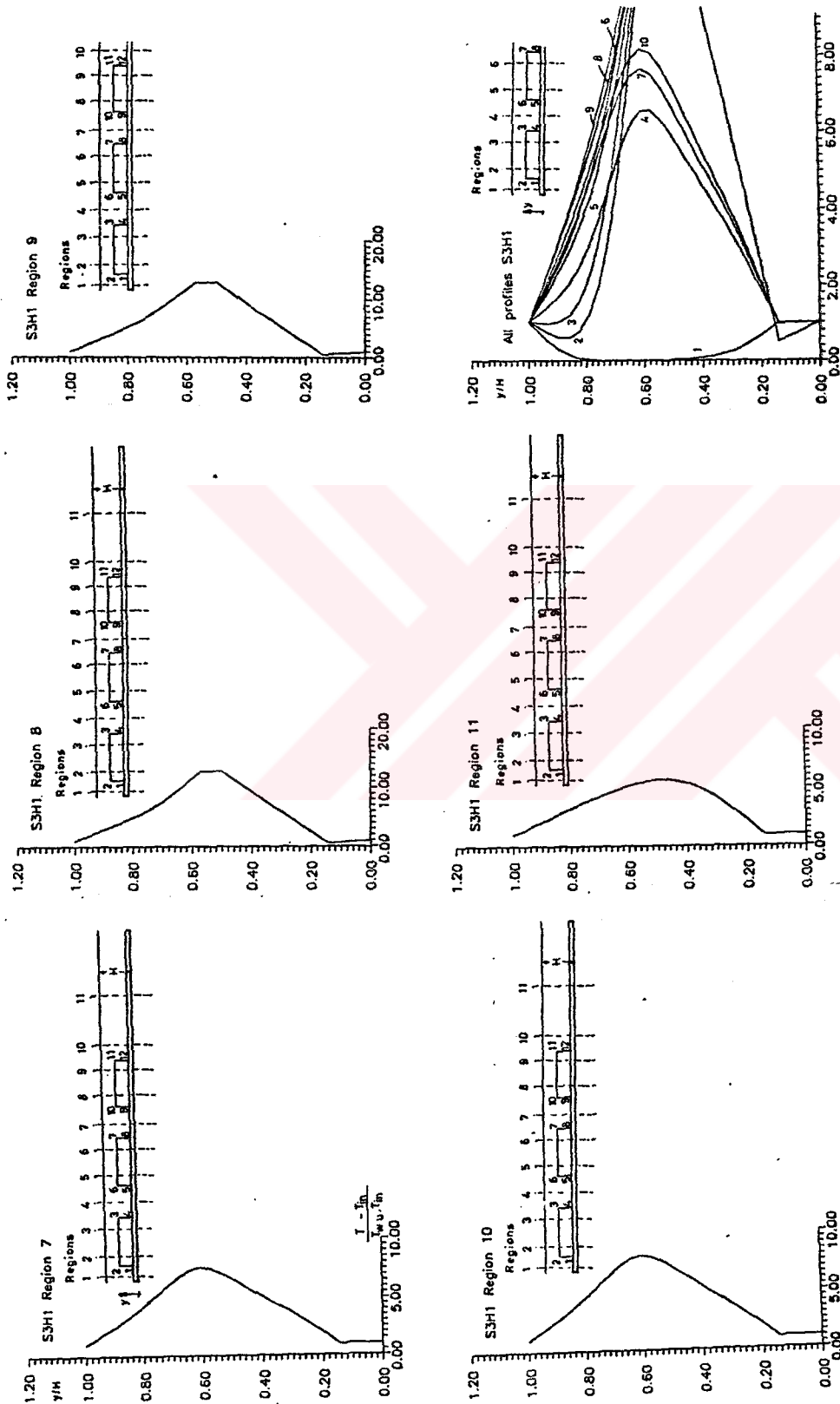


Figure 7.9 Temperature distribution at various section in three-step channel case with source location at a position,  $H'/H=5/6$ , ( $Re=200$ ,  $Pr=0.7$ )

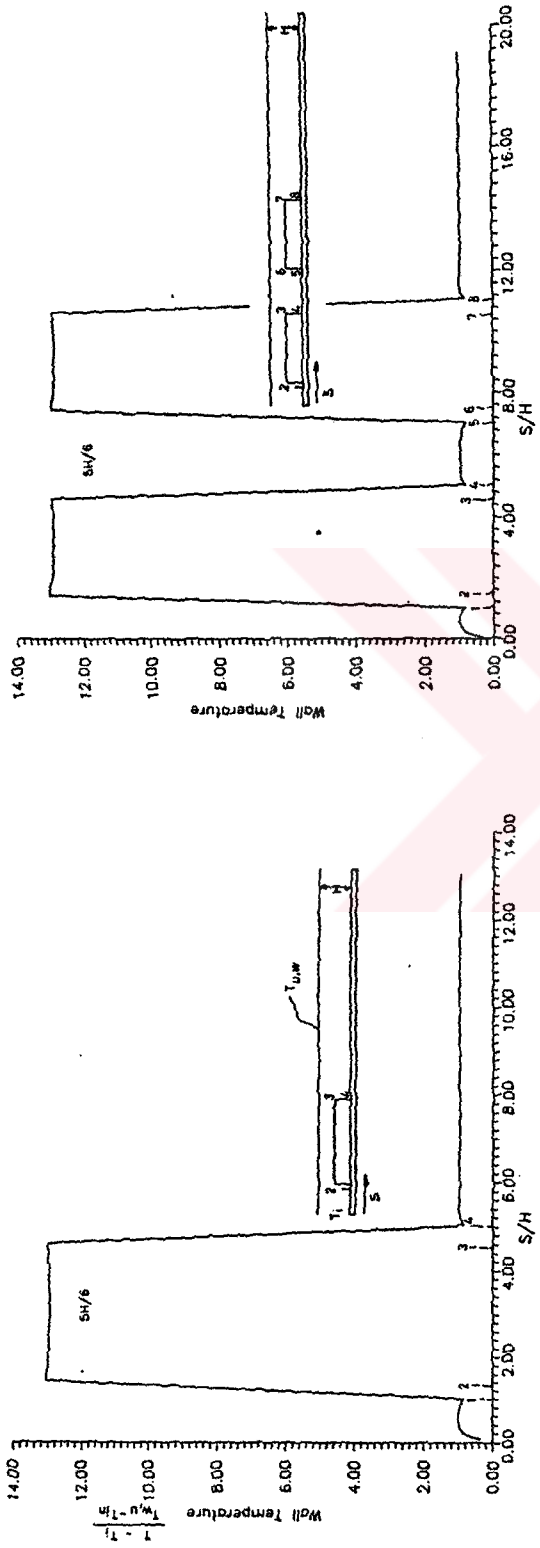
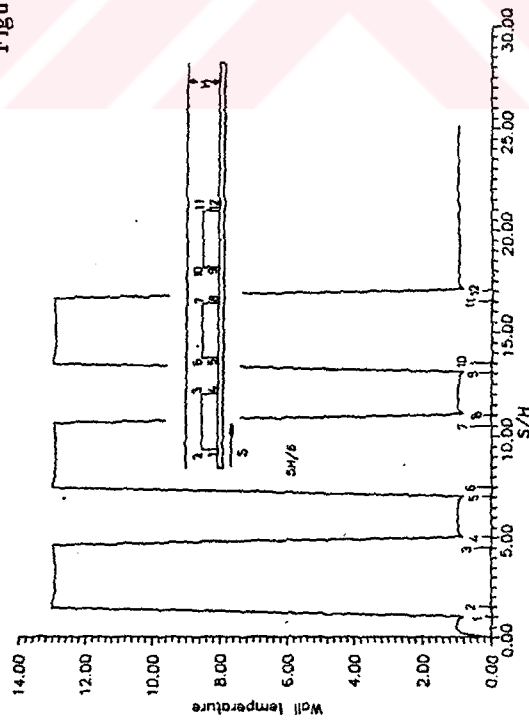


Figure 7.10a) Wall temperature distribution in flow direction for one, two, three step channel ( $Re=200$ ,  $Pr=0.7$ )



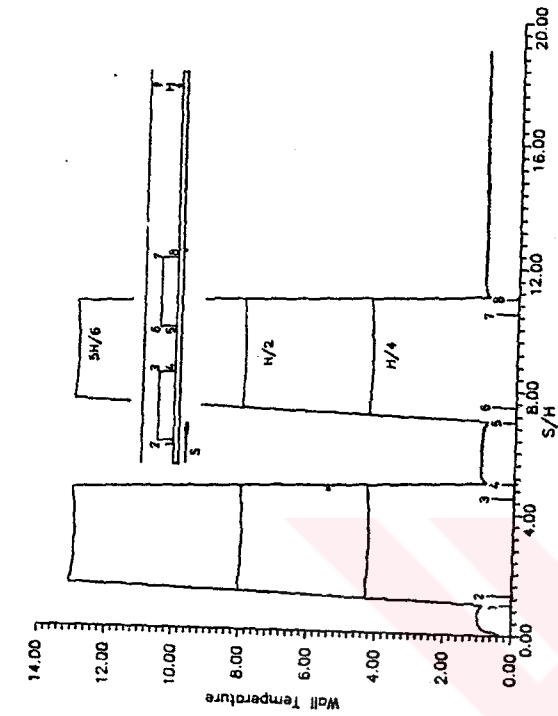
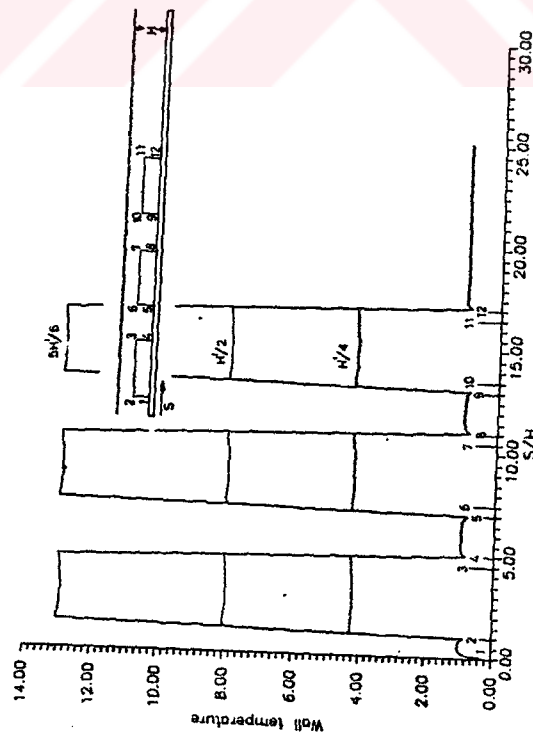
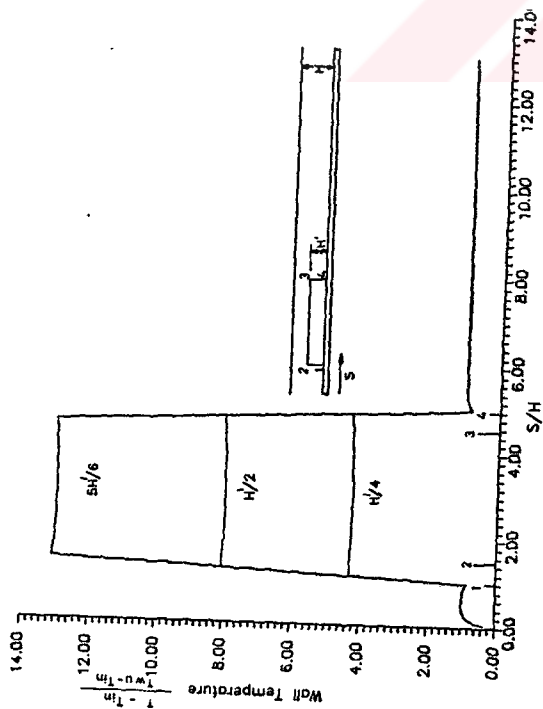


Figure 7.10b) Wall temperature distribution in flow direction for various source locations. ( $Re=200$ ,  $Pr=0.7$ )



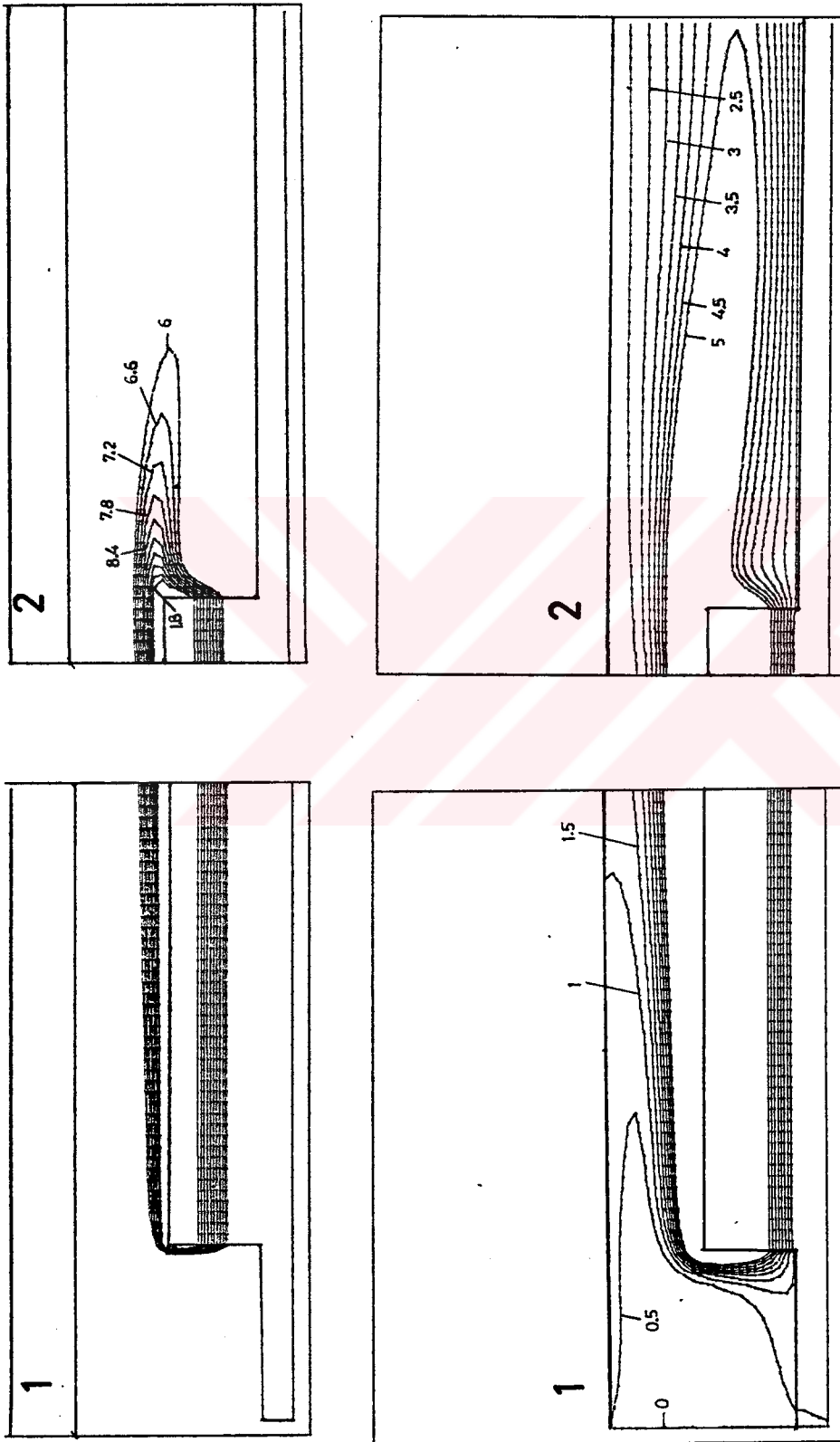


Figure 7.10c) Temperature contours in one-step channel with source location at a position,  
 $H'/H=5/6$ , ( $Re=200$ ,  $Pr=0.7$ ).



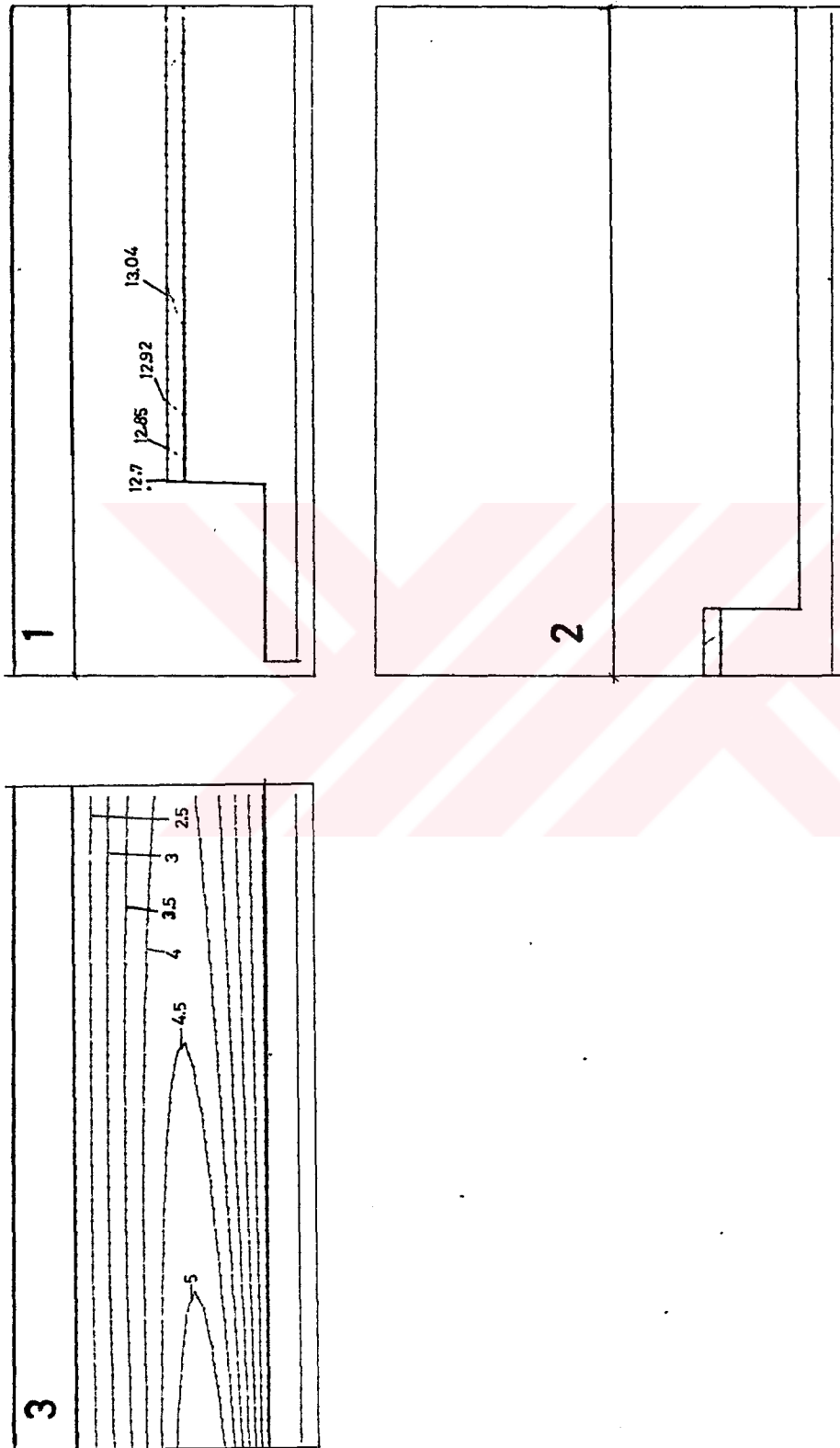


Figure 7.10d) Temperature contours in one-step channel with source location at a position,  $H'/H=5/6$ , ( $Re=200$ ,  $Pr=0.7$ ).

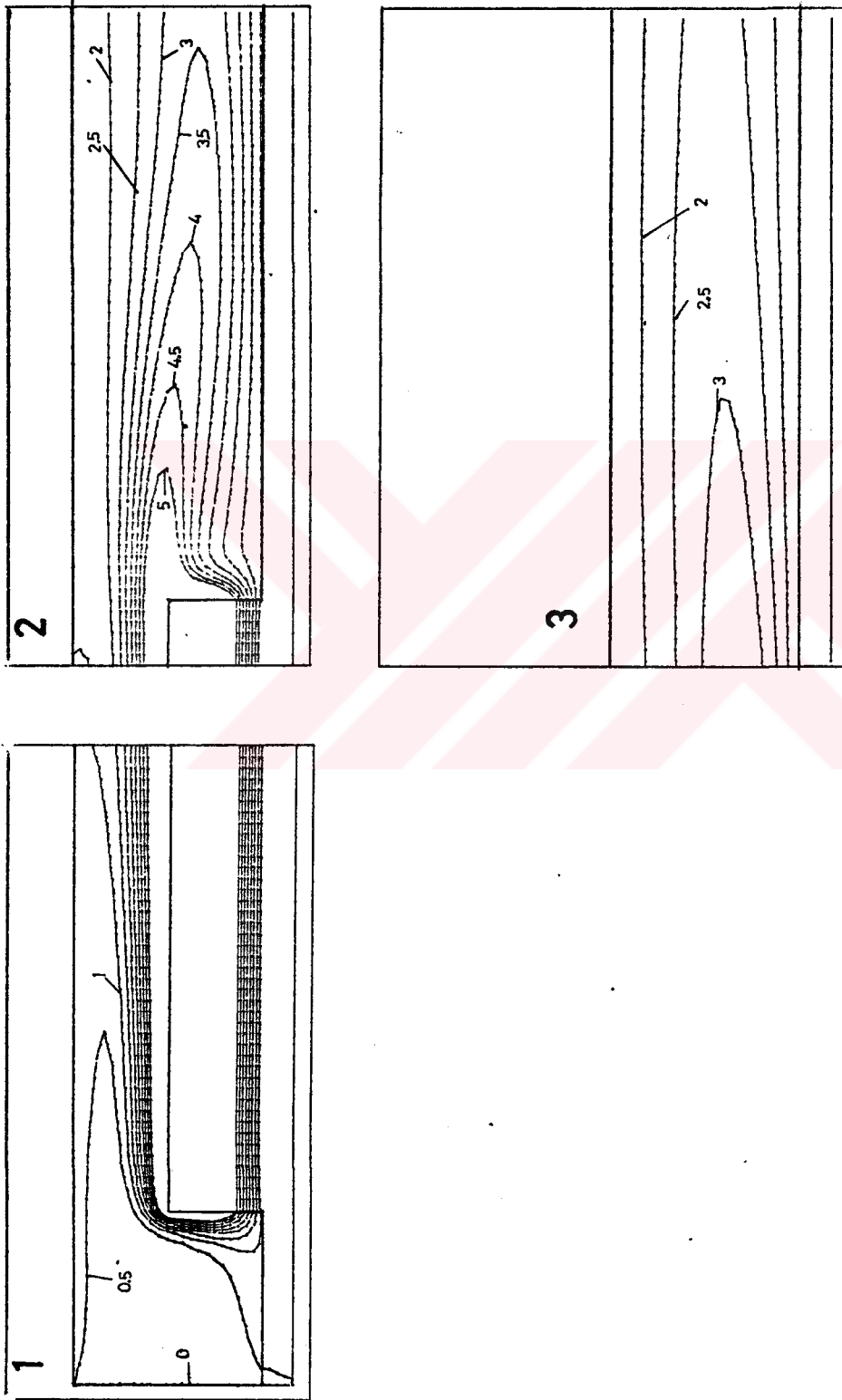


Figure 7.10e) Temperature contours in one-step channel with source location at a position,  $H'/H=1/2$ , ( $Re=200$ ,  $Pr=0.7$ ).

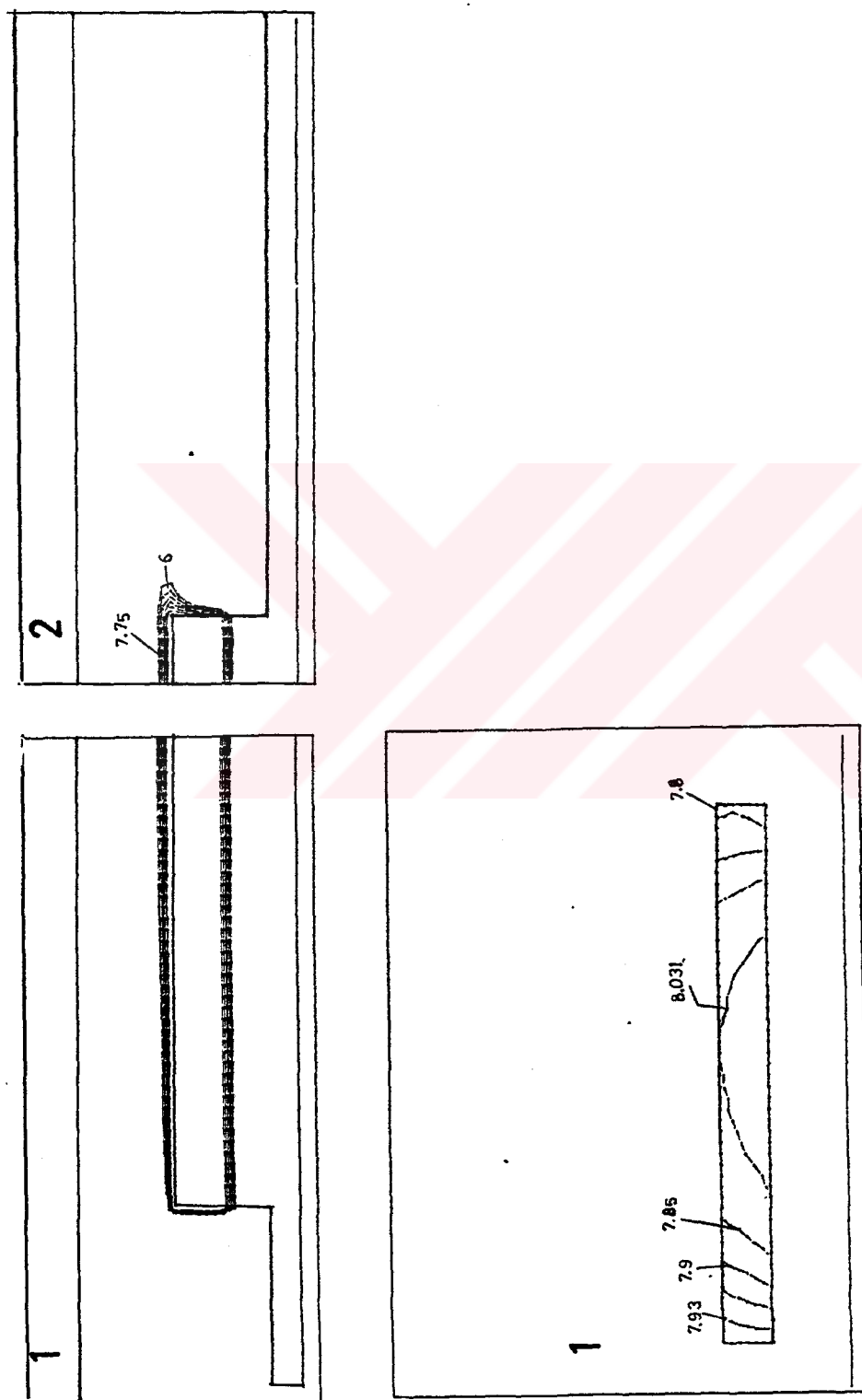


Figure 7.10f) Temperature contours in one-step channel with source location at a position,  $H'/H=1/2$ , ( $Re=200$ ,  $Pr=0.7$ ).

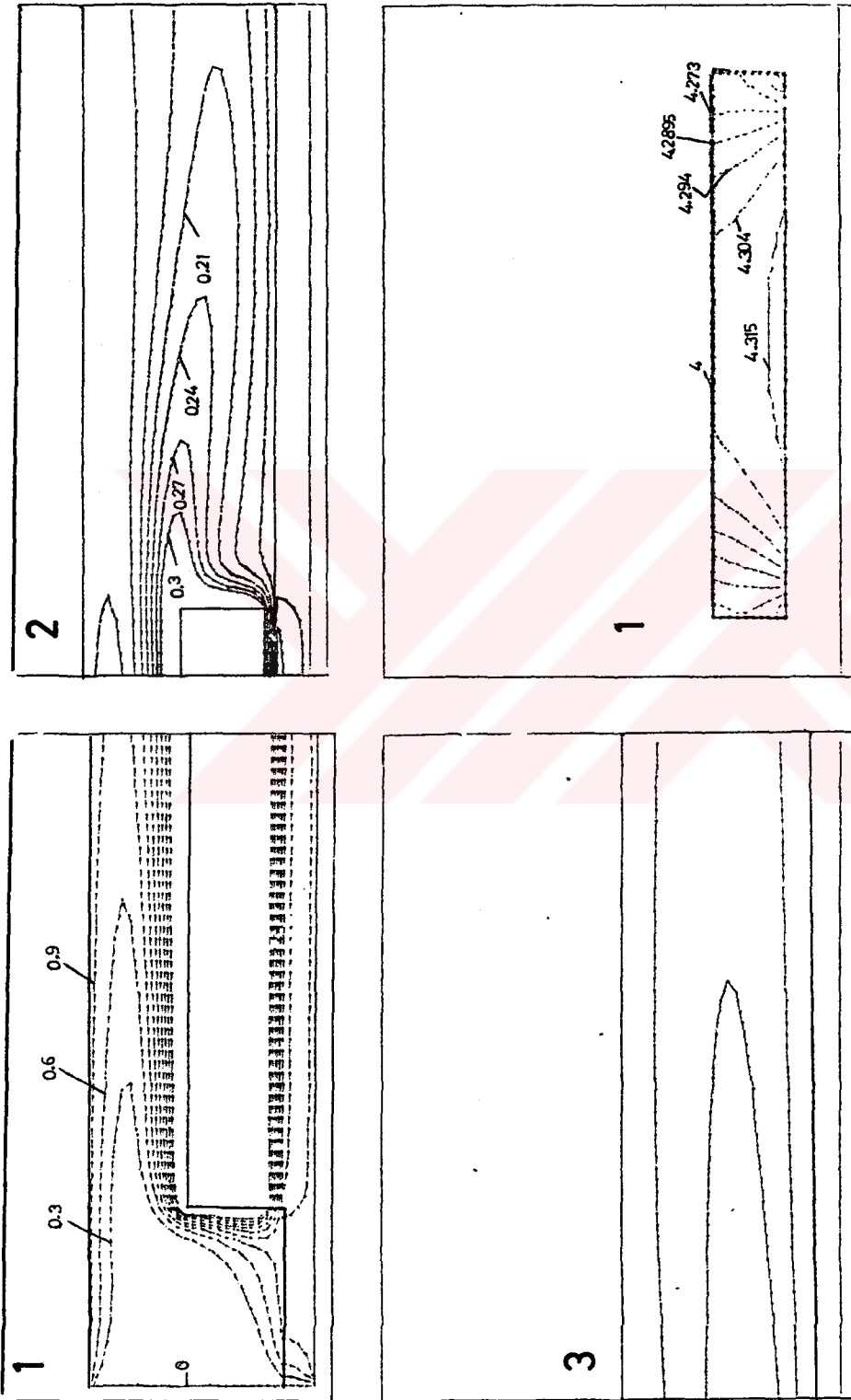


Figure 7.10g) Temperature contours in one-step channel with source location at a position,  
 $H'/H=1/4$ , ( $Re=200$ ,  $Pr=0.7$ ).

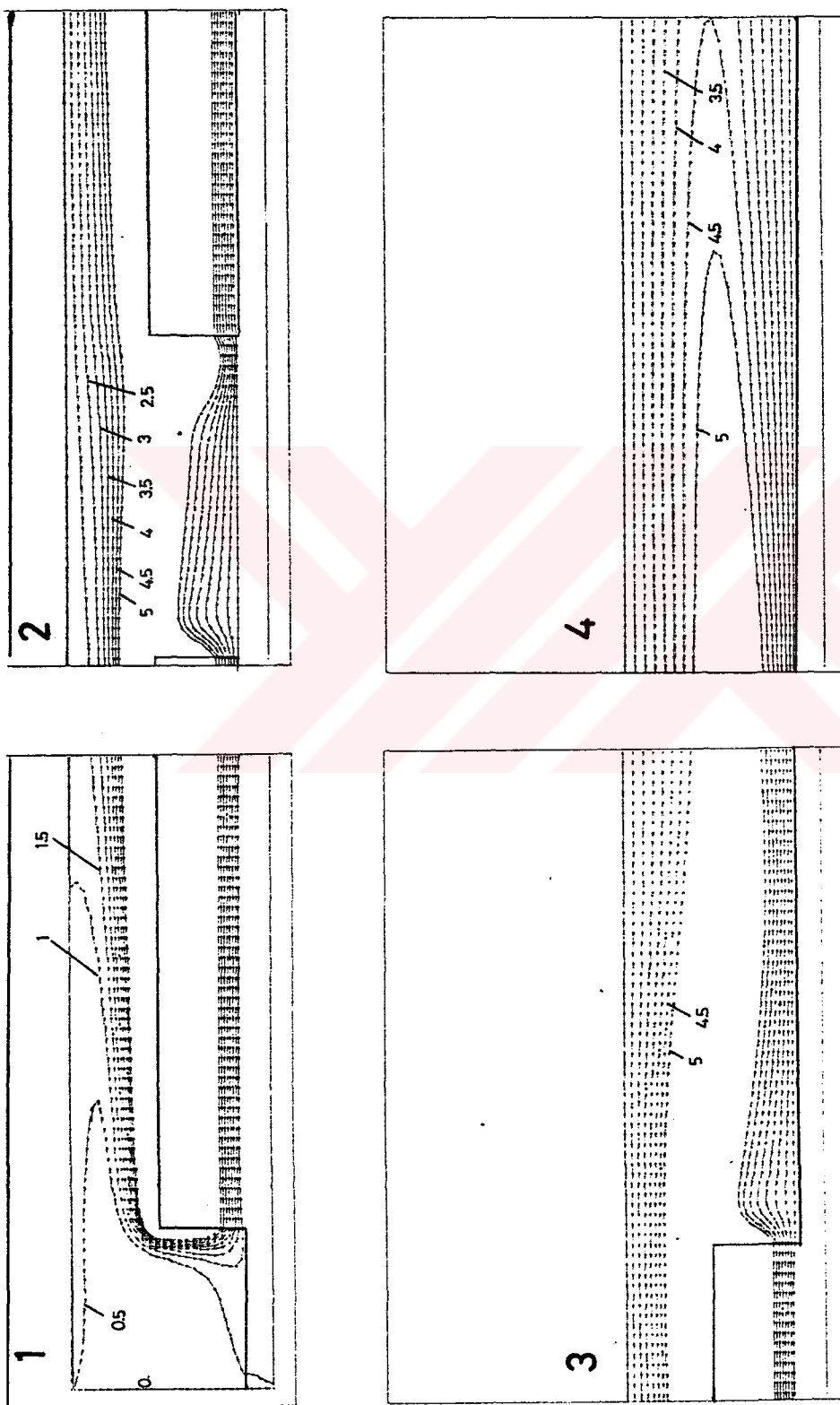
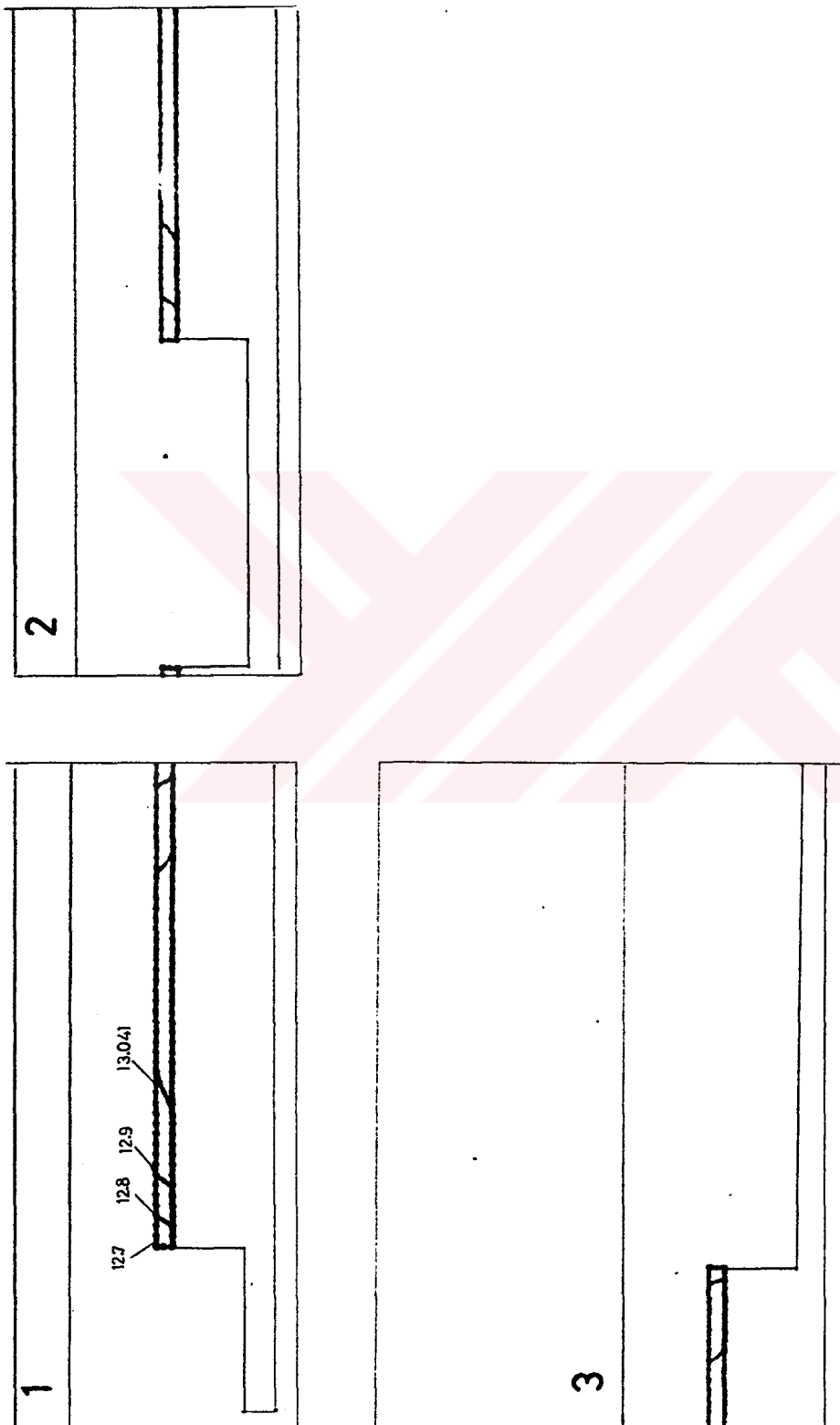


Figure 7.11a) Temperature contours in two-step channel with source location at a position,  $H'/H=5/6$ , ( $Re=200$ ,  $Pr=0.7$ ).



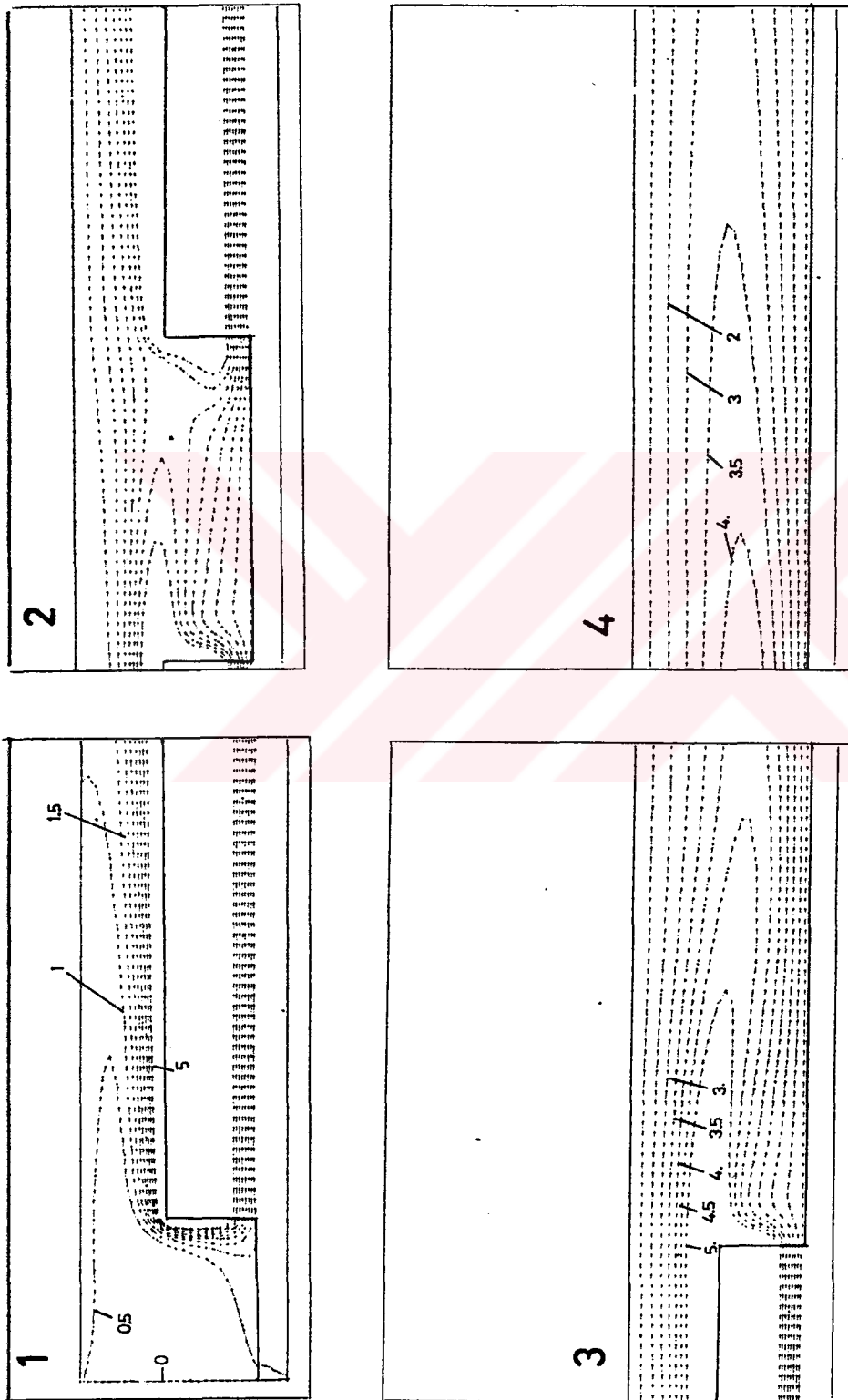


Figure 7.11c) Temperature contours in two-step channel with source location at a position,  $H'/H=1/2$ , ( $Re=200$ ,  $Pr=0.7$ ).

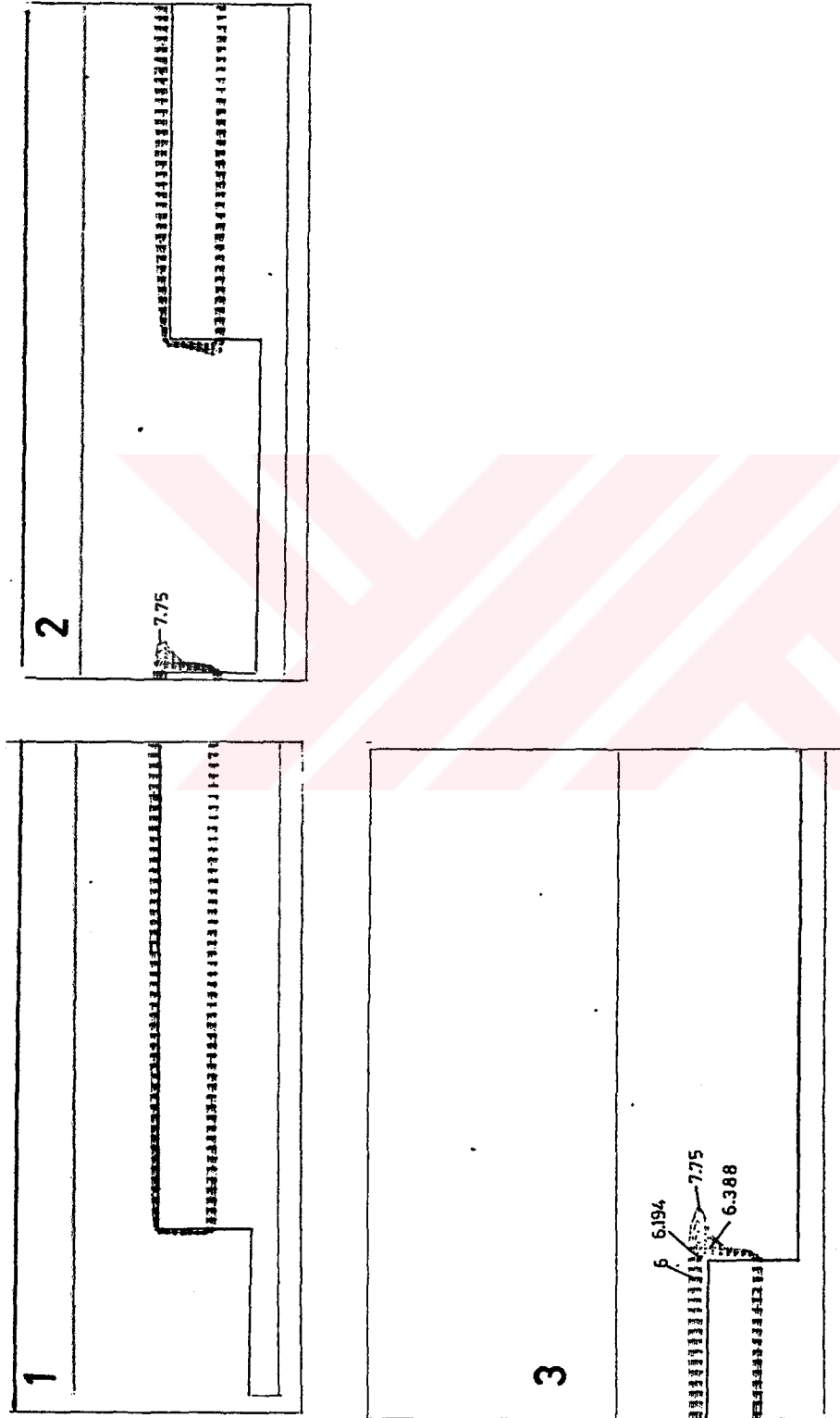


Figure 7.11d) Temperature contours in two-step channel with source location at a position,  $H'/H=1/2$ , ( $Re=200$ ,  $Pr=0.7$ ).



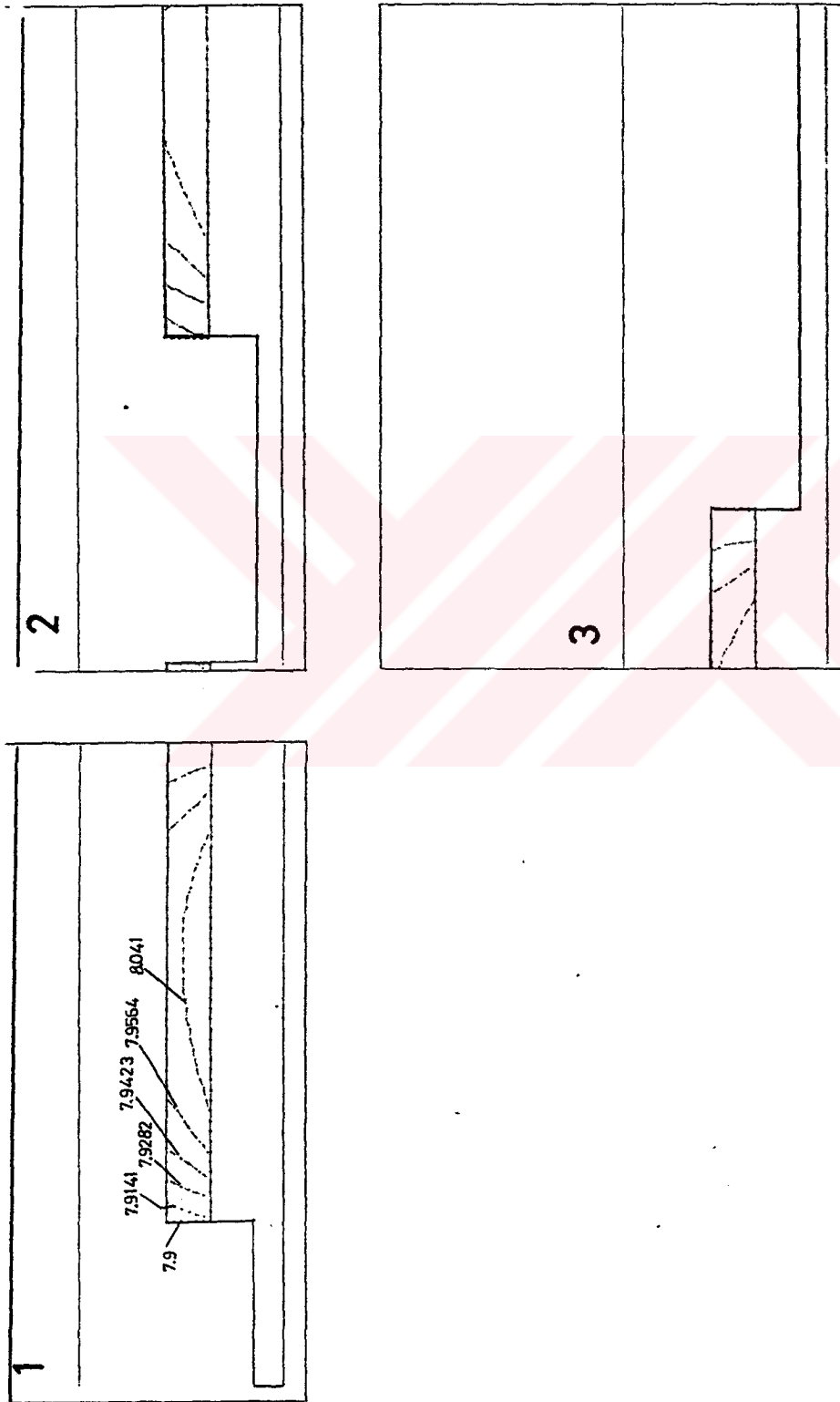


Figure 7.11e) Temperature contours in two-step channel with source location at a position,  $H'/H=1/2$ , ( $Re=200$ ,  $Pr=0.7$ ).

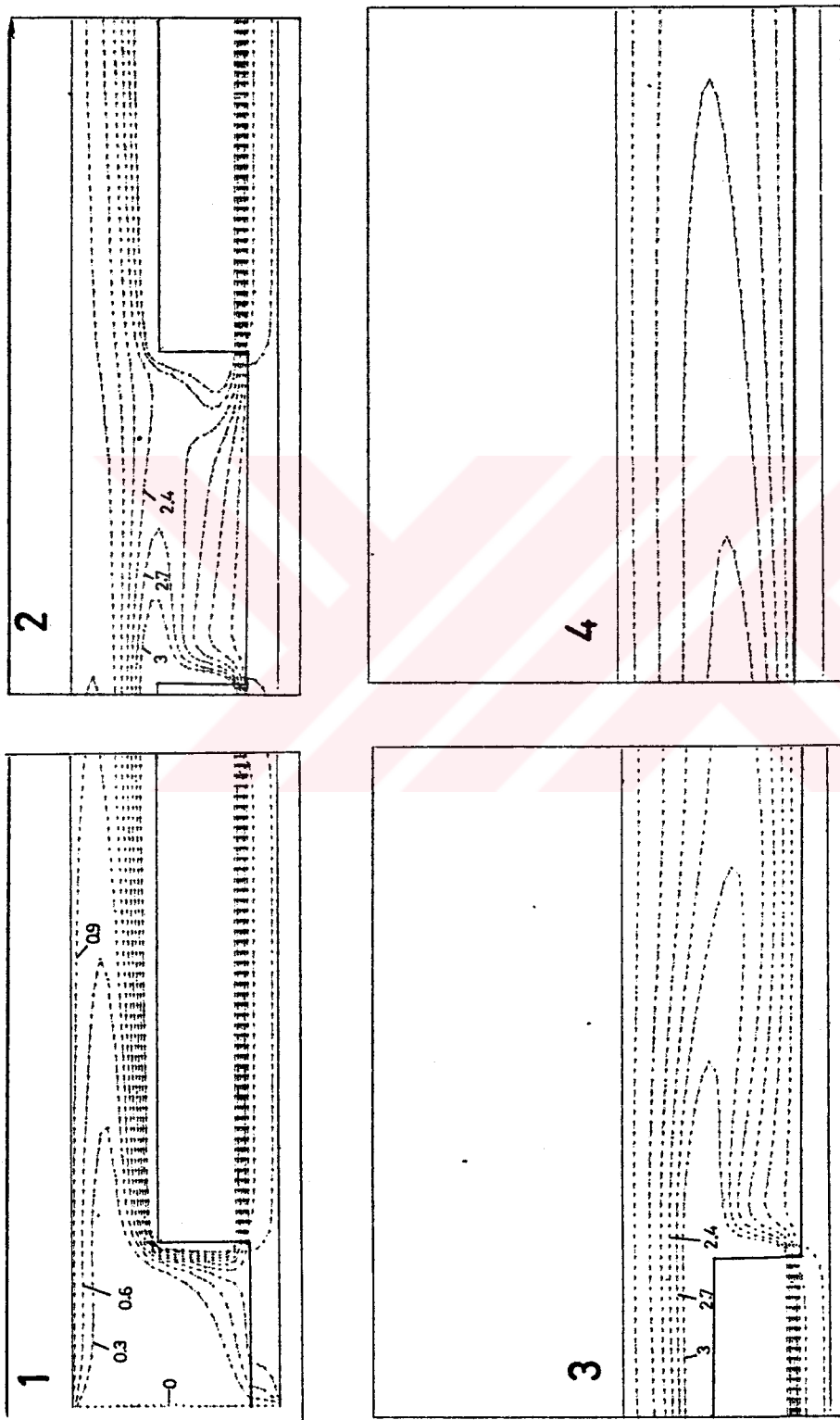


Figure 7.11f) Temperature contours in two-step channel with source location at a position,  $H'/H=1/4$ , ( $Re=200$ ,  $Pr=0.7$ ).

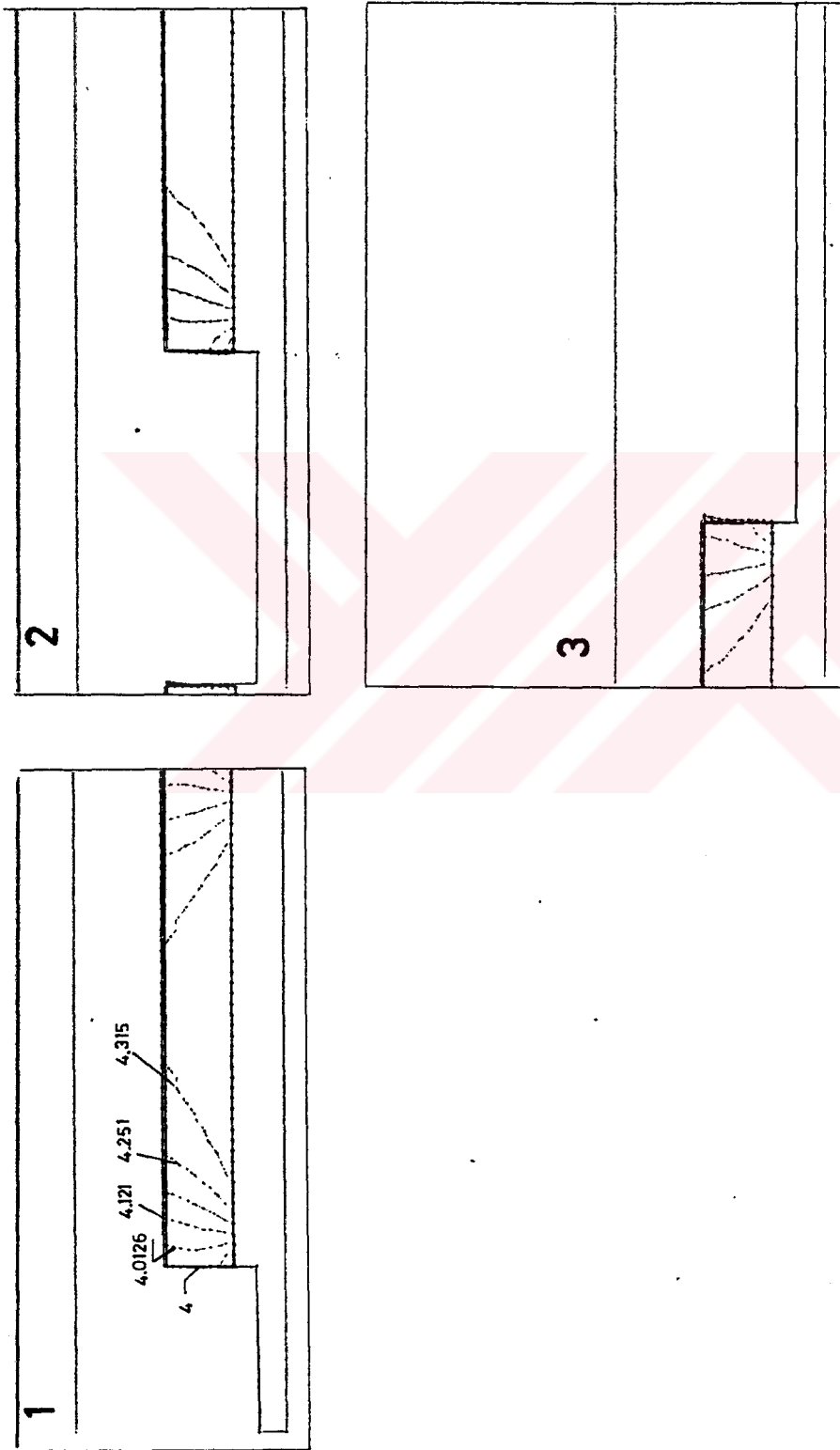


Figure 7.11g) Temperature contours in two-step channel with source location at a position,  $H'/H = 1/4$ , ( $Re=200$ ,  $Pr=0.7$ ).

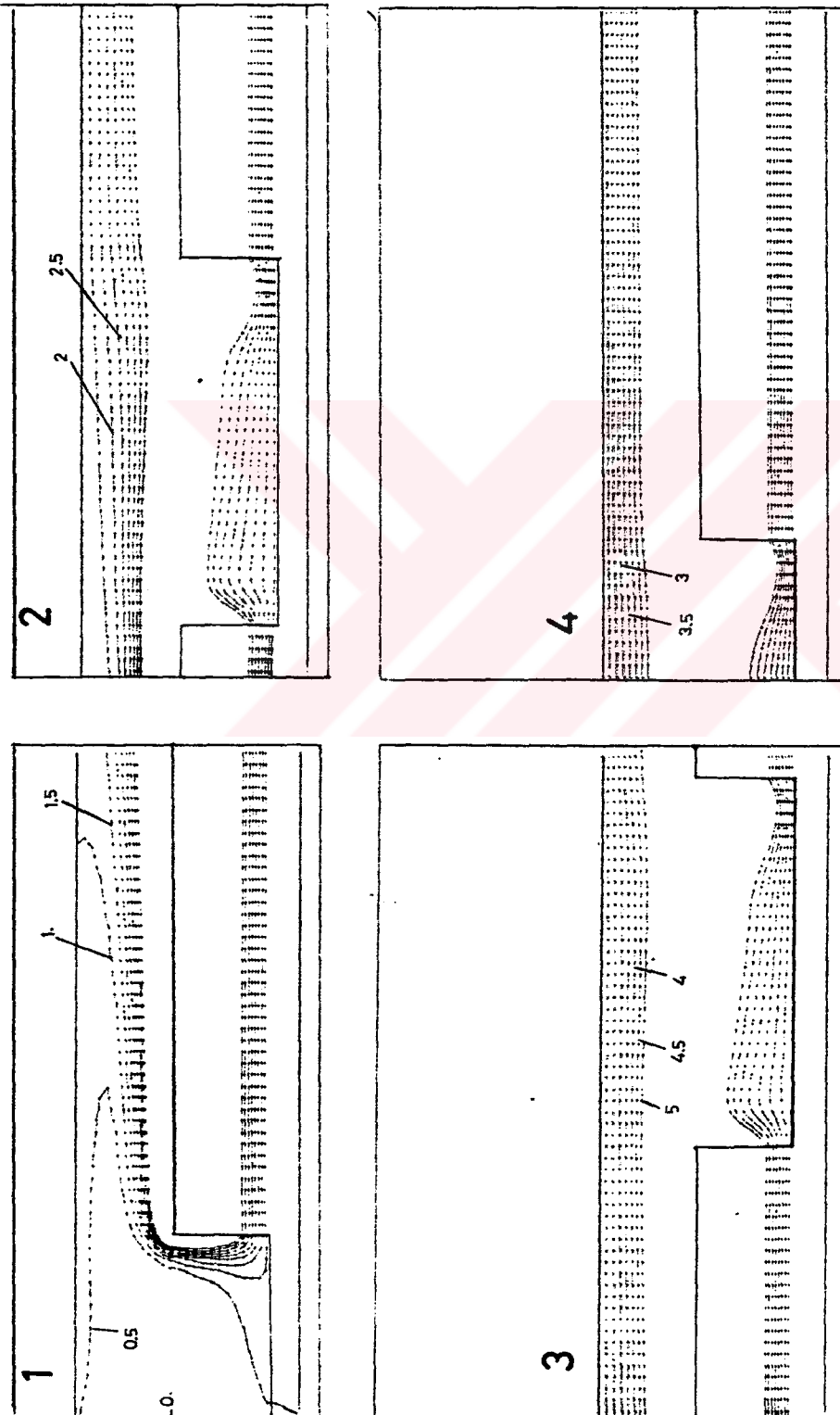


Figure 7.12a) Temperature contours in three-step channel with : source location at a position,  
 $H'/H=5/6$ , ( $Re=200$ ,  $Pr=0.7$ ).

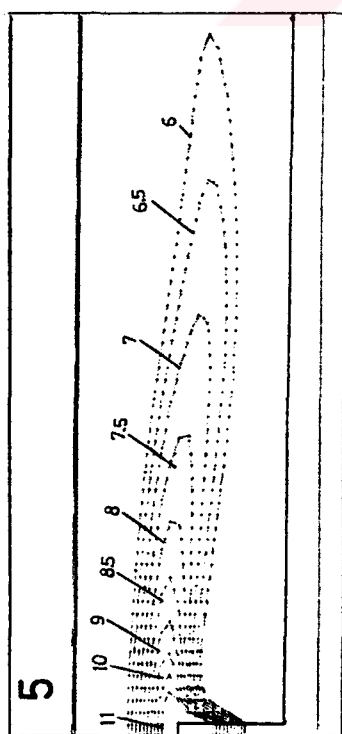


Figure 7.12c) Temperature contours in three-step channel with source location at a position,  $H'/H=5/6$ , ( $Re=200$ ,  $Pr=0.7$ ).

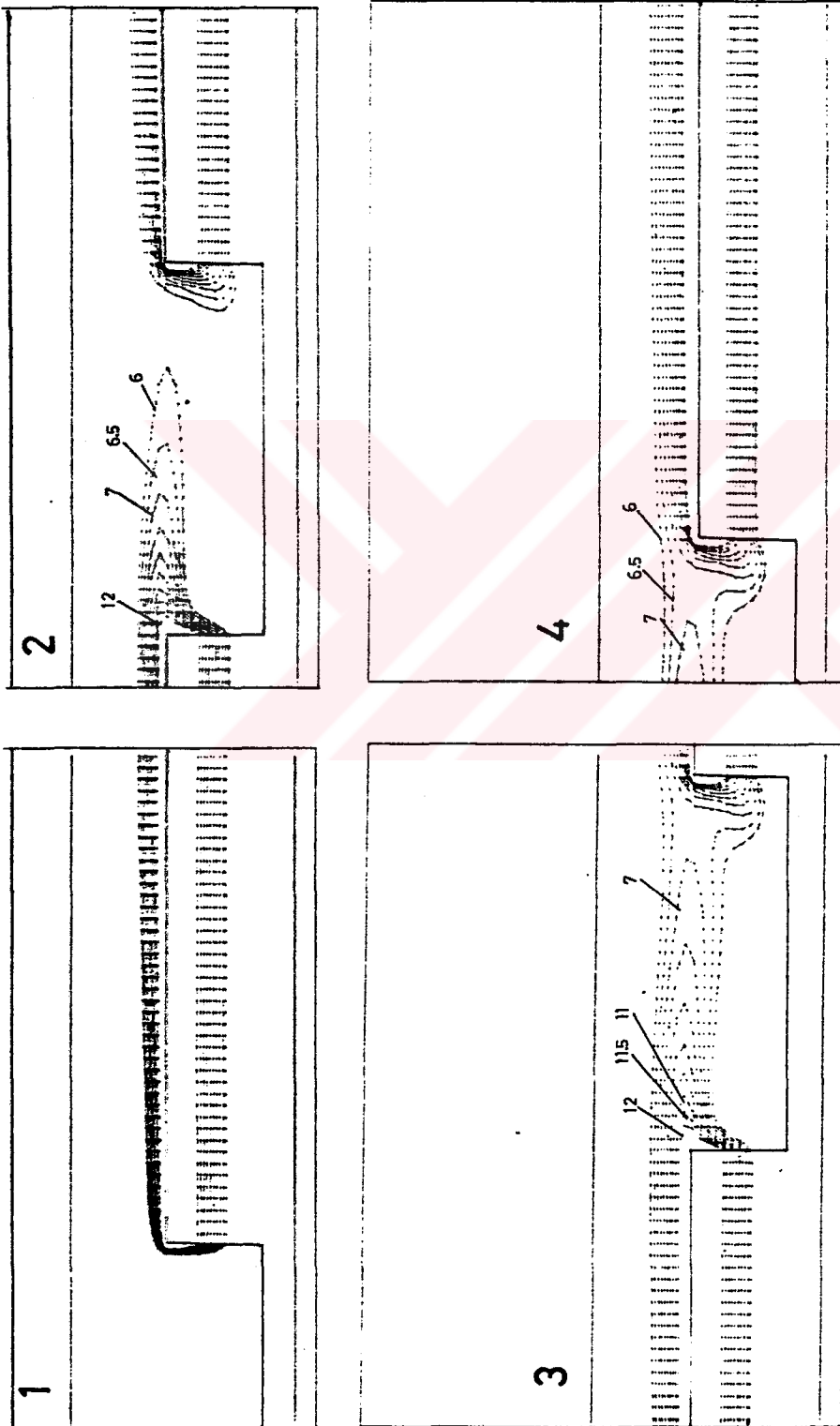


Figure 7.12b) Temperature contours in three-step channel with source location at a position,  $H'/H=5/6$ , ( $Re=200$ ,  $Pr=0.7$ ).

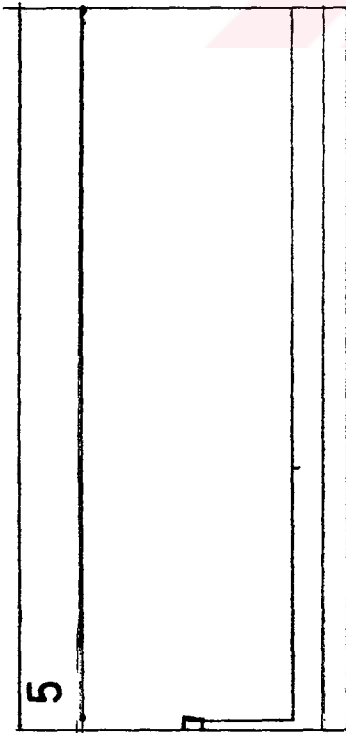


Figure 7.12e) Temperature contours in three-step channel with source location at a position,  $H'/H=5/6$ , ( $Re=200$ ,  $Pr=0.7$ ).

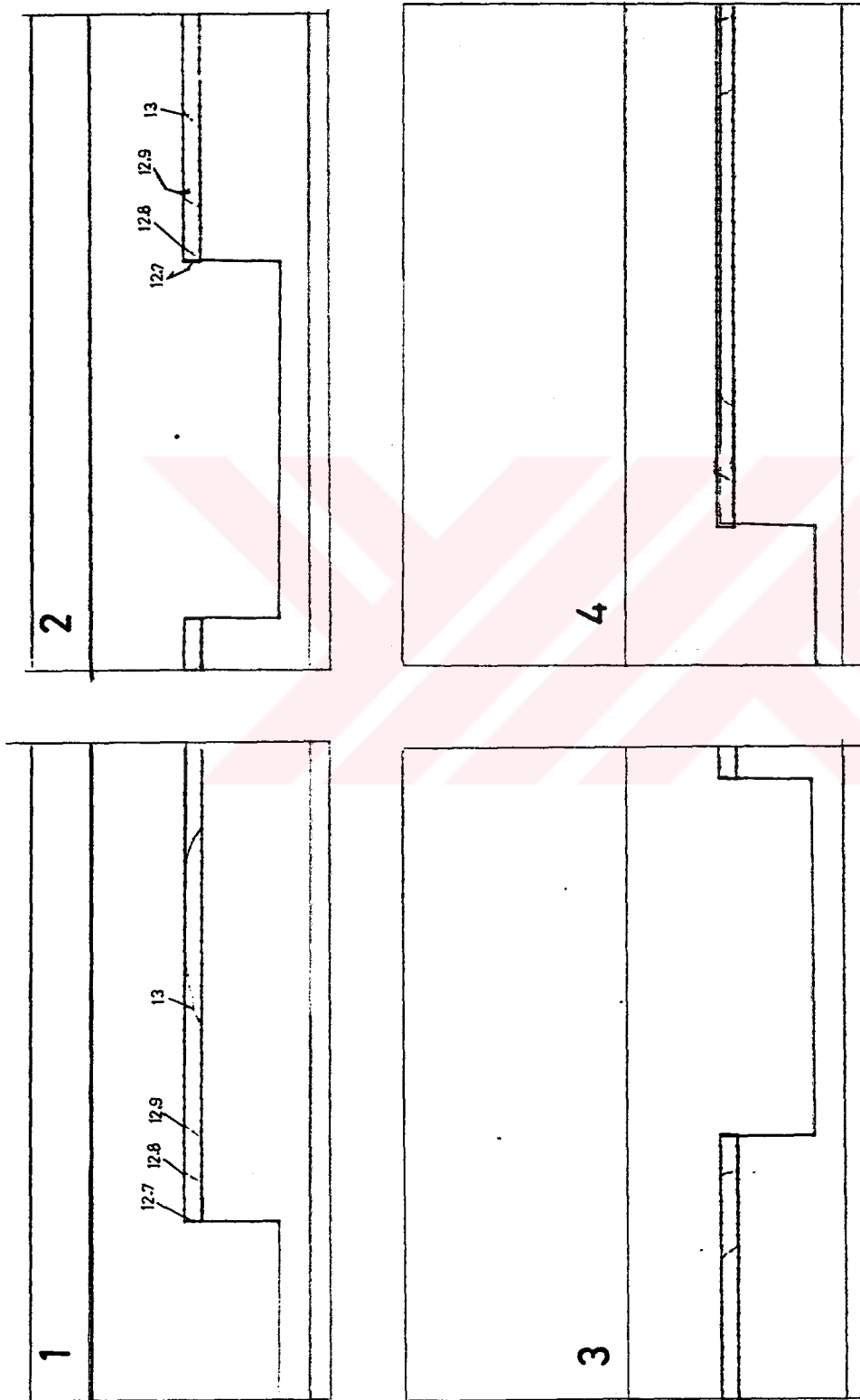


Figure 7.12d) Temperature contours in three-step channel with source location at a position,  $H'/H=5/6$ , ( $Re=200$ ,  $Pr=0.7$ ).



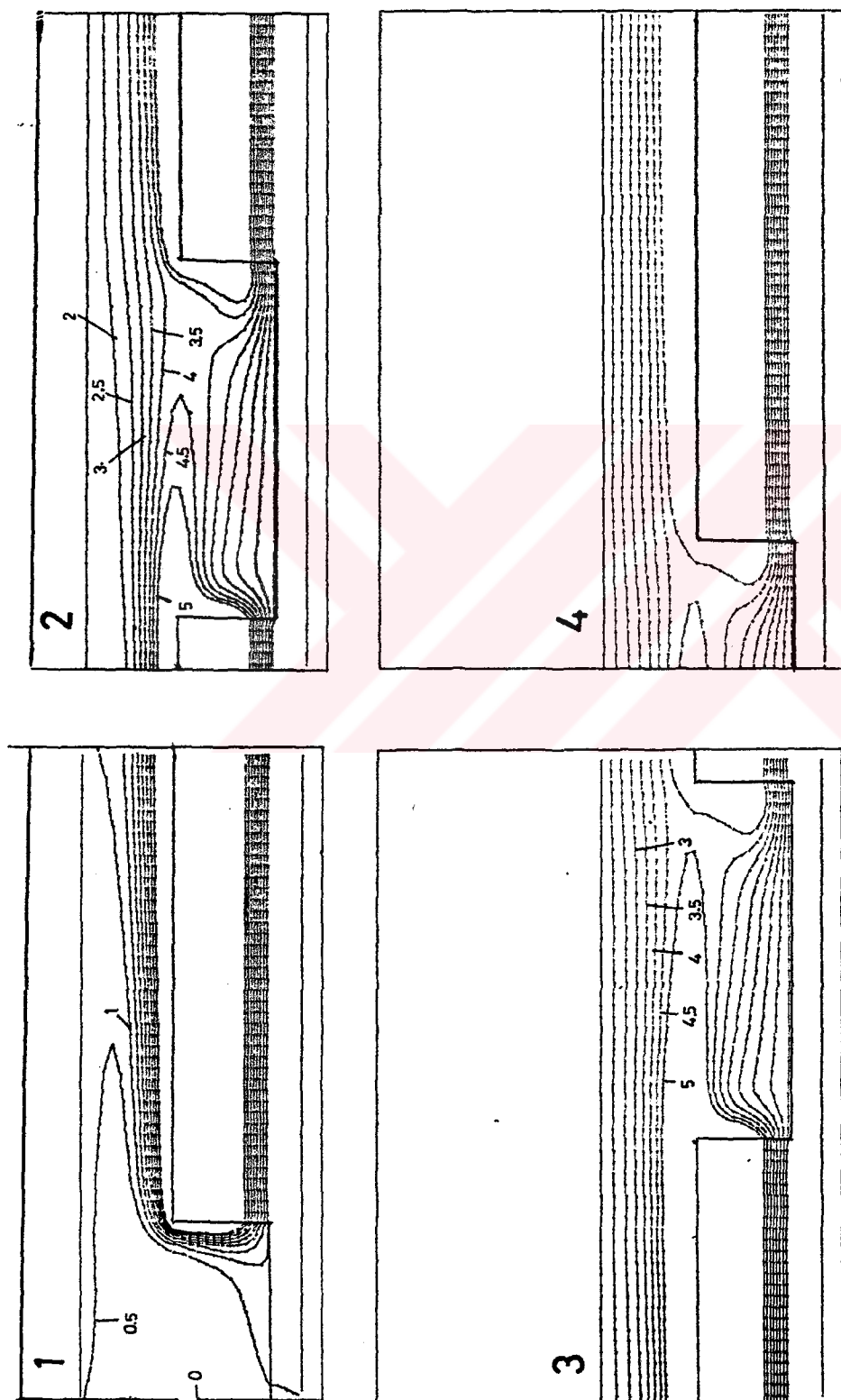


Figure 7.12f) Temperature contours in three-step channel with source location at a position,  $H'/H=1/2$ , ( $Re=200$ ,  $Pr=0.7$ ).

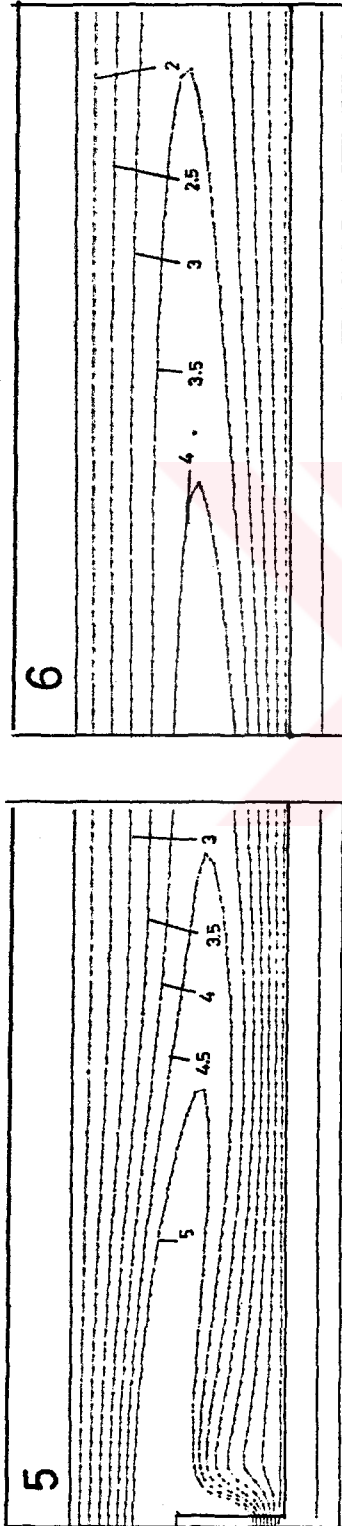


Figure 7.12g) Temperature contours in three-step channel with source location at a position,  $H'/H=1/2$ , ( $Re=200$ ,  $Pr=0.7$ ).

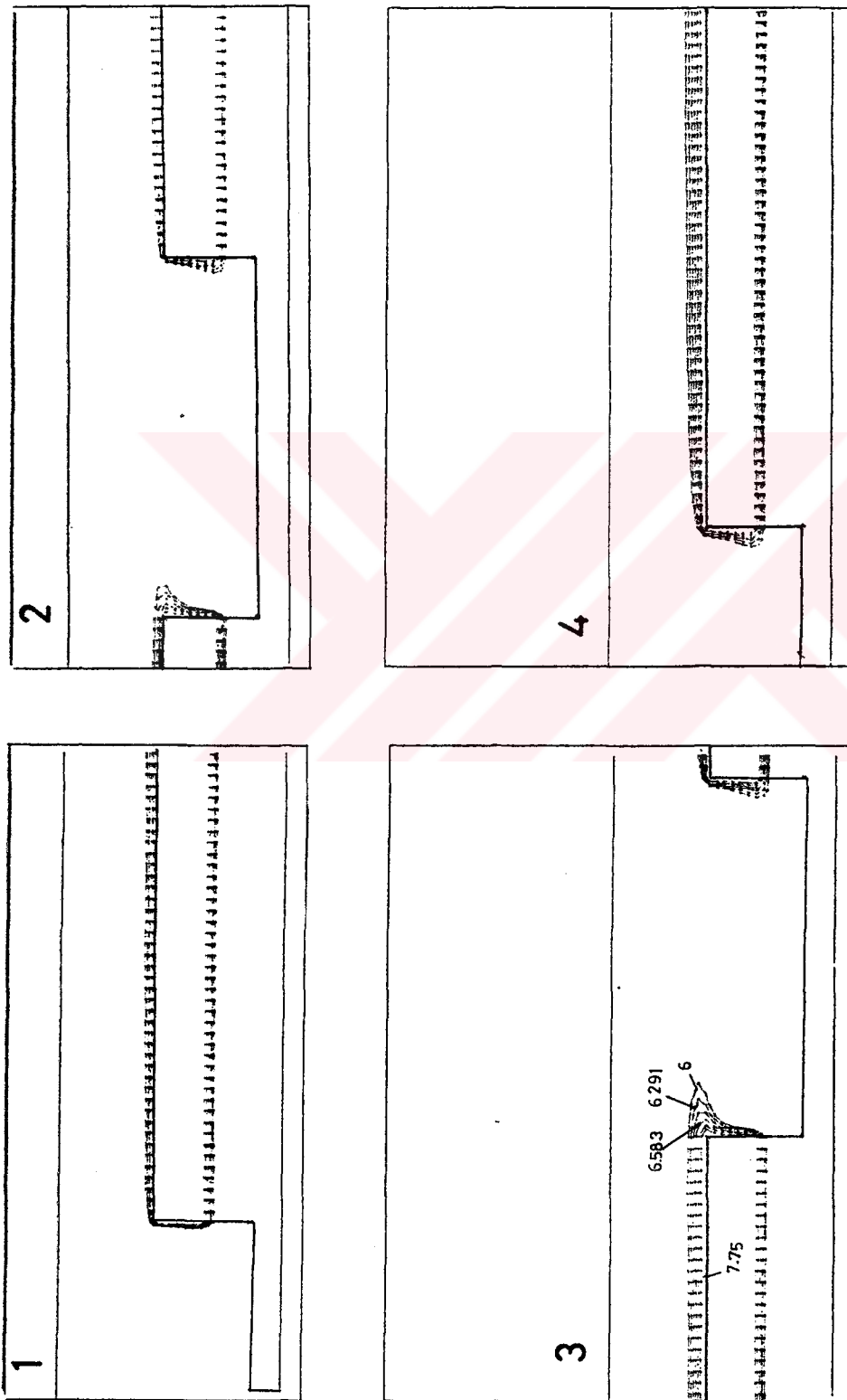


Figure 7.12h) Temperature contours in three-step channel with source location at a position,  $H'/H=1/2$ , ( $Re=200$ ,  $Pr=0.7$ ).

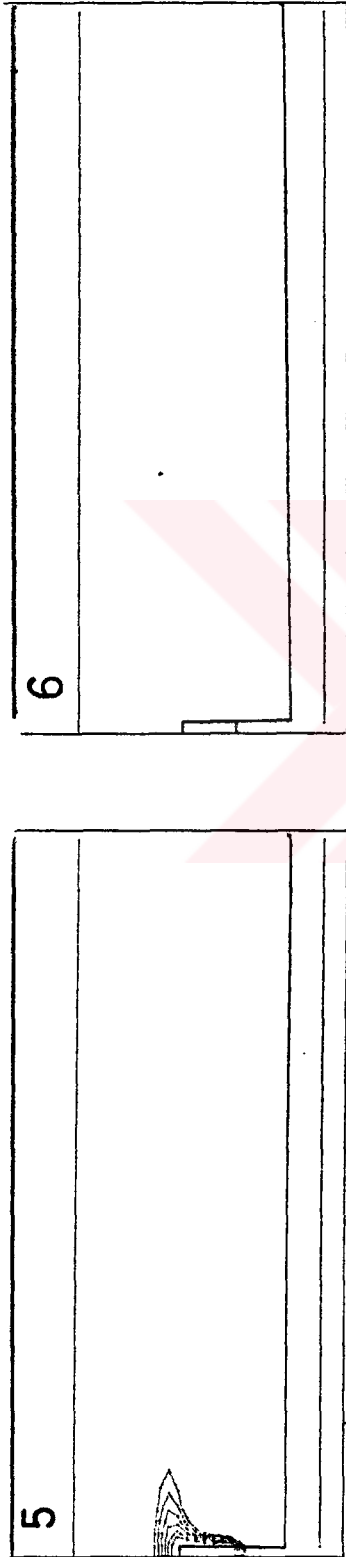


Figure 7.12k) Temperature contours in three-step channel with source location at a position,  $H'/H=1/2$ , ( $Re=200$ ,  $Pr=0.7$ ).

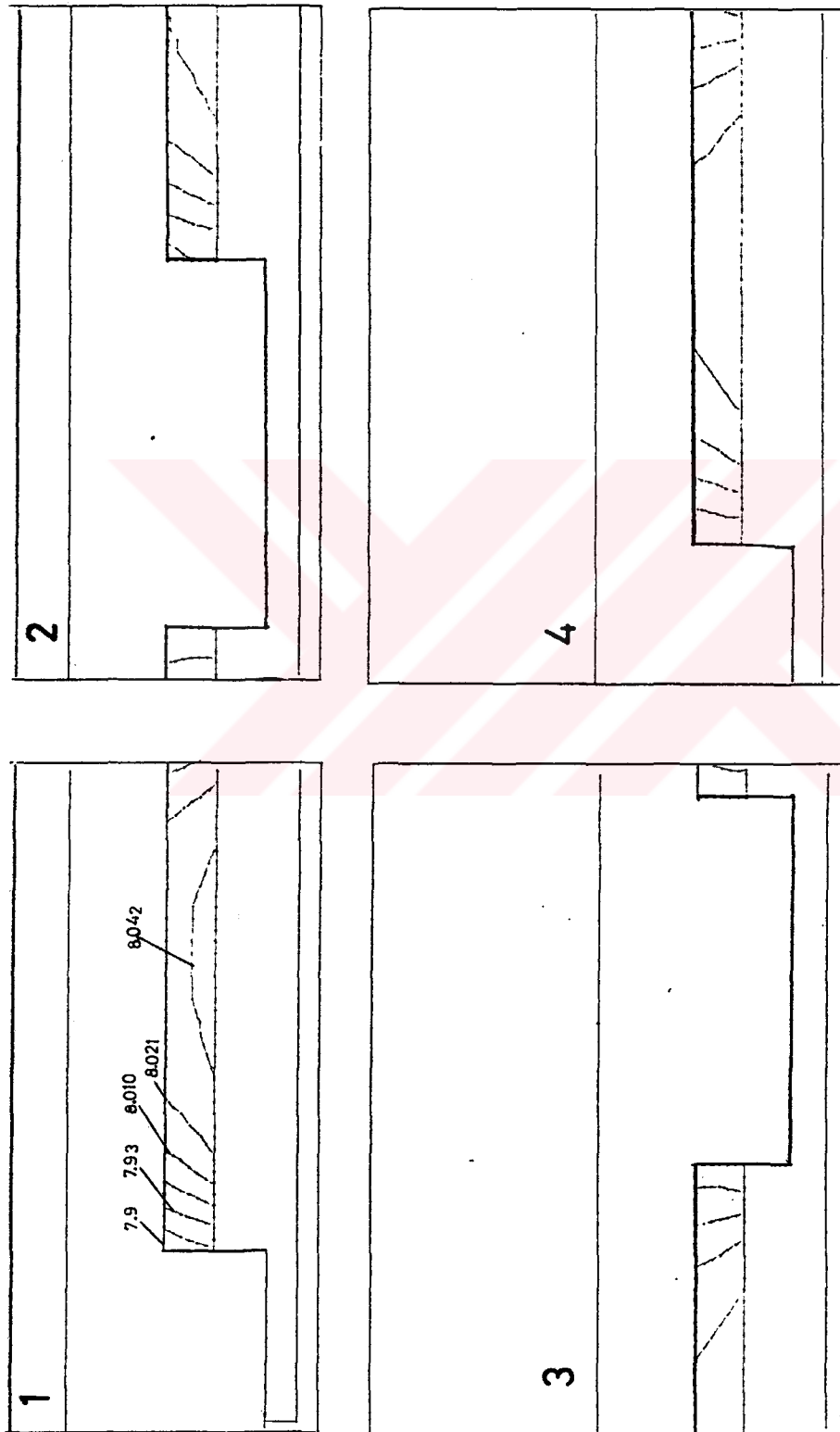


Figure 7.12l) Temperature contours in three-step channel with source location at a position,  $H'/H=1/2$ , ( $Re=200$ ,  $Pr=0.7$ ).

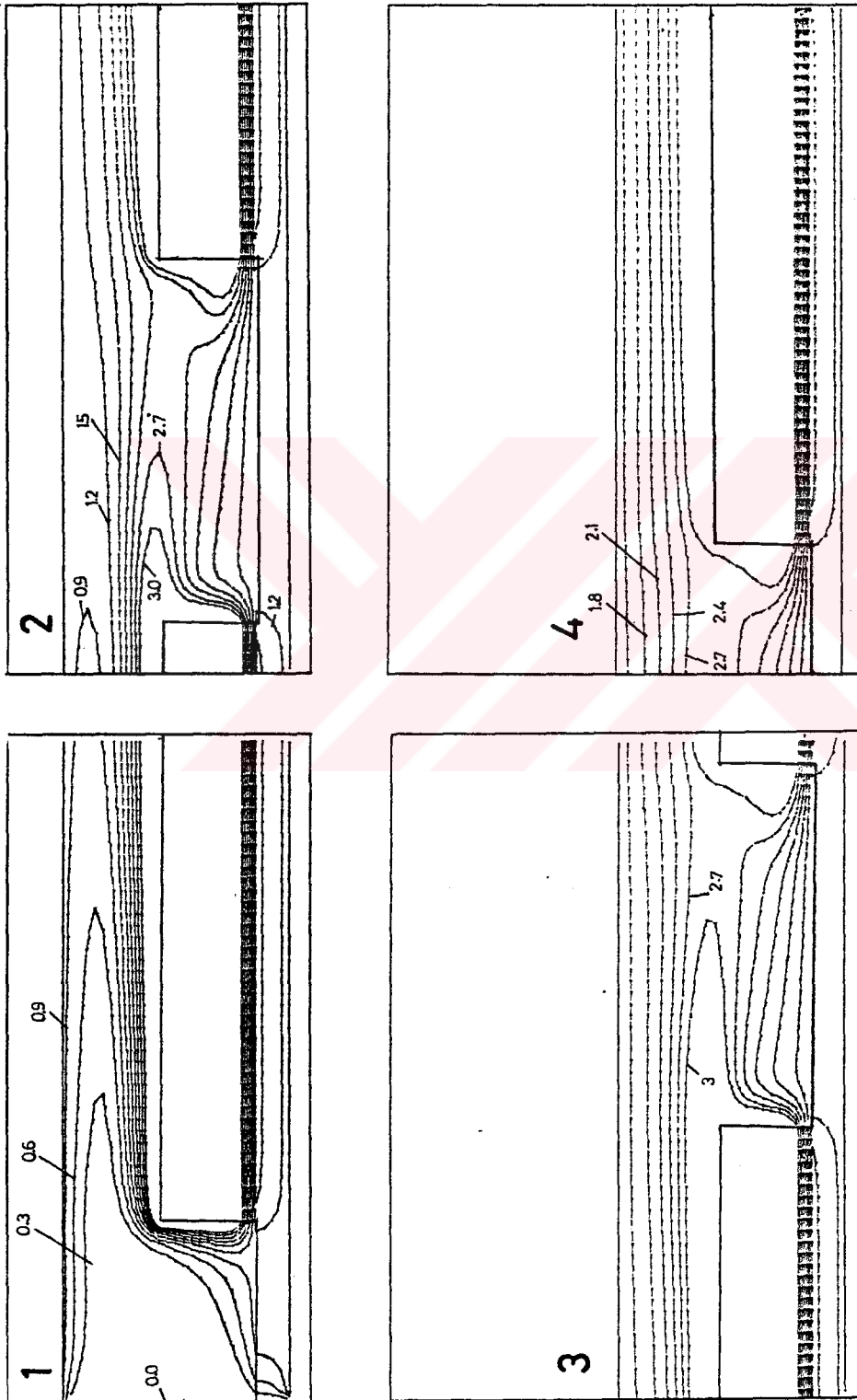


Figure 7.12m) Temperature contours in three-step channel with source location at a position,  $H'/H=1/4$ , ( $Re=200$ ,  $Pr=0.7$ ).

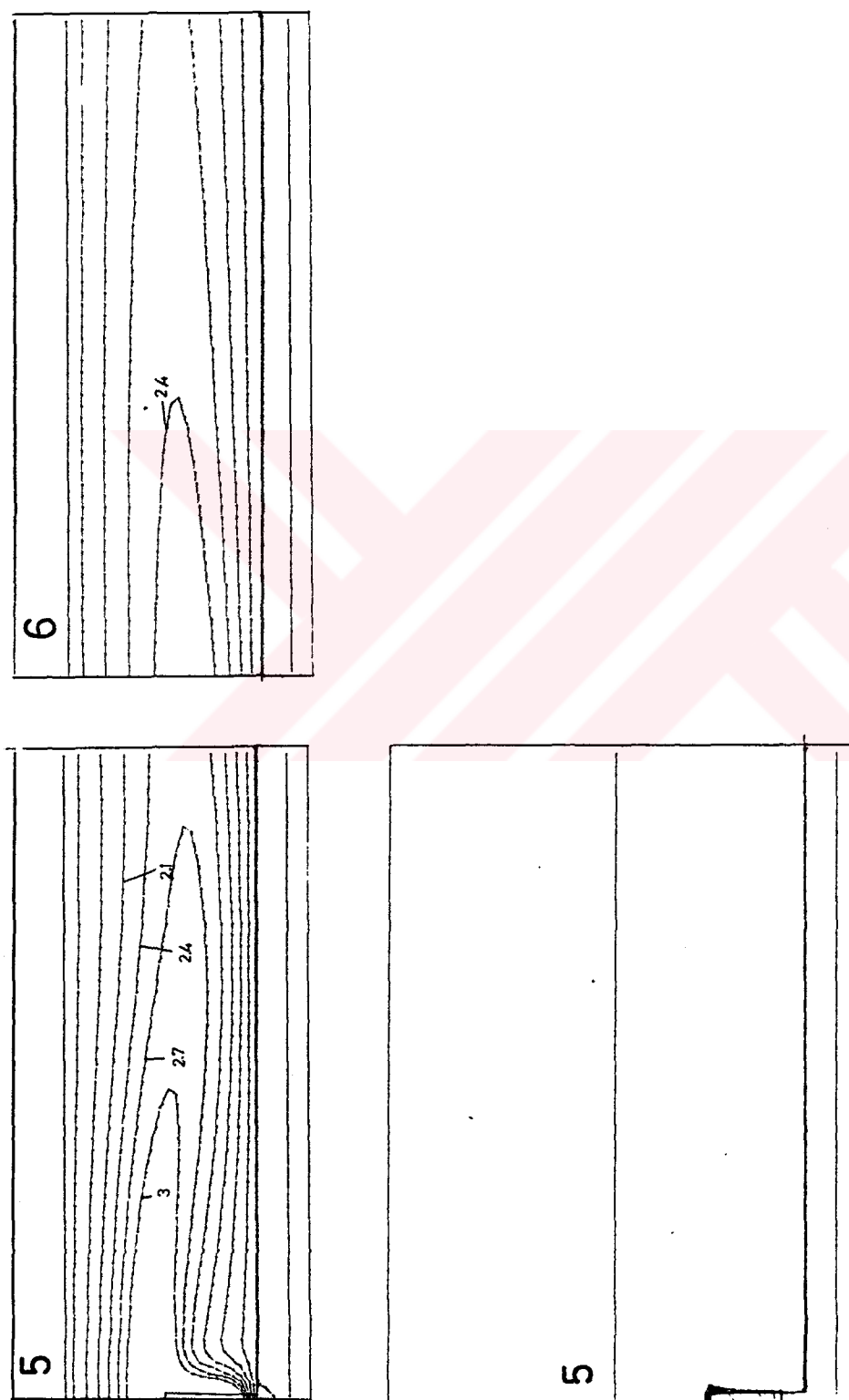


Figure 7.12n) Temperature contours in three-step channel with source location at a position,  $H'/H=1/4$ , ( $Re=200$ ,  $Pr=0.7$ ).

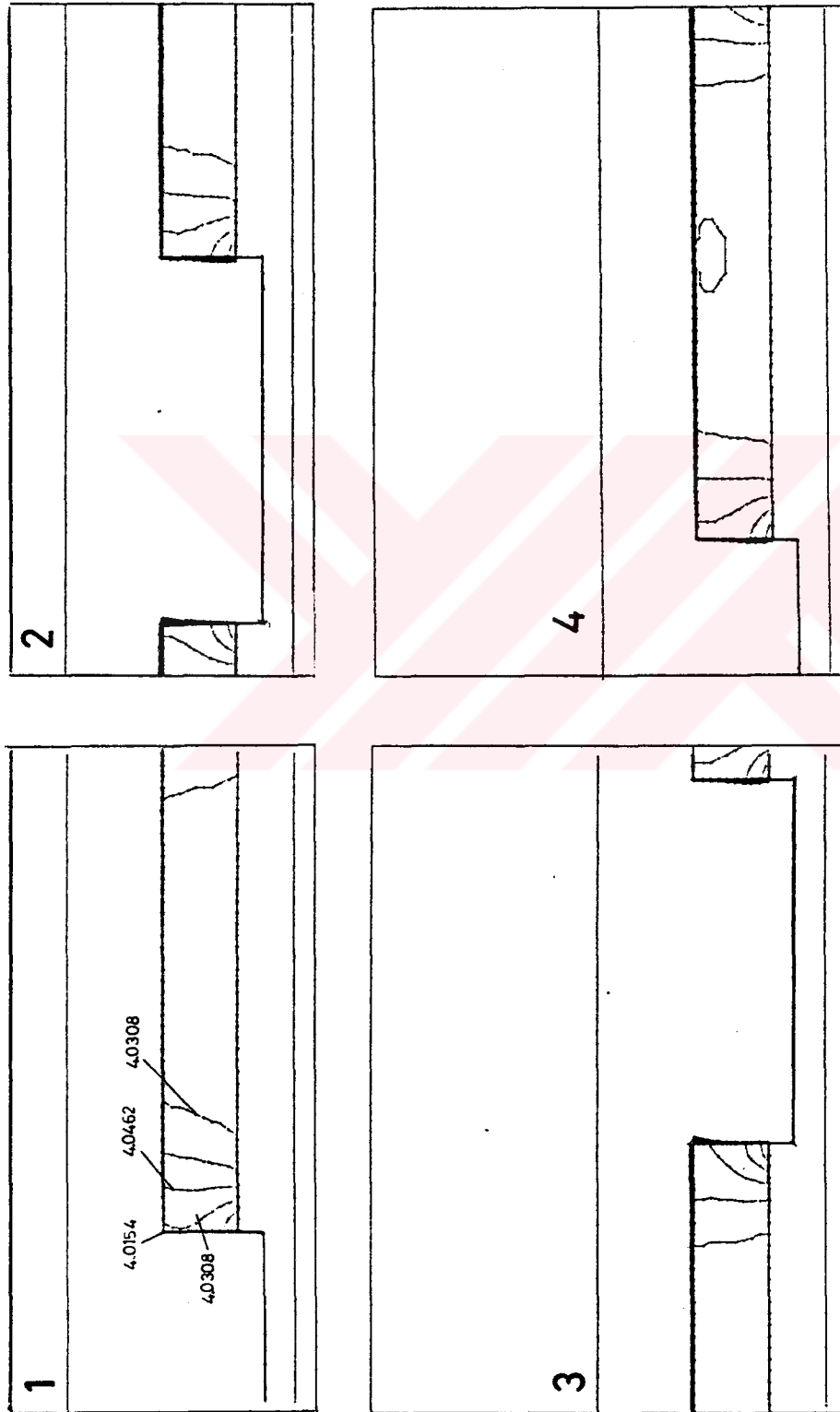


Figure 7.120) Temperature contours in three-step channel with source location at a position,  $H'/H=1/4$ , ( $Re=200$ ,  $Pr=0.7$ ).



## CHAPTER 8

### HEAT TRANSFER CHARACTERISTICS

In this section important heat transfer properties of the model problem are given. These properties are,

1) Figure 8.1a shows the fluid temperature variation along the flow direction in the case of  $Re=200$ ,  $Pr=0.7$ , along the flow direction fluid temperature naturally increases, though a sharp decrease on the step portion occurred. However, with same boundary conditions and nondimensionalized coefficients,  $Nu$  number continuously decreases along the flow direction. In Figure 8.1b, heat carried by convection along the  $X$  direction decreases. At the forward step and backward step portions,  $Nu$  number decreases since heat conduction becomes dominant.

2) In Figure 8.1c, the fluid temperature distributions are shown against various Prandtl numbers for  $Re=200$ . Decrease in Prandtl number results in increase in fluid temperature distribution along the flow direction. Since decreasing  $Pr$  number results in increasing molecular diffusivity of heat, this results in increase in temperature.

3) Figure 8.1d shows Nusselt number distribution at various Prandtl numbers. Increase in convection heat transfer is occurred in case of increasing molecular diffusivity. General trend for each case along the flow direction is same.

4) Figure 8.2 shows Nusselt number distributions for channels having one, two and three steps. On the steps Nusselt number is positive. The detailed explanation will be made for Figure 8.3.

5) Figure 8.3 shows Nusselt number distributions for channels having one, two and three steps. On the steps, for each case, Nusselt number is positive. Since convection heat transfer becomes dominant and velocities are comparatively high. On the other hand, in the cavity region, flow makes circulation and velocities continuously change their directions. Any fluid particles observed must be passed the same points where it was a while ago. If this period goes to zero, fluid particles likely stop, and the heat transfer by conduction becomes dominant. This mechanism results in negative Nusselt number in the cavity regions. The pick value of Nusselt number distributions is seen in this cavity regions where flow leaves the cavity wall, that is forward face of the next step of the bottom part.

6) Figure 8.4a shows the percentage of  $(T_{max} - T_{w,u})$  temperature values in the step. When the Prandtl number increases, percentage of  $(T_{max} - T_{w,u})$  distribution decreases. Higher the molecular diffusivity, higher the heat transfer. The temperatures, around the maximum, become dominant in the block but their values are comparatively lower than the temperature in case of high Prandtl number.

7) Figure 8.4b shows three-step channel fluid temperature distribution trend in case where the heat sources are located in the higher positions of the steps. But the general trends for each cases are the same except only the maximum temperature values.

8) Figure 8.5 shows bulk temperature distributions along the one, two, and three step channel cases with the source location at the higher position. General trend is the same along the flow direction: bulk temperature increases and makes out some peaks, on the step bulk temperature steadily increases. However, on the cavities walls, from upper part to the bottom part, it is possible to see the maximum and the minimum of the peaks, since, from the wall of the cavity, heat lost into the cooled substrate by conduction.

9) Figure 8.6 shows bulk temperature distribution along the one, two and three step channel case with heat sources at various locations. The location of the sources results in different maximum temperature values on the domain, though general trends are the same for each cases. Physical interperation of these figures can be done, as it is for Figure 8.4.

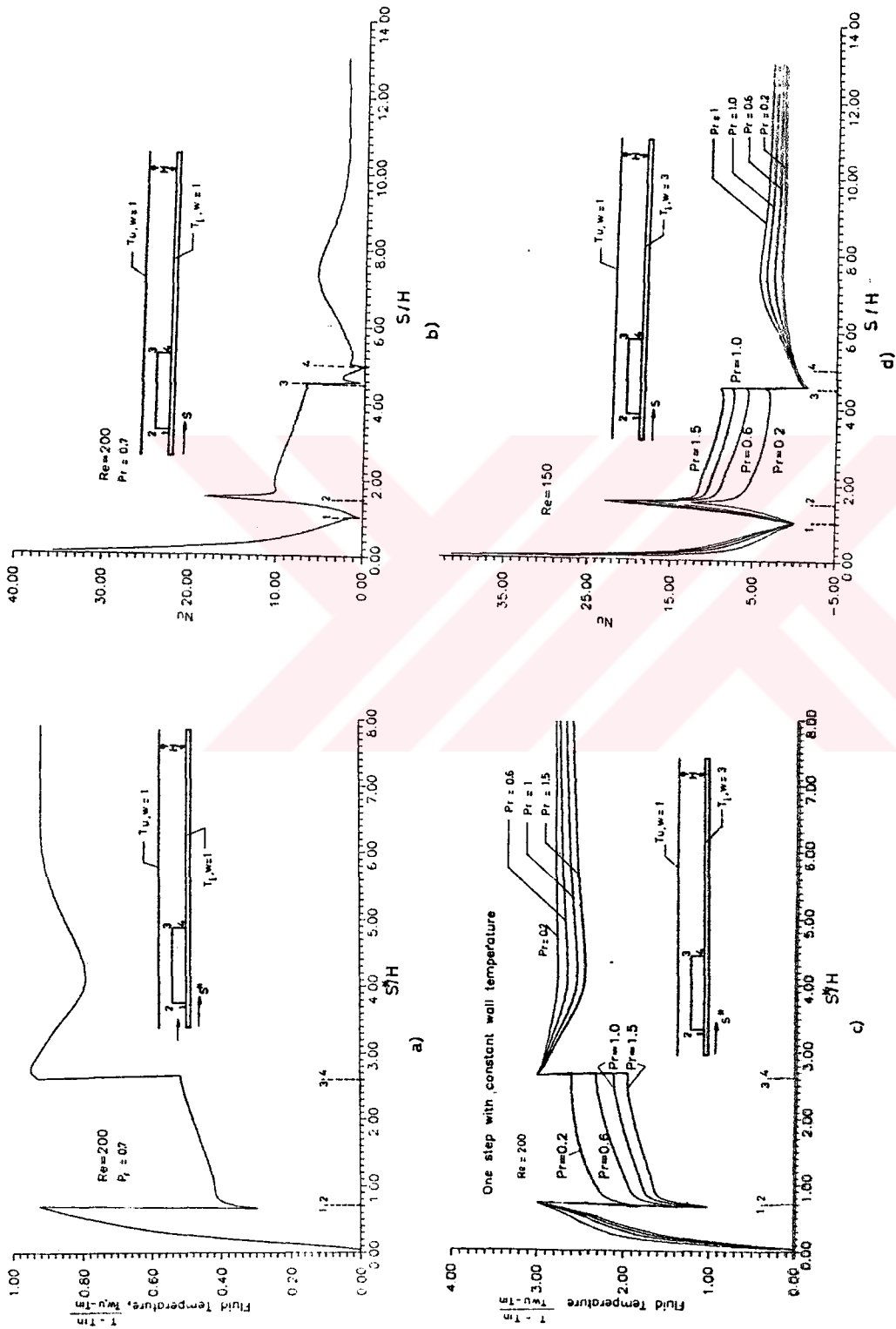


Figure 8.1) Fluid temperature and Nusselt number distribution at various Pr numbers.

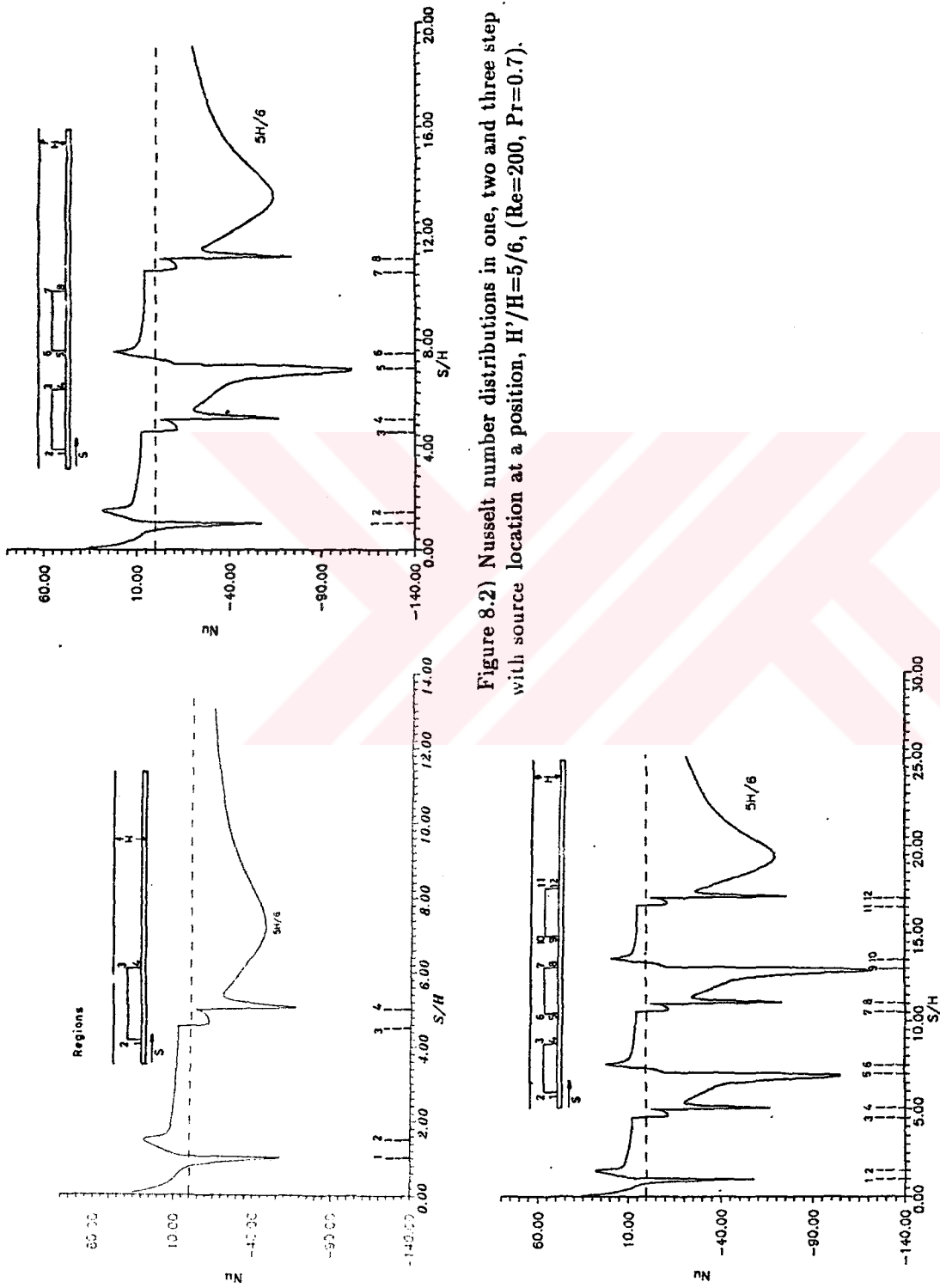


Figure 8.2) Nusselt number distributions in one, two and three step with source location at a position,  $H'/H=5/6$ , ( $Re=200$ ,  $Pr=0.7$ ).

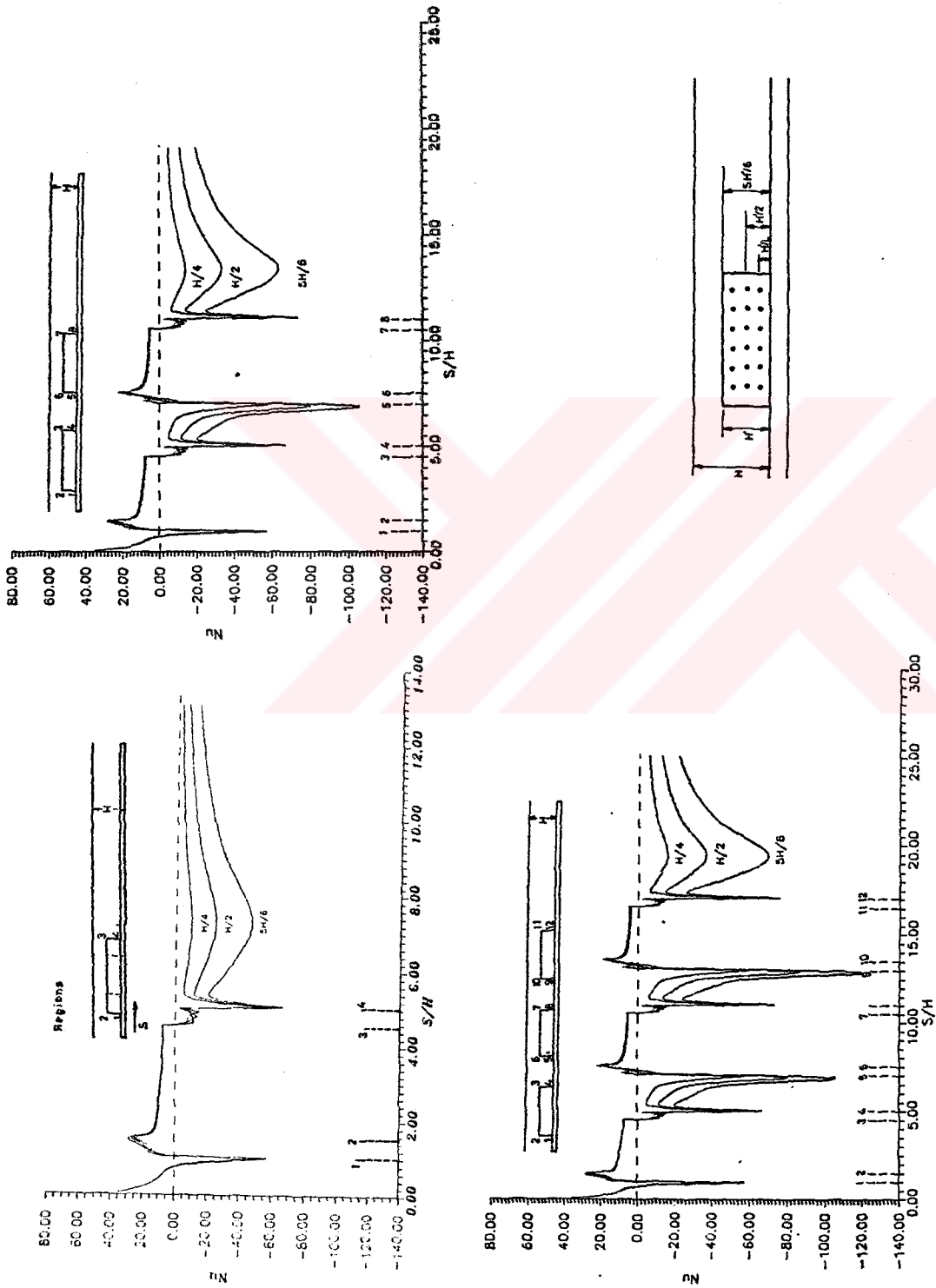


Figure 8.3) Nusselt number distribution in one, two, and step channels with source at various positions.

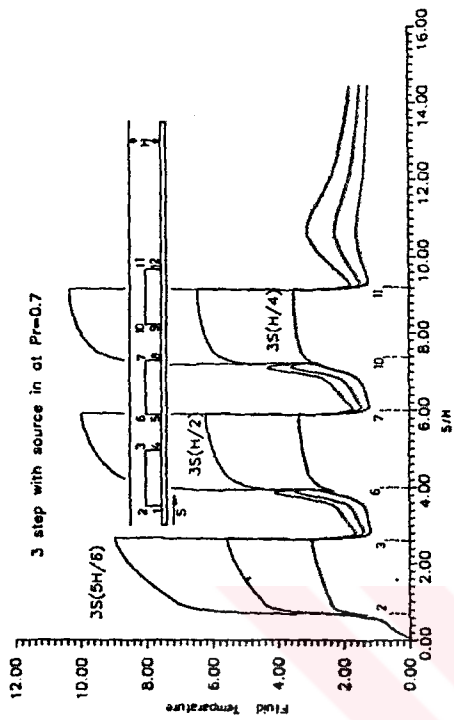


Figure 8.4b) Fluid temperature distribution along the three step channel.

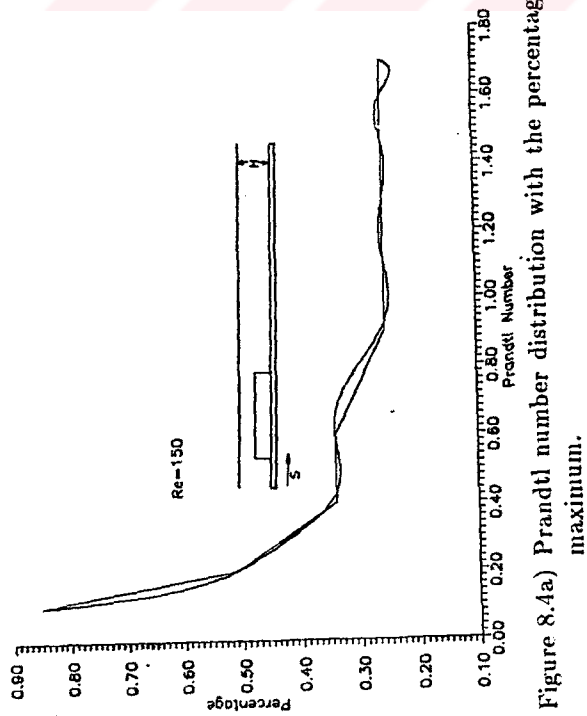


Figure 8.4a) Prandtl number distribution with the percentage of temperature around the maximum.

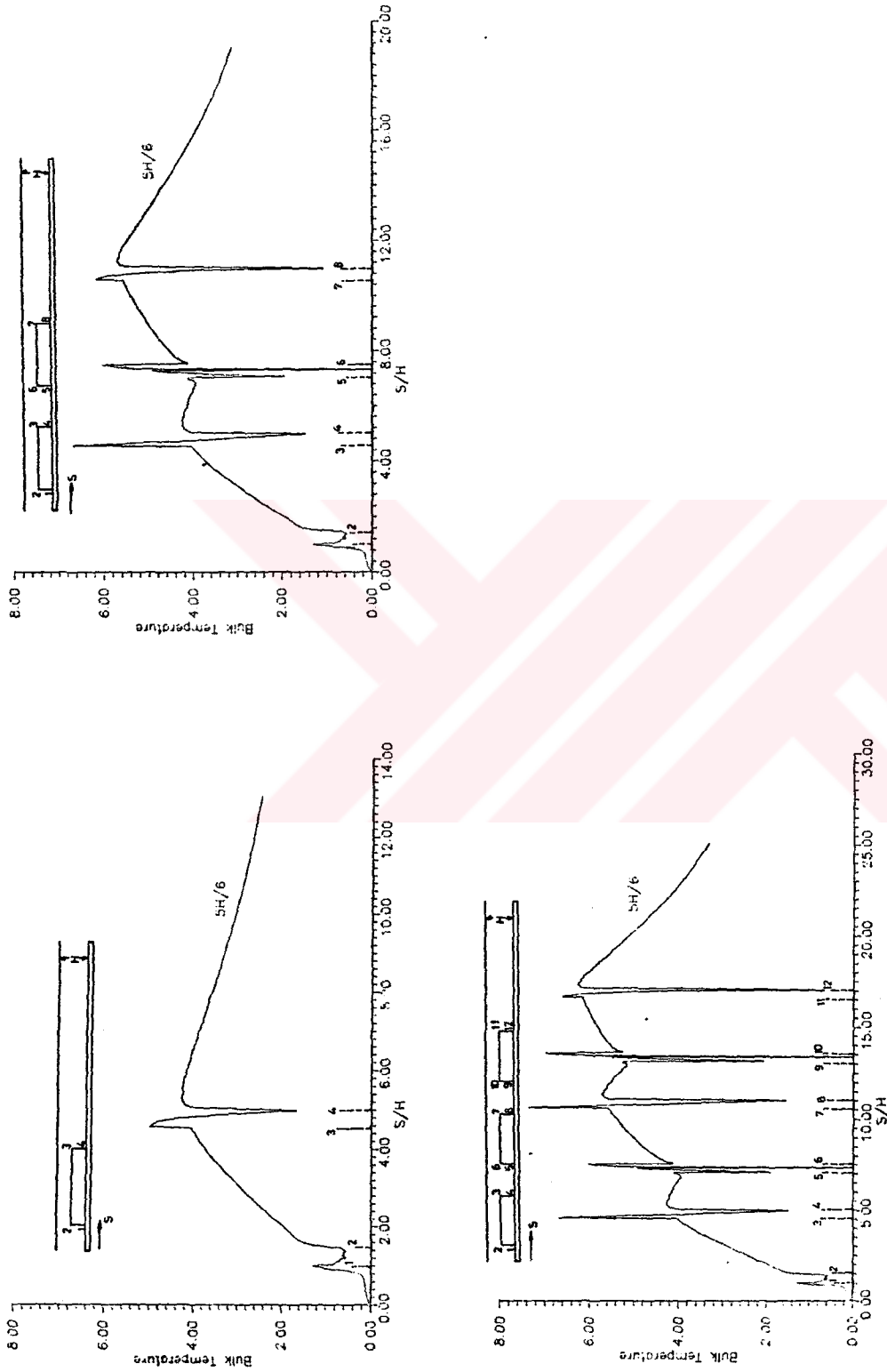


Figure 8.5) Bulk temperature distribution along the one, two and three step with source location at a position,  $W'/H=5/6$ , ( $Re=200$ ,  $Pr=0.7$ ).



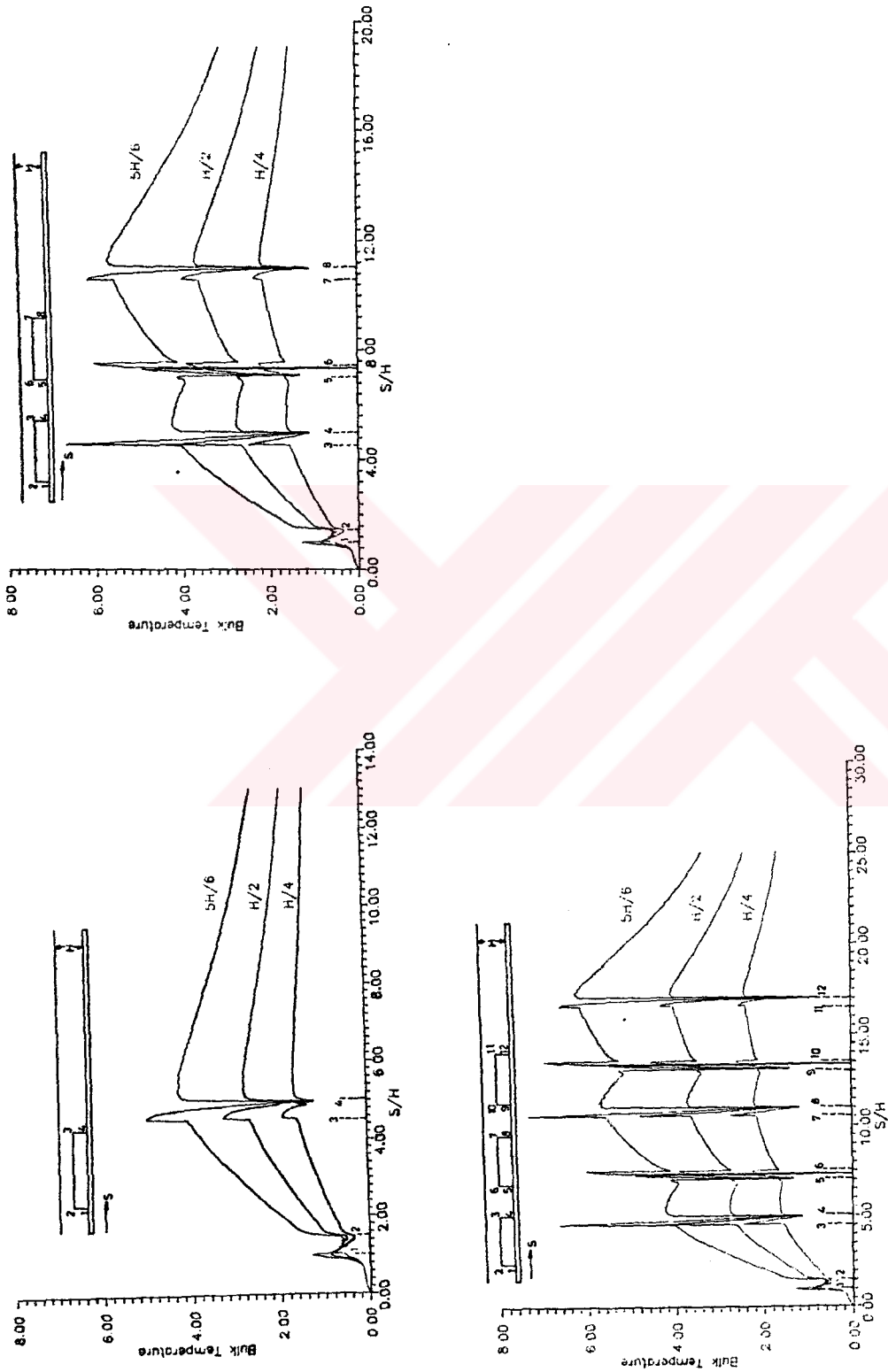


Figure 8.6) Bulk temperature distribution along the one, two and three step with heat sources at various location,  $H'/H=5/6$ , ( $Re=200$ ,  $Pr=0.7$ ).

## **CHAPTER 9**

### **COLOR GRAPHICS PRESENTATIONS**

In this chapter the flow field and thermal field solutions are presented for one, two and three-step channel cases. The source locations for three cases, shown individually by full color graphics.

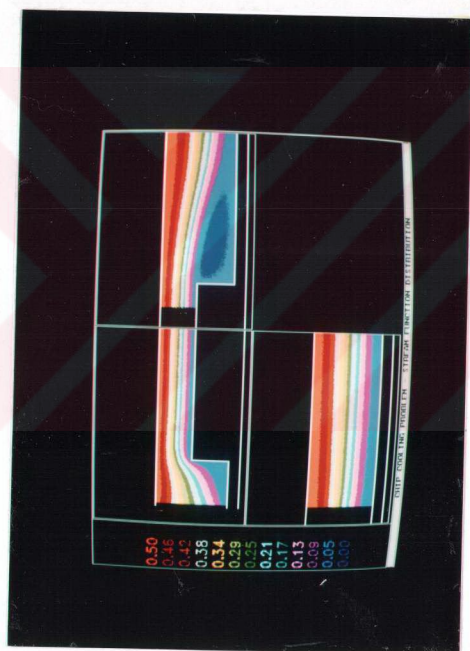


Figure 9.1) Stream function distribution in one-step channel.

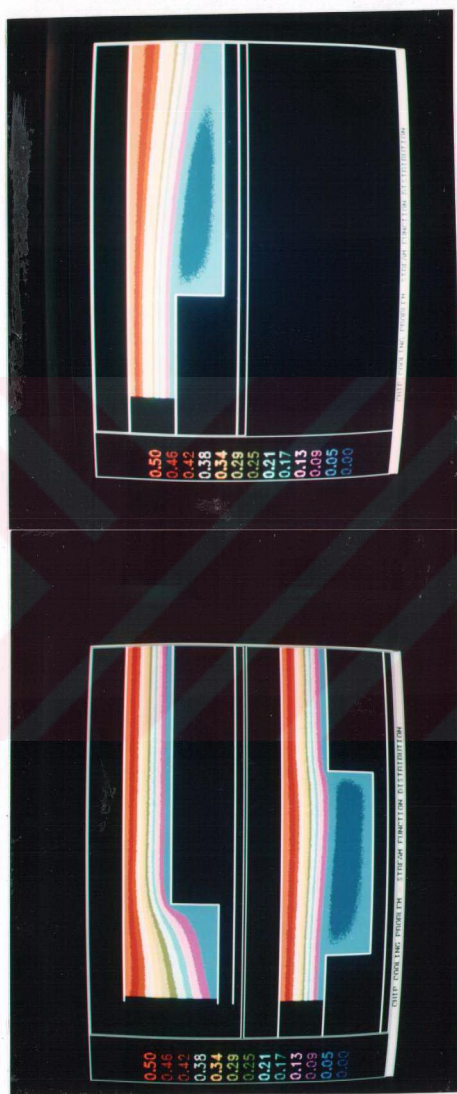


Figure 9.2) Stream function distribution in two-step channel.

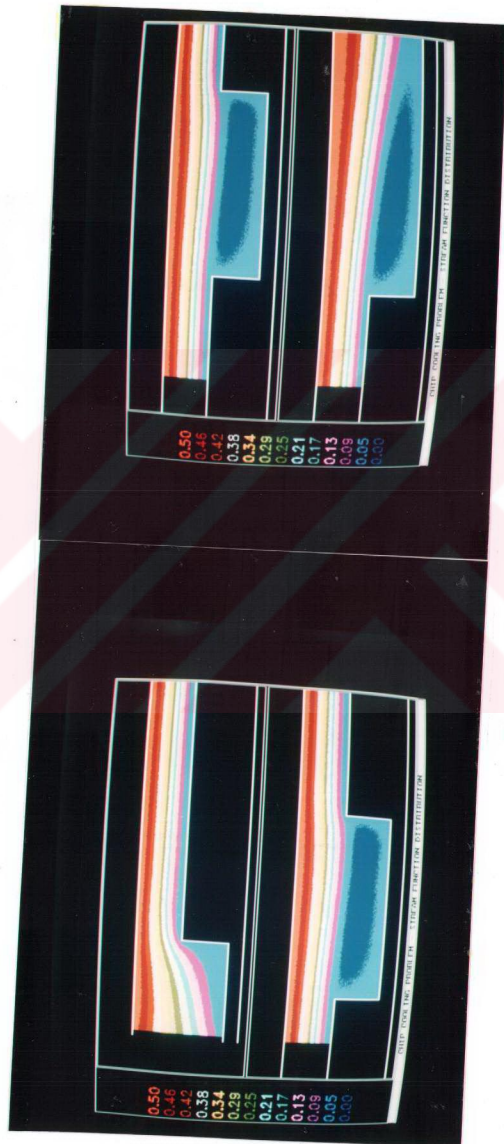


Figure 9.3) Stream function distribution in three-step channel.

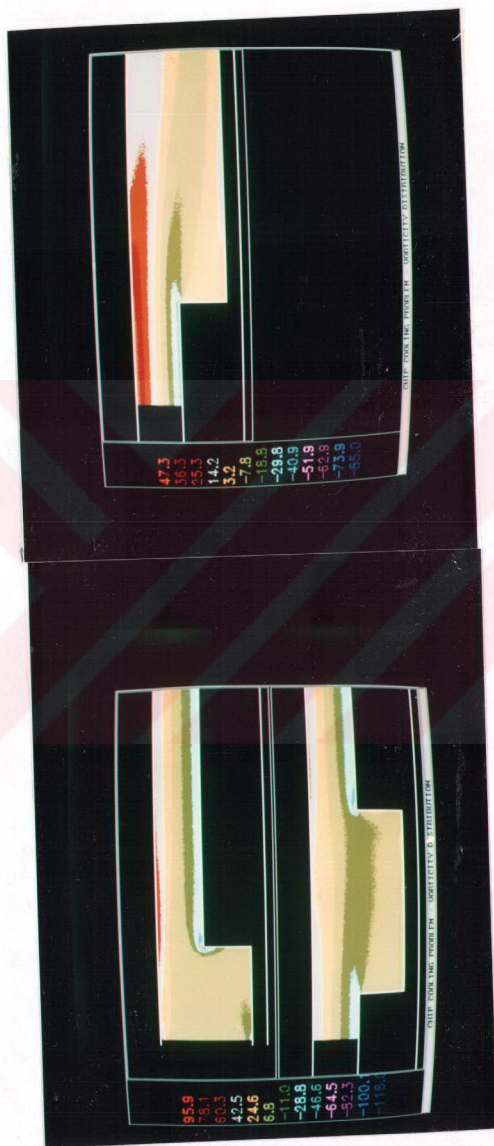


Figure 9.5) Vorticity distribution in two-step channel.

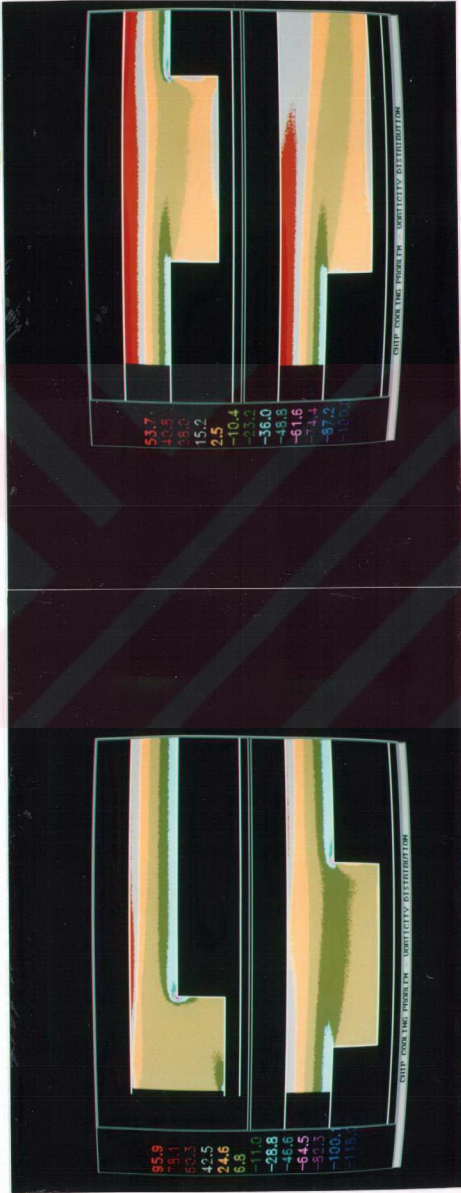


Figure 9.6) Vorticity distribution in three-step channel.



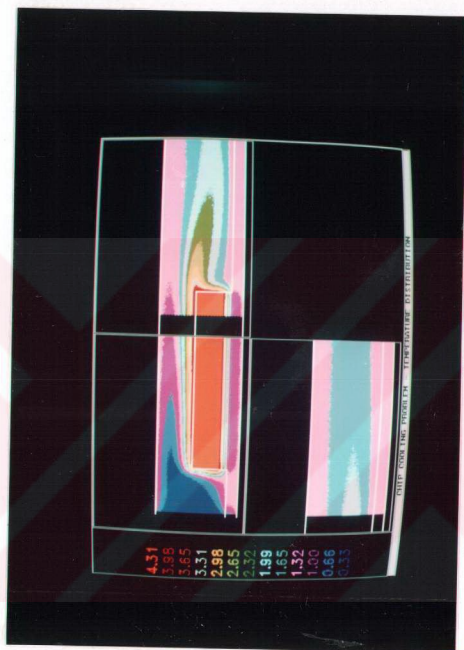


Figure 9.7) Temperature distribution in one-step channel with source location at a position  $H'/H=1/4$ , ( $Re=200$ ,  $Pr=0.7$ )



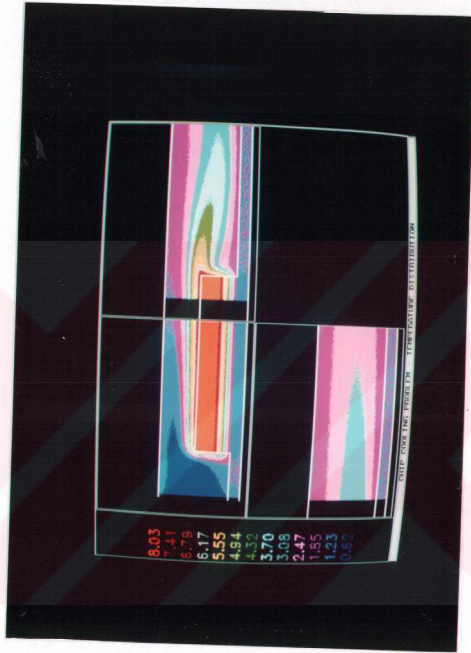


Figure 9.8) Temperature distribution in one-step channel with source location at a position  $H/H=1/2$ , ( $Re=200$ ,  $Pr=0.7$ )

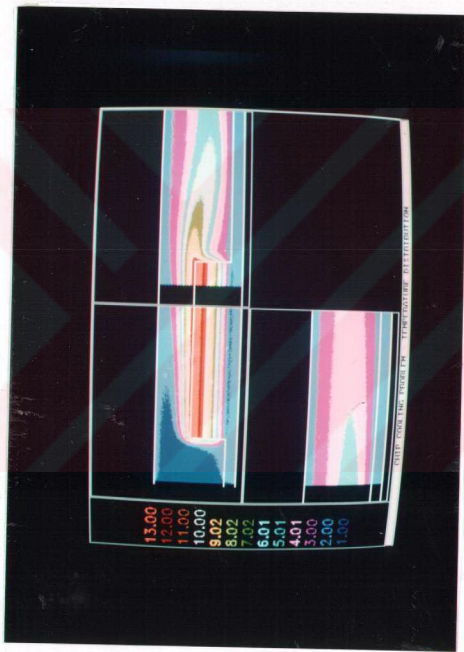


Figure 9.9) Temperature distribution in one-step channel with source location at a position  $H'/H=5/6$ , ( $Re=200$ ,  $Pr=0.7$ )

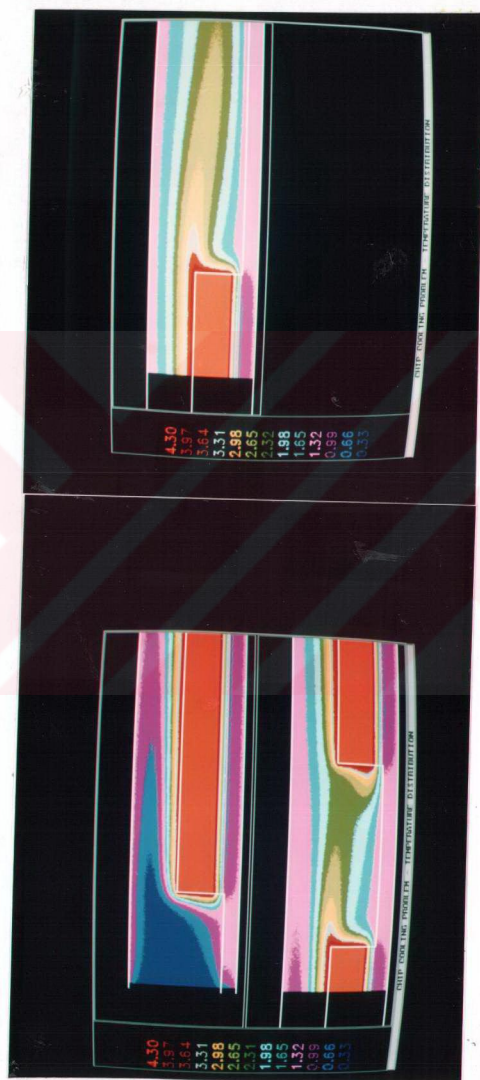


Figure 9.10) Temperature distribution in two-step channel with source location at a position  $H'/H=1/4$ , ( $Re=200$ ,  $Pr=0.7$ )

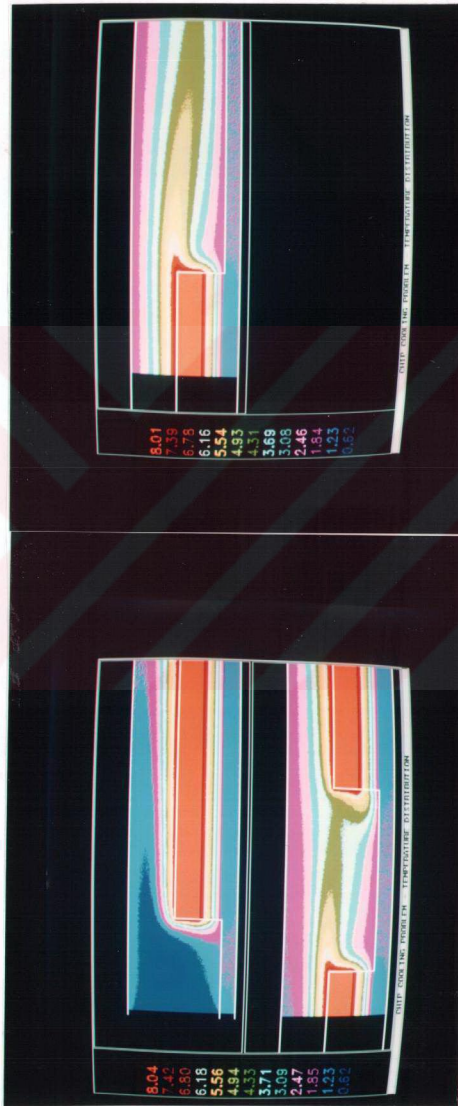


Figure 9.11) Temperature distribution in two-step channel with source location at a position  $H'/H=1/2$ , ( $Re=200$ ,  $Pr=0.7$ )

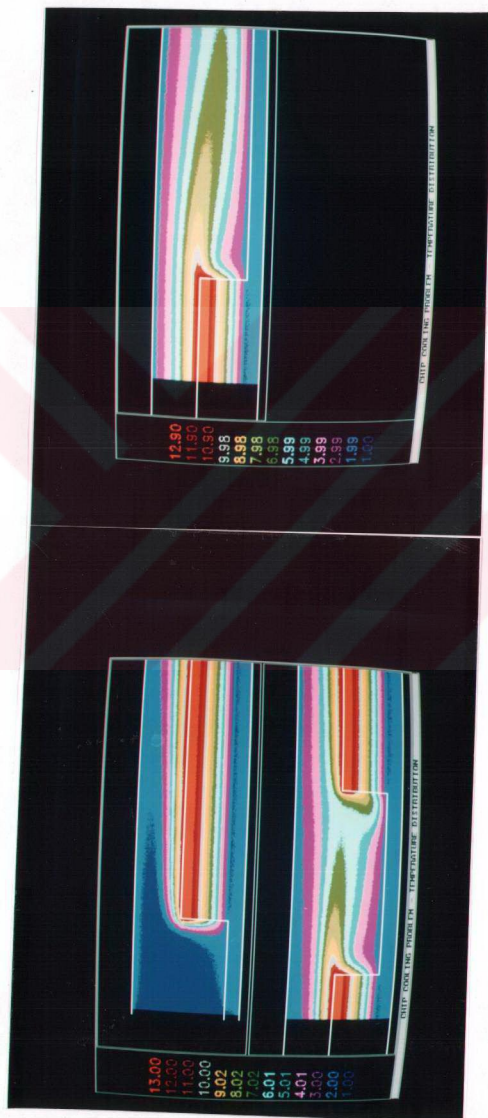


Figure 9.12) Temperature distribution in two-step channel with source location at a position  $H'/H=5/6$ , ( $Re=200$ ,  $Pr=0.7$ )





Figure 9.13) Temperature distribution in three-step channel with source location at a position  $H'/H=1/4$ , ( $Re=200$ ,  $Pr=0.7$ )

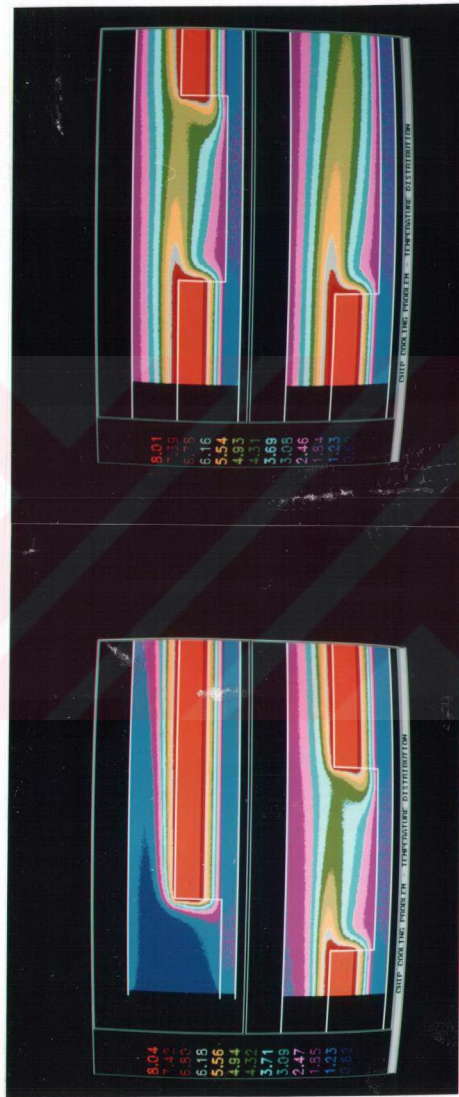


Figure 9.14) Temperature distribution in three-step channel with source location at a position  $H'/H=1/2$ , ( $Re=200$ ,  $Pr=0.7$ )

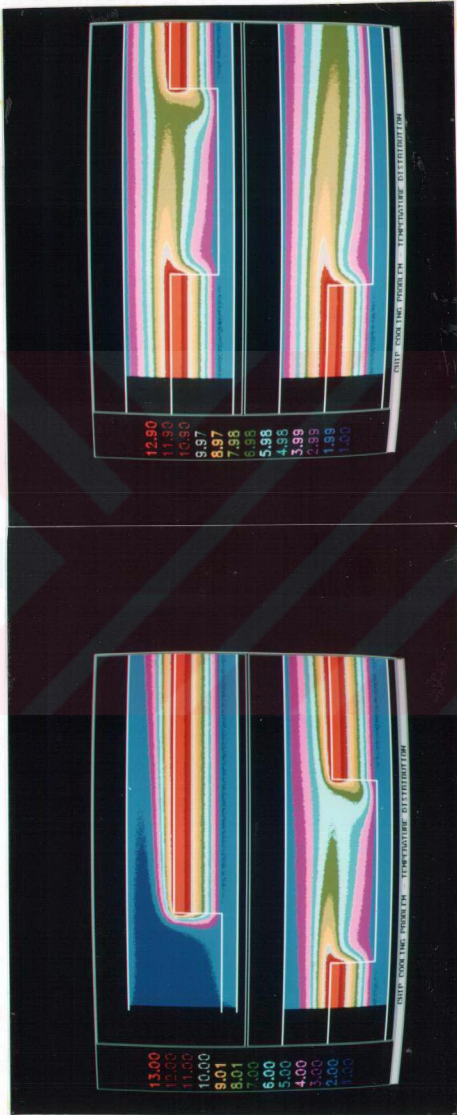


Figure 9.15) Temperature distribution in three-step channel with source location at a position  $H'/H=5/6$ , ( $Re=200$ ,  $Pr=0.7$ )



## CHAPTER 10

### RECOMMENDATION AND FUTURE ASPECTS

An investigation of conjugate problem which makes complex fluid-solid and solid-solid interaction is presented in this thesis. Author believes there are ample rooms for future developments. These are listed below :

1) Developed computer code has been applied for relatively low Reynolds number flows. This was mainly due to the computer limitations. Since high Reynolds number flows require more grid points near the solid surface, one has to have a high speed computer. Preliminary runs show that the code is capable of simulating Reynolds number of 1000-4000 value. The Reynolds number is defined with respect to twice the channel width.

2) The investigation was conducted for 2-D geometry and flow field. Further studies should be done to evaluate the flow field in channels with obstacles, using the turbulence and 3-D models. Adding turbulence and 3-D model will slightly change the results which are evaluated from 2-D models.

3) From the numerical experiments on the thermal field, the best cooling scenerous can be given out, choosing the source location as close as to cooled substrate. Quite high percentage of heat loses in to the cooled substrate by means of conduction. Thin substrate accelerates conduction process and drops critical temperature in the domain. Shortly one has to choose thin substrate with lowest source position in the block. Or, even, if it is possible, block must be cooled bu means of direct conduction process, surrounded by thin solids.

## REFERENCES

- [1 ] HaCohen, Y., Convective Heat Transfer Coefficients for Elements On a Packed Board, M.Sc. Thesis, Ben-Gurion University of The Negev, 1985.
- [2 ] Nakayama, W., Thermal Management of Electronic Equipment: a Review of Technology and Research Topics, Appl. Mech., Rev Vol. 39, No 12, Dec. 1986.
- [3 ] Incropera, F.P., Convection Heat Transfer in Electronic Equipment Cooling, Journal of Heat Transfer, Vol. 110/1097 November 1988.
- [4 ] Torok, D. and Gronseth, R., Developing Flows In Narrow Channel Containing Heated Obstacles, International Journal For Numerical Methods In Fluids, Vol. 8, 1543-1561 (1988).
- [5 ] Lehman, G.L. and Wirtz, R.A, Effect of Variations in Streamwise Spacing and Length on Convection From Surface Mounted Rectangular Components, HTD-48, 23rd National Heat Transfer Conf., Denver, CO, August 1985, pp. 39-47.
- [6 ] Arvizu, D.E. and Moffat, R.J., The Use of Superposition in Calculating Cooling Requirements for Circuit Board Mounted Electronic Components, IEEE Paper, CH1781-4/48-0133 (1982).
- [7 ] Ashiwake, N., Nakayama, W. and Daikoku, T., Forced Convection Heat Transfer From LSI Packages in An Air-Cooled Wiring Card Array, HTD-28, ASME Winter Annual Meeting, Boston, MA., November 1983, pp. 35-42.

- [8] Sparrow, E.M., Neithammer, J.E. and Chaboki, E.A., Heat transfer and Pressure Drop Characteristics of Arrays of Rectangular Modules Encountered in Electronic Equipment, *Int. J. Heat Mass Transfer*, 25, 469-473 (1982).
- [9] Bradley, R.G., Current Capabilities and Future Directions in Computational Fluid Dynamics, *Natioanal Academy of Sciences and National Research Council*, Washington, DC, 1986.
- [10] Pletcher, R.H., Patankar, S.V., Computers in Analysis and Design, *Mech. Eng.*, 105, 73-79, June 1983.
- [11] Patankar, S.V and Braater, M.E., Analysis of Laminar Mixed Convection in Shrouded Arrays of Heated Rectangular Blocks, *ASME HTD-32, National Heat Transfer Conf.*, Niagara Falls, NY, August 1984, pp. 77-84.
- [12] Torok, D.F, Augementing Experimental Methods for Flow Visualization and Thermal Performance Predicting in Electronic Packaging Using Finite Elements, *HTD-32, ASME Heat Transfer Conf.*, Niagara Falls, NY, August 1984, pp, 49-57.
- [13] Patera, A.T, A Spectral Element Method for Fluid Dynamics, *J. Comput. Phys.*, 54, 468, 1984.
- [14] Asaka, Y. and Faghri, M., Three Dimensional Heat Transfer and Fluid Flow Analysis of Arrays of Rectangular Blocks Encountered In Electronic Equipment, *ASME Preprint 87-HT-73, National Heat Transfer Conf*, Pittsburg, 1987.
- [15] Engelman, M., Computatioanal Fluid Dynamics: Pouring It on Too Thick ?, *Comput. Mech. Eng.*, 6, 52-56, Jaunary 1987.

- [16] Mahaney, H.V, Incropera, F.P and Ramadhyani, S., Comparasion of Predicted and Measured Mixed Convection Heat Transfer From An Array of Discrete Sources In a Horizontal Rectangular Channel, *Int. J. Heat Mass Transfer*. Vol. 33, No 6, pp 1233-1245, 1990.
- [17] Lin, J.T, Armaly, B.F and Chen, T.S, Mixed Convection In Buoyancy-Assisting, Vertical Backward-Facing Step Flows. *Int. J. Heat Mass Transfer*. Vol. 33, No 10, pp 2121-2132, 1989.
- [18] Kelkar, M.K and Patankar, S.V., Numerical Prediction of Flow and Heat Transfer in A Parellel Plate Channel With Staggered Fins, *Journal of Heat Transfer*. Vol. 109/25, 1987.
- [19] Hsieh, S.S and Huang, D.Y., Flow Characteristics of Laminar Separation on Surface Mounted Ribs, *AIAA Journal*. Vol 25, No 6, June 1987.
- [20] Ghia, K.N, Osswald, G.A and Ghia, U., Analysis of Incompressible Massively Separated Viscous Flows Using Unsteady Navier-Stokes Equations. *International Journal For Numerical Methods In Fluids*, Vol. 9, 1025-1050, 1989.
- [21] Pereira, J.C.F and Durst, F, Finite Difference Methods in Recirculating Flows.
- [22] Cheng, C.H, and Huang, W.H, Laminar Forced Convection Flows in Horizontal Channels With Transverse Fins Placed in Entrance Regions, *Numerical Heat Transfer, Part A*, Vol, 16, pp, 77-100, 1989
- [23] Anderson, D.A., Tannehill, J.C. and Pletcher, R.H., *Computational Fluid Mechanics and Heat Transfer*, Hemisphere Publishing Corporation, New York, 1984.
- [24] White, F.M., *Viscous Flow*, McGraw-Hill, Inc. 1974.



- [25 ] Roach, P.J., Computational Fluid Dynamics, Hermos Publishers, 1976.
- [26 ] Peyret, R and Taylor, T.D. computational Methods for Fluid Flow, Springer-Verlag, 1990.
- [27 ] Schlichting, H., Boundary Layer Theory, McGraw-Hill Book Company, 1958.
- [28 ] W.F Ames, Numerical Methods for Partial Differential Equations, Academic Press, 1977.
- [29 ] A.Lin, Towards Generation and Optimization of Implicit Medhods, International Journal for Numerical Methods In Fluids, Vol5,pp 357-380, 1985.
- [30 ] A.V Luikov, V.A Aleksaslenkes and A.A Aleksaslenkes, Analytical Methods of Solution of Conjugate Problems in Convective Heat Transfer, Int. I. Heat Mass Transfer, Vol 14, pp 1047-1050, 1971.
- [31 ] Mari, S., Sakakibana, M. Tanimoto, A. , Steady Heat Transfer to Laminar in a Circular Tube With Conduction in The Wall, Heat Tranfer: Jap. Res., Vol3, No2, 37-47, 1974.
- [32 ] Davalth, J., Beyazitoglu, Y., Forced Convection Cooling Across Rectangular Blocks, Journal of Heat Transfer, Vol. 109/321 May 1987.
- [33 ] Incropera, F.P., Kerbey, J.S., Moffatt, D.F, and Ramadhyani, S., Convection Heat Transfer, From Discrete Heat Sources in A Rectangular Channel, Int, J. Heat Mass Transfer Vol 29, No 7, pp. 1051-1058, 1986.
- [34 ] Garg, V.K. and MaJi, P.K., Laminar Flow And Heat Transfer in A Periodically Converging-Diverging Channel, International Journal For Numerical Methods In Fluids, Vol. 8, 579-597 (1988).

- [35] Kang, B.H. and Jaluria, Y., Natural Convection Heat Transfer Characteristics of Protruding Thermal Source Located on Horizontal And Vertical Surfaces, *Int. J. Heat Mass Transfer*. Vol33, No. 6. pp 1347-1357, 1990.
- [36] Kumar, S.G.R., Narayana, P.A.A., Seetharamu, K.N. and Ramaswamy.B, Laminar Flow and Heat Transfer Over A Two-Dimensional Triangular Step, *International Journal For Numerical Methods In Fluids*, Vol. 9, 1165-1177 (1989)
- [37] Biringen, S. and Kao, K.H., On The Application of Pseudospectral FFT Techniques To Non-Periodic Problems, *International Journal For Numerical Methods In Fluids*, Vol. 9, 1235-1267, 1989.
- [38] Holman, J.P., *Heat Transfer*, McGRAW-Hill Kogakusha, LTD., 1976.
- [39] Haugen, R.I. and Dhanak, A.M., Heat Tranfer in Turbulent Boundary-Layer Separation Over a Surface Cavity, *Journal of Heat Transfer*, November 1967.
- [40] Thoman, D.C. and Szewczyk, A.A., Time Dependent Viscous Flow Over a Circular Cylinder, *The Physics of Fluids Supplement II, High-Speed Computing in Fluid Dynamics*, pp 76-87, 1969.
- [41] Stone, H.L., Iterative Solution of Implicit Approximation of Multidimensinal Partial Differential Equations. *SIAM J. Num. Anal.* Vol. 5, Nr. 3, pp. 530-558, 1968.
- [42] Vemuri, V., Karplus, W.J., *Digital Computer Treatment of Partial Differential Equations*. Prentice-Hall, Inc., Englewood Cliff, New Jersy, 1981.
- [43] Arpaci, V.S. and Larsen, P.S, *Convection Heat Transfer*, Printince - Hall, Inc. 1984.

- [44 ] Denhem, M.K and Patrick, M.A, Laminar Flow Over a Downtstream-Facing Step in a Two-Dimensional Flow Channel, Trans. , Inst. Chem., Eng., 52, 361-367 (1974).



## APPENDIX A

### A) Nusselt Number Calculation

Using the wall heat flux equivalence to the lost by means of convection.

Hence,

$$q_w = h(T_w - T_\infty) = -k \left( \frac{\partial T}{\partial y} \right)_w$$

Take the characteristic length, say  $2H$ , for considered geometry in this study,

$$\frac{2hH}{k} = - \frac{\frac{\partial T}{\partial (y/2H)}}{T_w - T_\infty}$$

The definition of Nusselt number,

$$Nu = \frac{2hH}{k} = - \frac{\frac{\partial T}{\partial (y/2H)}}{T_w - T_\infty}$$

where,

$h$  is heat transfer coefficient,  $k$  and  $2H$  are the thermal conductivity and characteristic length of the fluid.

## B) Bulk Temperature Calculation

When the geometry of fluid is finite  $T_\infty$  is conveniently replaced by mean temperature for fluid. Say the bulk temperature for incompressible flow thus,

$$T_b = \frac{1}{AU_a} \int_A u(x, y) T(x, y) dA$$

$A$ : Transversal area to the motion.

$U_a$ : Transversally averaged velocity

$$U_a = \frac{\int_A u(x, y) dA}{\int_A dA}$$

Bulk Temperature becomes,

$$T_b = \frac{1}{A} \frac{\int_A u(x, y) T(x, y) dA}{\frac{\int_A u(x, y) dA}{\int_A dA}}$$

**CURRICULUM VITAE**

İbrahim ÖZKOL was born in İzmir, TURKEY on January 1, 1962. He completed high school in 1979. He got his B.Sc. degree from Istanbul Technical University (ITU), Faculty of Aeronautics and Astronautics, Department of Aeronautical Engineering in 1985. He obtained his M.Sc. degree from ITU Institute of Science and Technology, Aeronautics and Astronautics Engineering Program in 1988. He has been working as a research assistant in the Faculty of Aeronautics and Astronautics of ITU since 1987.